C4R

Capacity for Rail

Towards an affordable, resilient, innovative and high-capacity European Railway System for 2030/2050

Innovative concepts and designs for resilient S&Cs (final)

Submission date: 15/09/2017

Deliverable 13.3

This project has received funding from the European Union's Seventh Framework Programme for research, technological development and demonstration under grant agreement n° 605650








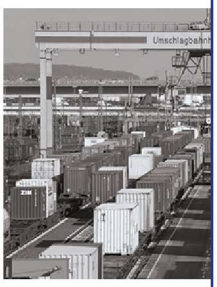

Collaborative project SCP3-GA-2013-60560
Increased Capacity 4 Rail networks through enhanced infrastructure and optimised operations
FP7-SST-2013-RTD-1

Lead contractor for this deliverable:

- Trafikverket

Contributors:

- University of Huddersfield
- VAE
- VCSA
- INECO
- TCDD
- CHALMERS

Project coordinator

- International Union of Railways, UIC

Executive Summary

The turnout (Switch & Crossing, S&C) is a vital component in railway networks as it provides flexibility to traffic operation by allowing trains to switch between tracks. However, the flexibility comes at a cost as the variation and discontinuities in rail profiles in the switch and crossing panels result in increased dynamic loading during wheel passage and thus increased degradation of track (and vehicle) components compared to plain line track. Common damage mechanisms on rails are wear, plastic deformation and rolling contact fatigue (RCF), while components suffer from fatigue (cracked casting) and support degrades (uneven ballast settlement and voids). The present deliverable is describing the work carried out in Capacity4Rail WP1.3, tasks 2, 3 and 4.

The main focus of the report is to investigate and propose innovative designs aiming towards improved S&Cs that reduces material deterioration and failures (task 1.3.2). Based on numerical simulations with validated models and software, the approach is focused on improved understanding of dynamic wheel-rail interaction in S&C and on how the rail degradation can be reduced by optimisation of geometrical and stiffness properties of the turnout. Examples of design variables are rail profiles and the selection of dynamic stiffness for the resilient elements, such as rail pads, base plate pads and under sleeper pads. The influence of rail grade selection and the introduction of friction management in the wheel-rail interface is also covered. The objective is to reduce rail degradation by improved wheel-rail contact conditions leading to a reduction of wheel-rail contact forces (stresses) and creepages. Reduced rail degradation rates will reduce the Life Cycle Cost (LCC) for turnouts. One particular challenge in the optimisation of S&C is to reach a design that is robust in terms of allowing for large variations in traffic conditions due to different vehicle types and worn wheel profiles.

The adopted approach incorporates studies of *short-term design measures* for improving current S&Cs, a *medium-term strategy* where improved solutions are incorporated in an existing railway system and a *long-term vision* where radically new solutions can be introduced without a need for compromising with existing structures. The WP focuses on medium/long distance mixed traffic. However, the design framework developed in the task can be applied to other operational scenarios, e.g. very high speed.

The investigated *short-term solutions* for minimising loads and rail profile degradation in the switch panel include selection of (1) rail profile and rail inclination, (2) rail grade, and (3) friction management. The calculations show that a design with inclined rails (1:30) is superior to the case with vertical rails. The selection of rail grade R350HT instead of R260 leads to a confirmed large reduction in wear. However, the predicted influences of rail grade and friction management on RCF are uncertain due to the wide range of factors influencing RCF initiation, such as the important interaction between crack growth and wear. Thus, the applied RCF damage model needs to be validated by future field observations and measurements. It is shown that both wear and RCF are reduced significantly by maintaining a low friction coefficient in the wheel-rail contact. In particular, situations with dry wheel-rail contact (high friction) should be avoided as these lead to very high RCF damage impact.

The investigated *medium-term solutions* focus on improving the performance of the crossing panel. These solutions include (1) geometry optimisation of the crossing to minimise impact loads and reduce the steering force damage in the contact areas, (2) dynamic load mitigation (ballast protection) through rail pad stiffness optimisation and the use of under sleeper pads (USP) or connecting elements between sleepers, and (3) novel materials in crossing nose and wing rails to resist fatigue, wear and plastic deformation. The investigation in crossing geometry has highlighted key differences in current design practice and machining tools used for half and full cant (UK terminology, where half cant produces a canted wing rail over half its width, while full cant produces a canted wing over its entire width, see Section 3.2.4.2 for more details) geometries, leading to quantifiably different damage behaviour. Damage has also been predicted on the opposite rail due to imposed creep steering forces in the crossing panel. On that basis, a methodology has been proposed to enable fast and effective optimisation of the crossing wing rail geometry to minimise vertical impact loads, wear and RCF on wing rail and crossing nose. Here also the requirement for additional material behaviour observations (field measurements and lab tests) are highlighted, especially the need to address the specific case of cast manganese steels with different hardening laws and processes than rails in plain line track. A methodology has also been proposed for the optimisation of rail pad stiffness in crossing panel, showing that low stiffness rail pads (ca 80 kN/mm) provide a suitable mitigation for ballast pressure, sleeper acceleration and minimising contact forces, while maintaining acceptable bending stresses of rail components.

The overall design of the S&C has been fundamentally unchanged over at least the last 30 years. To tackle the significant increases in line speed, axle load and volume of traffic the S&C system has been incrementally developed, but from a sub-system or component level. The ambition of the S&C next generation (*long-term solution*) is to consider a whole-system approach by enhanced design, materials and components and to incorporate modern mechatronics for improved system kinematics and control. One example of a long-term solution that is discussed in the report is the Modular Continuous Support (MCS) track, which is a ballast-less track design offering an efficient lower cost rail technology based on pre-fabricated modules and continuously supported rails.

Operation of S&Cs in extreme weather conditions is a challenge to railway administrations (task 1.3.3). Examples of common problems are the difficulty to move the switch rails in situations with heavy snow fall, track instability due to buckling at high temperatures, and deterioration of track support conditions due to heavy rainfall and flooding. Increased awareness when severe situations will occur and planning of maintenance personnel as well as reduction in traffic is part of good management strategy as well as preventative actions in the S&C. Some of the preventative actions are:

- Paint operational-critical switches with heat reflecting white-paint (warm weather)
- Regulary check the stress free temperature. Introduce minimal rules about how to design the turnout to avoid weak areas (warm weather)

- Ensure that there are no high trees close to the track (heavy winds)
- Ensure that track (and track off) drainage system are designed and maintained to lead water so the ballast not is affected (heavy rain)
- Installation of heating equipment that can remove snow fast (heavy snow, cold weather)

The last section of the report includes a brief survey of optimised maintenance and sensor strategies (task 1.3.4). The most essential information that should be collected is the information of movement of switch blade, track geometry and rail profile.

The present work and the writing of this deliverable were performed by Chalmers, University of Huddersfield, VAE, VCSA, INECO, TCDD and Trafikverket (lead contractor).

Table of contents

Abbreviations and acronyms

Abbreviation / Acronym	**Description**
AMS	Austenitic Manganese Steel
FB	Flash butt welding
LCC	Life cycle cost
RCF	Rolling contact fatigue
S&C	Switch and crossing
TCDD	Turkiye Chumhuriyeti Devlet Demir Yollari Isletmesi Genel Mudurlugu
TRV	Trafikverket
TSI	Technical System Interoperability
UoH	University of Huddersfield
USP	Under Sleeper Pad
VAE	VAE Gmbh
VSCA	Vossloh Cogifer SA

1 Background

The turnout (Switch & Crossing, S&C) is a vital component in railway networks as it provides flexibility to traffic operation by allowing trains to switch between tracks. However, the flexibility comes at a cost as the variation and discontinuities in rail profiles in the switch and crossing panels result in higher rail (and wheel) degradation rates than in plain line track. Turnouts are often built without transition curves, causing high vehicle jerk (time derivative of lateral vehicle acceleration) at entry and exit of the diverging route. Further, space constraints often prevent the provision of adequate length of support transitions on either side of the S&C unit. Due to the planar nature of a turnout, track inclination (cant) to compensate for the lateral acceleration is not possible.

There are many different railway turnout configurations to fulfil the needs of varying traffic demands. Figure 1.2.1 illustrates a common layout featuring a straight section called the through route and a curved deviating part called the diverging route. The 'front of the turnout' is defined as the start of the deviating curve in the switch panel. The switching function is realised by switching machines or actuators that position the switch rails according to the desired traffic route. The closure panel connects the switch and crossing panels, whereas the crossing panel allows for wheels to travel along both intersecting paths. Opposite to the crossing, and next to the adjacent through (stock) rails, are the check rails that enforce a constraint on the lateral position of passing wheelsets. This is to avoid interference contact between wheel and crossing nose.

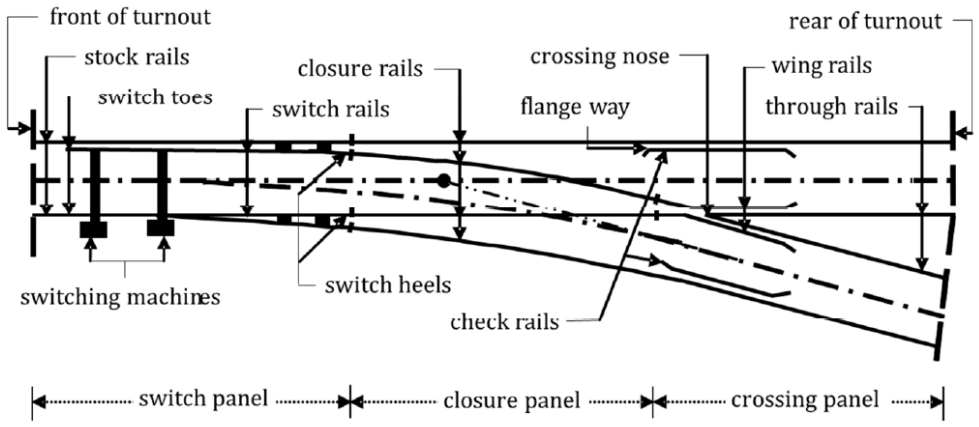

Figure 1.2.1 Schematic illustration of a turnout (S&C) and its components

The costs for S&C are high as they constitute a key component in railway systems all over the world and consume large capital resources for their construction and maintenance. Turnouts stand for a

considerable contribution to reported track faults. In Sweden there are over 12 000 turnouts in some 17 000 km of track [1.1], and the cost for turnout operation and maintenance was 250 – 300 MSEK per year in 2001 to 2004 [1.2]. In the EC FP6 sponsored European project INNOTRACK [1.3], LCC models were used to find cost drivers for S&C and to study the cost benefits of innovative solutions. Within INNOTRACK, Deutsche Bahn (DB) analysed a set of 458 turnouts on a high-speed line with a mixed traffic volume of about 17.5 mega gross tonnes (MGT) per year [1.4]. It was concluded that 50% of the overall costs were for inspection, service and test measures. Out of the remaining costs it was found that renewal of switch rails, crossings and large elements such as check rails stood for 65% of the costs while other maintenance activities such as welding and tamping constituted the remainder of the costs. With such a large contribution to the overall costs, it was quite naturally found that optimized components such as switch rails and crossings with a longer service life can help to reduce the life cycle costs for turnouts [1.3].

1.2 REFERENCES

[1.1] A. Nissen, *Development of life cycle cost model and analyses for railway switches and crossings*, PhD Thesis, Division of Operation and Maintenance Engineering, Luleå University of Technology, Luleå, 2009

[1.2] A. Nissen, *Analys av statistik om spårväxlars underhållsbehov (analysis of statistics of maintenance requirements for railway turnouts, in Swedish)*, Licentiate Thesis, Division of Operation and Maintenance Engineering, Luleå University of Technology Luleå, 2005

[1.3] A. Ekberg, and B. Paulsson (eds.), *INNOTRACK: Concluding technical report*, International Union of Railways (UIC), Paris, 2010, 288 pp

[1.4] W. Grönlund, and G. Baumann (eds.), *INNOTRACK: D3.1.1/D3.1.2 Definition of key parameters and Report on cost-drivers for goal-directed innovation*, www.innotrack.net, 2008, 37 pp

2 Objectives

The objectives of WP1.3 in Capacity4Rail are to:

- Identify current and future operational failure modes of S&Cs and related root causes (task 1.3.1). This was reported in deliverable D1.3.1.
- Propose innovative designs to minimize material deterioration and failures (task 1.3.2)
- Suggest innovative designs and operational practices to ensure resilience to extreme weather conditions and improved maintainability (task 1.3.3)
- Survey optimized maintenance and sensor strategies (task 1.3.4)
- Perform in-field demonstration of key concepts (task 1.3.5). This work is not covered in separate reports.

Part of this report (deliverable D13.3) is presenting the work performed in task 1.3.2 aiming towards an optimisation of the design of S&C. It is focused on the understanding of dynamic wheel-rail interaction in S&C and on how the rail degradation can be reduced by optimisation of geometrical and stiffness properties of the track superstructure, such as the design of rail profiles and the selection of stiffness of resilient elements (rail pads, base plate pads, under sleeper pads). The influence of rail grade selection and the introduction of friction management in the wheel-rail interface is also covered. The objective is to reduce rail degradation by improved wheel-rail contact conditions leading to a reduction of wheel-rail contact forces (stresses) and creepages. Reduced rail degradation rates will reduce the Life Cycle Cost (LCC) for turnouts.

Further, this report surveys problems occurring with S&C in extreme weather conditions (warm and cold climate, flooding) and suggests remedial actions.

3 Innovative designs minimizing S&C loads and material deterioration (C4R task 1.3.2)

Capacity4Rail WP1.3 aims to provide for a drastic improvement in S&C design and operations. To a successful end, the strategy outlined incorporates short-term objectives in improving current S&Cs, a medium term strategy where improved solutions are incorporated in an existing railway system and a long-term vision where radically new solutions can be introduced without a need for compromising with existing structures. The WP focuses on medium/long distance mixed traffic. However, the design framework developed in the task can be applied to other operational scenarios, e.g. very high speed and in spin-off projects.

This chapter covers work performed in Capacity4Rail task 1.3.2. Short-term design solutions, with particular focus on the switch panel, have been studied by Chalmers and are presented in Section 3.1. Medium-term design solutions, with focus on the crossing panel, have been the focus of the work by University of Huddersfield, see Section 3.2. Long-term design solutions are briefly described by VAE and VCSA, see Section 3.3.

References to Section 3.1 are listed in Section 3.1.8, while references to Section 3.2 are listed in Section 3.2.8.

3.1 SHORT-TERM DESIGN SOLUTIONS

In this section, focus is on short-term design solutions for mitigation of accumulated damage in the switch panel. In this part of the turnout, the combined profile of the stock and switch rail assembly results in non-smooth rolling radius difference characteristics due to contact between wheel flange and switch rail. As the rolling radius difference that can be generated is reduced (compared to for a standard rail profile), this contact condition reduces the steering capability of the wheelset leading to a magnification of the lateral wheel–rail contact force [3.1.1]. Further, the two-point contact situation with one contact point on the switch rail and one on the stock rail induces relative motion and slip between wheel and rail leading to high energy dissipation, in this section referred to as $T\gamma$ (creep force multiplied with creepage).

Examples of wear and RCF damage in the switch panel are shown in Figure 3.1.1, where severe wear is observed on the switch rail, while RCF has been generated on the crown of the stock rail. This particular RCF defect mainly occurs in the wheel transfer area from stock rail to switch rail, caused by high tangential contact stresses leading to near surface crack initiation. However, RCF damage does also occur on the switch rail. Subsequent merger of cracks leads to detachment of material (spalling). Corrective measures include grinding or replacement of the switch and stock rail assembly.

Means to mitigate the insufficient rolling radius difference and improve the contact conditions include prescribed track gauge widening and optimisation of switch rail profiles [3.1.3, 3.1.4]. For example, it

has been shown that a variation of prescribed track gauge widening along the switch panel is efficient in the through route and improves the situation in the diverging route. Optimisation of switch rail profile to allow for an earlier full transition from stock rail to switch rail (facing move) is particularly efficient in the diverging route. However, limits on switch rail loading need to be established to determine the feasible design space. Combining the two measures can be an effective solution for reduced damage because the track gauge widening makes it possible to increase the thickness and strength of the front section of the switch rail.

Thus, short-term design solutions for minimising loads and rail profile degradation in the switch panel include (1) prescribed track gauge widening and (2) rail profile optimisation (also considering rail inclination). Other short-term solutions include (3) different rail grades and (4) friction management. Based on numerical simulations, solutions (2), (3) and (4) will be studied in this section.

Section 3.1 has been written by Chalmers, except Section 3.1.1 which has been written by INECO.

Figure 3.1.1 Wear on the switch rail and RCF on the stock rail caused by high tangential contact stresses. From [3.1.2]

3.1.1 In situ measurement of profile damage of the switch rails

3.1.1.1 Background

The acquisition of real data from railway lines in service is a valuable work that helps to understand the wearing processes of the components in a turnout. The periodical inspections of the track superstructure, i.e. rail condition, track geometry, S&C performance, etc. are complemented with rolling stock inspections and the conditions of traffic operation. Correct management of all this information leads to a better understanding of the ageing and degradation processes of turnout components.

In some situations, it may be very interesting to select an S&C in the network where particular defects are recurrent or are showing at an early stage. More intense inspections can be done to monitor the evolution of these defects, and the data can be combined with the information from the rolling stock side (wheel profile condition, number of MGT, intensity of traffic, etc.). The implementation of all sources of information gives clues of the causes of a particular defect, e.g. the excessive damage of a stock rail after a relatively short time in track.

However, taking this information to the research projects related with the study of damage in particular parts of S&Cs is also very important. It definitely helps to fit the results of the laboratory models to the real conditions of a turnout in operation. Reciprocally, railway maintenance staff can be advised on the future condition of track elements and plan actions to prevent some defects reaching a critical level.

3.1.1.2 Procedure for measurements in an S&C

In order to apply the methodology explained in the background, an S&C has been selected out of all turnouts of a particular metropolitan network. Measuring on this type of railway systems has some advantages:

- Traffic parameters are known and constant (mass, frequency, axles, …)
- Rolling stock is almost mono-type
- Wheel profiles are homogeneous and easy to measure
- Turnouts are operated in the same position and direction at most of cases (except in manoeuvring, redirecting to depots, etc.)
- Maintenance protocols and actions are mostly periodical and well reported

A full inspection of the turnout components has been performed, which includes the following aspects:

- Geometry (track gauge, inclination, alignment, safety parameters, …)
- Coupling of the switch rail
- Sitting of the switch rail on the slide baseplates
- Curving of the switch rail in the diverging route

- Proper work of the locking system
- Condition of the crossing
- Presence of damage (wear or any other rail defect)
- Measurement of the rail profile at several locations

Figure 3.1.2 shows a general view of the selected S&C. The turnout characteristics are diverging curvature 154 metres and tangent 1:8.5. Manufactured in rail 54E1 with an inclination 1:20 on straight route and vertical on the switch part.

Figure 3.1.2 Photo of selected S&C

3.1.1.3 STUDY OF DEFECTS

In this study, the aim is to detect the causes for excessive damage on the left-side switch rail and stock rail when both rails are coupled in diverging track, see Figure 3.1.3. Besides, on the right-side stock rail there is a noticeable vertical wear, see Figure 3.1.4. On this stock rail, there is also a plastic deformation on the gauge corner at the field side, see Figure 3.1.5. This premature damage has been noticed in several S&C that are installed in the same line, so it is important to detect the causes and set actions to prevent the defect to damage a large number of turnouts. There is an irregular running surface along the switch rails and a notable wearing from the corner gauge to the top of the coupled stock rail. Thus, the profile of both rails has been carefully measured during the inspection.

Figure 3.1.3 View of coupled switch rail and stock rail (allowing for diverging track)

Figure 3.1.4 Stock rail on the right side. When uncoupled, it allows for traffic to diverging track

Figure 3.1.5 Stock rail on the right side. View of the field side seen from the switch toe

3.1.1.4 RAIL PROFILE MEASUREMENT

The transverse profiles of the switch rail and stock rails have been measured by using the Miniprof tool. Specific measurements have been performed on each set of switch rail and stock rail at 200 mm and at 1000 mm from the toe of the swith rail. The results are reported in the following template, see Figure 3.1.6.

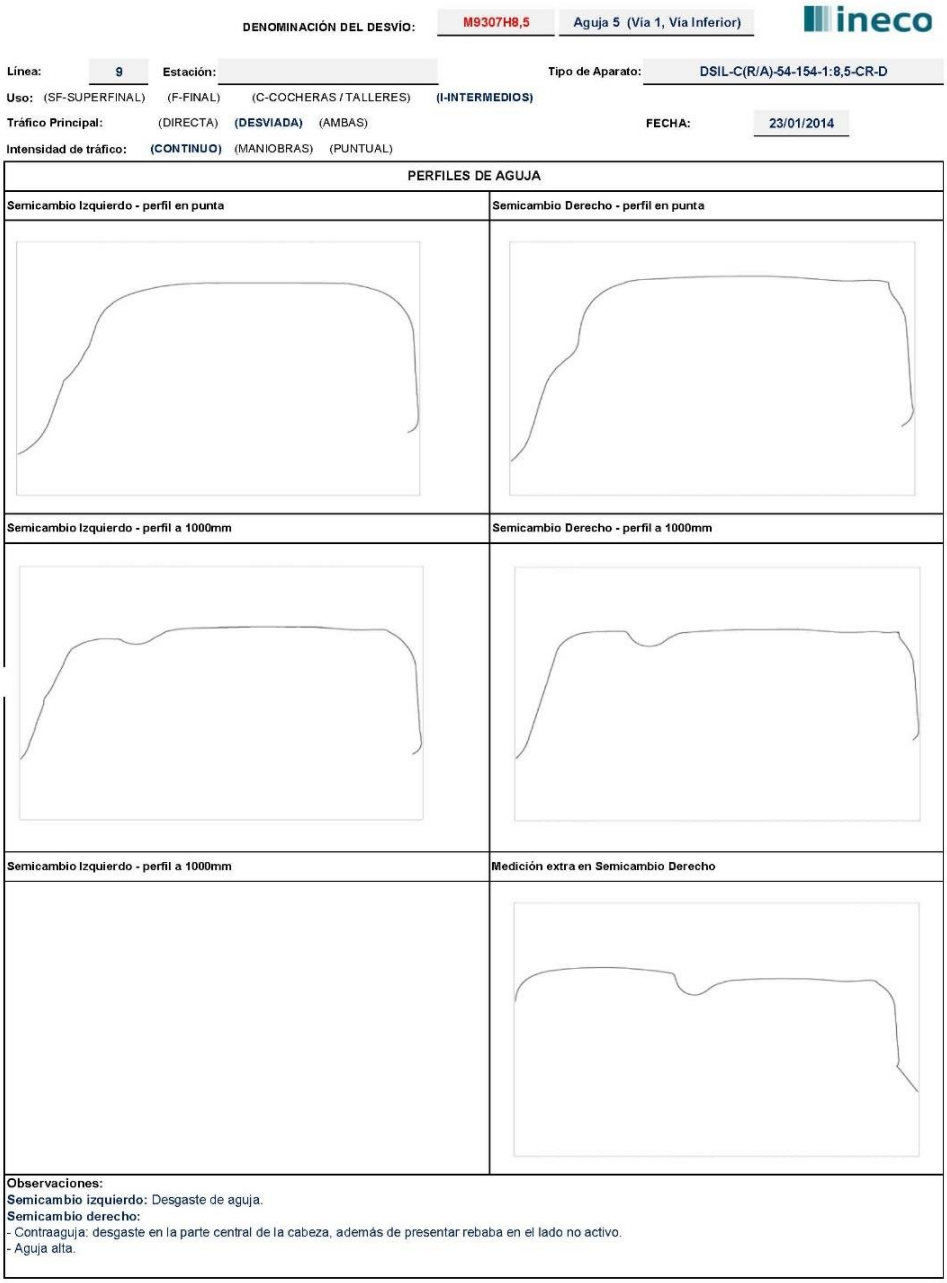

Figure 3.1.6 Graphic reporting. Left column shows profiles of the left hand side rails at (from top down) 200 mm and 1000 mm. Right column shows profiles of the right hand side rails at (from top down) 200 mm, 1000 mm and 1600 mm

3.1.1.5 WHEEL PROFILE MEASUREMENT

In order to have good information about the interaction between the switch rails and the wheels of the rolling stock, several measurements of wheel profile for the trainsets in operation have been performed, see Figure 3.1.17. As the type of trains are similar and all of them work in the same conditions, this information helps greatly in the understanding of the damages observed.

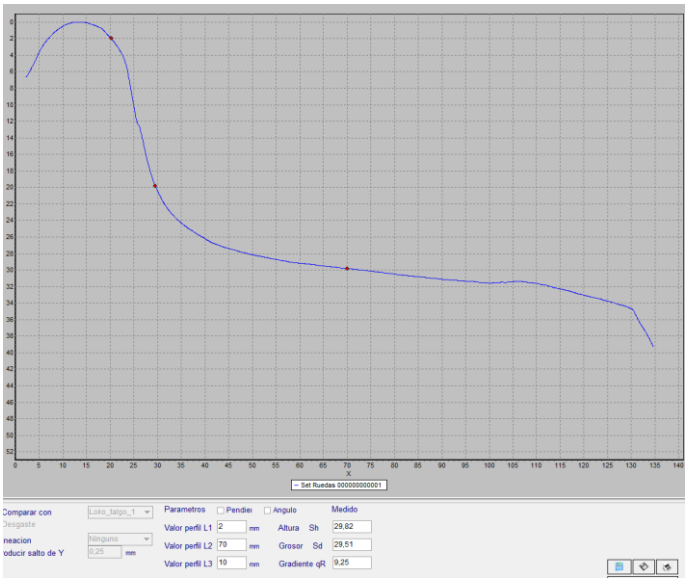

Figure 3.1.7 Measurement of wheel profile

3.1.1.6 TRAFFIC CONDITIONS

- Type of traffic: there is an intense traffic, one trainset every 4 min. Most trains run in the diverging route.
- Type of trains: Trainset series 9000, 5 coaches, 20 axles, axle payload: 10 t.
- Annual tonnage (estimated) = 12.4 MGT per year.

3.1.1.7 POSTPROCESSING OF THE PROFILE MEASUREMENTS

The combination of the real profile and the original one (as designed) is done in order to detect any distortion of shape, excessive wearing, etc. In this case, the damage observed is caused by an irregular wheel/rail interaction, which causes diverse defects.

The thickness of material removed from the running surface of the switch rails is calculated from the graphic results, see examples in Figures 3.1.8 – 3.1.10.

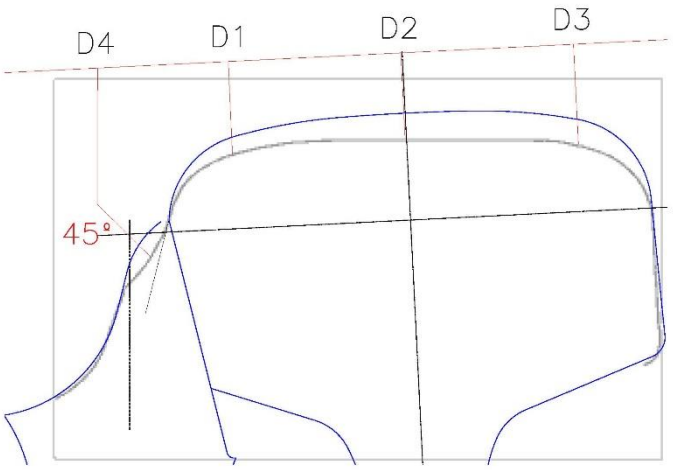

Switch rail	Stock rail		
D4 [mm]	D1 [mm]	D2 [mm]	D3 [mm]
3.265	3.13	4.7	4.53

Figure 3.1.8 Combination of profiles at 200 mm from the beginning of the switch rail (switch rail and stock rail coupled). Blue is new rail and grey is measured rail. The matching point is the down gauge corner of the field side, then the worn profile is adapted to the nominal inclination. Results of thickness of material removed

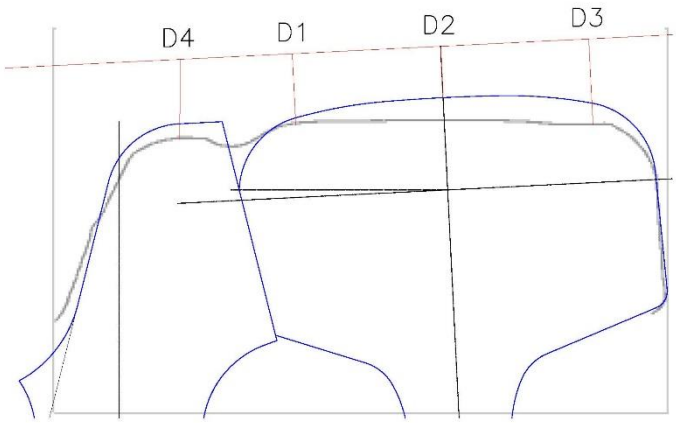

Switch rail	Stock rail		
D4 [mm]	D1 [mm]	D2 [mm]	D3 [mm]
3.33	1.575	4.795	4.585

Figure 3.1.9 Combination of profiles at the 1000 mm from the beginning of the switch rail (switch rail and stock rail coupled). Results of thickness of material removed. See also caption to Figure 3.1.8

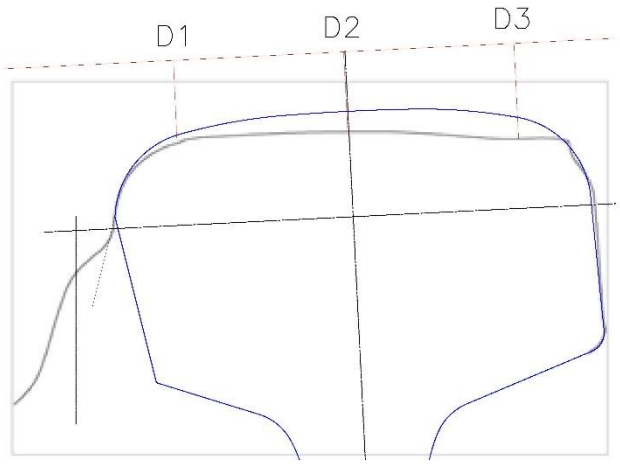

Switch rail	Stock rail		
D4 [mm]	D1 [mm]	D2 [mm]	D3 [mm]
-	1.095	3.48	3.875

Figure 3.1.10 Combination of profiles at the beginning of the right stock rail 200 mm from the switch rail toe (as reference). Results of thickness of material removed. See also caption to Figure 3.1.8

3.1.1.8 COMMENTS TO THE MEASUREMENT PROCEDURE

The methodology for the acquisition of data from S&C in operation and the processing of this information to analyse the damage due to wheel/rail interaction is useful from the point of view of the treatment of particular defects on the rails in an S&C. In a further study, it may be useful to study the influence of tonnage and type of traffic on accumulated wear. Eventually the results can be applied to validate the developed models to simulate damage and improve designs.

It is observed that the combination of the theoretical switch profile and the measured profile is sometimes difficult due to shape of the running surface after some time in operation. There are some defects, i.e. plastic deformations or abnormal wear, which makes an accurate matching difficult. Therefore, an accurate procedure for matching both images is necessary and even more so when there is a need to measure thin layers of removed material.

It is also observed that a poor condition of the wheel profile – on an average basis – is detrimental as it creates damage in areas where the wheel/rail contact is not expected. Nonetheless, the geometry of the S&C and the proper coupling of the switch rail and sitting to the slide base plates is determinant for the occurrence of premature damages.

3.1.2 METHODOLOGY FOR NUMERICAL PREDICTION OF ACCUMULATED RAIL DAMAGE

A brief overview and description of the methodology applied by Chalmers in numerical prediction of accumulated rail damage (wear and RCF) is given below. Further details can be found in [3.1.5].

Two different wear regimes, mild and severe wear, in terms of wear rate and characteristics of wear debris were identified in [3.1.6]. Different parts of the rail profile may be subjected to different wear regimes, the wear rate at the gauge corner being up to ten times higher than on the rail crown [3.1.7]. This can be accounted for in a prediction model by implementing a wear map where the wear coefficient in the wear model is dependent on normal contact pressure p_z and sliding velocity **s** [3.1.8], see also Section 3.1.4.

Two models for evaluation of rail wear have been applied in this study. Model A (often referred to as the *Tγ* method) is based on the calculated energy dissipation given by the summed products of force and corresponding creepage in each wheel–rail contact. For each wheel *i* passing through the switch panel on the side where the wheel transfers from stock rail to switch rail (the damage on the opposite rail is not considered here as it is significantly lower) and each evaluated instant in time, the energy dissipation W_i is calculated by summing the work in up to two considered contact points/patches (j=1, 2) as

$$W_i = \sum_{j=1}^{2} T_{x,j}\gamma_{x,j} + T_{y,j}\gamma_{y,j} \tag{1}$$

where T_x and T_y are the tangential contact forces in the contact plane, and γ_x and γ_y are the associated creepages (note that the contribution due to spin has been dropped here). From the output of each simulation of dynamic vehicle-track interaction, the energy dissipation at N_i discrete time steps is assembled in the vector $\mathbf{W}_i$ ($N_i \times 1$), collecting data for the most loaded front section of the switch and stock rail assembly, see [3.1.3]. For each wheel passage, a scalar damage value D_i^{w} ('w' for wear) is then evaluated as

$$D_i^{\mathrm{w}} = \frac{\sqrt{\mathbf{W}_i^{\mathrm{T}}\mathbf{W}_i}}{N_i} \tag{2}$$

The vector norm of the damage value is used to obtain a weighted average of the total friction work, thus indicating the total material removal, while providing a penalty to high local values. Model A allows for a fast assessment of the influence of switch panel geometry on damage over the switch panel as it requires no further post-processing of the output from GENSYS.

Model B applies the Archard model of sliding wear. The distributions of contact stress and sliding distance are determined from a FASTSIM discretisation of the contact area. According to the Archard wear model, the volume V_{wear} of worn material is calculated as

$$V_{\text{wear}} = k_{\text{w}}(p_z, s) \cdot \frac{Nd}{H} \tag{3}$$

where k_w is the non-dimensional wear coefficient given by a wear map, N is the normal contact force, d is the sliding distance and H is the hardness of the softer material. For further details about wear model B, see [3.1.5].

The development of surface initiated RCF cracks is due to accumulated plastic deformation (ratchetting) of the surface material caused by cyclic loading leading to compressive and shear stresses acting at the wheel-rail contact surface [3.1.9, 3.1.10]. Cracks are formed if the plastic deformation exceeds the fracture strain of the material. Crack growth is promoted not only due to subsequent rolling contact loading, but also due to hydro-pressurisation caused by fluid trapped in the crack.

Based on shakedown theory (assuming full slip and Hertzian wheel–rail contact conditions), an index for time-efficient prediction of rolling contact load levels resulting in ratchetting was introduced in [3.1.9] as

$$FI_{\text{surf}} = f - \frac{2\pi abk}{3N} \tag{4}$$

where f is the traction coefficient given by the ratio of resultant tangential contact force and normal contact force, while a and b are the semi-axes of the Hertzian contact patch. For rail grade R260, the yield stress in shear for the work-hardened material is taken as k = 300 MPa. Surface initiated RCF is predicted to occur if

$$FI_{\text{surf}} > 0 \tag{5}$$

Using this model, the risk for surface initiated RCF can be predicted by straight-forward assessment of output from a simulation of vehicle-track interaction. However, in an assessment of different RCF prediction models [3.1.11], it was pointed out that disadvantages of the FI_{surf} model are the assumption of full slip and that it does not consider that wear is generally the dominating type of damage at high levels of slip. High levels of wear will wear away cracks and lead to an increase of fatigue life. Wear (and plastic deformation) will also alter the contact geometry that may lead to an increase or decrease in contact stresses. More general slip conditions (partial slip) will be accounted for in this study by relating the RCF damage to the local shear stress [3.1.12].

An alternative approach to predict RCF on rails is to relate a fatigue damage index to the energy dissipation $T\gamma$ in the wheel–rail contact [3.1.13, 3.1.14]. At high levels of energy dissipation, the wear rate is higher than the crack growth resulting in no RCF damage. This is reflected in the model by a multi-linear relationship between damage index and $T\gamma$. A disadvantage of this model is that it is empirical and needs to be calibrated for different applications of rail grades and traffic conditions. Based on validation of the model versus field observations of surface initiated RCF on various curves

with rail grade R260 or R350HT, it was concluded that no RCF damage occurs for $T\gamma$ > 175 J/m and $T\gamma$ > 400 J/m, respectively, see [3.1.14]. For wheel–rail contact occurring between wheel flange and gauge side of the switch rail, it can be concluded that evaluated $T\gamma$-values generally exceed the limit values indicating that wear is the dominating damage mechanism. As this is in agreement with field observations, it is proposed here to apply the model based on shakedown theory (see Equation (4)) but to multiply the predicted damage with a penalty function $f_p(T\gamma)$ that is reflecting the damage index in [3.1.13, 3.1.14]. Thus, for all grid elements of a given contact patch, this means that there is no RCF damage if $T\gamma$ evaluated for the complete contact patch exceeds the threshold value (175 J/m for R260 and 400 J/m for R350HT). If $T\gamma$ evaluated for the complete contact patch is in the range between the maximum in the damage index function and the threshold value, the RCF damage will be scaled down by the suggested penalty function.

The model used here for prediction of accumulated damage (wear and RCF) in the switch panel is described in further detail in [3.1.5]. The model is inspired by the approach presented by Dirks et al [3.1.11, 3.1.15], where Archard's model is applied for the calculation of wear, while the shakedown approach and the empirical damage index model are compared for the calculation of RCF. It was shown that fatigue life prediction based on the two RCF models can differ, in particular in situations with severe wear such as in small radius curves. However, if wear is considered in the shakedown approach model (as is already the case in the damage index model), it was shown that the two models give comparable results. It was also concluded that the two RCF models lead to different results in cases with poor adhesion conditions (high slip) since the influence of creepage is only explicitly implemented in the damage index model. In [3.1.15], the two RCF models were extended with a computationally efficient model for propagation of short cracks. The extension leads to that two material parameters need to be determined by calibration with field measurements.

3.1.3 Influence of rail grade on wear and head check growth – review of laboratory tests and field observations

The measured influence of rail grade on wear rate and head check initiation and growth on standard (curved) track has been investigated in several references. In this section, a summary of important results and conclusions from laboratory tests (twin disk tests and wheel/rail roller rig tests) and field observations is given with particular focus on the compared performance of R260 and R350HT. The section ends with a recommendation on rail grade selection from the INNOTRACK project [3.1.16], see also [3.1.17].

Results from twin disk tests (performed by Corus) with various pearlitic rail steels are reported in [3.1.16] and are copied in Figure 3.1.11 and Figure 3.1.12. The tests show an increasing resistance to wear and RCF initiation with increasing hardness of the rail.

Twin disk tests performed at DB with different combinations of wheel and rail materials are reported in [3.1.18]. The prescribed normal contact pressure in the tests was 1250 MPa and the slip was 3%. A

drop of water was applied to the contact at 20 s intervals (wet conditions). The results are shown in Figure 3.1.13. For pairing with wheel material R7, it is observed that rail wear was increased by a factor of about 1.2 if R260 was used for the rail instead of R350HT.

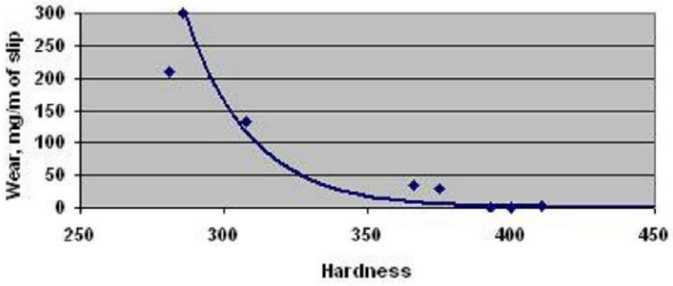

Figure 3.1.11 Influence of hardness on wear rate. Twin disk test. From [3.1.16]

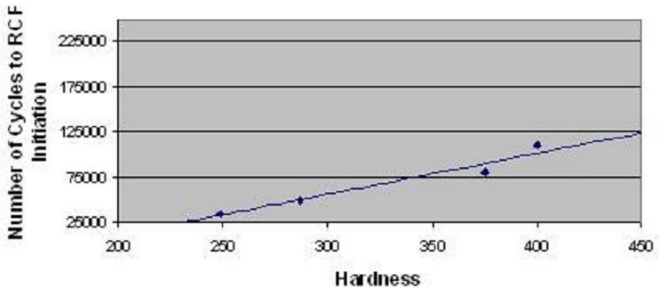

Figure 3.1.12 Influence of hardness on number of cycles to RCF initiation. Twin disk test. From [3.1.16]

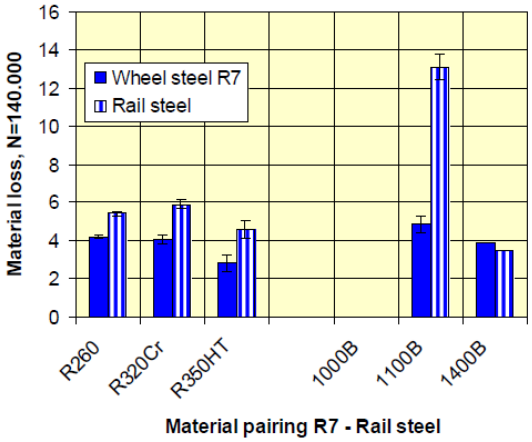

Figure 3.1.13 Influence of wheel and rail material on wear. Twin disk test (wet conditions). From [3.1.18]

Extensive laboratory tests have been performed in a full-scale wheel/rail test rig at DB Kirchmöser [3.1.19]. In this case, the applied contact forces are similar to the contact forces in a real application in the field and realistic vehicle speeds can be simulated. This means there is no need to use a scaling of contact forces and slip, which may lead to uncertain results in a twin disk test. However, note that the

laboratory tests are conducted with the same wheel profile whereas the rail in track sees a wide variety of wheel profiles and vehicles. Although the laboratory tests were successful in initiating RCF, the nature and magnitudes of the crack were different to those seen in samples taken out of track. Corus (Tata) also examined samples from the full-scale rig and the results were reported in INNOTRACK. Different combinations of rail and wheel materials were tested in dry conditions, see Figure 3.1.14. For pairing with wheel steel ER7, it is observed that rail wear was reduced by a factor of about 6 if R350HT was used instead of R260. Further, it was concluded that neither more wear nor more RCF damage was detected on either wheel or rail when using a harder contact partner.

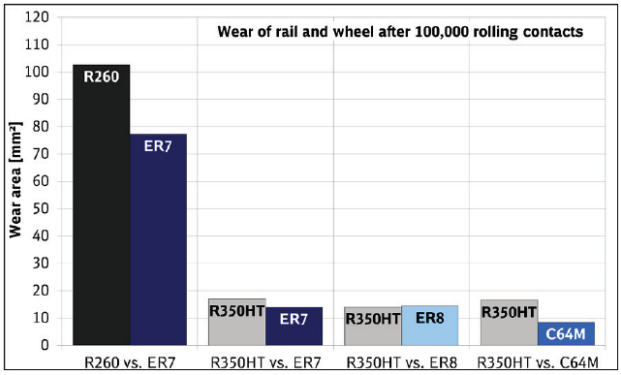

Figure 3.1.14 Wear of wheel and rail for different combinations of material (rail wear in the left columns). Full-scale wheel/rail test rig (dry conditions). From [3.1.19]

A comprehensive database containing field measurements from the years 1998-2012 has been compiled by DB [3.1.20, 3.1.21]. The database has been used to determine rates of head check growth and wear in R260 and R350HT grade rail steels, see Figure 3.1.15 and Figure 3.1.16. For R260, it was concluded that the depth of head check cracks grows at a rate of 0.8-2.8 mm/ 100 MGT, while for R350HT the growth rate is 0.1-1.2 mm/100 MGT. The database indicates no influence of curve radius on head check growth for radii in the interval 300-6000 m and no influence of cant, cant deficiency or permissible speed. Further, it was observed that head checks were avoided by using a bainitic steel. However, it should also be pointed out that three different grades of bainitic steels are available to the railways: a low carbon carbide free bainitic steel from Tata that has shown very high resistance to RCF, a high carbon heat treated bainitic steel from voestalpine whose performance has been found to be not as good as R400HT, and the final bainitic steel with a chemistry developed by DB whose performance is also believed to be good.

In curves with radius greater than 1000 m, wear rates for R260 were between 0.5 and 1.0 mm/100 MGT and between 0.2 and 0.4 mm/100 MGT for R350HT [3.1.20]. In small radius curves, wear rates increase exponentially with decreasing curve radius reaching values of several millimetres per 100 MGT of traffic. For a given curve with two different rail grades, it was found that wear rates for R260 were 1.5 – 3 times greater than for R350HT [3.1.20].

Note that it is important to differentiate between vertical wear and side wear as the mechanisms causing these two types of wear are different. Large radii curves do not suffer from side wear, whereas in tight curve radii the rail is subjected to both vertical and side wear. In tight radii curves, it is largely the magnitude of side wear that determines rail life.

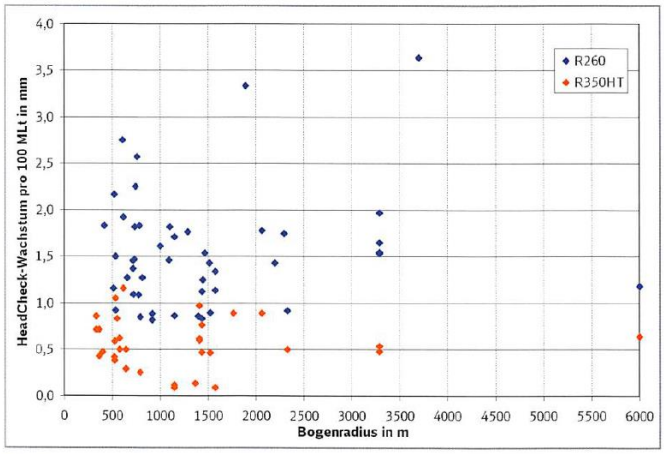

Figure 3.1.15 Influence of curve radius and rail grade on head check growth per 100 MGT. From [3.1.21]

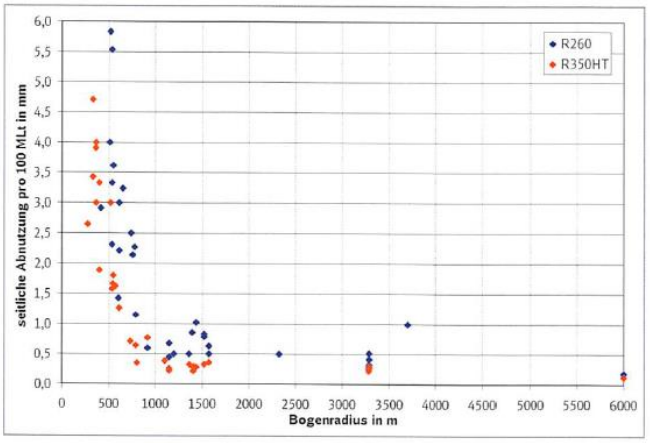

Figure 3.1.16 Influence of curve radius and rail grade on gauge corner rail wear per 100 MGT. From [3.1.21]

The database [3.1.20] also shows that modern traction units with electric power transmission and automatic traction control facilitate the formation of head checks. Homogeneous vehicle fleets tend to produce a narrow band for the wheel-rail contacts. This could be the reason for early onset of RCF observed in suburban rapid transit systems and on homogeneous high-speed lines. The combination of wheel and rail profiles has a major effect on the stresses in the wheel-rail contact patch, and the contact patch becomes smaller the closer the contact point is to the gauge corner and the smaller the gauge corner radius. In Germany since 2010, an anti-head-check (AHC) profile is used on all outer rails in curves with radius up to 3000 m. The AHC profile corresponds to the 60E2 profile with a rail

inclination 1:40 and with a radial deviation (material removal) at the gauge corner of at most -0.6 mm. It was also concluded that the stability of the wheel/rail profiles is larger when using higher-strength steels.

In a long-term field test (part of the Optikon project), DB placed eight different steel grades in a 791 m curve near Vilshofen [3.1.22]. The test curve with curve radius 791 m, 60E1 rail profile and mixed traffic conditions (maximum speed 130 km/h) was prepared by welding 15 m sections of different rail grades. Gauge corner wear and RCF were monitored during 10 years corresponding to an accumulated traffic load of 170 MGT, see Figure 3.1.17. It was concluded that the higher strength pearlitic steels resulted in less wear than R260, the factor between R260 and R350HT being about 1.8. The heat-treated pearlitic grades revealed head checks but not as deep as for R260. The three hard pearlitic R320Cr grades showed low levels of wear but head checks were not completely eliminated. The bainitic rail steels showed differences in performance. The high manganese and low carbon (1100Mn) bainitic steel showed no head checks but a high level of wear. Finally it was pointed out that the 1400Cr bainitic grade had low wear and no head checks but requires more demanding welding techniques.

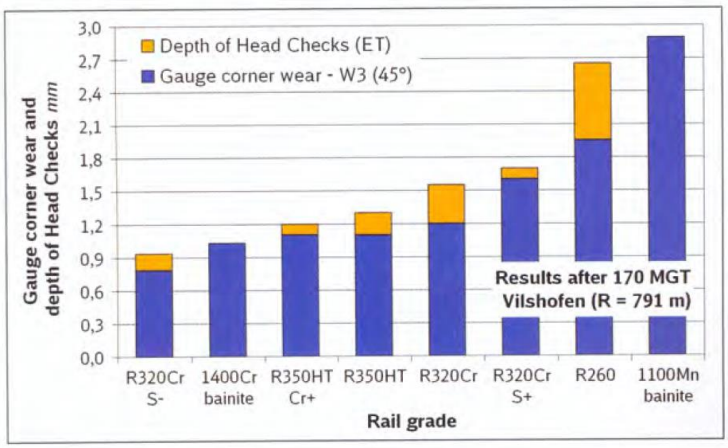

Figure 3.1.17 Influence of rail grade on gauge corner wear and depth of head checks (field conditions). From [3.1.22]

Field tests to compare the performance of R260 and R350HT have also been reported in [3.1.23]. It was concluded that for a medium-speed track with curve radius 3300 m, the wear of the R260 rail was about 1.6 times higher than for R350HT. For a high-speed tangent track and curve with radius 6000 m, the corresponding factors were about 1.6 and 1.4, respectively.

Based on track data collected by Corus and voestalpine in the INNOTRACK project, it was found that gauge corner (45°) wear is significantly dependent on curve radius with higher wear occurring on tighter radius curves [3.1.24]. It was concluded that the influence of rail grade is reduced wear in inverse proportion to the increasing hardness, with a pronounced influence for the smaller radius curves, see Figure 3.1.18. Empirical formulae for mean wear rate for three rail grades are given in Figure 3.1.18. No formula could be determined for R350HT due to a limited number of test sites with

this rail grade. It should also be noted that there is a significant scatter in the data and that there are many unknown/uncontrolled variables that could have affected the measured wear rates resulting in the observed scatter of results.

A guideline for selection of rail grade for standard track leading to improved durability and reduced need for maintenance was one of the key results of the INNOTRACK project [3.1.16]. The guideline is based on various laboratory and field (track) tests, many of them being referred to above. For given applications, recommendations of different rail grades are provided, either in terms of curve radius and tonnage or based on accepted track degradation (wear rate and head check crack depth rate). The recommended use of a range of rail steel grades for different applications (curve radius and tonnage) is shown in Figure 3.1.19. In INNOTRACK, it was concluded that the use of heat treated rail grades, such as R350HT, to reduce both wear and RCF is beneficial for curves with radius up to 3000 m.

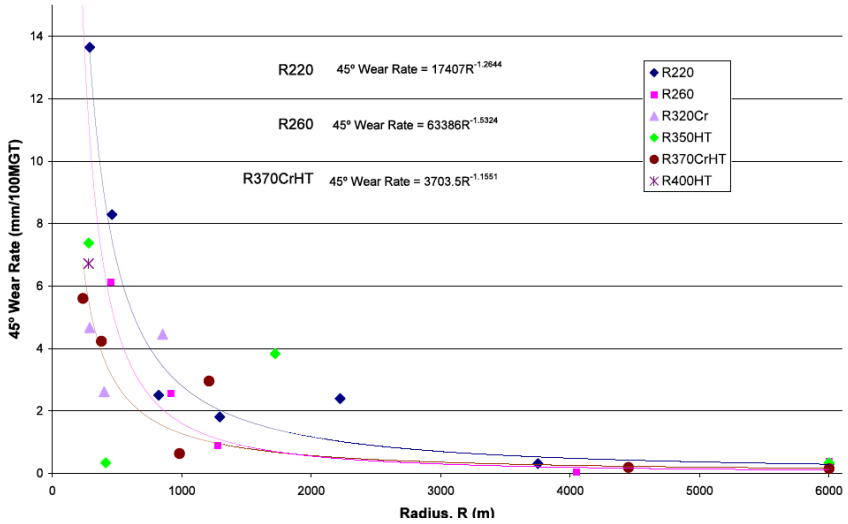

Figure 3.1.18 Influence of curve radius and rail grade on gauge corner (45°) wear rate. From [3.1.16]

According to [3.1.16], wear is dominant in curves with radius less than 1000 m, while RCF occurs for radii in the range 500 to 5000 m. Increasing hardness of pearlitic rail steels leads to higher resistance to both wear and RCF, where the improvement in terms of wear for R350HT relative to R260 is in the order of a factor 3 (and higher for small radius curves), and at least a factor 2 for RCF.

Wear and RCF initiation are influenced by the conditions (contact stresses) in the wheel-rail contacts. The contact stresses are determined by the normal and tangential contact forces, the combination of wheel/rail profiles and the size of the contact patch. This means that conditions in a curve of a standard track and subsequent rail damage cannot be directly translated to the conditions in a switch panel.

Unfortunately, official documents reporting results from field studies of influence of material in a switch panel have not been found. However, for a given S&C geometry and tonnage, the expected

improvement in terms of wear has been stated to be in the order of a factor 2 when using switch rails manufactured with rail grade R350HT instead of R260 [3.1.25]. For a switch panel with curve radius smaller than 300 m, the expected improvement is higher than a factor 2. However, it should also be emphasised that the harshness of contact conditions can vary very considerably from one S&C unit to another and hence comparative evaluation of different rail grades becomes more challenging.

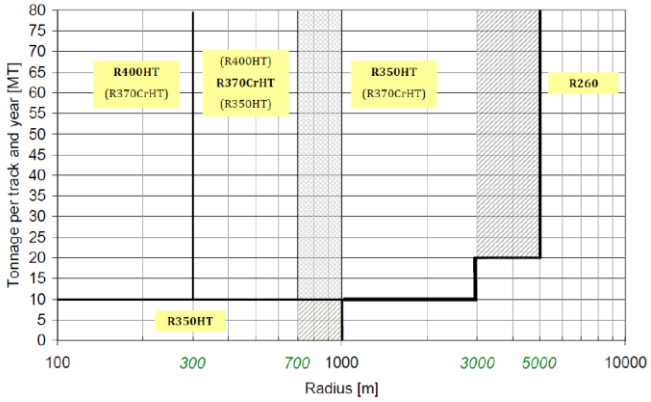

Figure 3.1.19 INNOTRACK recommendation on rail grade selection. From [3.1.16]

3.1.4 Input data to damage models – focus on R260 and R350HT

The concept of wear maps was introduced by Lim and Ashby [3.1.26] to classify the influence of different dry wear mechanisms (delamination, mild and severe oxidation, melting, seizure, etc.) on wear data. Based on pin-on-disk and twin disc tests (dry conditions), wear coefficient maps for different wheel/rail material combinations were derived in [3.1.27]. The results showed that wear coefficient is dependent on sliding velocity and contact pressure. This agrees with observations from a curve at Älvsjö in Sweden, where wear measured at the rail gauge (high sliding velocity) was six times higher than on the rail head (low sliding velocity). In a pin-on-disc test, the wear rate in the so-called catastrophic wear regime was four times higher than in the mild regime. The wear rates measured in the field test were lower than in the laboratory due to differences in environmental control between the two tests (humidity, presence of biological material). Further, it was concluded that wear rates for R8T and R260 are similar to those for R7 and R260.

Thus, wear maps allow for the contributions of sliding velocity and contact pressure to the wear rate to be isolated and give an understanding of where transitions occur between acceptable and more severe wear conditions [3.1.27]. Wear maps for different wheel/rail material combinations have shown that there is a clear difference in wear rates in the severe wear regime. For example, comparing standard carbon rail material with R260, rail wear rates were reduced by an order of magnitude by using the latter material. In the mild wear regime, however, it was hard to distinguish any difference in wear rate between different material combinations. Note that, at present, available data required

to set up detailed wear maps is very limited (in particular for combinations of high contact pressure and high sliding velocity and for materials other than R260). This calls for further measurements to increase understanding of the influence of material on wear coefficient and to extend the usefulness of wear maps and wear models.

A wear map for R260 is shown in Figure 3.1.20[3.1.28]. Based on these measurements, a wear map was set up by Jendel [3.1.29], see Figure 3.1.21. The horizontal line is indicating the so-called seizure limit according to the original wear map suggested by Lim and Ashby [3.1.26]. This limit can be estimated by Tabor's equation [3.1.26] and is dependent on hardness and friction coefficient. The wear map in Figure 3.1.21 has been used as input in this study for predicting wear in switch panels with R260 rail grade. To account for the influence of field conditions (weather, contamination, lubrication, etc), all wear coefficients have been scaled down by a factor 5.5, see [3.1.29].

Unfortunately, data for R350HT are very scarce. However, according to [3.1.30] and based on two twin disc tests with one combination of contact pressure (1500 MPa) and sliding velocity (0.01 m/s, slip 1%), the Archard wear coefficient for R8T/R260 is about 8 times higher than for R8T/R350HT. The wear map in Figure 3.1.21 has been used also for predicting wear in switch panels with R350HT rail grade but wear coefficients have been divided by a factor 3 (a more conservative value compared to the single test referred to above) and the seizure limit has been raised due to the higher hardness. Note that these assumptions need to be verified by future measurements.

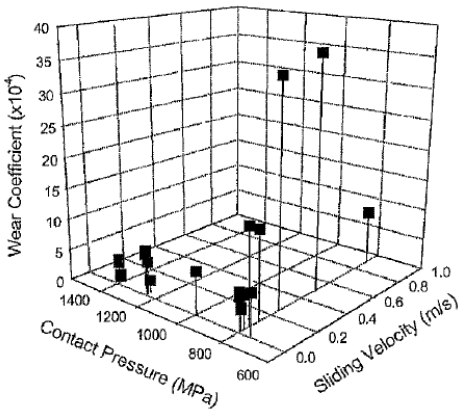

Figure 3.1.20 Wear coefficient map for wheel/rail combination R7 and R260 (dry conditions). From [3.1.28]

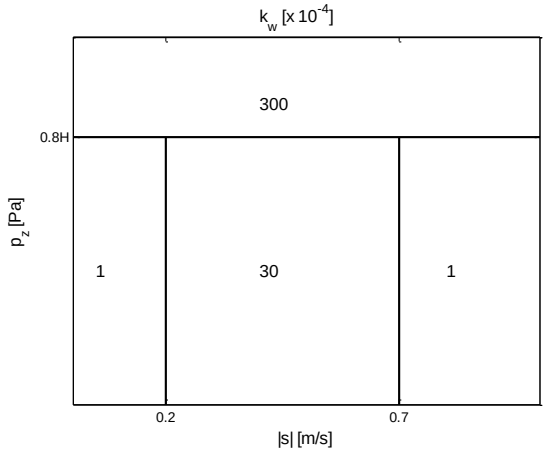

Figure 3.1.21 Map for coefficient k_w [×10^{-4}] in Archard's wear model. Based on laboratory measurements with wheel (R7) and rail (R260) steels, dry conditions, H = 3.4 GPa for run-in R260 rails (virgin material H = 2.7 GPa). For R350HT (run-in rails), it is assumed that all wear coefficients are reduced by a factor 3 and H = (350/260)*3.4 = 4.6 GPa

To predict RCF damage by the shakedown approach, the cyclic yield stress in shear k is required, see Equation (4). For rail grade R260, the yield stress in shear for work-hardened material is taken as k = 300 MPa [3.1.9].

Based on a database including laboratory measurements on 150 different non-austenitic steels, there is a linear correlation between the static yield strength in pure tension and Vickers hardness H_v, see Figure 3.1.22 [3.1.31]. This observation was used to derive a linear regression equation for the static yield strength in pure tension of non-martensitic steels.

$$\sigma_Y = -84.8 + 2.646 H_V \tag{6}$$

According to von Mises, the corresponding static yield strength in pure shear is obtained as

$$k_{stat} = \sigma_Y / \sqrt{3} \tag{7}$$

This results in k_{stat} = 370 MPa for R260 (H_V=274 GPa) and k_{stat} = 516 MPa for R350HT (H_V=370 GPa), corresponding to a ratio 1.4. Note that the static yield strength is normally higher than the cyclic yield strength.

For three levels of total strain amplitude (0.4, 0.6 and 1.0%), uniaxial, strain-controlled fatigue tests on R260 and R350HT specimens were performed in the INNOTRACK project [3.1.32, 3.1.33]. During the tests the maximum and minimum stress values were logged for each load cycle, see Figure 3.1.23 and Figure 3.1.24. For R260, stable stresses were measured at N/2 as 465, 530 and 640 MPa, respectively. For R350HT, the corresponding stresses were 650, 750 and 885 MPa. This corresponds to a consistent ratio of about 1.4, which is in agreement with the ratio from the monotonic tests. In the present study,

for R350HT the cyclic yield stress in shear is taken as k = 1.4·300 = 420 MPa. Further, (based on the data for R260 and R350HT) it is here assumed that the cyclic yield stress for other rail grades can be obtained by linear inter/extrapolation depending on the Brinell hardness. Thus,

$$k = \frac{4}{3} H_{\mathrm{B}} - 47 \quad \text{[MPa]} \tag{8}$$

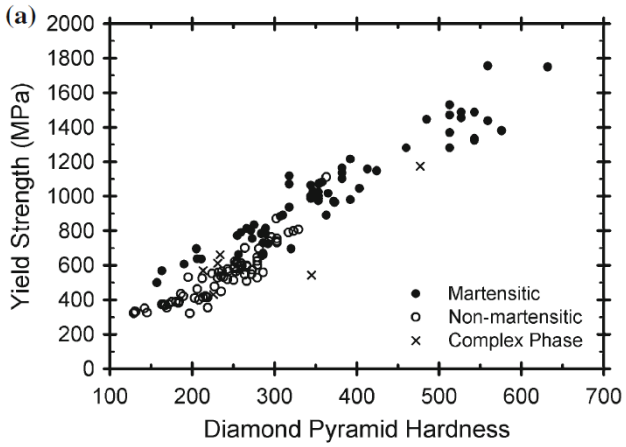

Figure 3.1.22 Influence of Vickers hardness on static yield strength in pure tension. From [3.1.31]

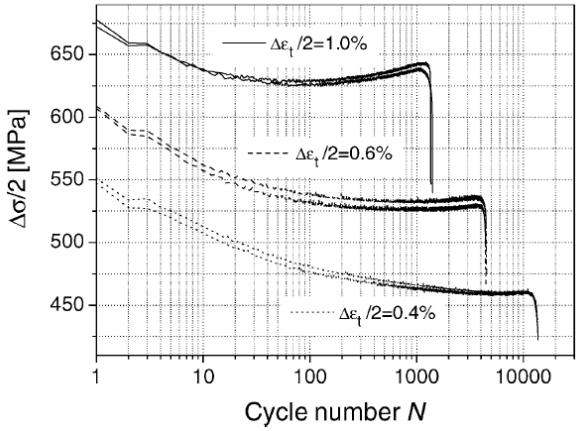

Figure 3.1.23 Stress amplitude versus cycle number in a uniaxial, strain-controlled fatigue test on rail grade R260. From [3.1.32]

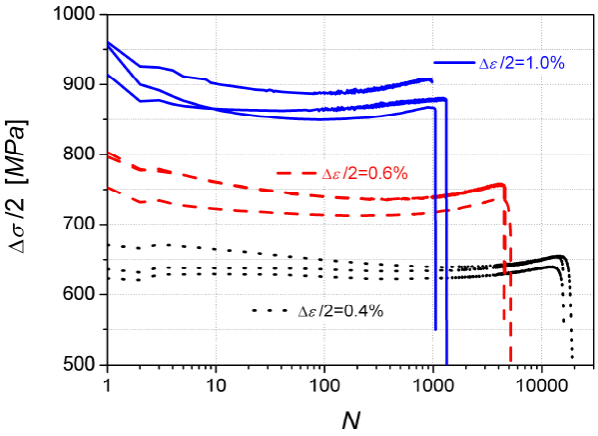

Figure 3.1.24 Stress amplitude versus cycle number in a uniaxial, strain-controlled fatigue test on rail grade R350HT. From [3.1.33]

As described in Section 3.1.2, an alternative approach to predict RCF on rails is to relate a RCF damage index to the energy dissipation *Tγ* in the wheel-rail contact (neglected influence of spin) [3.1.13]. Based on validation of this model versus field observations of surface initiated RCF on various curves with rail grade R260 or R350HT, the multi-linear damage functions in **Figure 3.1.25** were derived [3.1.14]. In this study, the model based on shakedown theory is used but the predicted damage is multiplied with a penalty function $f_p(T\gamma)$ that is reflecting the damage index in Figure 3.1.25. Thus, for all grid elements of a given contact patch, it is assumed that there is no RCF damage if *Tγ* evaluated for the complete contact patch exceeds the threshold value (175 J/m for R260 and 400 J/m for R350HT), see Figure 3.1.26. Note that the empirical functions in **Figure 3.1.25** and **Figure 3.1.26** were derived for wheel-rail contact conditions in curves and may not be representative for the wheel-rail contact conditions in a switch panel. Note that these assumptions need to be verified by future measurements.

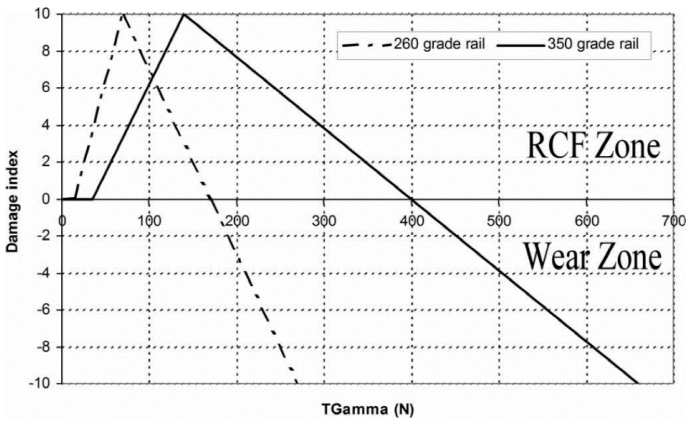

Figure 3.1.25 Empirical assessment of RCF damage index based on energy dissipation in the wheel–rail contact. From [3.1.14]

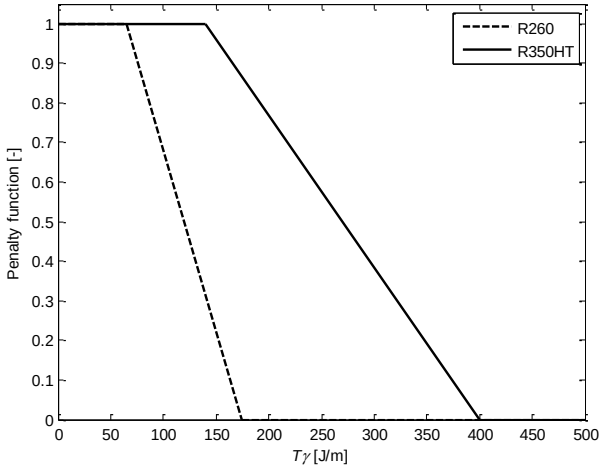

Figure 3.1.26 Penalty function applied in evaluation of surface-initiated RCF damage for rail grades R260 and R350HT

3.1.5 VEHICLE-TRACK INTERACTION MODEL

Dynamic interaction between vehicle and the switch panel of a railway turnout is studied in the time domain using the commercial software GENSYS [3.1.34]]. The vehicle model represents a freight vehicle (one car) with Y25 bogies and axle load 25 tonnes. For a detailed description of this vehicle and the simulation set-up, see [3.1.35, 3.1.36]. For traffic in the through route, the nominal vehicle speed is 100 km/h, whereas for traffic in the diverging route the speed is 70 km/h. The geometry of the nominal (reference) turnout is the standard design 60E1-760-1:15 with rail profile 60E1 (rail inclination 1:30 and a 60° chamfer milled on the front section of the switch rail), curve radius 760 m and turnout angle 1:15. In nominal configuration, the switch rails begin at 805 mm from the start of the turnout.

The track flexibility is modelled by systems of springs and dampers, with one such moving system following each wheelset. Each track model consists of two rails with neglected inertia that are attached to rigid ground by linear spring-damper elements in the lateral and vertical directions to account for the stiffness of the track. The vertical track properties used here are taken from track model TM1 in [3.1.37] with input data based on the measured track stiffness in a turnout using the rolling stiffness measurement vehicle developed by the Swedish Transport Administration (Trafikverket) [3.1.38]. The vertical track stiffness between rail and ground is 60 kN/mm and the viscous damping coefficient is 535 kNs/m. The corresponding stiffness and damping in the lateral direction were not available from these measurements but are set to 30 kN/mm and 270 kNs/m, see the discussion in [3.1.3]. The properties of the moving track models are taken as independent of the position along the switch panel. Note that this simple track representation, with neglected track inertia, should be sufficiently accurate as vehicle dynamics in the switch panel is dominated by low frequencies (< 20 Hz) [3.1.37].

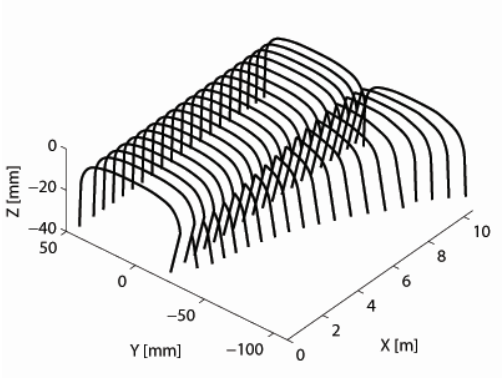

Figure 3.1.27 Switch rail assembly based on 60E1 rail profile, no rail inclination and nominal milling tool path

The manufacturing process of a switch rail is briefly described in [3.1.4]. For a given tool profile, the complete switch rail is milled from a nominal stock rail profile as determined by the prescribed vertical and lateral motion of the tool along the longitudinal milling tool path. In addition, the front part of the switch rail is milled to generate a 60° chamfer to avoid contact with the wheel flange where the switch rail is thin.

Using an in-house computer program inspired by this manufacturing process, the switch rail profile geometry is parameterised in two levels, see [3.1.4]. The milling tool profile is parameterised using a B-spline, and the vertical milling tool path for the profiling tool is parameterised by adding a deviation from the nominal profiling path. The implemented nominal design is based on drawing 9-511401 (Trafikverket), which describes a turnout with 60E1 rails with no rail inclination. However, alternative switch rail designs can also be generated by setting different parameters for the tool profile and the tool path. Based on this procedure, and for any given combination of rail profile, rail inclination and selected vertical milling tool path, the variation in rail profile in the switch panel is here represented by 68 pairs of rail cross-sections (one set of rail cross-sections per rail side). The stock rail and switch rail assembly is considered as rigid. Note that the switch rail is manufactured from a rail with the same inclination as the stock rail but the tool profile is not rotated.

One example of a generated nominal rail assembly is illustrated in Figure 3.1.27. Samples of rail profiles created by the in-house program are compared with the corresponding rail sections supplied by Vossloh Cogifer (representing the INNOTRACK turnout at Eslöv in Sweden with rail inclination 1:30) in Figure 3.1.28. Good agreement between the generated sections and the true profiles is observed (the small deviations are mainly explained by small differences in longitudinal coordinates for the Vossloh and generated profiles). This serves as a validation of the in-house program, which will be used to generate also other switch panel designs with different combinations of stock rail profile and rail inclination.

For each combination of wheel profile and rail cross-section, the wheel-rail contact geometry problem is solved in advance using the GENSYS module KPF. Based on a linear interpolation procedure between

rail sections, tabulated contact geometry functions are used in the subsequent time integration analysis. Further, each wheel-rail contact is modelled by a Hertzian spring with linearised stiffness 1500 kN/mm in the normal direction and an implementation of Kalker's simplified theory FASTSIM [3.1.39] in the tangential direction. The software accounts for the two-point contact situations occurring on the stock and switch rail assembly.

Time histories of normal and tangential forces, creepages and positions for each wheel–rail contact are calculated with a sampling frequency of 1 kHz. All results are then filtered with a low-pass (fourth-order Butterworth) filter with cut-off frequency 20 Hz before calculating the damage (wear and RCF).

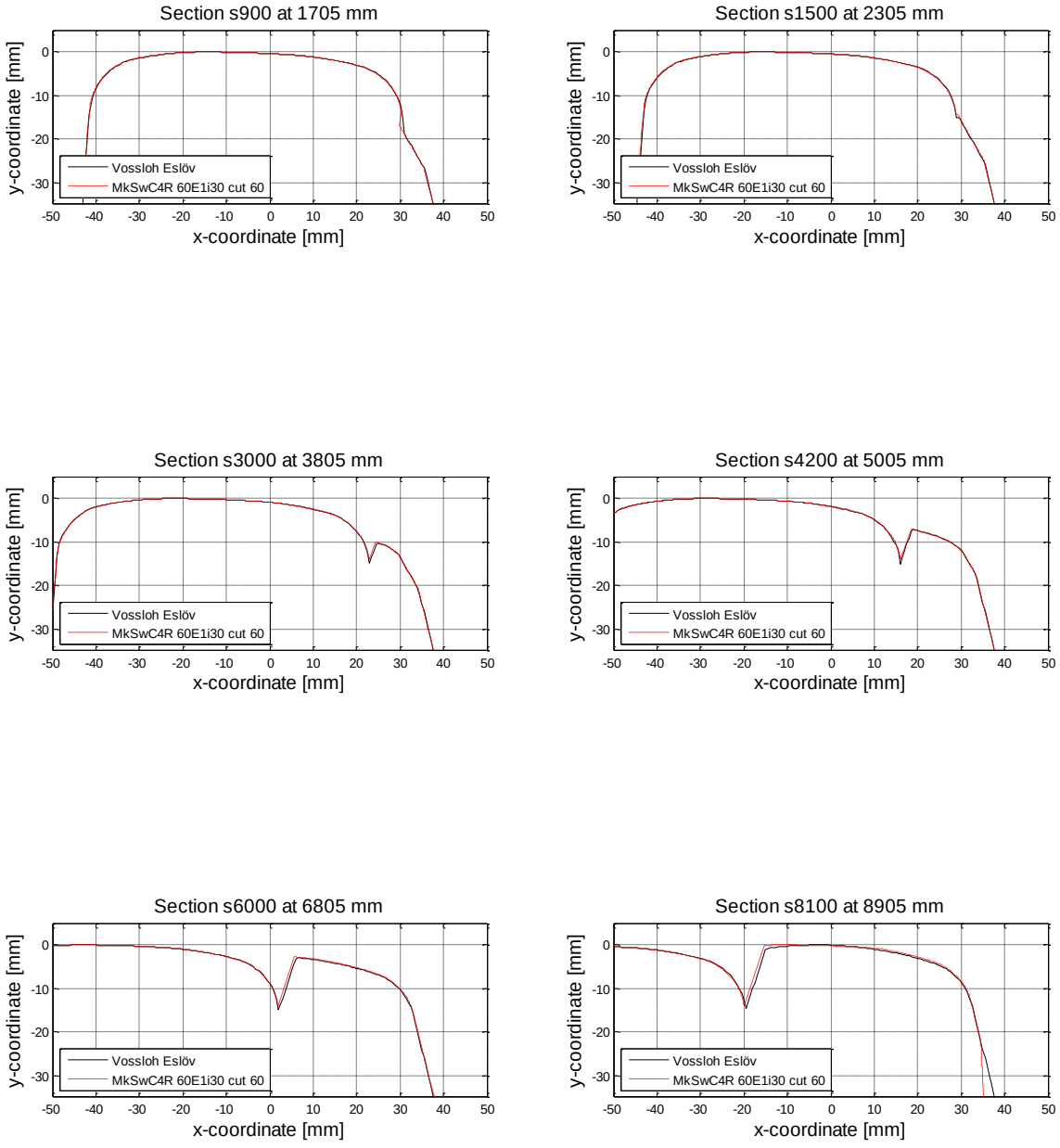

Figure 3.1.28 Samples of rail profile in the switch panel. Comparison of rail profiles generated by parameterised in-house program and rail profiles supplied by Vossloh Cogifer representing the INNOTRACK turnout at Eslöv in Sweden with 60E1 stock rail profile and rail inclination 1:30

3.1.6 SWITCH RAIL PROFILE, RAIL INCLINATION AND RAIL GRADE

The influence of switch rail profile and rail inclination on damage in the switch panel has been investigated using the model described in the previous sections. Two rail inclinations (vertical rails and 1:30) and the influence of a 60° chamfer along the front section (up to 4.98 m from the switch rail tip) of the switch rail have been studied. Examples of rail cross-sections from the three different designs used as input are compared in Figure 3.1.29.

For freight traffic in facing move of the diverging route at speed 70 km/h, and with nominal (non-worn) S1002 wheel profiles, time histories of $T\gamma$ and contact positions on the rails are illustrated in Figure 3.1.30(leading wheel in leading bogie) and Figure 3.1.31(trailing wheel in leading bogie). The shaded area indicates the range of $T\gamma$-values that according to Figure 3.1.25 corresponds to the RCF zone for rail grade R260. In particular, the horizontal dashed line within the shaded area indicates the $T\gamma$-value where there is a maximum in RCF damage. Rail inclination has a significant influence on contact position on the stock rail, see Figure 3.1.26(a) and Figure 3.1.27(a), but not for the contact position on the switch rail since the switch rail profile is the same independent of rail inclination, see Figure 3.1.26(b) and Figure 3.1.27(b). Further, it is observed in Figure 3.1.30(b) and Figure 3.1.31(b) that there is two-point wheel-rail contact for both leading and trailing wheels from about 4 m to 9 m from the front of the turnout. Thus, the full transition to the switch rail occurs at about 9 m from the front of the turnout for all the studied switch panel designs. Two-point contact occurs slightly earlier for the inclined rail (60E1i30) and in particular if there is no 60° chamfer. Very high values of $T\gamma$ (and normal contact pressure, not shown here) are generated in the contact between wheel flange and switch rail indicating that the dominating damage mechanism is wear (wear zone in Figure 3.1.25). For the contact between wheel tread and stock rail (during the situation with two-point contact), the leading wheel generates $T\gamma$-values in the upper end of the RCF zone (see Figure 3.1.30(a)), whereas the trailing wheel generates $T\gamma$-values closer to the maximum in the RCF damage function (see Figure 3.1.31(a)). Thus, for this load case, it is concluded that the maximum wear damage is generated on the switch rail due to contact with the wheel flange of both leading and trailing wheels. Further, RCF damage on the stock rail before the full transition to the switch rail is mainly generated by the trailing wheel (see Figure 3.1.31(a)), whereas the RCF damage on the switch rail after the full transition to the switch rail is generated by the leading wheel (see Figure 3.1.30(a)).

The corresponding plots for freight traffic in trailing move of the diverging route are shown in Figure 3.1.32 (leading wheel in leading bogie) and Figure 3.1.35 (trailing wheel in leading bogie). It is observed that the leading wheel is in two-point contact from about 9 m to 2 m from the front of the turnout, whereas the trailing wheel is generally only making one-point contact. The model indicates there is intermittent (irregular) contact between wheel flange and switch rail when there is a 60° chamfer, and that severe wear damage is generated (high $T\gamma$-values, see Figure 3.1.32(b)). The leading wheel generates severe RCF damage on the stock rail while there is two-point contact ($T\gamma$-values close to the maximum in the RCF damage function), see Figure 3.1.32(a). The trailing wheel generates low damage (both wear and RCF), see Figure 3.1.33.

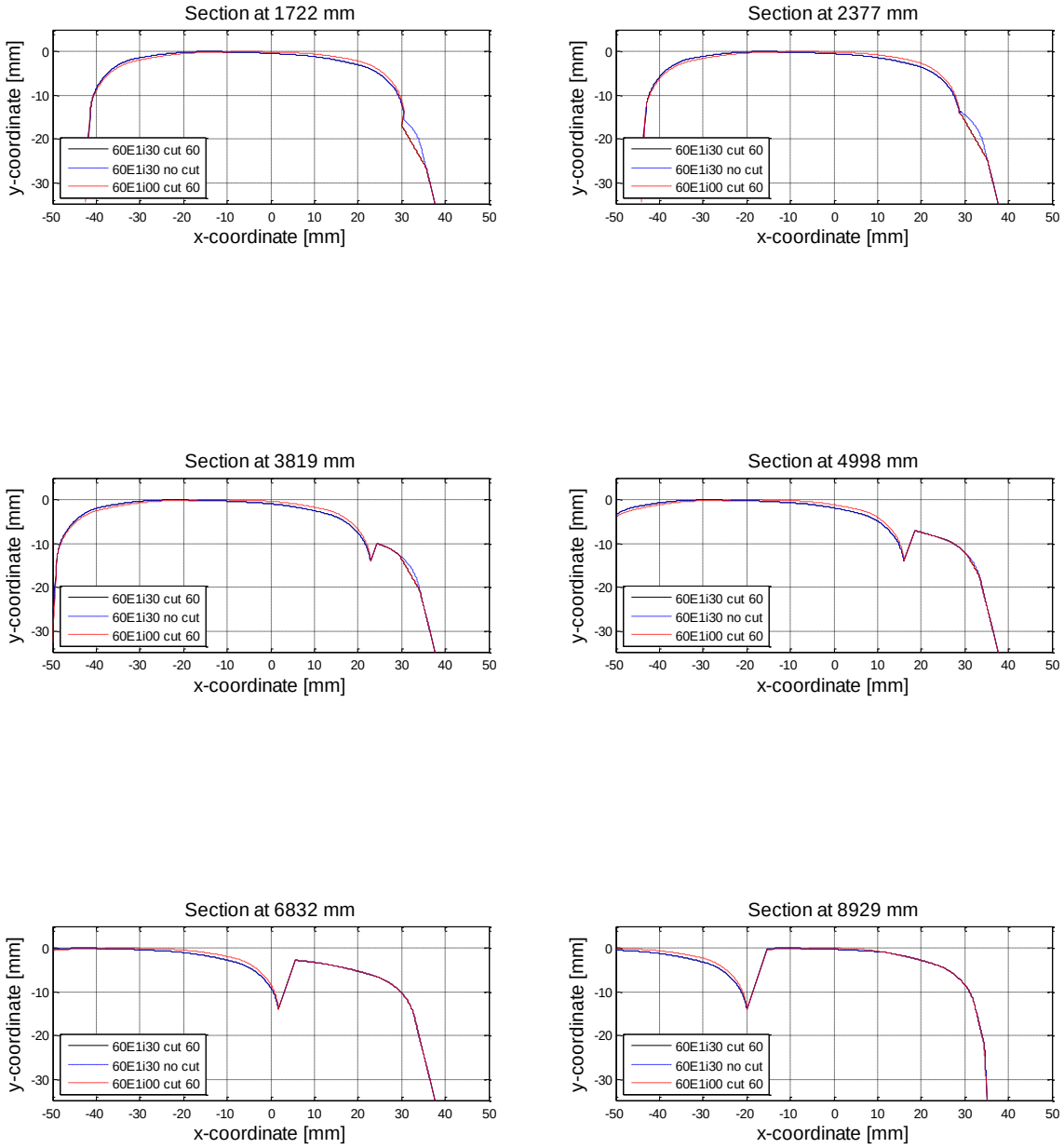

Figure 3.1.29 Samples of rail profile in the switch panel. Comparison of rail profiles generated by in-house computer program: two different rail inclinations and with or without 60° chamfer

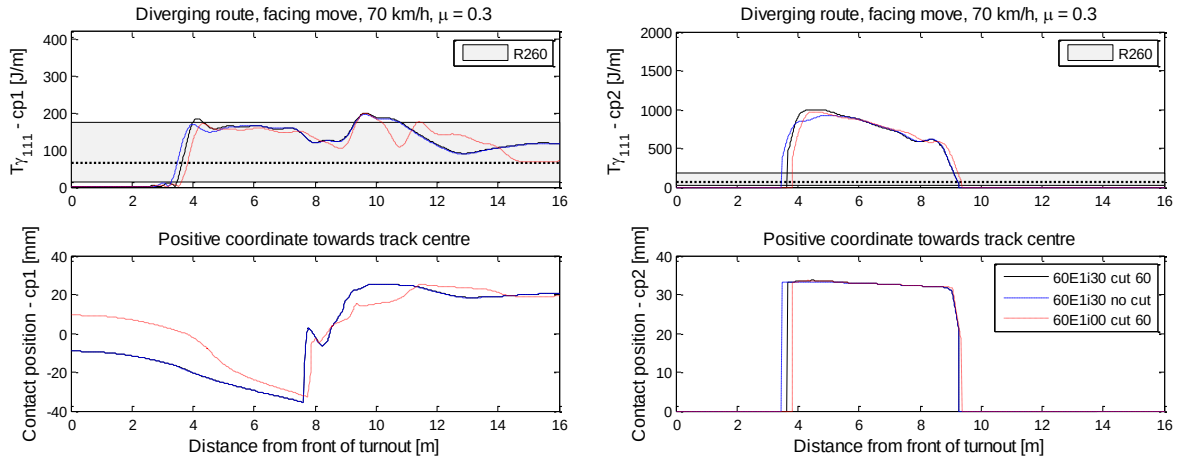

(a) (b)

Figure 3.1.30 Influence of rail inclination and 60° chamfer on damage function *Tγ* and contact position (two contact points) in diverging route. S1002 wheel profile, vehicle speed 70 km/h, friction coefficient 0.3. *Leading wheel* in leading bogie, facing move

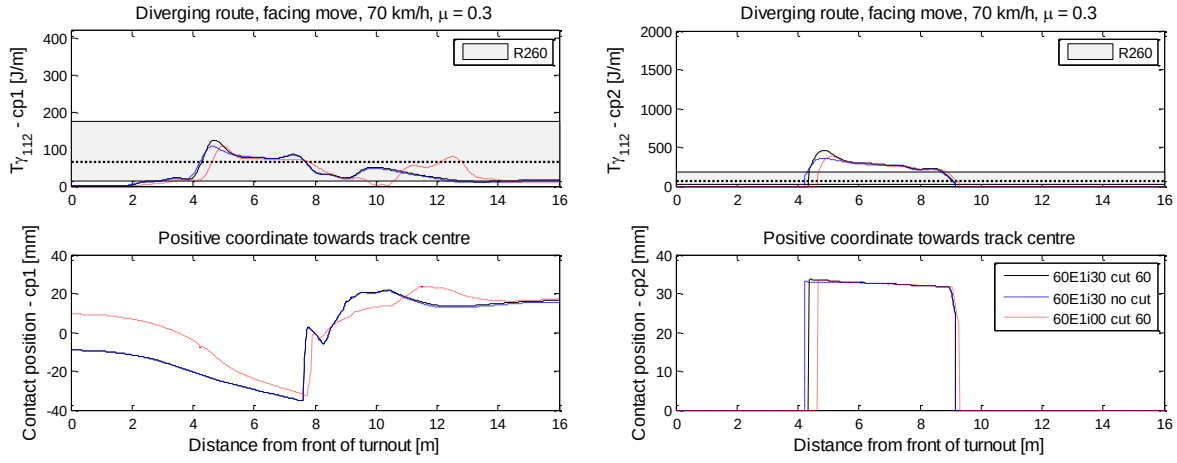

(a) (b)

Figure 3.1.31 Influence of rail profile and rail inclination on damage function *Tγ* and contact position (two contact points) in diverging route. S1002 wheel profile, vehicle speed 70 km/h, friction coefficient 0.3. *Trailing wheel* in leading bogie, facing move

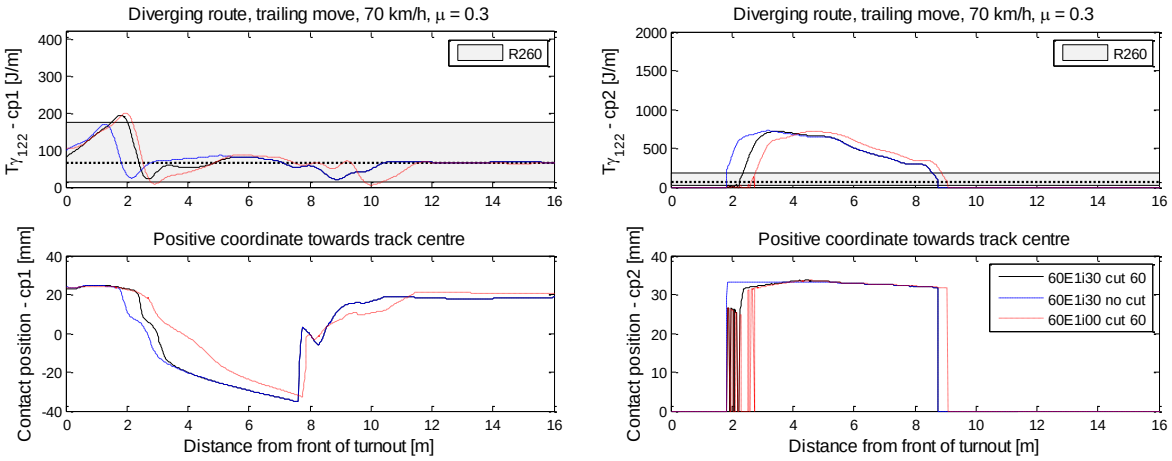

(a) (b)

Figure 3.1.32 Influence of rail profile and rail inclination on damage function *Tγ* and contact position (two contact points) in diverging route. S1002 wheel profile, vehicle speed 70 km/h, friction coefficient 0.3. *Leading wheel* in leading bogie, trailing move

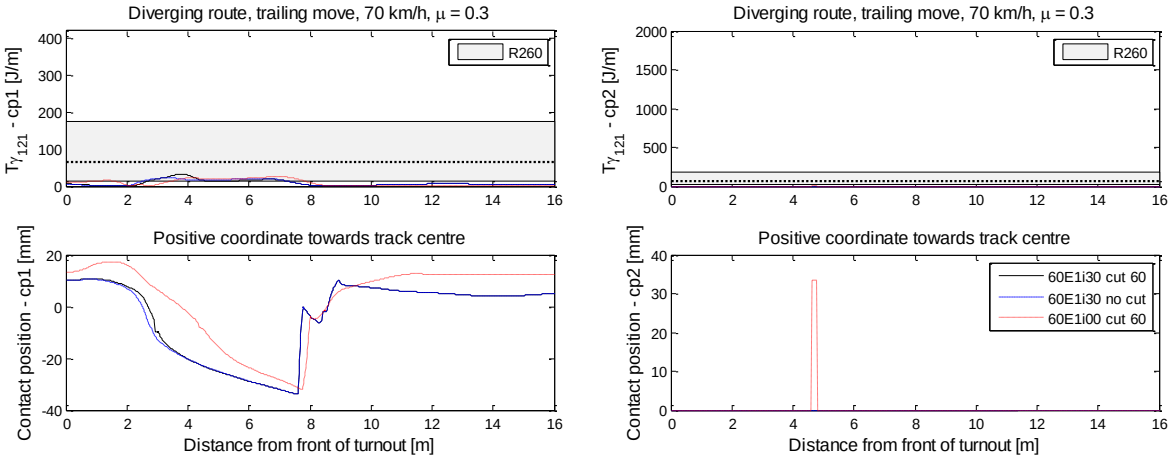

(a) (b)

Figure 3.1.33 Influence of rail profile and rail inclination on damage function *Tγ* and contact position (two contact points) in diverging route. S1002 wheel profile, vehicle speed 70 km/h, friction coefficient 0.3. *Trailing wheel* in leading bogie, trailing move

Table 3.1.1 Influence of rail profile and rail inclination on maximum accumulated wear and RCF damage for one Y25 vehicle (*four wheelsets*) in diverging route. S1002 wheel profile, vehicle speed 70 km/h, friction coefficient 0.3. Damage is normalised with respect to damage calculated for the case marked with grey colour

Rail profile	Move	Max wear [μm]	Position [m]	Max RCF damage [10^{-6}]	Position [m]	Max wear [μm]	Position [m]	Max RCF damage [10^{-6}]	Position [m]
		R260				R350HT			
60E1i30 cut 60	Facing	1	x=5.12 m y=3.33 cm	1	x=5.64 m y=3.27 cm	0.15	x=4.45 m y=3.37 cm	2.68	x=4.35 m y=3.37 cm
60E1i30 no cut	Facing	0.90	x=5.06 m y=3.31 cm	1.51	x=4.24 m y=3.31 cm	0.08	x=3.66 m y=3.33 cm	2.48	x=4.24 m y=3.31 cm
60E1i00 cut 60	Facing	1.38	x=4.73 m y=3.35 cm	3.92	x=9.60 m y=1.17 cm	0.18	x=4.67 m y=3.35 cm	3.08	x=10.96 m y=1.85 cm
60E1i30 cut 60	Trailing	1.10	x=4.06 m y=3.35 cm	1.34	x=8.66 m y=3.17 cm	0.16	x=4.06 m y=3.35 cm	1.31	x=1.01 m y=2.47 cm
60E1i30 no cut	Trailing	1.50	x=2.35 m y=3.33 cm	3.08	x=2.60 m y=3.31 cm	0.24	x=2.55 m y=3.33 cm	3.64	x=1.84 m y=2.93 cm
60E1i00 cut 60	Trailing	1.13	x=4.67 m y=3.35 cm	2.80	x=2.55 m y=1.95 cm	0.15	x=4.19 m y=3.35 cm	2.80	x=2.37 m y=2.11 cm

The calculated accumulated damage (wear and RCF) due to the passage of one vehicle (four wheelsets with nominal S1002 wheel profiles) in either facing or trailing move is summarised in Table 3.1.1. The calculated damage has been normalised with respect to the corresponding damage calculated for the inclined rail with 60° chamfer (60E1i30 cut 60) and rail grade R260 in facing move traffic (shaded area). For comparison, damage has also been calculated assuming rail grade R350HT. The positions (longitudinal coordinate measured from the front of the turnout and lateral coordinate on the rail, see Figure 3.1.29 for reference) of calculated damage maxima are also presented in the table. Based on the calculated results, the following conclusions can be made:

- Wear is significantly reduced by selecting R350HT instead of R260. This is as expected as it has been assumed that R350HT corresponds to a factor 3 lower wear coefficients and the higher hardness of R350HT raises the seizure limit in the wear map, see Figure 3.1.21.
- The maximum wear damage is generated on the side of the switch rail, typically at 4.5 – 5 m from the front of the turnout). However, for the design without the 60° chamfer the position of maximum wear in trailing move is shifted closer to the switch rail tip where the switch rail is thinner.

- The 60° chamfer leads to increased wear in the facing move.
- There seems to be no clear correlation between initiation of RCF damage and rail grade selection. Depending on rail profile design and move, RCF damage may increase or decrease when selecting R350HT instead of R260. This can be explained by the assumed penalty function, see Figure 3.1.26, which depending on rail grade scales the evaluated RCF damage. For the higher rail grade, the evaluated $T\gamma$ may be closer to the maximum in the RCF damage function.
- The inclined rail profile leads to reduced damage (both wear and RCF) compared to the vertical profile for all cases except one (wear in trailing move, R350HT).
- The 60° chamfer reduces wear and RCF damage in the trailing move.
- The rail inclination has a significant influence on the position of maximum RCF damage.

The influence of switch rail profile and rail inclination on damage in the switch panel has also been investigated for a traffic situation with a more representative selection of measured (worn) wheel profiles. Ten wheel profiles were sampled (Latin hypercube sampling) from a pool of 120 profiles measured on 120 unique and randomly selected Y25 wheelsets. To obtain the representative selection, before sampling the wheel profiles were sorted with respect to equivalent conicity $\lambda_{eq,3mm}$ as this has been shown to be the wheel profile parameter correlating best to damage in S&C [3.1.40].

The scalar damage value D_i^w (i = 1, 2, 3 and 4), see Equation (2), was evaluated for each wheel passage i and each contact point to determine which wheel profile is the most detrimental to the switch panel. Note that the damage value is a weighted average of $T\gamma$ evaluated along the switch panel (1 – 11 m from the front of the turnout). Thus, while providing a penalty to high local values, it does not necessarily indicate which wheel profile generates the maximum local damage. For traffic in facing move and for each combination of wheel profile, switch rail profile and rail inclination, the maximum value D^w evaluated for all four wheels in the vehicle model is shown in Figure 3.1.34. It was observed (not shown here) that the maximum value was always generated by the leading wheel in the leading bogie. Further, it is noted in Figure 3.1.34 that all wheels generate maximum D^w-values in the same order of magnitude although wheel profile 4 is slightly worse than the other profiles. It is observed that the influence of switch rail profile and rail inclination on D^w is moderate. The corresponding plot for traffic in trailing move is presented Figure 3.1.35. In this case, it was observed (not shown here) that the maximum value was always generated by the leading wheel in the trailing bogie.

Calculated accumulated damage (wear and RCF) due to the passage of 10 vehicles (total of 40 wheelsets and each vehicle with a different worn wheel profile) in either facing or trailing move is summarised in Table 3.1.2. Again, the calculated damage has been normalised with respect to the corresponding damage calculated for the inclined rail with 60° chamfer (60E1i30 cut 60) and rail grade R260 in facing move traffic (shaded areas). The variation in wheel profile leads to a more realistic distribution of wheel-rail contact positions (a wider running band). In comparison with the nominal S1002 profile, the worn wheel profiles can make contact with the switch rail closer to the front of the

turnout. The damage has also been calculated assuming rail grade R350HT. The following conclusions can be made:

- Wear is reduced significantly by selecting R350HT instead of R260 (same conclusion as for the case with S1002 profiles).
- The maximum wear damage is generated on the switch rail (same conclusion as for the case with S1002 profiles). For the switch rails with the 60° chamfer, the use of worn wheel profiles leads to a shift of the position of maximum wear closer to the switch rail tip, compare Table 3.1.1 and Table 3.1.2.
- Wear and RCF damage are higher in the trailing move.
- The 60° chamfer leads to increased wear in both moves.
- RCF damage increases with the selection of R350HT. As discussed above, this is a consequence of the assumed penalty function. To confirm that this is a correct result, the penalty function (RCF damage function) needs to be calibrated for switch panels in the field.
- The inclined rail profile leads to significantly reduced RCF damage compared to the vertical profile for both moves and both rail grades. However, the wear on the switch rail is in most cases slightly increased by the inclined stock rail.
- The maximum RCF damage in facing move is on the switch rail in the area where the full wheel transition to the switch rail has just occurred, while the maximum RCF damage in trailing move is on the stock rail in the area where the full wheel transition to the stock rail has just occurred.

To summarise, the calculations show that the design with inclined rails (1:30) is superior to the case with vertical rails. However, it seems that the 60° chamfer of the switch rail does not have a positive effect. It is possible that this chamfer design would be improved by adding also a so-called secondary cut where the vertical milling tool path is changed to reduce the height of the front sections of the switch rail. The use of R350HT instead of R260 leads to a significant reduction in wear although the results obtained here indicate are more dramatic reduction than has been observed in the field. This is probably explained by the lack of input data in the wear maps for both rail grades, in particular for R350HT and for combinations with high contact pressure and high sliding velocity. The predicted positions of maximum RCF damage and the influence of rail grade on RCF damage (R350HT leads to increased RCF damage compared to R260) need to be confirmed by field observations.

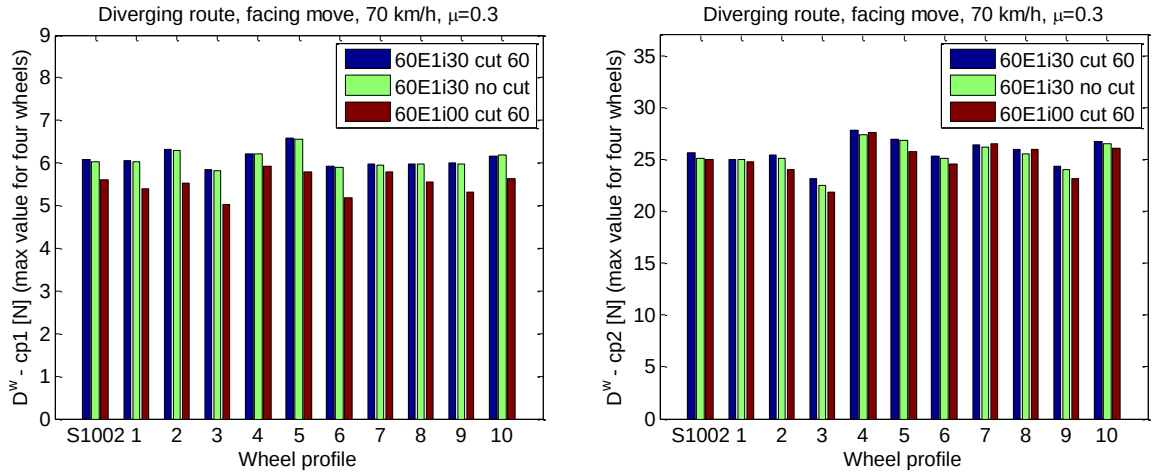

(a) (b)

Figure 3.1.34 Influence of wheel profile, switch rail profile and rail inclination on damage value *D* – maximum value evaluated for all four wheels in vehicle model (two contact points). Diverging route, facing move, vehicle speed 70 km/h, friction coefficient 0.3

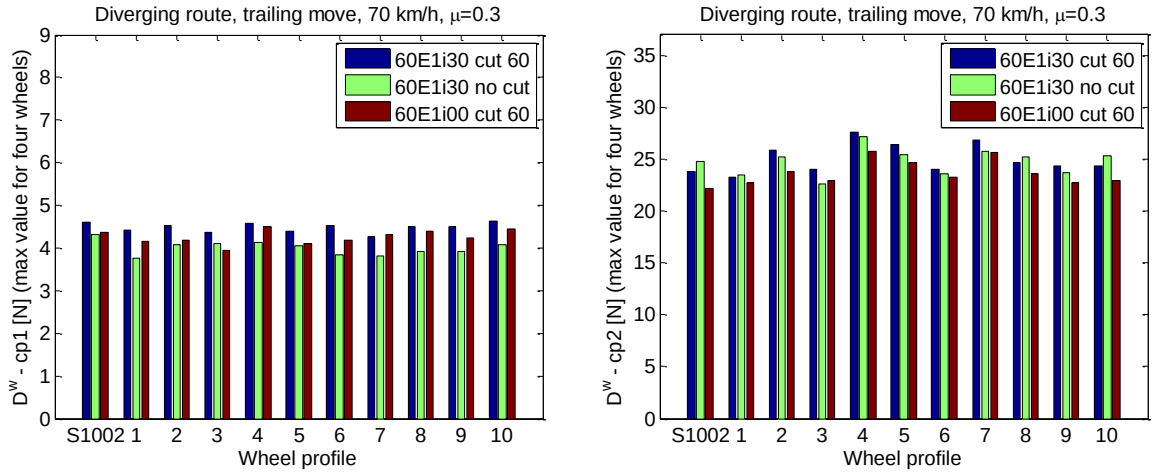

(a) (b)

Figure 3.1.35 Influence of wheel profile, switch rail profile and rail inclination on damage value *D* – maximum value evaluated for all four wheels in vehicle model (two contact points). Diverging route, trailing move, vehicle speed 70 km/h, friction coefficient 0.3

Table 3.1.2 Influence of rail profile and rail inclination on maximum accumulated wear and RCF damage for 10 Y25 vehicles (*40 wheelsets*) in diverging route. 10 combinations of worn wheel profile and vehicle speed 70 km/h. Friction coefficient 0.3. Damage is normalised with respect to damage calculated for the case marked with grey colour

Rail profile	Move	Max wear [μm] R260	Position [m]	Max RCF damage [10^{-6}]	Position [m]	Max wear [μm] R350HT	Position [m]	Max RCF damage [10^{-6}]	Position [m]
60E1i30 cut 60	Facing	1	x=4.14 m y=3.39 cm	1	x=9.23 m y=2.15 cm	0.08	x=3.97 m y=3.41 cm	2.88	x=10.47 m y=2.43 cm
60E1i30 no cut	Facing	0.26	x=3.91 m y=3.35 cm	1.06	x=9.18 m y=2.19 cm	0.04	x=5.86 m y=3.31 cm	3.23	x=10.82 m y=2.41 cm
60E1i00 cut 60	Facing	1.09	x=4.69 m y=3.37 cm	2.18	x=10.88 m y=1.79 cm	0.07	x=4.07 m y=3.39 cm	4.72	x=10.98 m y=1.87 cm
60E1i30 cut 60	Trailing	2.70	x=3.93 m y=3.41 cm	2.97	x=2.33 m y=1.99 cm	0.19	x=3.36 m y=3.43 cm	4.06	x=2.00 m y=2.21 cm
60E1i30 no cut	Trailing	1.26	x=3.01 m y=3.37 cm	2.15	x=1.77 m y=2.21 cm	0.07	x=2.06 m y=3.35 cm	5.02	x=1.44 m y=2.33 cm
60E1i00 cut 60	Trailing	2.33	x=3.98 m y=3.41 cm	6.66	x=2.44 m y=1.95 cm	0.17	x=3.51 m y=3.43 cm	6.81	x=2.24 m y=2.07 cm

3.1.7 FRICTION MANAGEMENT

The influence of friction coefficient in the wheel-rail interface on damage in the switch panel has been investigated using the model described in the previous sections. The studied switch panel design is the reference design in Section 3.1.6 with the 1:30 inclined rails and the 60° chamfer of the front section of the switch rail. The background for this investigation is the possibility to use friction management in the switch panel with a friction coefficient designed to be on a moderate level (in the order of 0.3) independent of weather conditions.

For freight traffic in facing move of the diverging route at speed 70 km/h, and with nominal (non-worn) S1002 wheel profiles, time histories of $T\gamma$ and contact positions on the rails are illustrated in Figure 3.1.36 (leading wheel in leading bogie). The shaded area indicates the range of $T\gamma$-values that according to Figure 3.1.25 corresponds to the RCF zone for rail grade R260. In particular, the horizontal dashed line within the shaded area indicates the $T\gamma$-value where there is a maximum in RCF damage. Very high values of $T\gamma$ are observed on the switch rail during two-point contact and $T\gamma$ is increasing with increasing wheel-rail friction, see Figure 3.1.36(b). Contact positions on the rails are only influenced by friction coefficient after the full transition to the switch rail. Based on the damage function for R260 in Figure 3.1.25, there is no RCF damage on the switch rail during two-point contact for any studied value

of friction coefficient. RCF damage may occur on the stock rail during two-point contact and on the switch rail after the transition to one-point contact, and in particular for the low friction coefficient as the *Tγ*-values are close to the maximum in the RCF damage function. However, the high *Tγ*-values indicate that RCF is to some degree suppressed by wear.

The tangential forces in the wheel-rail contact (in longitudinal and lateral directions) are presented in Figure 3.1.37. During two-point contact (from about 3.5 m to 9 m from the front of the turnout), the longitudinal wheel-rail contact force on the stock rail is acting in positive X-direction (same as facing move) and in the negative X-direction on the switch rail, see Figure 3.1.37(a). The lateral (in the contact plane) wheel-rail contact forces on stock rail and switch rail are acting towards the inside of the curve, see Figure 3.1.37(b). The magnitudes of the tangential contact forces are increasing with increasing friction. Calculated levels of FI_{surf} indicates RCF damage impact on both rails during two-point contact and on the switch rail after the transition to one-point contact, see Figure 3.1.38. The damage index FI_{surf} is increasing significantly with increasing wheel-rail friction. However, as stated above, note that FI_{surf} does not account for the influence of wear on crack growth.

Figures 3.1.39 – 3.1.41 illustrate the corresponding results for the trailing wheel in the leading bogie, while Figures 3.1.42 – 3.1.47 present the corresponding results for the leading and trailing wheels in the leading bogie in trailing move. It is concluded that friction management to maintain a controlled friction level and avoid situations with dry wheel-rail contact conditions with high friction coefficients has a significant potential to reduce energy dissipation, tangential contact forces and damage (wear and RCF) in the wheel-rail contacts.

The calculated accumulated damage (wear and RCF) due to the passage of one vehicle (four wheelsets with nominal S1002 wheel profiles) in either facing or trailing move is summarised in Table 3.1.3. As in Table 3.1.1, the calculated damage has been normalised with respect to the corresponding damage calculated for the reference switch panel design (60E1i30 cut 60) with rail grade R260 and friction coefficient 0.3 in facing move traffic (shaded areas). For comparison, damage has also been calculated assuming rail grade R350HT. The positions (longitudinal coordinate measured from the front of the turnout and lateral coordinate on the rail, see Figure 3.1.29 for reference) of calculated damage maxima are presented in the table. The following conclusions can be made:

- Wear is reduced significantly by selecting rail grade R350HT instead of R260.
- Wear is reduced by maintaining a low friction coefficient in the wheel-rail contacts. Note that according to the Archard model, wear is only occurring in sliding contact.
- Independent of friction coefficient and move, the maximum wear damage is generated on the side of the switch rail at 4 – 5 m from the front of the turnout.
- RCF damage (prediction based on shakedown theory and the use of a penalty function to suppress damage in cases with very high energy dissipation *Tγ*) is reduced significantly by

maintaining a low friction coefficient in the wheel-rail contact. In particular, cases with dry wheel-rail contact (high friction) lead to very high RCF damage impact.

- In facing move, for friction coefficient ≤ 0.3 the maximum RCF damage occurs on the switch rail at about 3.5 – 5.5 m from the front of the turnout (during two-point contact). For higher friction coefficients, the maximum RCF damage occurs on the switch rail after the full wheel transition from the stock rail (about 10 – 11 m from the front of the turnout).
- In trailing move, the maximum RCF damage is generally occurring on the stock rail after the full wheel transition from the switch rail (about 1 – 2.5 m from the front of the turnout).

Calculated accumulated damage (wear and RCF) due to the passage of 10 vehicles (total of 40 wheelsets and each vehicle with a different worn wheel profile) in either facing or trailing move is summarised in Table 3.1.4. The damage has also been calculated assuming rail grade R350HT. The following conclusions can be made:

- Wear is reduced significantly by selecting rail grade R350HT instead of R260 (same conclusion as for the case with S1002 profiles).
- Wear is reduced by maintaining a low friction coefficient in the wheel-rail contacts (same conclusion as for the case with S1002 profiles).
- Independent of friction coefficient and move, the maximum wear damage is generated on the side of the switch rail. However, in contract to the case with S1002 profiles, the position of maximum wear is shifted closer to the switch rail tip to about 3 – 4.5 m from the front of the turnout.
- RCF damage is reduced significantly by maintaining a low friction coefficient in the wheel-rail contact. In particular, cases with dry wheel-rail contact (high friction) lead to very high RCF damage impact (same conclusion as for the case with S1002 profiles).
- In facing move, independent of friction coefficient, the maximum RCF damage occurs on the switch rail after the full wheel transition from the stock rail (about 9 – 11 m from the front of the turnout).
- In trailing move, independent of friction coefficient, the maximum RCF damage occurs on the stock rail after the full wheel transition from the switch rail (at about 2 m from the front of the turnout).

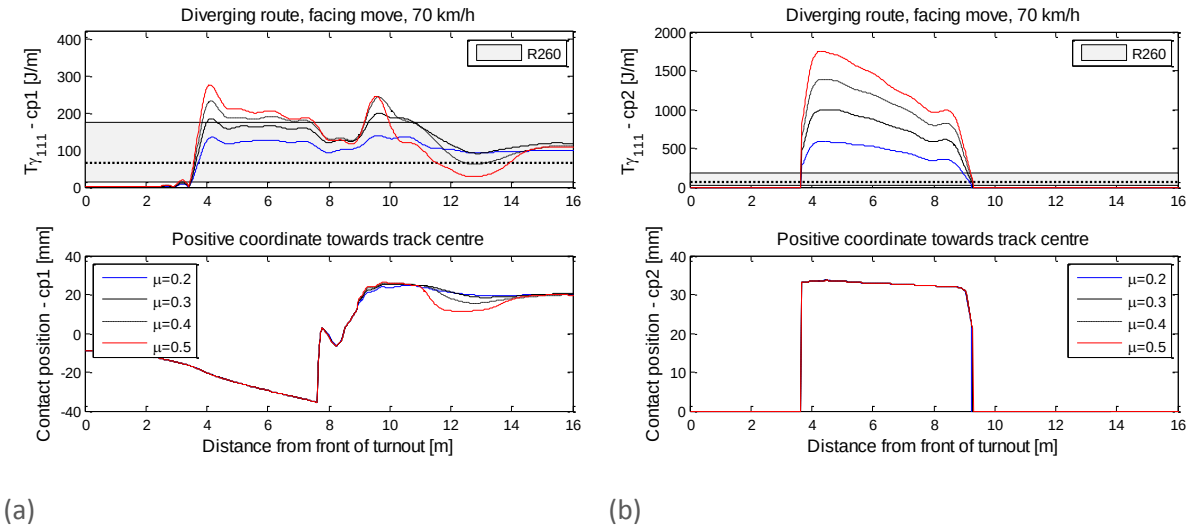

Figure 3.1.36 Influence of friction coefficient on damage function *Tγ* and contact position (two contact points) in diverging route. S1002 wheel profile, vehicle speed 70 km/h, rail profile 60E1i30 cut 60. *Leading wheel* in leading bogie, facing move

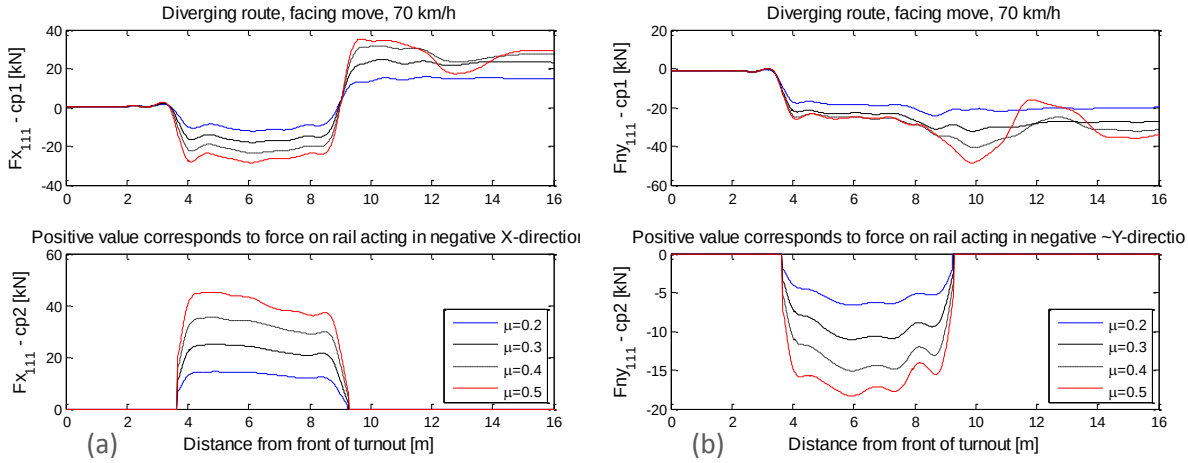

Figure 3.1.37 Influence of friction coefficient on tangential wheel-rail contact forces (two contact points) in diverging route. S1002 wheel profile, vehicle speed 70 km/h, rail profile 60E1i30 cut 60. *Leading wheel* in leading bogie, facing move

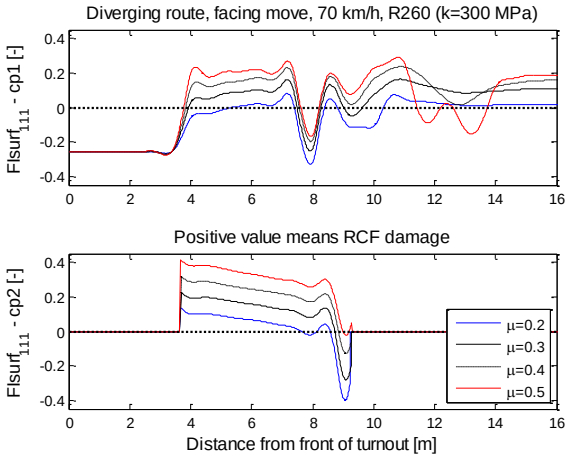

Figure 3.1.38 Influence of friction coefficient on FI_{surf} (two contact points) in diverging route. S1002 wheel profile, vehicle speed 70 km/h, rail profile 60E1i30 cut 60. *Leading wheel* in leading bogie, facing move

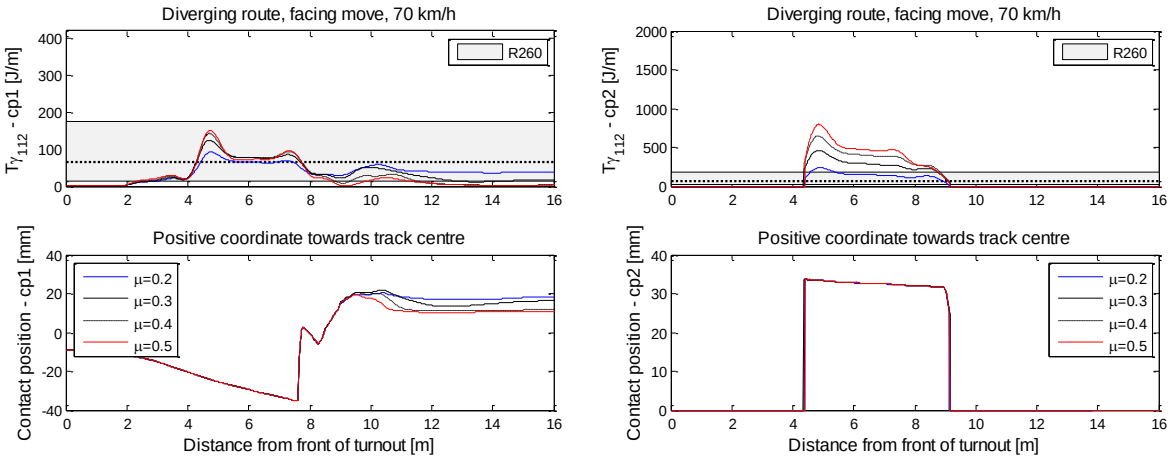

(a) (b)

Figure 3.1.39 Influence of friction coefficient on damage function *Tγ* and contact position (two contact points) in diverging route. S1002 wheel profile, vehicle speed 70 km/h, rail profile 60E1i30 cut 60. *Trailing wheel* in leading bogie, facing move

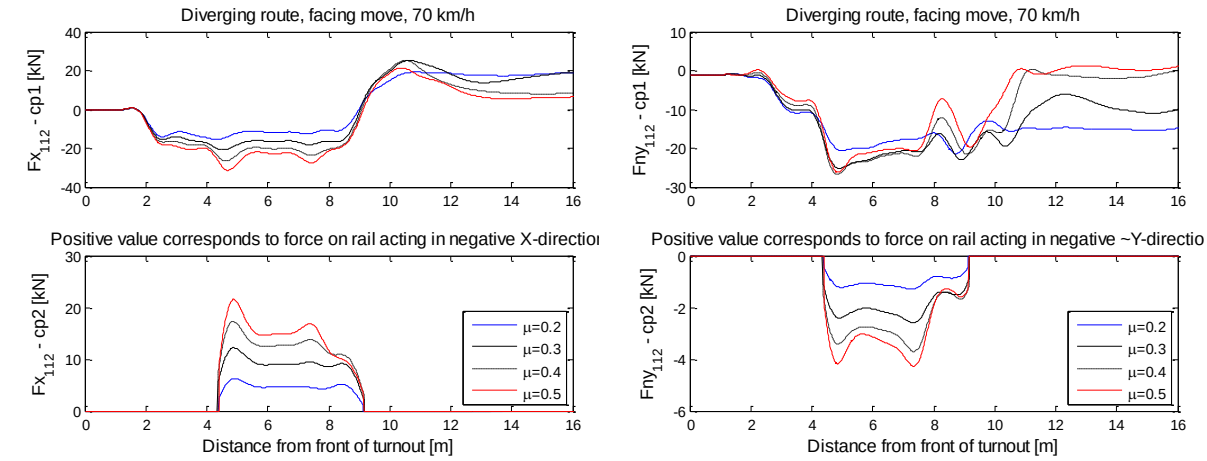

(a) (b)

Figure 3.1.40 Influence of friction coefficient on tangential wheel-rail contact forces (two contact points) in diverging route. S1002 wheel profile, vehicle speed 70 km/h, rail profile 60E1i30 cut 60. *Trailing wheel* in leading bogie, facing move

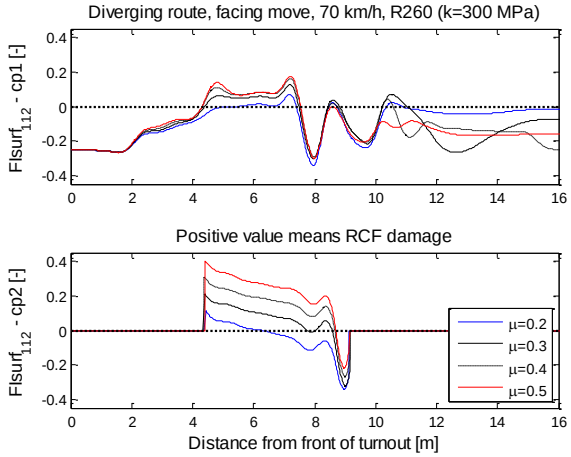

Figure 3.1.41 Influence of friction coefficient on FI_{surf} (two contact points) in diverging route. S1002 wheel profile, vehicle speed 70 km/h, rail profile 60E1i30 cut 60. *Trailing wheel* in leading bogie, facing move

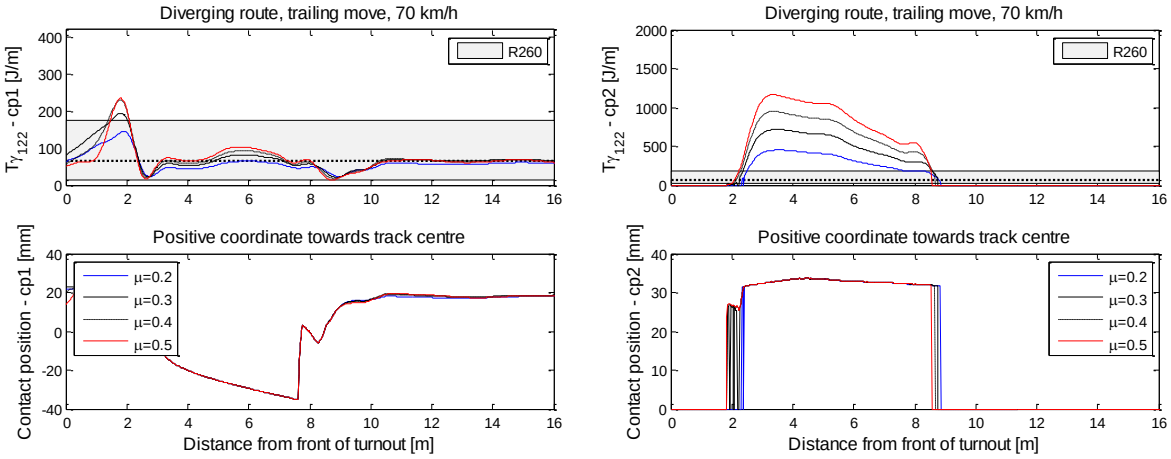

(a) (b)

Figure 3.1.42 Influence of friction coefficient on damage function *Tγ* and contact position (two contact points) in diverging route. S1002 wheel profile, vehicle speed 70 km/h, rail profile 60E1i30 cut 60. *Leading wheel* in leading bogie, trailing move

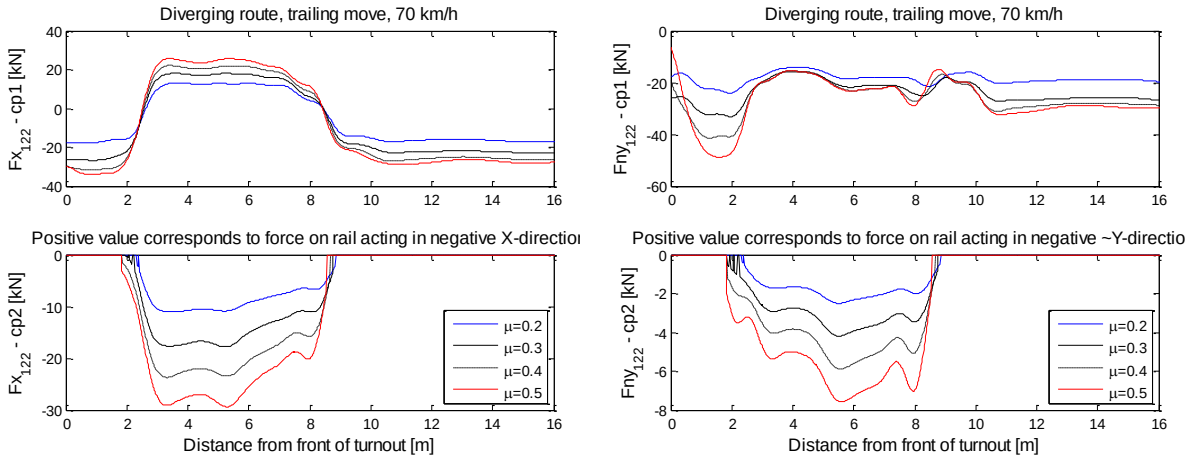

(a) (b)

Figure 3.1.43 Influence of friction coefficient on tangential wheel-rail contact forces (two contact points) in diverging route. S1002 wheel profile, vehicle speed 70 km/h, rail profile 60E1i30 cut 60. *Leading wheel* in leading bogie, trailing move

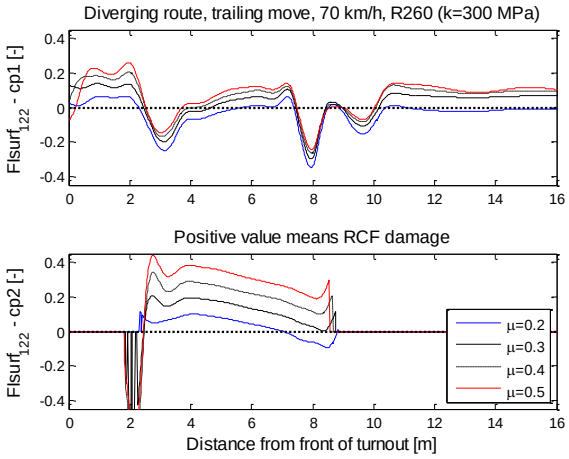

Figure 3.1.44 Influence of friction coefficient on FI_{surf} (two contact points) in diverging route. S1002 wheel profile, vehicle speed 70 km/h, rail profile 60E1i30 cut 60. *Leading wheel* in leading bogie, trailing move

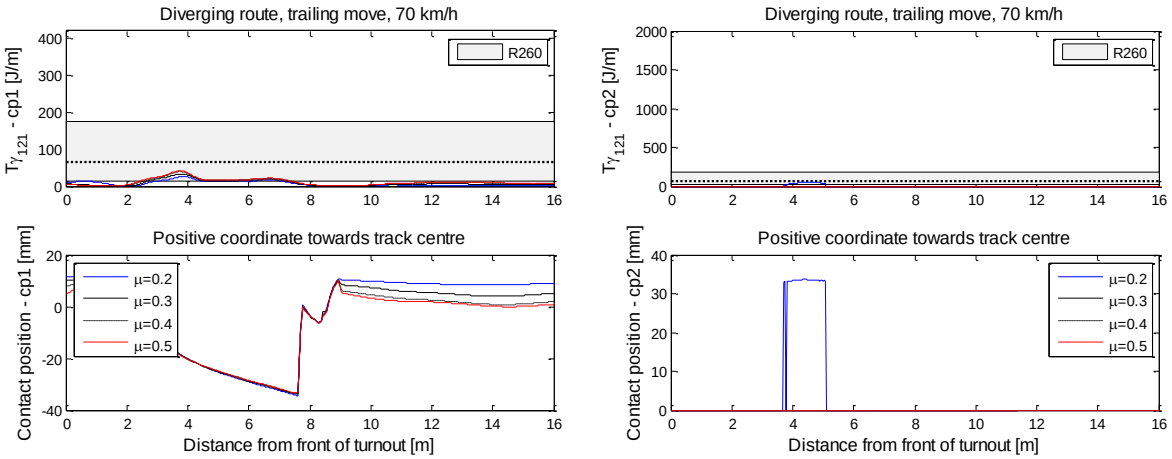

(a) (b)

Figure 3.1.45 Influence of friction coefficient on damage function *Tγ* and contact position (two contact points) in diverging route. S1002 wheel profile, vehicle speed 70 km/h, rail profile 60E1i30 cut 60. *Trailing wheel* in leading bogie, trailing move

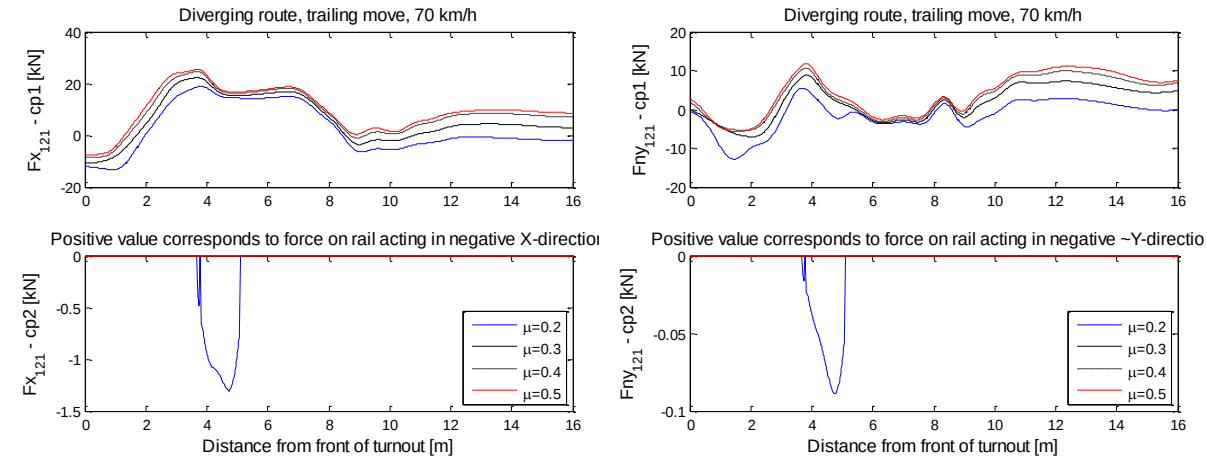

(a) (b)

Figure 3.1.46 Influence of friction coefficient on tangential wheel-rail contact forces (two contact points) in diverging route (direction of forces as explained in the figure). S1002 wheel profile, vehicle speed 70 km/h, rail profile 60E1i30 cut 60. *Trailing wheel* in leading bogie, trailing move

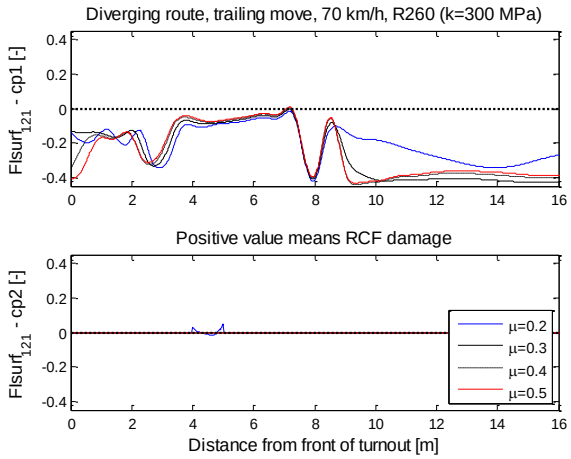

Figure 3.1.47 Influence of friction coefficient on FIsurf (two contact points) in diverging route. S1002 wheel profile, vehicle speed 70 km/h, rail profile 60E1i30 cut 60. *Trailing wheel* in leading bogie, trailing move

Table 3.1.3 Influence of friction coefficient on maximum accumulated wear and RCF damage for one Y25 vehicle (*four wheelsets*) in diverging route. S1002 wheel profile, vehicle speed 70 km/h, rail profile 60E1i30 cut 60. Damage is normalised with respect to damage calculated for the case marked with grey colour

Rail profile	Move	Max wear [μm]	Position [m]	Max RCF damage [10^{-6}]	Position [m]	Max wear [μm]	Position [m]	Max RCF damage [10^{-6}]	Position [m]
		R260				R350HT			
μ=0.2	Facing	0.77	x=4.45 m y=3.37 cm	0.52	x=4.39 m y=3.37 cm	0.12	x=4.45 m y=3.37 cm	0.43	x=3.66 m y=3.31 cm
μ=0.3	Facing	1	x=5.12 m y=3.33 cm	1	x=5.64 m y=3.27 cm	0.15	x=4.45 m y=3.37 cm	2.68	x=4.35 m y=3.37 cm
μ=0.4	Facing	1.15	x=5.06 m y=3.33 cm	1.44	x=10.97 m y=2.45 cm	0.16	x=4.45 m y=3.37 cm	13.17	x=10.80 m y=2.49 cm
μ=0.5	Facing	1.18	x=5.02 m y=3.35 cm	12.61	x=10.21 m y=2.59 cm	0.16	x=4.49 m y=3.37 cm	33.61	x=10.48 m y=2.57 cm
μ=0.2	Trailing	0.99	x=4.06 m y=3.35 cm	0.40	x=2.32 m y=3.15 cm	0.12	x=4.06 m y=3.35 cm	0.21	x=2.32 m y=3.15 cm
μ=0.3	Trailing	1.10	x=4.06 m y=3.35 cm	1.34	x=8.66 m y=3.17 cm	0.16	x=4.06 m y=3.35 cm	1.31	x=1.01 m y=2.47 cm
μ=0.4	Trailing	1.10	x=4.06 m y=3.35 cm	7.29	x=2.39 m y=1.89 cm	0.16	x=4.06 m y=3.35 cm	7.00	x=1.01 m y=2.53 cm
μ=0.5	Trailing	1.07	x=4.06 m y=3.35 cm	16.81	x=2.35 m y=2.01 cm	0.16	x=4.06 m y=3.35 cm	28.01	x=1.07 m y=2.51 cm

Table 3.1.4 Influence of friction coefficient on maximum accumulated wear and RCF damage for 10 Y25 vehicles (*40 wheelsets*) in diverging route. 10 combinations of worn wheel profile and vehicle speed 70 km/h, rail profile 60E1i30 cut 60. Damage is normalised with respect to damage calculated for the case marked with grey colour

Rail profile	Move	Max wear [μm]	Position [m]	Max RCF damage [10^{-6}]	Position [m]	Max wear [μm]	Position [m]	Max RCF damage [10^{-6}]	Position [m]
		R260				R350HT			
μ=0.2	Facing	0.69	x=4.08 m y=3.39 cm	0.11	x=9.02 m y=1.99 cm	0.06	x=3.95 m y=3.41 cm	0.19	x=10.58 m y=2.39 cm
μ=0.3	Facing	1	x=4.14 m y=3.39 cm	1	x=9.23 m y=2.15 cm	0.08	x=3.97 m y=3.41 cm	2.88	x=10.47 m y=2.43 cm
μ=0.4	Facing	1.19	x=4.24 m y=3.39 cm	2.85	x=10.08 m y=2.43 cm	0.09	x=3.97 m y=3.41 cm	15.42	x=10.47 m y=2.47 cm
μ=0.5	Facing	1.31	x=4.38 m y=3.39 cm	6.74	x=9.06 m y=2.85 cm	0.11	x=3.97 m y=3.41 cm	24.61	x=9.17 m y=2.59 cm
μ=0.2	Trailing	2.14	x=3.69 m y=3.43 cm	0.15	x=2.37 m y=1.95 cm	0.14	x=3.36 m y=3.43 cm	0.36	x=1.75 m y=2.25 cm
μ=0.3	Trailing	2.70	x=3.93 m y=3.41 cm	2.97	x=2.33 m y=1.99 cm	0.19	x=3.36 m y=3.43 cm	4.06	x=2.00 m y=2.21 cm
μ=0.4	Trailing	2.78	x=3.93 m y=3.41 cm	14.59	x=2.19 m y=2.09 cm	0.19	x=3.42 m y=3.45 cm	18.99	x=2.00 m y=2.23 cm
μ=0.5	Trailing	2.74	x=3.67 m y=3.43 cm	23.54	x=2.10 m y=2.15 cm	0.18	x=3.42 m y=3.45 cm	44.19	x=1.98 m y=2.29 cm

3.1.8 REFERENCES

[3.1.1] B.A. Pålsson, Optimisation of railway switches and crossings, PhD thesis, Department of Applied Mechanics, Chalmers University of Technology, Gothenburg, Sweden, 2014

[3.1.2] C4R Deliverable 13.1, Operational failure modes of S&C, September 2014, 51 pp

[3.1.3] B.A. Pålsson and J.C.O. Nielsen, Track gauge optimisation of railway switches using a genetic algorithm, *Vehicle System Dynamics*, 2012, **50**(S1), pp 365-387

[3.1.4] B.A. Pålsson, Design optimisation of switch rails in railway turnouts, *Vehicle System Dynamics*, 2013, **51**(10), pp 1619-1639

[3.1.5] J.C.O. Nielsen, B.A. Pålsson and P.T. Torstensson, Switch panel design based on simulation of accumulated rail damage in a railway turnout, *Proceedings 10th International Conference on Contact Mechanics and Wear of Rail/Wheel Systems*, Colorado Springs, CO, USA, September 2015

[3.1.6] J.F. Archard and W. Hirst, The wear of metals under unlubricated conditions, *Proceedings of the Royal Society of London. Series A. Mathematical and Physical Sciences,* 1956, **236**, pp 397-410

[3.1.7] U. Olofsson and T. Telliskivi, Wear, plastic deformation and friction of two rail steels – a full-scale test and a laboratory study, *Wear*, 2003, pp 80-93

[3.1.8] R. Enblom and M. Berg, Proposed procedure and trial simulation of rail profile evolution due to uniform wear, *Proceedings IMechE, Part F, Journal of Rail and Rapid Transit*, 2008, **222**, pp 15-25

[3.1.9] A. Ekberg, E. Kabo and H. Andersson, An engineering model for prediction of rolling contact fatigue of railway wheels, *Fatigue Fract Engng Mater Struct*, 2002, **25**, pp 899-909

[3.1.10] A. Ekberg, B. Åkesson and E. Kabo, Wheel/rail rolling contact fatigue – Probe, predict, prevent, *Wear*, 2014, **314**(1), pp 2-12

[3.1.11] B. Dirks and R. Enblom, Prediction model for wheel profile wear and rolling contact fatigue, *Wear*, 2011, **271**, pp 210-217

[3.1.12] B. Dirks, R. Enblom, A Ekberg and M. Berg, The development of a crack propagation model for railway wheels and rails, *Fatigue and Fracture of Engineering Materials and Structures*, 2015, **38**(12), pp 1478-1491

[3.1.13] M.C. Burstow, Whole life rail model application and development for RSSB – continued development of an RCF damage parameter, Rail Standards and Safety Board, London, 2004

[3.1.14] J.R. Evans, T.K.Y. Lee, and C.C. Hon, Optimising the wheel/rail interface on a modern urban rail system, *Vehicle System Dynamics*, 2008, **46**, pp 119-127

[3.1.15] B. Dirks, Simulation and measurement of wheel on rail fatigue and wear, PhD thesis, Department of Aeronautical and Vehicle Engineering, Royal Institute of Technology, Stockholm, Sweden, 2015

[3.1.16] INNOTRACK D4.1.5, Definitive guidelines on the use of different rail grades, 2009 (downloaded from www.innotrack.net/Reports in November 2015)

[3.1.17] TATA Steel Rail technical guide, 2014 (downloaded from www.tatasteeleurope.com/static_files/Downloads/Rail/Rail%20technical%20guide%20Eng.pdf in March 2016)

[3.1.18] K. Mädler, A. Zoll, R. Heyder and M. Brehmer, Rail materials – alternatives and limits, *Proc 8th World Congress on Railway Research (WCRR2008)*, Seoul, Korea, 2008

[3.1.19] R. Heyder and K. Mädler, The influence of wheel and rail material on the wear of the respective contact partner, *Proceedings 10th International Conference on Contact Mechanics and Wear of Rail/Wheel Systems*, Colorado Springs, CO, USA, September 2015

[3.1.20] R. Heyder and M. Brehmer, Empirical studies of head check propagation on the DB network, *Wear* 314, 36-43, 2014

[3.1.21] R. Heyder and M. Brehmer, Empirische Erkenntnisse zum HeadCheck-Wachstum und zur Verschleissentwicklung, ZEVrail 137, 4 April, 2013

[3.1.22] R. Heyder and T. Hempe, Extending rail life on DB's core network, *Railway Gazette International*, April 2010

[3.1.23] R. Heyder and G. Girsch, Testing of HSH rails in high-speed tracks to minimize rail damage, *Wear* 258, 1014-1021, 2005

[3.1.24] INNOTRACK D4.1.4, Rail degradation mechanisms, 2009 (downloaded from www.innotrack.net/Reports in November 2015)

[3.1.25] H. Ossberger, VAE GmbH, personal communication, 2015-11-18

[3.1.26] S.C. Lim and M.F. Ashby, Wear-mechanism maps, *Acta Metallurgica* 35(1), 1-24, 1987

[3.1.27] R. Lewis and U. Olofsson, Mapping rail wear regimes and transitions, *Wear* 257, 721-729, 2004

[3.1.28] U. Olofsson and T. Telliskivi, Wear, plastic deformation and friction of two rail steels – a full-scale test and a laboratory study, *Wear* 254, 80-93, 2003

[3.1.29] T. Jendel, Prediction of wheel profile wear – comparisons with field measurements, *Wear* 253, 89-99, 2002

[3.1.30] G. Vasic, Modelling of wear and crack initiation in rails, PhD thesis, The University of Newcastle, 2013

[3.1.31] E.J. Pavlina and C.J. van Tyne, Correlation of yield strength and tensile strength with hardness for steels, *Journal of Materials Engineering and Performance* 17(6), 888-893, 2008

[3.1.32] J. Ahlström and B. Karlsson, Fatigue behavior of rail steel – a comparison between strain and stress controlled loading, *Wear* 258, 1187-1193, 2005

[3.1.33] M. Schilke and J. Ahlström, Laboratory tests of material properties, In INNOTRACK deliverable 3.1.6, Recommendation of, and scientific basis for, optimization of switches & crossings – part 2, www.innotrack.net/Reports

[3.1.34] GENSYS [Internet]. Available from www.gensys.se

[3.1.35] T. Jendel, Dynamic analysis of a freight wagon with modified Y25 bogies, M.Sc. thesis, Department of Vehicle Engineering, Royal Institute of Technology, Stockholm, Sweden, 1997

[3.1.36] E. Kassa, C. Andersson, and J.C.O. Nielsen, Simulation of dynamic interaction between train and railway turnout, *Vehicle System Dynamics*, 2006, **44**(3), pp 247-258

[3.1.37] B.A. Pålsson, and J.C.O. Nielsen, Dynamic vehicle–track interaction in switches and crossings and the influence of rail pad stiffness – field measurements and validation of a simulation model, *Vehicle System Dynamics*, 2015, **53**(6), pp 734-755

[3.1.38] E. Berggren, Railway track stiffness – dynamic measurements and evaluation for efficient maintenance, Ph.D. thesis, Aeronautical and Vehicle Enginering, Royal Institute of Technology, Stockholm, Sweden, 2009

[3.1.39] J.J. Kalker, A fast algorithm for the simplified theory of rolling contact, *Vehicle System Dynamics*, 1982, **11**(1), pp 1-13

[3.1.40] B.A. Pålsson, and J.C.O. Nielsen, Wheel–rail interaction and damage in switches and crossings, *Vehicle System Dynamics*, 2012, **50**(1), pp 43-58

3.2 MEDIUM-TERM DESIGN SOLUTIONS

While Section 3.1 focuses on short-term solutions in switch panels, this section focuses on medium-term solutions in crossing panels. Crossing panels also suffer from discontinuity in both support and kinematic guidance of the vehicle's axles, leading to a large range of damage such as rail wear and rolling contact fatigue, cast crossings structural fatigue, ballast support deterioration (voids) and fatigue of components (pads and bearers) – see the failure catalogue report [3.2.1]. Section 3.2 has been written by the University of Huddersfield, exception made of Section 3.2.7 written by VCSA.

3.2.1 SOURCE OF DAMAGE IN CROSSING PANELS

Similarly to the switch panel, the wheelset traversing a crossing experiences rapid changes in contact conditions. The point of contact on the wheel running on the crossing is moving outwards (towards field side) as the wheel passes the throat of the crossing and the wing rail diverges at the crossing angle. The wheel therefore rolls onto a decreasing rolling radius and its centre of gravity moves down, assuming a conical wheel shape, until contact is made with the crossing nose in the area of the wheel flange root; this is what is called the load transfer (from wing to nose and vice versa in facing and trailing move respectively). This leads to a sudden upward motion of the wheel on the nose topping which resembles an inverted triangle (Figure 3.2.1) characterised by a dip angle [3.2.2] which value is known to be directly related to the magnitude of the vertical dynamic impact force induced by this load transfer (see analogy with dip joints [3.2.3]), as evidenced by simulation output in Figure 3.2.3. A similar behaviour occurs in the reverse direction of movement. The dynamic impact force contains a very high frequency peak value (P1) and a medium frequency oscillatory response (P2) as illustrated in Figure 3.2.2. Jenkins in his original work on rail joint [3.2.3] reported that the P1 force corresponds to the wheel unsprung mass moving against the rail mass on the contact spring stiffness. It is of very short duration (fraction of a millisecond) and it is generally ignored within standard practice when dealing with track damage, however due to the high magnitude of stress generated it may arguably be a key driver for material damage within the rail. Jenkins also characterised the P2 force as associated with the coupled movement of the wheel and track (rail/sleeper) masses against the track support stiffness (ballast) and last for several milliseconds. Taking the assumption of Jenkins it can be observed that the frequency response of P1 and P2 are fixed by the vehicle-track properties (mass and stiffness). This allows us to derive in Table 3.2.1 the expected semi-wavelength for the P1 and P2 forces at which the force will be at its peak. The P1 is thus concentrated over a few tens of millimetres and matches the size of typical local fatigue defects observed on the crossing nose and wing rail, while the P2 force covers a longer span ranging from 0.1 to 2m, covering more or less that the sleeper spacing distance. It is therefore leading to differential damage of the support in crossing panels, especially linked to ballast deterioration and voids but also potential fatigue of the casting. Note that the table also shows that the location of the peak load is related to the vehicle speed.

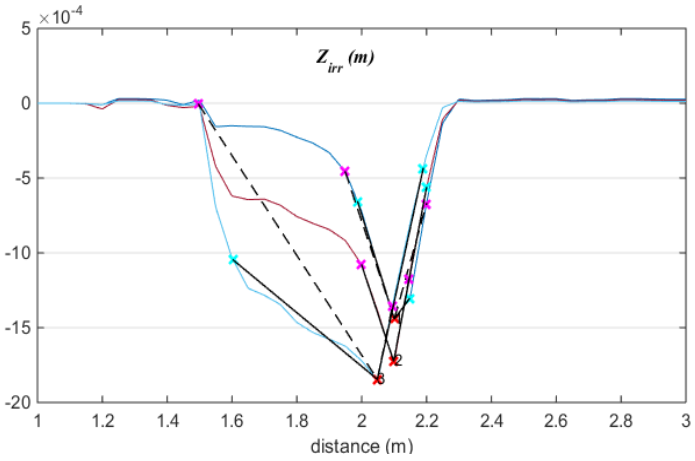

Figure 3.2.1 Wheel unsprung mass vertical motion (meters) and points used for corresponding equivalent dip angle calculation, for one wheel negotiating one crossing geometry at three different lateral positions [3.2.2]. Note the variation in equivalent dip angle obt

.

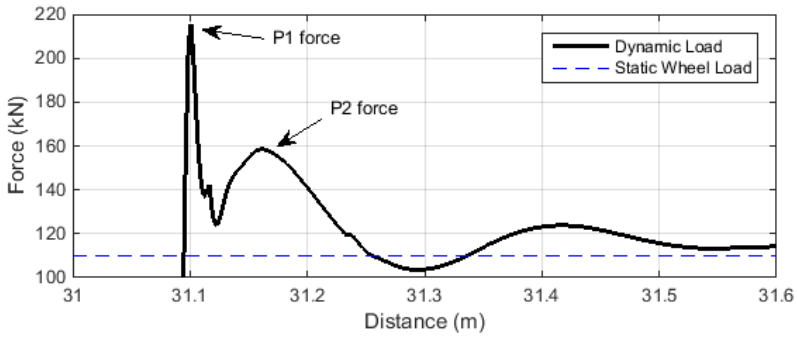

Figure 3.2.2 Typical P1 and P2 calculated force response against distance

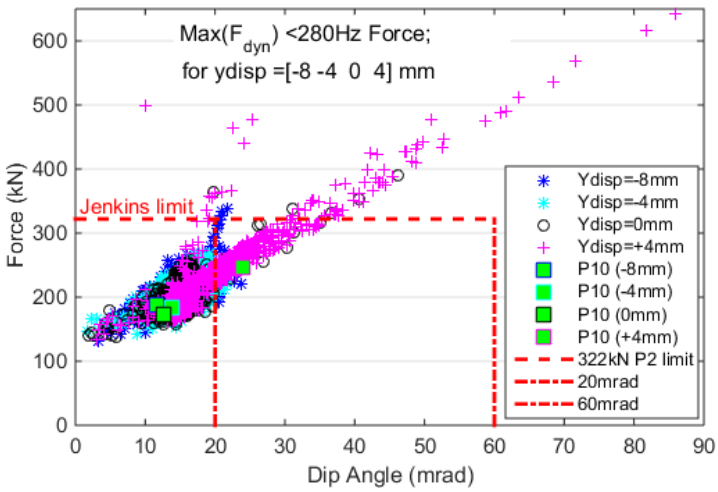

Figure 3.2.3 Relation between equivalent dip angle and P2 force level simulated for a range of wheel profiles [3.2.2] in SUSTRAIL project.

Table 3.2.1 Typical semi-wavelength for P1 and P2 impact forces

		P1		P2	
		low	high	low	high
Impulse frequency (Hz)		500	2000	20	100
Impulse duration (ms)		2.0	0.5	50	10
Vehicle speed		**Peak Load Position (1/2 wavelength)**			
km/h	*m/s*	*mm*		*mm*	
40	11.1	11	3	278	56
80	22.2	22	6	556	111
120	33.3	33	8	833	167
200	55.6	56	14	1,389	278
250	69.4	69	17	1,736	347
320	88.9	89	22	2,222	444

Examples of damage at crossing nose related to the P1 force are shown in Figure 3.2.4 and Figure 3.2.5 taken from [3.2.1]. The very local nature of the discrete damage can be observed in the narrow location of the LTA, on the crossing nose and on the wing rail. Examples of damage of support linked to the P2 force are shown in Figure 3.2.6, where damage location can be extended away from the load transfer area due to the longer wavelength of the P2 force. High stress concentration resulting from P2 force bending the cast crossing generally occurs on the edges of sleepers around the LTA and also near tri-metallic welds (e.g. Figure 3.2.6, right).

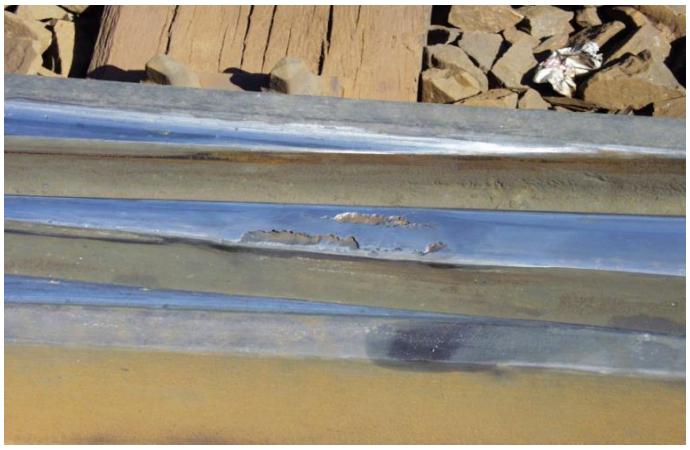

Figure 3.2.4 Example of damage on crossing nose – spalling

Figure 3.2.5 Example of damage on wing rail – plastic deformation and localised crushing in contact area. The damage is in the order of few 10s of mm, matching the definition of the P1 force.

Figure 3.2.6 Illustration of vertical support damage due to the P2 vertical force: voided sleeper (left) and fatigued cast crossing (right) occurring some distance away from the LTA

In addition to the vertical dynamic impact load, the rolling radius difference generated between left and right wheels induces a relatively rapid change of angle of attack around the load transfer area (LTA) (similar to that explained in the switch panel in Section 3.1) which leads to sudden lateral dynamic forces also impacting on rail damage as well as support and lateral geometry degradations. The magnitude of the dynamics lateral wheel force, although lower than the vertical impact, can be in the order of 30 to 40kN even on straight through route. Full details and examples of these results are presented in section 3.2.3.3.

3.2.2 PARAMETERS OF INFLUENCE

A range of parameters influencing the magnitude and location of the damaging dynamic forces are discussed below:

- Axle Payload: The vehicle axle load is one of the main drivers for vertical damage. The heavier the axle load (heavy freight and locomotives), the higher the wheel-rail contact stresses and therefore the higher the potential damage in rail materials. For heavy haul, the wheel-rail contact conditions are often beyond the yield resistance of the materials, especially in areas where rail shapes have been compromised by component machining (high geometrical curvatures) and where dynamic loading occur.
- Vehicle type (*PYS*): running gears properties like primary yaw stiffness (*PYS*) influence steering ability and creep forces in the LTA, as well as wheelset attitude in diverging route - angle of attack and lateral shifted position – both of which are key parameters in predicting dynamic forces, contact conditions and resulting damage (see Figure 3.2.3 for the effect of axle lateral displacement on force level). In curves, the leading axle in a bogie will typically tend to move towards the high rail with a higher angle of attack, while the trailing axle can move in opposite direction or be closer to the track centreline. Friction based freight bogies running gears are particularly prone to generate poor steering conditions in turnouts and exhibit non-linear dynamics responses. Therefore, both axles in a bogie need to be considered in terms of cumulative damage in S&C.
- Vehicle type ($M_{unsprung}$): P1 and P2 forces are directly proportional to the wheelset unsprung mass ($M_{unsprung}$) – heavy running gears such as motor bogies with partly unsuspended gear box and traction motors and brake discs lead to higher impact loads.
- Vehicle speed (*V*): The faster the speed of the vehicle (*V*) the more the energy spent in making the unsprung mass change direction in the LTA, therefore the higher the potential for damage. However in practice this is dealt with having different S&C categories for specific ranges of speed (C, D, E, etc… types in the UK) and higher speed category have shallower crossing angles or even movable crossing for dedicated high speed making damage more controllable. The work in this project is concentrated on improving medium speed category and mixed traffic (C to E types).
- Vehicle wheel shapes: In combination with PYS and V, the wheel shapes are a key driver for the axle behaviour in the crossing panel and the resulting dynamic forces and wheel-rail contact conditions. In [3.2.2] it was demonstrated that the wheel shape can have a strong influence on the vertical wheel motion and equivalent dip angle and therefore on the magnitude of the P1 and P2 forces. Table 3.2.3 shows the scatter in force level as a function of the equivalent dip angle for a large range of wheel shapes and lateral offset positions. It was also demonstrated that some characteristics of the wheel shape can influence the peak force, for example as the equivalent slope at the nominal radius increases with wear this tend to lead to higher dynamic load factor. This is because the wheel tends to drop faster along the wing

rail and also contact the nose in a region where the topping angle is steeper. Hollow worn wheels also lead to very different dynamic behaviour and damage, and therefore a representative range of wheels need to be considered in the design and optimisation of a crossing.

- Rail material: The type of crossing and associated material governs the behaviour under high load conditions. Two main categories are in use. On the one hand fabricated or built up crossing generally use standard grade R260 steel but can also easily accommodate higher resisting steels (see Section 3.2.7 on material consideration). On the other hand, cast manganese (Mn) block, which are more expensive, are primarily used because they offer work hardening under initial loading to increase the material hardness and the resistance to wear and plastic deformation. Additionally, the one-piece casting ensures good bending strength and resistance in track. There can also be Explosive Depth Hardened (EDH) cast manganese crossings so that high resistance is achieved form the start, thus limiting the initial deformation in traffic. It is all the more important to get the geometry right with these types of crossing, as they will retain their shape for a long while, without complying with the running traffic wheel shapes. Within Section 3.2.7.1, a new bainitic steel material is proposed and tested on Swedish track for improved performance of crossing nose.
- Wheel-rail interface properties: the materials, surface roughness, weather conditions and any other types of lubrication influence the coefficient of friction between wheel and rail and therefore influence dynamic behaviour and energy expenditure in the contact. Artificial lubrication is not a subject of study but a realistic range of friction values needs to be taken into account in the optimisation process.
- Crossing geometry: The shape of the crossing geometry and in particular the cross-sections at specific locations along its length, are key to the wheel-rail contact dynamic behaviour. Key areas of optimisation concern the nose shape and its topping angle – how fast it rises, as well as the wing rail slope and its height with respect to the nose. A number of research has been looking at the crossing nose optimisation [3.2.4 to 3.2.6] and so far little work has been done on the understanding of existing wing rail shapes and how they perform in relation to one another and for what reasons. This is a key area of research identified in this project.
- Track geometry: Poor and degraded vertical track geometry (horizontal irregularities) attributed to the poorly supported sleepers (ballast degradation) and uneven stiffness along the crossing panels lead to increased dynamic effects in and around the LTA. These conditions obviously result in a feedback loop mechanism where dynamic vertical forces and vertical degradation are amplified and accelerated.
- Crossing types: Two main types of crossing can be found which are acute or common crossing and obtuse. The first one is far more common as the name indicates. Obtuse although much less prominent in numbers are reported to have higher rate of damage and failures. The key difference is that on an obtuse crossing the wing rail is placed on one side and acts as load support for the wheel in both directions of travel. This means that at the crossing point, the

wing rail shape is compromised and cannot be optimised for a single direction independently from the other. This report focuses on common crossing as obtuse is a particular case to be dealt with separately, however modelling techniques presented in this report can also be employed for obtuse crossings in the future.

- Crossing angle (*1 in N*): This parameter has an obvious influence on the dynamic forces and damage observed as a wider angle (lower *N* value) leads to a shorter LTA with potential less support for the wheel tread as the wing rail diverges more rapidly. Turnout categories C to E switch lengths for NR56 and NR60 designs in the UK include natural angles from $9^{1/4}$ to 15 and from 9.5 to $15^{3/4}$ respectively. This range is of interest in the project as they are common types on intercity lines with mixed traffic. CV type switches tend to represent a large population in track and $9^{1/4}$ crossings can see significant speeds in the through routes, therefore leading to higher dynamics effects.
- Track support: Track support stiffness is a key driver for the P2 impact force. The overall resilient stiffness of the crossing panel governs the load spreading capabilities along the panel and therefore the peak load in the LTA. The quality of the ballast support underneath sleepers, mass/bending properties of the long bearers, their connection with the rest of the panel, the rail pads stiffness used between the cast crossing and the sleepers, the bending properties of the cast crossing and mass; all are governing parameters in terms of track stiffness reaction and damage level. In this project the influence of rail pad resilience stiffness as well as use of USP is discussed in terms of previous results [3.2.2] and additional study. The move away from conventional ballasted track towards more consistently supported track is also discussed with a preliminary study on linking sleepers together to effectively make the crossing panel closer to a slab in terms of its dynamic behaviour (Section 3.2.6).
- Check rail lateral position (tolerances and maintenance): maintaining correct check rail gauge position ensures that the wheels do not move too close to the crossing nose. The fact that flange contact increases the chances for high damage has been demonstrated in the SUSTRAIL project [3.2.2].

The key challenges in terms of medium-term optimisation have been identified as:

- Geometry optimisation of the crossing to minimise vertical dynamics impact loads and lower steering force damage in the contact areas. This involves parametric variation analysis related to wing rail angle, height and transversal length, wing topping gradient along the crossing length.
- Dynamic load mitigation (ballast protection) through rail pad stiffness optimisation and use of USP.
- Dynamic load mitigation (ballast protection) through use of connecting elements between sleepers.

- Validation of simulation prediction, including matching damage prediction with site observation
- Using advanced measurement techniques to be able to assess geometry shape evolution under traffic and match with predicted wear and plastic deformation.
- Assessment of novel material in crossing nose and wing rails to resist fatigue, wear and plastic deformation, through laboratory testing, on-site testing and simulations.

3.2.3 GEOMETRY OPTIMISATION OF WING RAIL BASED ON UK CROSSING GEOMETRY

The geometry of the wing rail significantly influences how the wheel load is transferred from the wing rail to the crossing nose and vice-versa, and therefore, the magnitude of the dynamic forces that occur in this region. In this section, the performance of two UK acute crossing geometries have been compared and assessed using multibody simulation software. A freight wagon and a passenger vehicle have been considered in the through route in both directions. Since the wheel shape strongly influences the wheel-rail interaction and the load transfer, a representative set of wheels composed of the P10 UK profile and 20 worn wheels was selected out of a population of more than 800 wheels for the freight vehicle and the UK P8 wheel for the passenger vehicle.

First the methodology of introducing the different geometries are summarised in section 3.2.3.1. Then the characteristics of each crossing are compared in section 3.2.3.2. The comparative numerical time results are then presented in section 3.2.3.3 while qualitative comparisons are made with site observation in section 3.2.3.8. Statistical results of a geometry optimisation are presented in section 3.2.3.12 as well as its comparison to the overall performance of the two reference crossings. Finally conclusions are given in section 3.2.3.15.

3.2.3.1 MODELLING OF THE 3D GEOMETRY OF THE CROSSING

The 3D geometry of the crossing is modelled using SOLIDWORKS software [3.2.29], as shown in Figure 3.2.7. This software allows quickly modifying and testing key design parameters in order to obtain an optimised solution. The model is created based on an initial solid block and then all the geometrical operations are defined sequentially by adopting a similar methodology to that used in the machining process. The main geometrical operations are illustrated in Figure 3.2.8. Since the crossing is symmetric, a half block is modelled and mirrored in the end. The back and end grooves are cut in steps (b) and (c) and the throat relief planning is performed in step (d). These three steps define a significant part of the crossing geometry. The rails are modelled in step (e) and the half-model is mirrored in step (f).

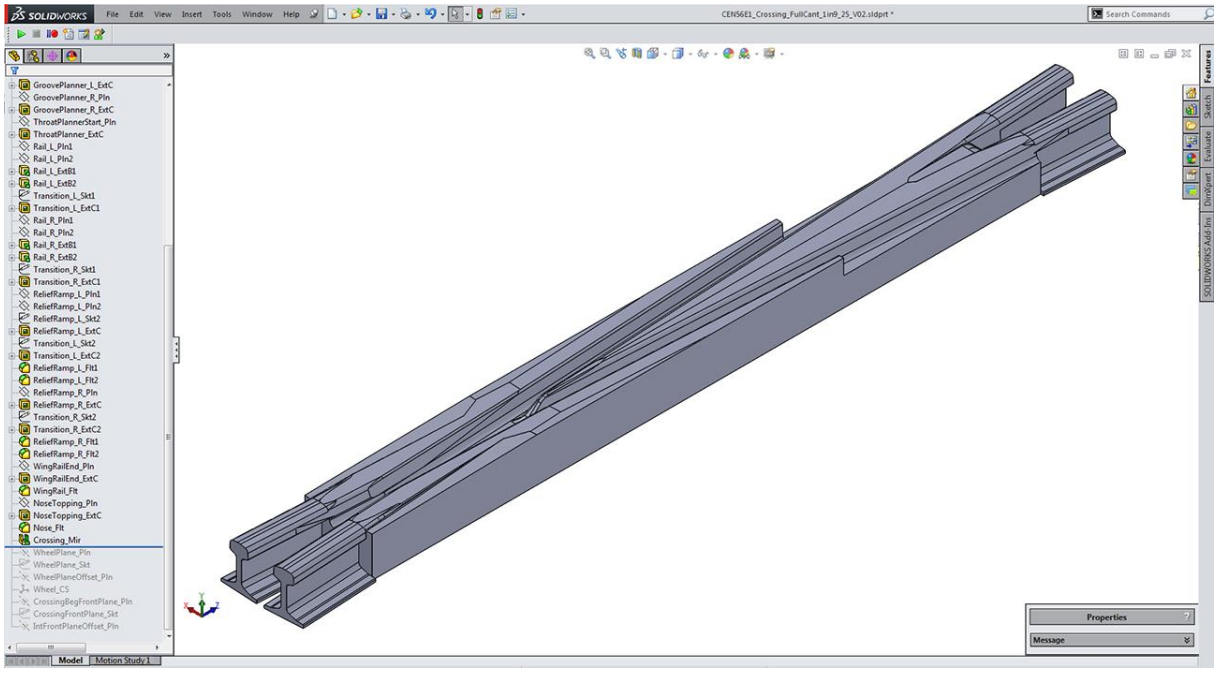

Figure 3.2.7 3D geometry of the crossing modeled in SolidWorks

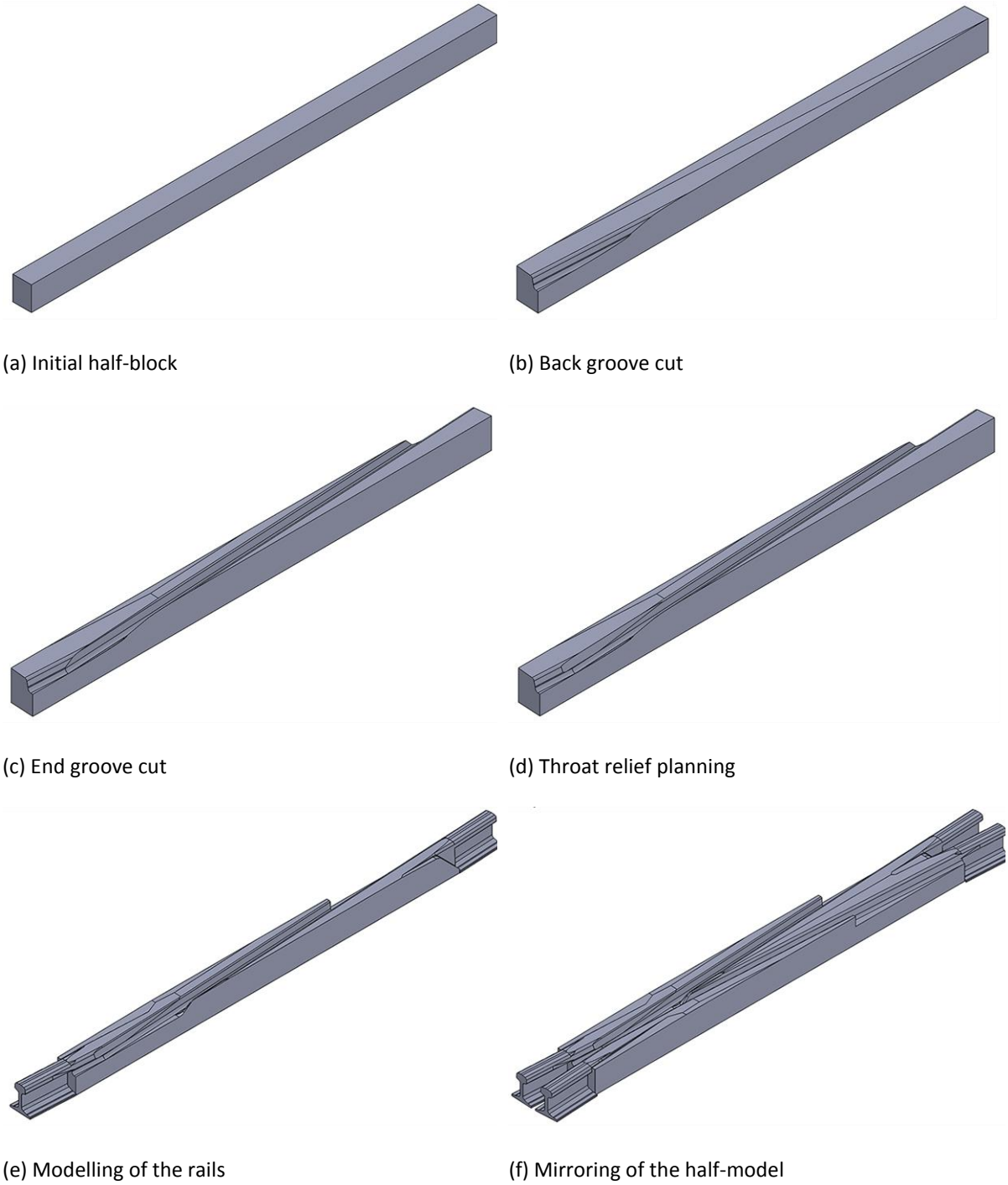

(a) Initial half-block

(b) Back groove cut

(c) End groove cut

(d) Throat relief planning

(e) Modelling of the rails

(f) Mirroring of the half-model

Figure 3.2.8 Main geometric operations used to create the crossing model

After the geometry is completely defined, the 2D cross-sections are exported to IGES using a computer code developed in Visual Basic for Applications for SOLIDWORKS. In order to optimise the computational time required by the multibody simulation software (MBS), only a key number of cross-

sections that accurately define the 3D surface are exported. The IGES files containing the information of the geometric entities of the cross-sections (see Figure 3.2.9) are imported to ANSYS program [3.2.30] and are meshed in order to obtain the keypoints that are used by the MBS software to define the cross-sections (see Figure 3.2.10). The lateral and vertical coordinates of the keypoints are then exported to text files. All these steps are performed automatically using ANSYS APDL scripting language [3.2.31].

The 2D cross-sections are imported to MATLAB and are further pre-processed (trimmed, smoothed, etc.) to obtain the final geometry that is used in the MBS software (e.g., see Figure 3.2.11). The dynamic analyses are performed using the software VI-Rail, which uses an online contact search algorithm that interpolates the profiles of the crossing for each time step in order to calculate the wheel-rail contact data. The 3D surface obtained is represented in Figure 3.2.12.

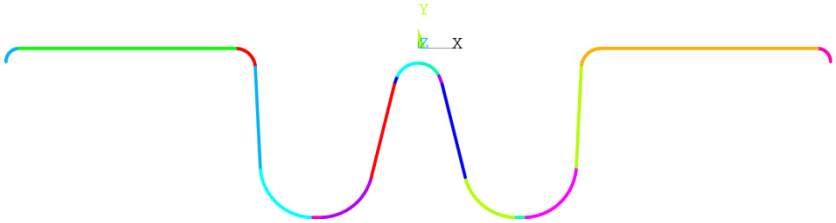

Figure 3.2.9 Geometric entities of the cross-section

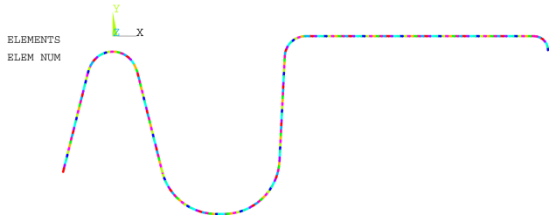

Figure 3.2.10 Mesh of the cross-section created using ANSYS

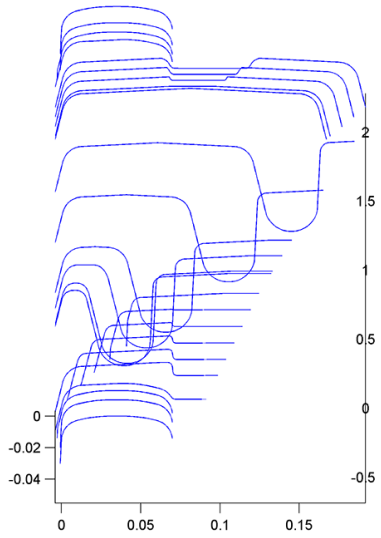

Figure 3.2.11 Example of the cross-sections used in VI-Rail

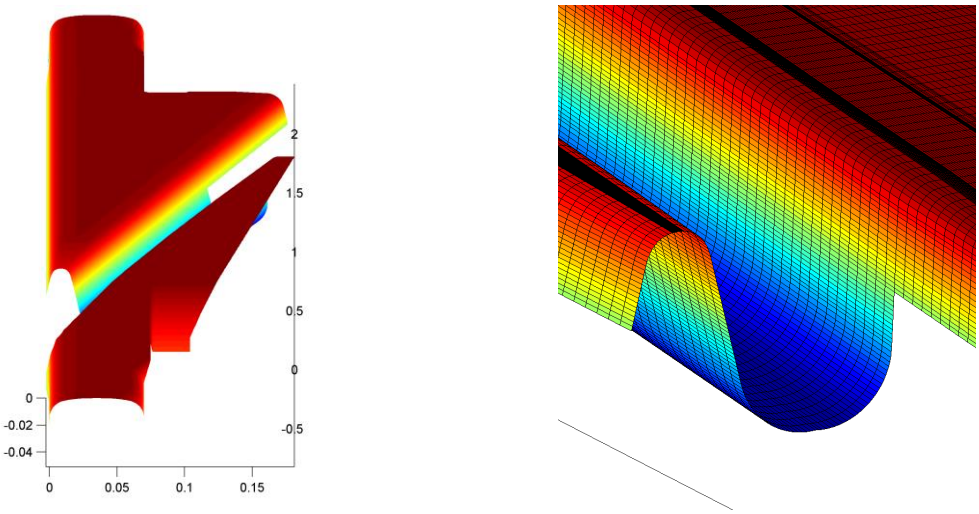

Figure 3.2.12 Example of the crossing 3D surface

3.2.3.2 COMPARISON OF THE DIFFERENT CROSSING GEOMETRIES

Two different UK crossing geometries from the same family of crossing (CEN56 vertical) have been analysed in this project. They are:

- Crossing with a CEN56 vertical rail design and a 1 in 20 cant over 102mm, followed by a horizontal plane; nicknamed Full Cant (FC) in the UK.
- Crossing with a CEN56 vertical rail design and a 1 in 20 cant over 35mm, followed by a horizontal plane; nicknamed Half Cant (FC) in the UK.

These crossings are still widely used in the UK despite the fact that the majority of new installations on modern intercity and high speed routes favour 60kg rails rather than 56 kg, and therefore use the more modern baseplate NR60 S&C design. However, the CEN56 design remains of interest as like for like replacements are still very common, and therefore there is an argument for optimising such design. Also, the HC and FC crossings lead to significantly different dynamic behaviours of the train-track system around the load transfer area, and therefore important lessons can be drawn from comparing the two designs.

The planners used to cut the back and end grooves of the HC crossing are represented in Figure 3.1.13 and Figure 3.1.14, respectively (see also Figure 3.2.9). The lower dashed line represents the height of the gauge corner and the upper line, located 14mm above, represents the top of the rail head. The left part of the planner of the end groove cuts the wing rail while the right part cuts the crossing vee. The planners used to cut the back and end grooves of the FC crossing are represented in Figure 3.1.15 and Figure 3.1.16, respectively.

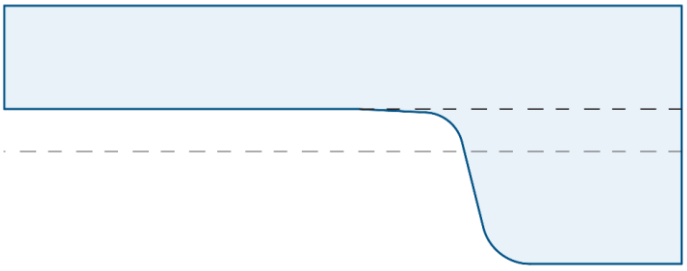

Figure 3.2.13 Planner used to cut the back groove of the HC crossing

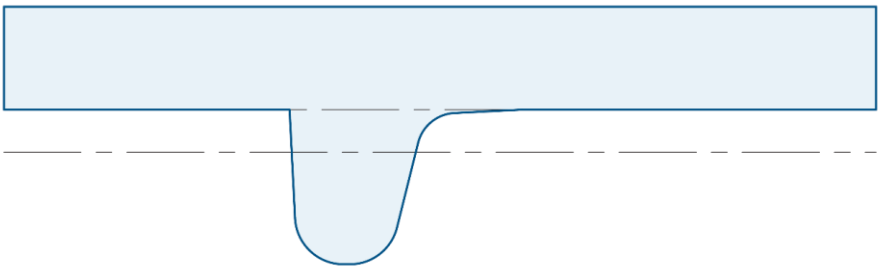

Figure 3.2.14 Planner used to cut the end groove of the HC crossing

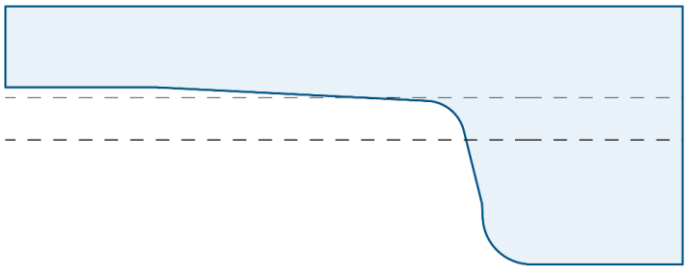

Figure 3.2.15 Planner used to cut the back groove of the FC crossing

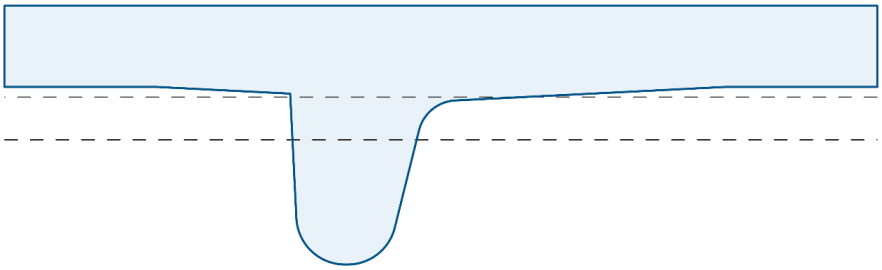

Figure 3.2.16 Planner used to cut the end groove of the FC crossing

The main difference between the cutters used to machine the cast blocks of the two crossings is illustrated in more detail Figure 3.1.17. In the HC design, the 35 mm cant of the cutter corresponds to half of the rail head width (therefore nicknamed half cant), whereas in the FC design, the cutter is inclined along the full width of the rail head (thus nicknamed full cant). As explained before, the FC design also has a horizontal plane after the 1 in 20 cant over 102mm. Figure 3.1.17 shows the comparison between the obtained FC and HC cross sections for input to the simulation, at a few key locations along the crossing.

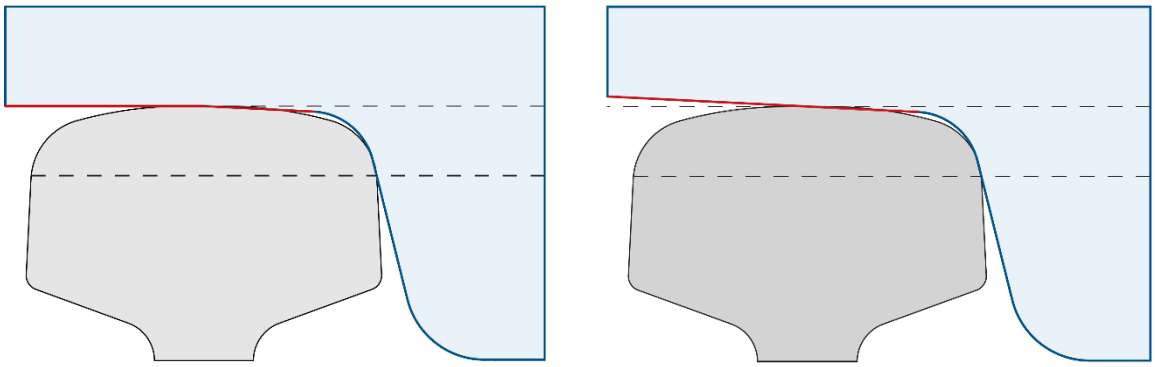

(a) (b)

Figure 3.2.17 Partial view of the cutters used for machining the (a) HC crossing and (b) FC crossings

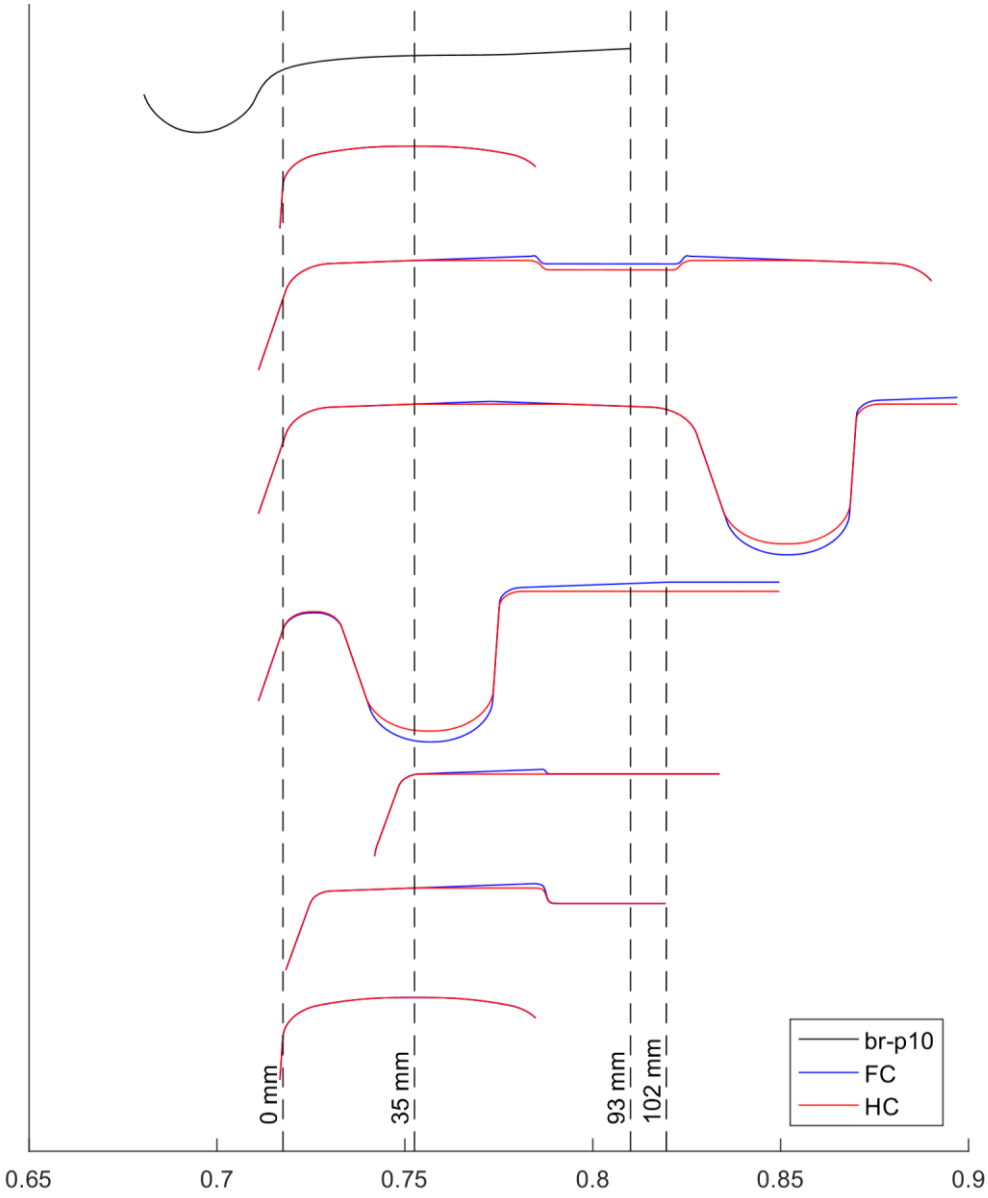

Figure 3.2.18 Comparison between some cross-sections of the HC and FC designs.

As concluded in Section 3.2.3.3, the better performance of the FC design, when compared with the HC design, significantly depends on the fact that the wheels are generally kept at a higher position before contacting with the crossing nose. In order to further enhance this desired behaviour, an optimized design, named Optimized Design 04 (OD04), has been developed based on the FC design. Figure 3.2.19 and Figure 3.2.20 show the planners used to cut this type of crossing (see also Figures 3.2.15 and 3.2.16). The planner used for the back groove of the OD04 design has a 1 in 20 cant till the end instead of just over 102mm. The planner used for the end groove of the OD04 design is the same as that of the FC except that it does not have the left part used to cut the wing rail.

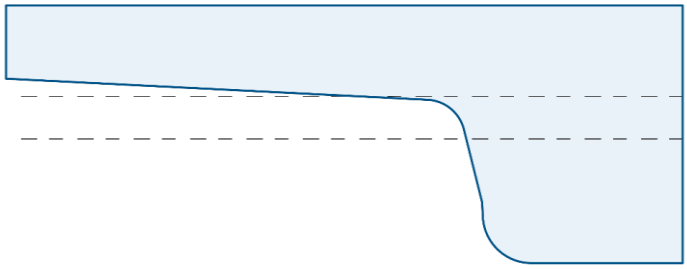

Figure 3.2.19 Planner used to cut the back groove of the OD04 crossing

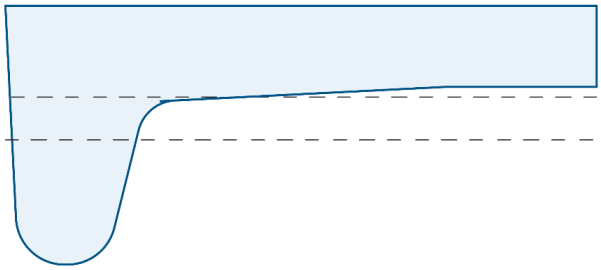

Figure 3.2.20 Planner used to cut the end groove of the OD04 crossing

3.2.3.3 DYNAMIC SIMULATION OF WING GEOMETRY CONSIDERING THE EFFECT OF WHEEL SHAPES

The two crossing geometry presented above are simulated to predict the wheel-rail contact response and predicted damage level. The software Vi-Rail is used which offers the advantage of a non-Hertzian multi-point contact algorithm with on-line calculation of contact condition (actual rail profile interpolation at each time step). The quality of the simulation therefore depends on the pre-processing work and assumption made while preparing the geometry as explained in Section 3.2.4.1 above. Simulation conditions are as follows:

- Vehicle: freight wagon with x2 Y-series friction damped bogies. 22.5T axle load.
- Speed: 40km/h
- Wheel profiles: variable with reference P10 wheel.
- Wheel-rail interface: coefficient of friction 0.35.
- Track: straight track (through routes only) – facing move only.
- Crossing angle: $9^{1/4}$

A sample of 20 worn wheels have been selected out of a population of over 800 wheel pairs using Latin Hypercube sampling method in three dimension so as to respect the characteristics of the original sample (Figure 3.2.21) in terms of (a) Flange height, (b) Flange thickness and (c) Slope in the root of the flange (ca 50-20). This is the measure of the cone angle 50 mm from flange back (20 mm inward from the nominal radius), over a distance of 20 mm. This selection also shows a very good coverage of the equivalent conicity distribution. The selected wheels are shown in Figure 3.2.22 showing a very

representative spread around the reference P10 (new) according to all characteristics above and also one selected hollow wheel.

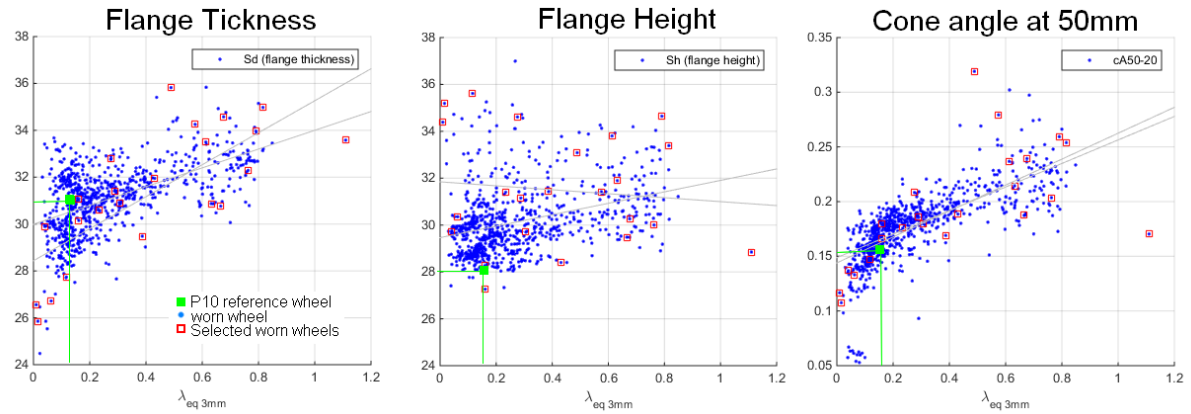

Figure 3.2.21 Selected wheels (red square) out of original population (blue dots) as a function of flange thickness (left), flange height (middle) and slope near flange root (right)

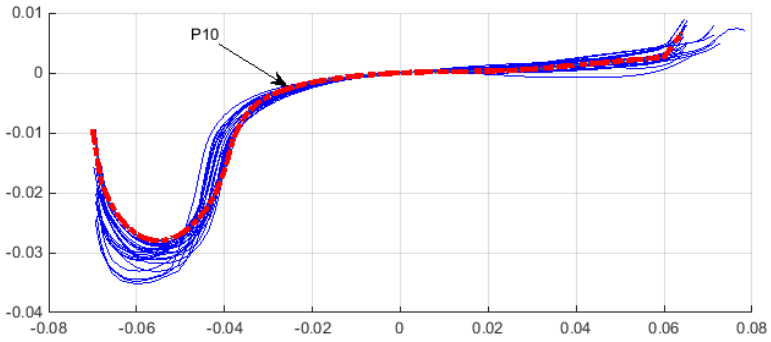

Figure 3.2.22 Selected worn wheels (solid blue) and reference P10 wheel (dashed red)

Results are hereafter presented for leading (solid lines) and trailing axle (dashed lines) of front bogie only (no major differences at straight through routes). Worn wheels are plotted in a range of blue-green hue colors while the reference P10 is plotted in bold back lines, and the one selected hollow wheel is in magenta color. Leg ends and theoretical crossing point locations are indicated with vertical dashed lines. The previous intermediate project report (D132) presented the wide range ofg output quantities available from the simulations, hereafter only the key quantities of interest are presented.

3.2.3.4 WHEEL VERTICAL DISPLACEMENT AND CONTACT POINT

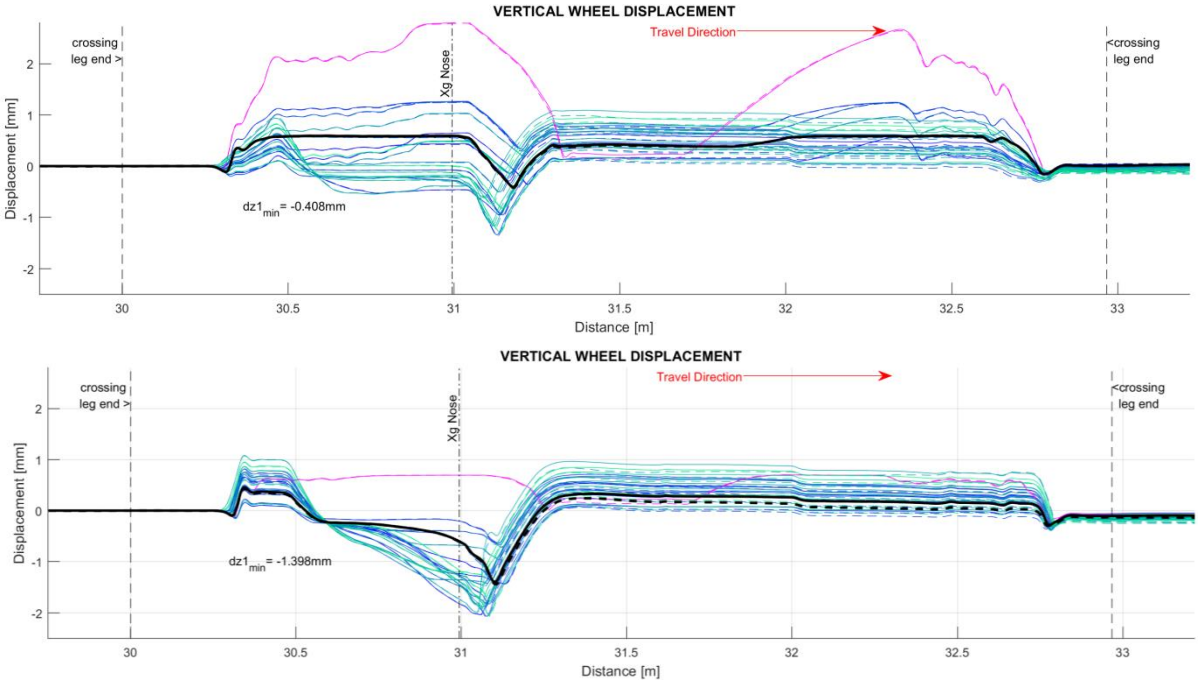

Figure 3.2.**23** shows the vertical motion of the wheel traversing the entire crossing geometry. Figure 3.2.24 shows the lateral coordinate of the contact point on the rail assuming zero as the centre of the normal reference CEN56 rail (negative values towards the gauge corner and positive values towards the wing rail and field side). Several general observations are made:

- On the entry (left leg end), the wheels tends to 'climb up' the wing rail over a rather short distance. This corresponds to a shift of contact onto the field side of the wing rail (FC) or gauge corner (HC).
- Passing the theoretical crossing nose, the wheels tend to move down starting from various positions and at different rates. This start when the wheel contacts the gauge corner of the laterally moving wing rail. Note that on the HC this start earlier (before the crossing nose position) and more gradually initially.
- At various distances passed the theoretical crossing point, the wheel transit onto the crossing nose and move back up at a certain angle. It can be seen from the contact plot that this jump from wing to nose occurs later and over a larger area of the nose for the FC, than for the HC.
- The wheels then run at various stable vertical positions onto the crossing vee, until they all merge back to the same vertical position passed the exit leg end.

The following specific observations are made:

- The worn wheels present a large scatter of behaviour surrounding that observed for the reference P10 wheel.
- For both crossing design the hollow worn wheel exhibit a noticeably different behaviour, rising higher (FC) or maintaining its height (HC) and dropping onto the back part of the crossing nose

(where it is higher and wider). Its contact with the field side of the wing rail and crossing nose is also obvious on the contact position plots.

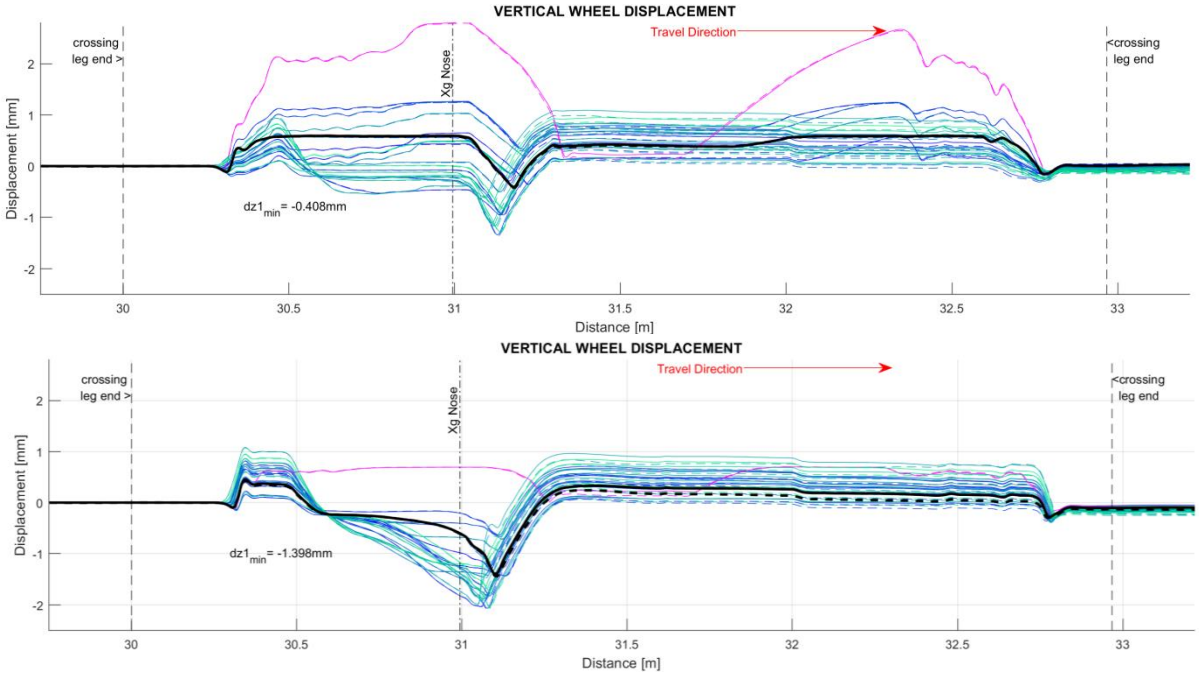

Figure 3.2.23 Wheel vertical displacement for FC (top) and HC (bottom)

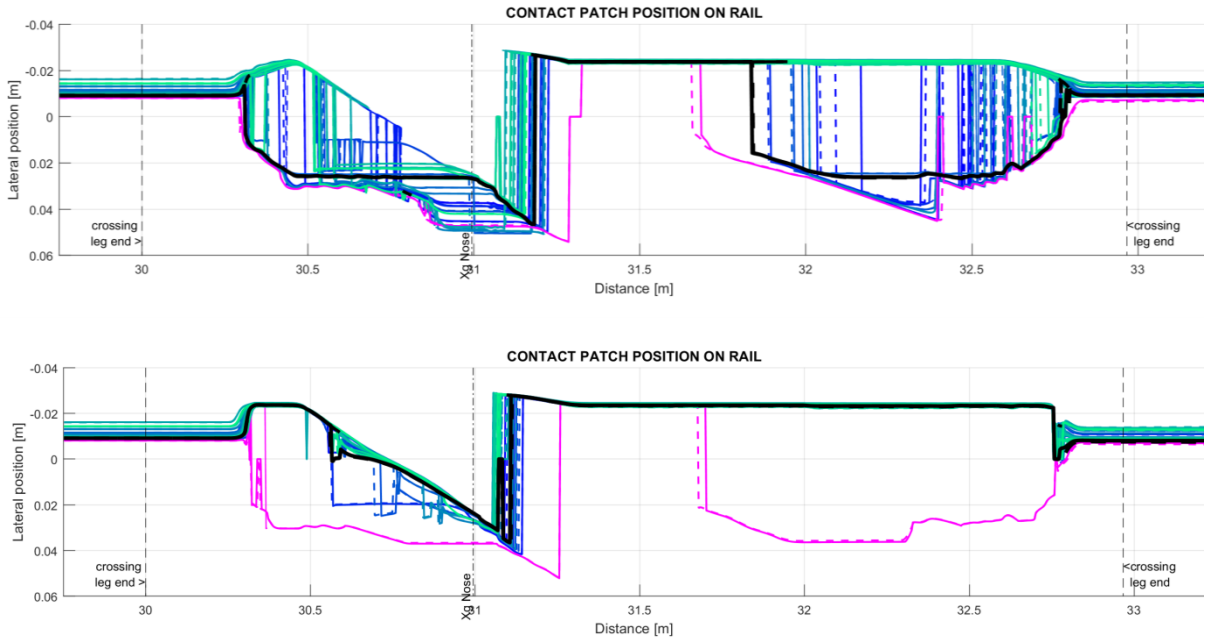

Figure 3.2.24 Contact point position on rail coordinate: zero = middle or normal rail crown, for FC (top) and HC (bottom)

3.2.3.5 CONTACT VERTICAL FORCE

Figure 3.2.25 shows the resulting vertical wheel-rail contact forces along the crossing geometry, starting from the quasi-static 110kN level on the left of the graph. A large number of transient responses are observed mainly at the two leg ends and in the area of load transfer from the wing to the nose. It has to be noted that the transient behaviour predicted here at the leg end is not entirely realistic because the details of the manual grinding taking places after manufacture in that region is not taken into account while producing the input profiles. Some dynamic effects are however expected in this area and discussed in later section 3.2.3.8 on site observations. For now the focus should be in the area of load transfer where the wheel goes down and then up (x-distance ranging between 31 and 31.5m), leading to the transient dynamic loads of interest. The following observations are made:

- As the wheel moves downwards, the force through the contact tend to reduce
- Beyond the theoretical crossing nose point (31m) initial low force transient behaviour is observed where the wheel sometime looses contact. This is the result of the wheel starting rolling along the edge of the wing rail gauge corner moving sideways at an angle 1 in N from the direction of travel.
- At the same time the wheel shape generally has a steeper conical shape towards the field side. This combines with the lateral displacement of the wing rail accelerates the downward motion of the wheel (and loss of contact).
- Next the wheel flange root suddenly comes into contact with the crossing nose (double contact for a short duration) and starts ramping up. The sudden change of direction and upward acceleration generates a high force of short duration (P1) visible in all results. There is a high degree of variation of this force depending on the wheel case.
- A lower frequency transient response ensues, which maintain a high forces response over a longer distance on the crossing nose (P2). There is some degree of variation of this force depending on the wheel case but less pronounced than for the P1.
- On both crossing the P1 and P2 forces generated by the hollow wheel occur later on the crossing nose. For the FC the impact load is higher than average because the high wing rail shape is not compatible with the hollowness of the wheel. On the other hand the fact that the HC wing rail is lower on the field side is more compatible with the hollowness of the wheel and leads to a lower impact force (smooth transition as seen on the vertical displacement figure).

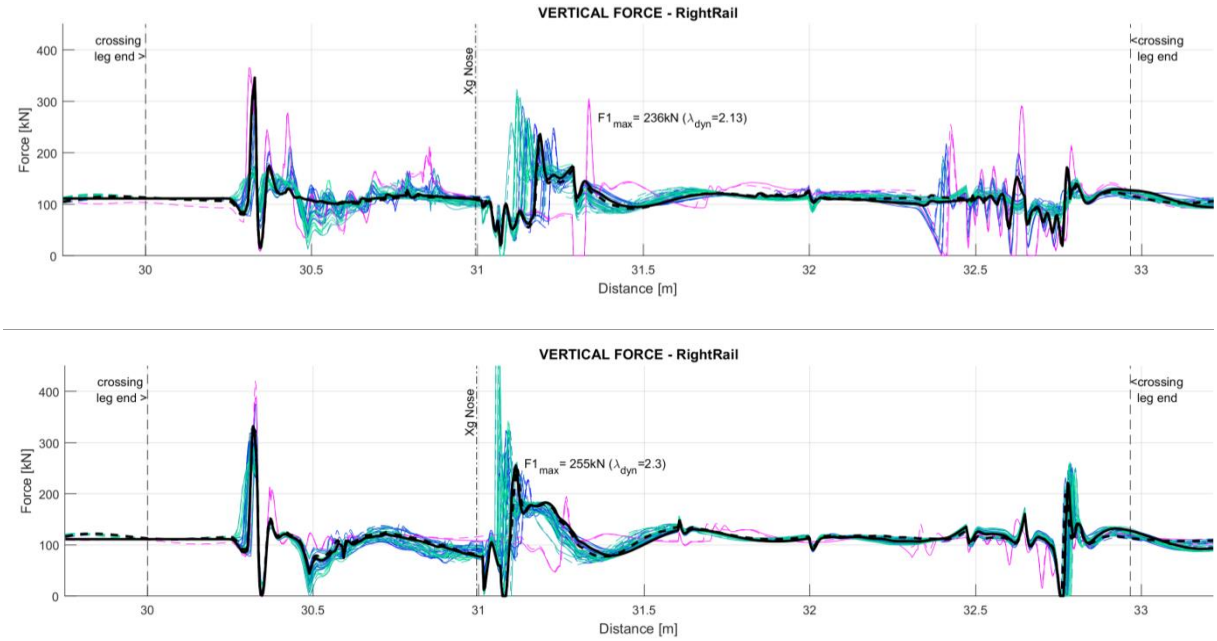

Figure 3.2.25 Wheel-rail contact vertical force along the crossing geometry for FC (top) and HC (bottom)

3.2.3.6 CONTACT LATERAL FORCE

Although the dynamic interaction in the crossing is mostly vertical in nature, there are non-negligible transient effects occurring in the lateral direction. Figure 3.2.26 shows the lateral forces resulting from the wheel-rail contact on the crossing. Apart from the effect around the leg ends, to be ignored for now, one can see short duration lateral forces of the order of minus 30-35kN (towards field side) to plus 15-20kN (towards centreline of track). Certain wheels on the FC generate negative forces larger than 40kN and the hollow wheel on the HC generates a positive peak force around 40kN.

Overall these force level are not an issue as we are only looking at straight through direction here and with respect to derailment risk for example, the Y/Q ratio would a fraction of the EN14363 limit of 1.2. However transient lateral forces may contribute to some of the local rail damage as well as local lateral disturbances (shaking) of the sleepers around the load transfer area. This may contribute to ballast rearrangement under the sleeper surface and therefore lead to increase differential settlement in the crossing panel. More analysis would be necessary using a discrete support beam model to confirm this or not. In diverging direction these forces would be however much more important and also transient in nature to the local geometry change.

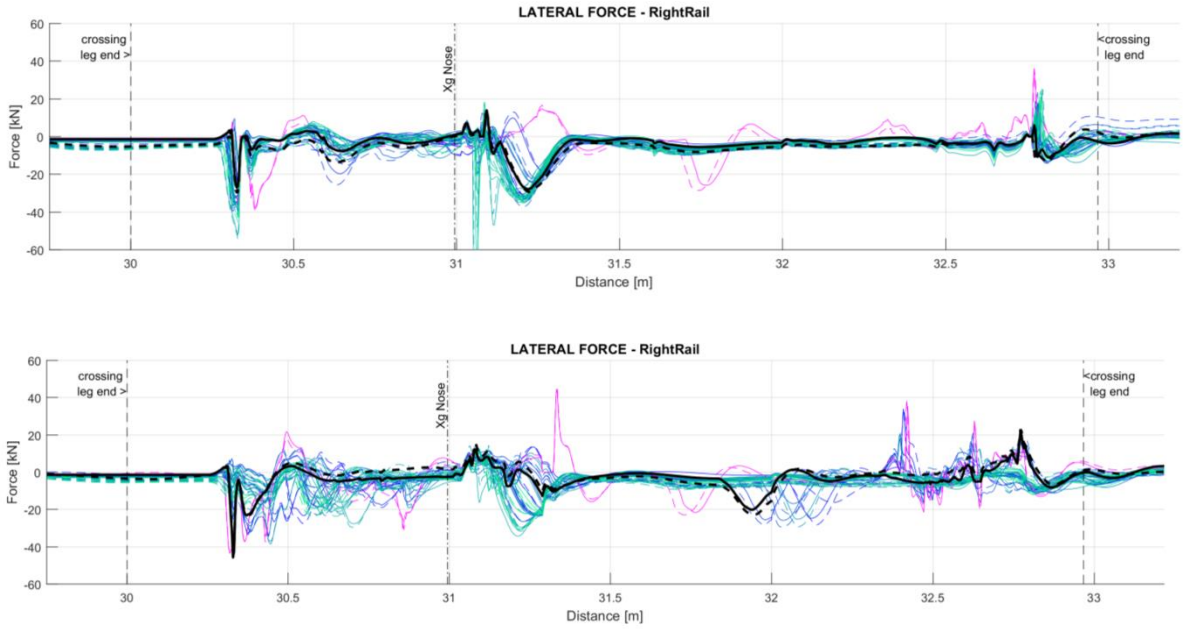

Figure 3.2.26 Wheel-rail contact lateral force along the crossing geometry for FC (top) and HC (bottom)

3.2.3.7 CONTACT STRESSES

Although the contact algorithm used for the dynamic calculation takes into account the local geometry (curvature) change in the contact, the output given are equivalent Hertzian ellipses. This can be converted into an approximate equivalent Hertzian contact stress dividing the normal force by the ellipse area. Materials are assumed to be purely linear elastic. Figure 3.1.27 shows the resulting contact stresses on along the surface of the crossing while Figure 3.1.28 shows the projection of the cumulative contact bands (exact width and location) as view from the top of the crossing. The colour of the contact band corresponds to the magnitude of the pressure: white below yield and grades or red to black as a function of magnitude above yield.

For both crossing high contact stresses can be observed on the wing rail between 30.4m and 30.9m. For the FC they appear to be partly the results of repeated transient vertical load effects following on from the harsh leg end contact conditions change partly due to modelling approximations. On the other hand the HC shows an area between 30.5 and 31m where some of the worn wheels lead to very high contact stresses. This is the fact that most worn wheel contact on the gauge corner of the wing rail where the fillet radius is small, therefore high curvature and small contact area. This would likely lead to significant plastic deformation in the area, as the Hertzian stresses are well above Yield stress.

For both crossing the highest values are seen under the influence of the P1 and P2 peak forces, very localised at various position on the crossing nose (between 31.1 and 31.2m). The worn wheels generally give rise to contact earlier on the crossing nose, with higher normal force and smaller contact radii.

Along the crossing nose the contact conditions are generally more stable and in the 'as new' configuration of the crossing (before any wear and plastic deformation occur), the contact stresses are two to three times higher than reference contact condition on the vertical CEN56 rail (see traces on the far left and right hand side of the plots). The hollow wheel and some worn wheel can clearly be seen contacting towards the field side of both wing rail and crossing nose.

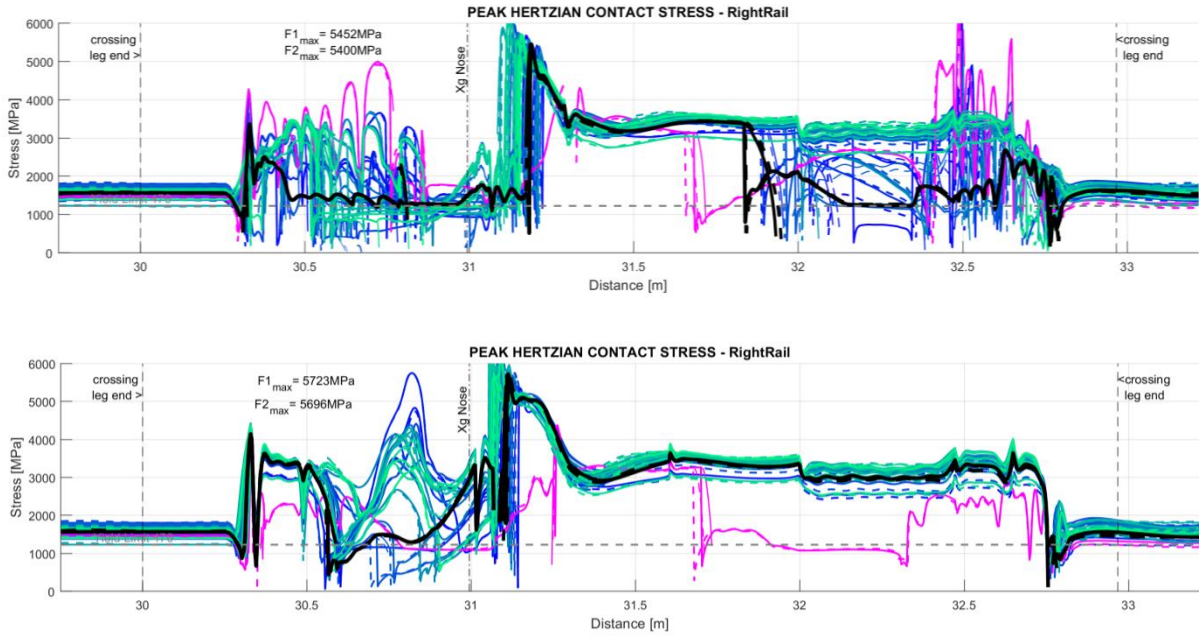

Figure 3.2.27 Wheel-rail contact equivalent Hertzian stresses for FC (top) and HC (bottom)

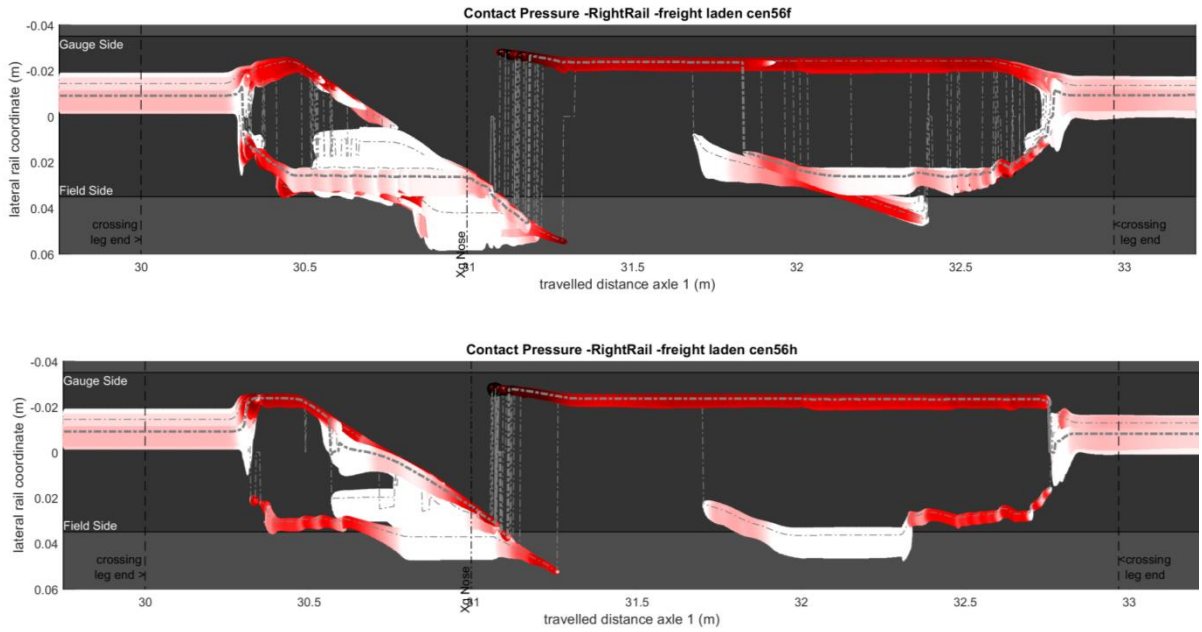

Figure 3.2.28 Cumulative contact band and coloured contact stress for FC (top) and HC (bottom)

3.2.3.8 QUALITATIVE COMPARISON WITH SITE OBSERVATIONS

In the course of the project, the University of Huddersfield had the opportunity to carry out a site visit with the support of Network Rail at a site on the East Coast Main Line to take profiles measurement and observations on a CEN56E1 vertical 1 in 13 turnout. This is the design geometry comparable to the FC presented previously. It is used almost entirely in the through facing direction on a good quality intercity track and long bearers. Traffic is dominated by locomotive hauled intercity train and mixed with freight traffic. A series of observations are made here after and discussed on the basis of photo evidence and compared with the simulation results.

3.2.3.9 OBSERVATION 1: LEG ENDS CONTACT CONDITIONS

The change in contact conditions predicted at the leg ends, can clearly be visible on site (Figure 3.2.29), where the consistent initial contact on the crown of the rail near the gauge side suddenly jumps over a short distance to a range of positions higher up the wing rail. This shift would coincide with a rapid upward motion of the wheel and some imposed dynamic loads (not measured at the time). High pressures are predicted and corresponding conformal wear is observed. Not much contact is seen on the gauge corner of the wing rail (as opposed to the simulations) because most of the traffic that ran other the geometry was passenger trains with expected consistent quality of wheels shapes.

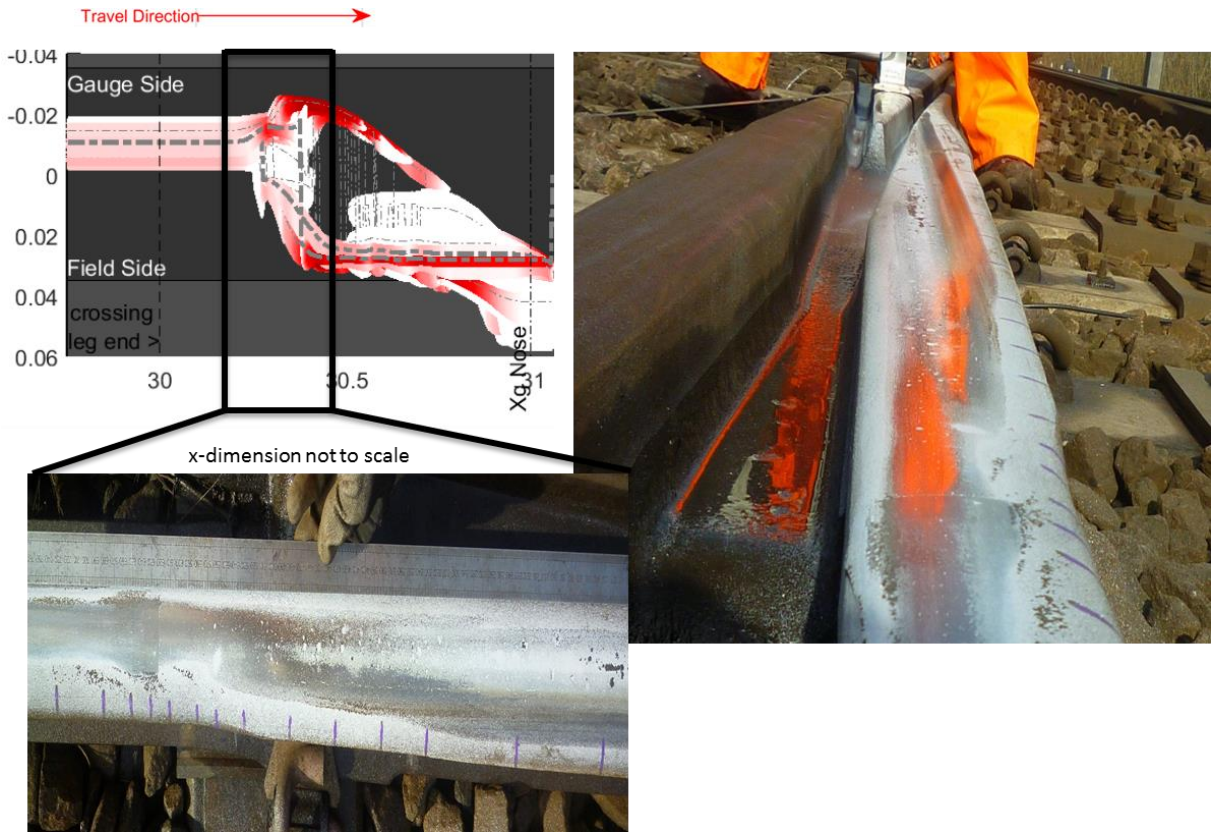

Figure 3.2.29 Leg end contact change observations on FC crossing

3.2.3.10 OBSERVATION 2: HIGH PRESSURE IN WING AND NOSE

In Figure 3.2.30 observation from the load transfer area show the white marks (high pressure and wear) on the wing rail corresponding to the run off of the wheel from the wing rail to the nose, and the corresponding white marks on the nose (high pressure and high wear) where the wheel start contacting the crossing nose. These correspond with the highlighted high pressure areas from the modelling.

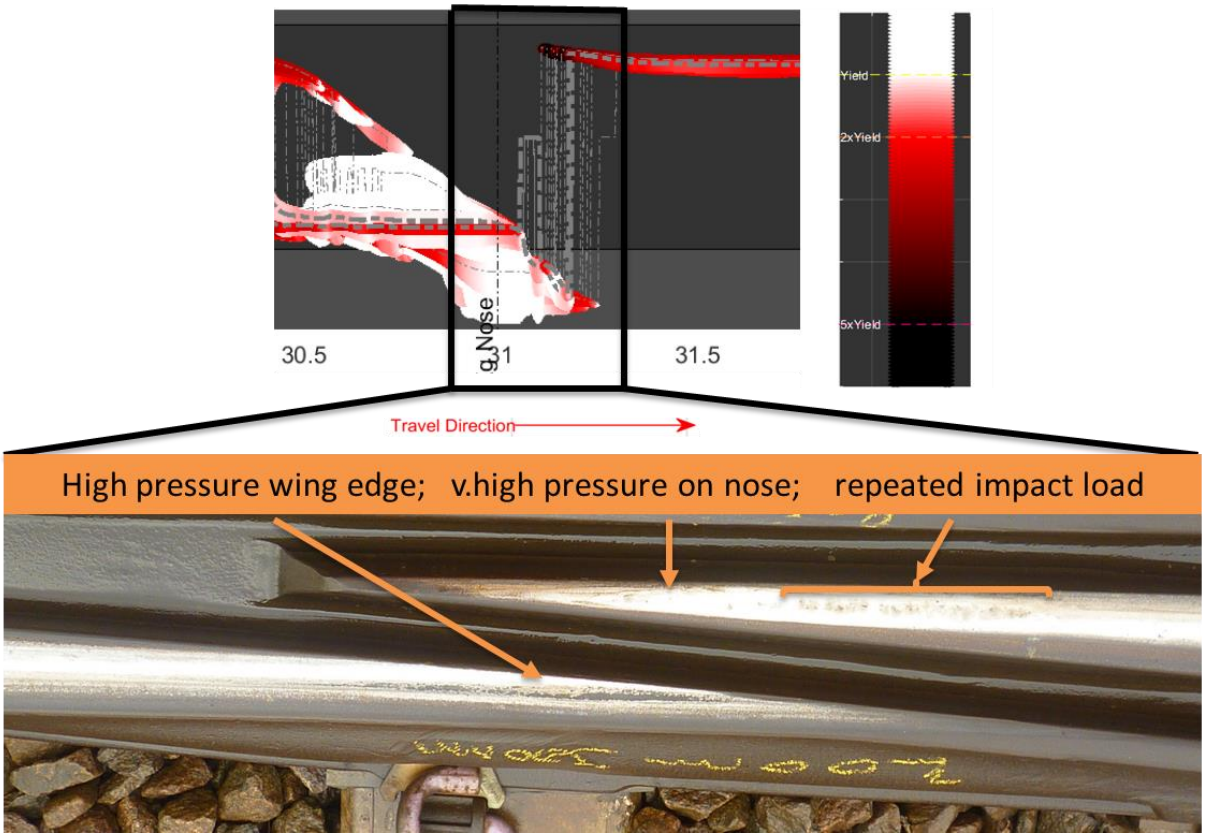

Figure 3.2.30 Contact deformation and marks in load transfer area

3.2.3.11 OBSERVATION 3: REPEATED IMPACT LOAD ON NOSE

In Figure 3.1.31 discrete material damage marks are clearly visible covering the same area covered by the predicted P1 peak loads form the simulations. These impact load can be a trigger mechanism for surface and sub-surface fatigue damage observed on this area of the crossing nose. This is not shown here but the associated shear energy in the contact is also high in correspondence with this location. Note that the overall P2 loading covers all of this area and will contribute to the overall plastic deformation/wear occurring that eventually makes the nose shape comply more with the range of wheel shapes it sees.

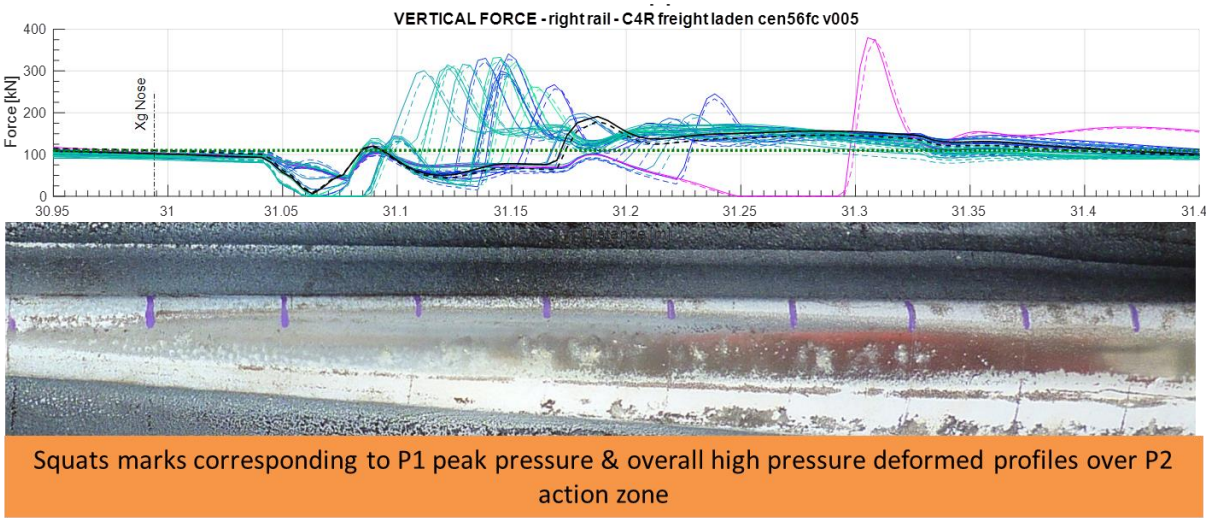

Figure 3.2.31 Crossing nose discrete damage marks in impact load transfer area

3.2.3.12 Design optimisation and statistical observations

Based on the two FC and HC design assessed in this work and the geometry generation methodology, respecting current manufacturing processes, the University of Huddersfield attempted a number of variations on the cutting operations, namely the cut-off point and slope of the secondary cut. Options in between the FC and HC did not bear any significant improvement, however one modification named OD04 and explained earlier in section 3.2.3.2 showed an overall improvement of the results. In this subsection the peak forces (P1 and P2) are compared for the entire range of simulations produced (facing/trailing, 40/80/120km/h) and for the two reference crossing (FC and HC) and the new optimised solution (OD04).

3.2.3.13 Dynamic force response (P1) as a function of speed and direction of travel for HC and FC crossings

Figure 3.2.32-34 show the peak dynamic unfiltered force (P1) for both reference crossings HC and FC as a function of the calculated equivalent dip angle (based on wheel vertical motion) for all three speeds: 40, 80 and 120km/h. On the left hand side we have the facing move results and on the right hand side we have the trailing move results. The horizontal black semi-dashed line represents the nominal wheel load for the freight vehicle results (110kN). The horizontal semi-dashed red line represent the UK P2 force limit of 320kN, normally applied to P2 filtered force, but used here as a reference. The P10 reference wheel results are highlighted with a bigger red circled marker. The P8 reference wheel results from the passenger vehicle runs are highlighted with a bigger greyscale and black circled marker. The following observations are made:

- There is a clear linear relationship between the wheel motion calculated dip angle and the resulting peak force (P1), in all cases.

- There is a clear increase of peak force with increasing speed as shown with the linear regression lines increasing slope with respect to dip angle.
- There are subtle differences due to the traveling direction but overall the force levels are very comparable.
- On both crossing the worn wheels show significant differences with respect to the reference P10 wheel.
    - On the FC the new P10 shows good performance, generally getting worst with wear of wheels (although some wheel show better performance).
    - On the HC the new P10 shows slightly worst performance than on the FC, with worn wheels being more equally distributed around (some worst some better).
- The linear regression line generally has a higher slop for the HC, indicating worst overall performances. However one wheel has been seen to show better behaviour, it is the hollow wheel.

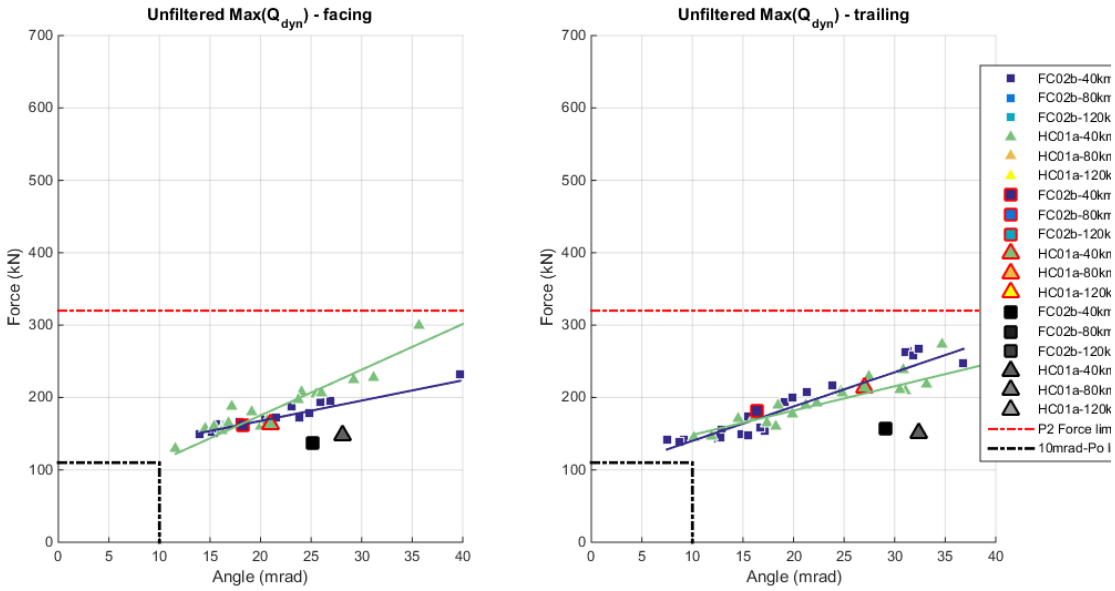

Figure 3.2.32 Peak P1 force against equivalent dip angle for HC and FC crossings at 40km/h, facing (left) and trailing (right) moves.

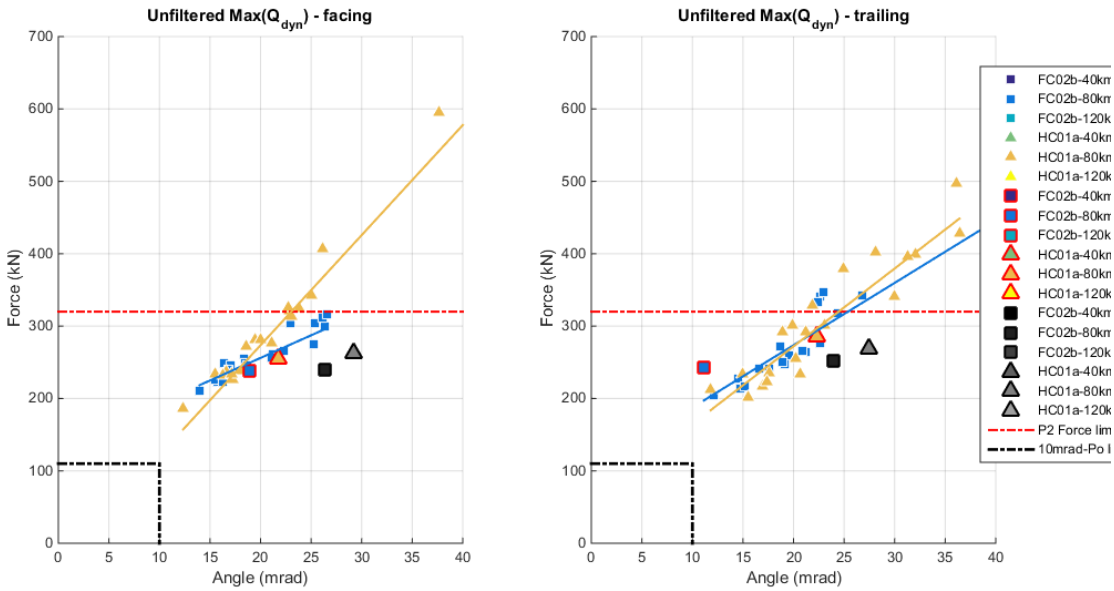

Figure 3.2.33 Peak P1 force against equivalent dip angle for HC and FC crossings at 80km/h, facing (left) and trailing (right) moves.

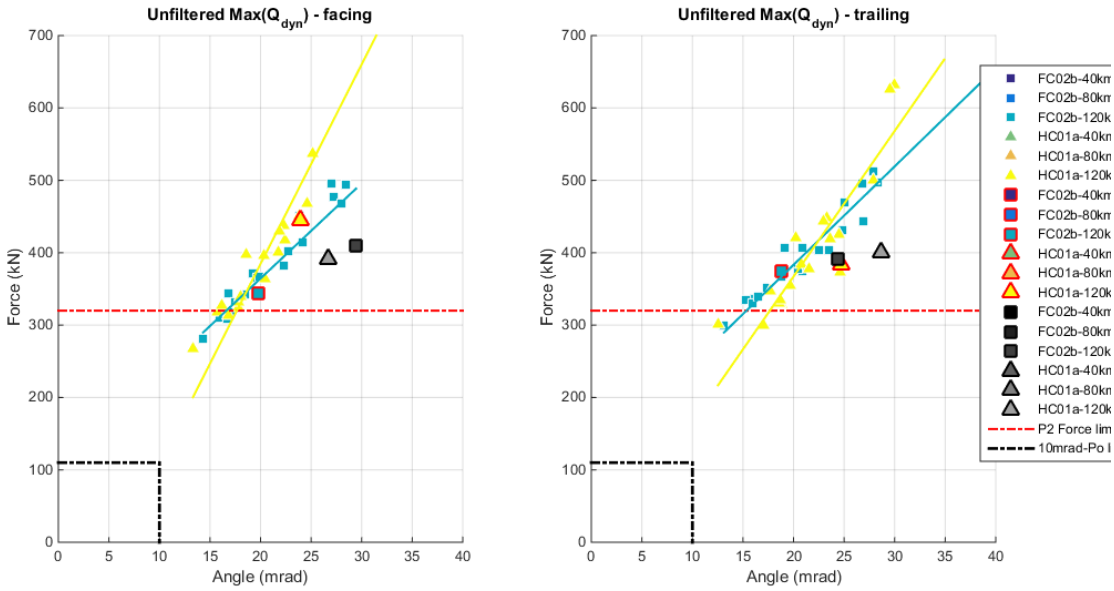

Figure 3.2.34 Peak P1 force against equivalent dip angle for HC and FC crossings at 120km/h, facing (left) and trailing (right) moves.

Figure 3.2.35 shows the peak dynamic unfiltered force (P1) for both reference crossings HC and FC as a function of the position of impact along the crossing nose 80km/h speed. On the left hand side we have the facing move results and on the right hand side we have the trailing move results. Here also horizontal lines indicate both the nominal wheel load (110kN) and UK P2 force limit (320kN). Key

location are indicated with black vertical lines: Theoretical crossing point, crossing nose and x84 the crossing angle N. The following observations are made:

- Peak force in the facing direction occur past the crossing nose (right hand side), while peak force in the trailing direction occur between the crossing nose and the theoretical crossing point, as expected.
- In the facing direction the higher forces occur very near the start of the crossing nose, corresponding to wheel transiting early and having to ramp up more suddenly up the nose slope.
- Wheel contacting later on, tend to maintain more height and have less of a rapid change of direction, contacting on the later shallower slope of the crossing nose. One exception is the hollow wheel.
- In the trailing direction the reciprocal behaviour is observed, whereby wheels transiting later on give rise to the highest force as they have to climb more to contact back onto the wing rail.
- Here also the reference P10 and P8 wheel are showing an average behaviour.

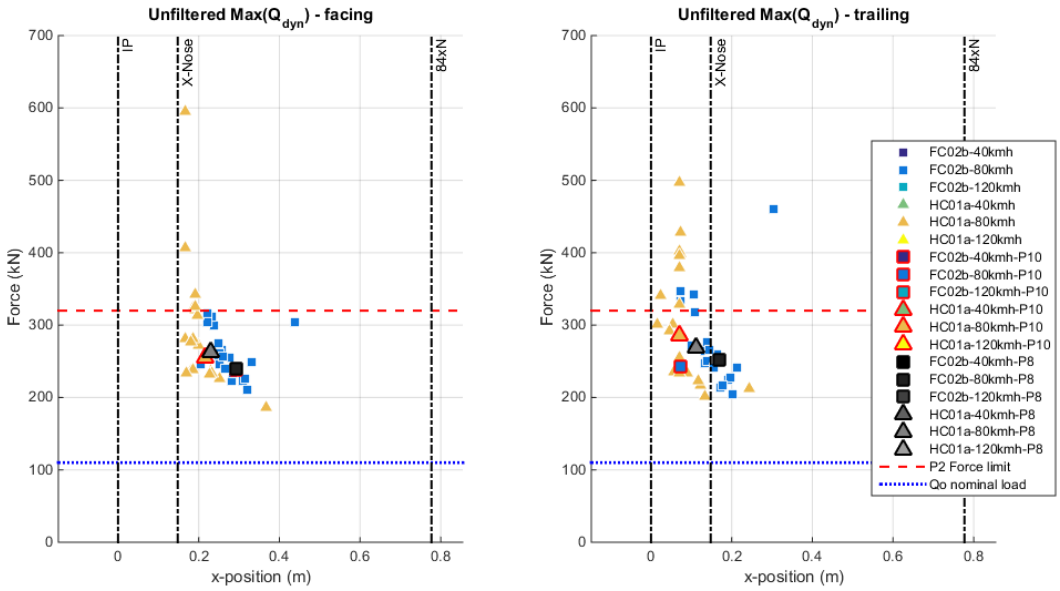

Figure 3.2.35 Peak P1 force against peak force position on HC and FC crossings nose at 80km/h, facing (left) and trailing (right) moves.

3.2.3.14 Dynamic force response (P1 & P2) as a function of speed and direction of travel for HC, FC and OD04 crossings

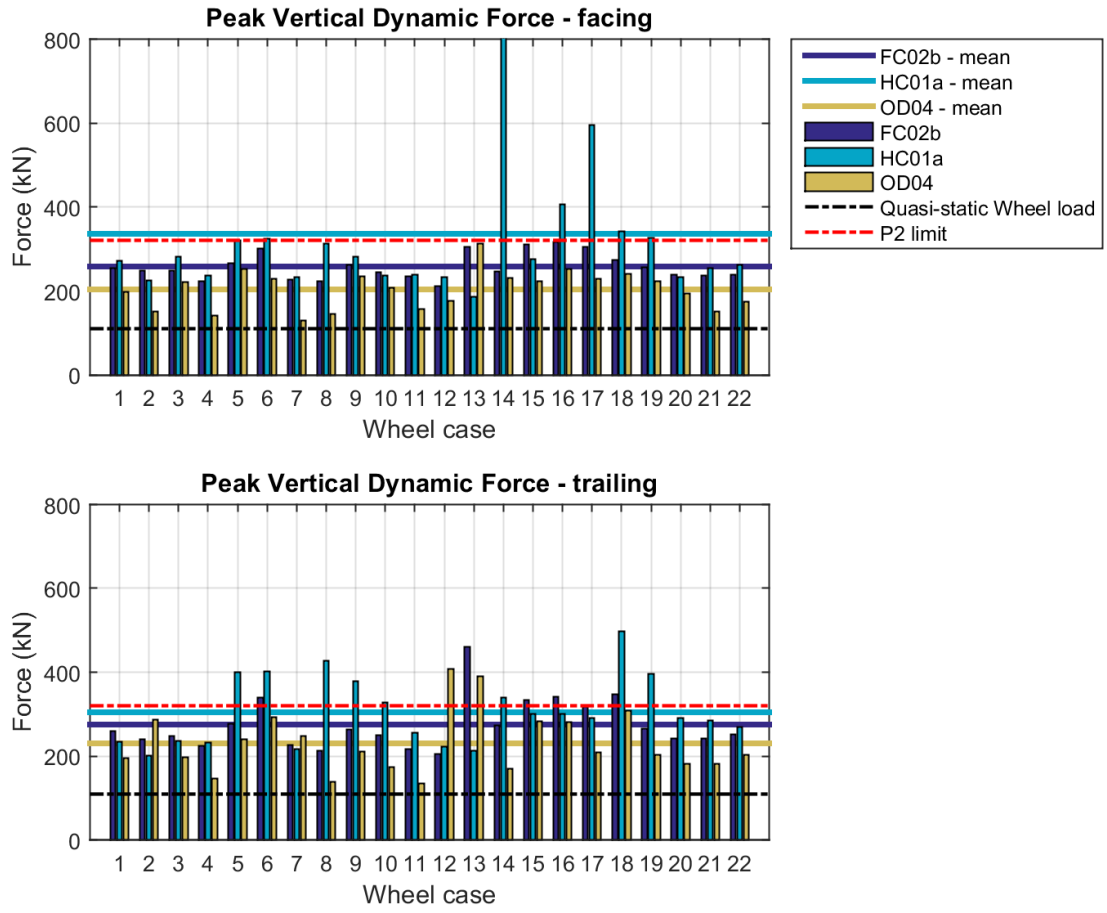

Figure 3.2.**36** shows the P1 force for all wheels and all three crossings.

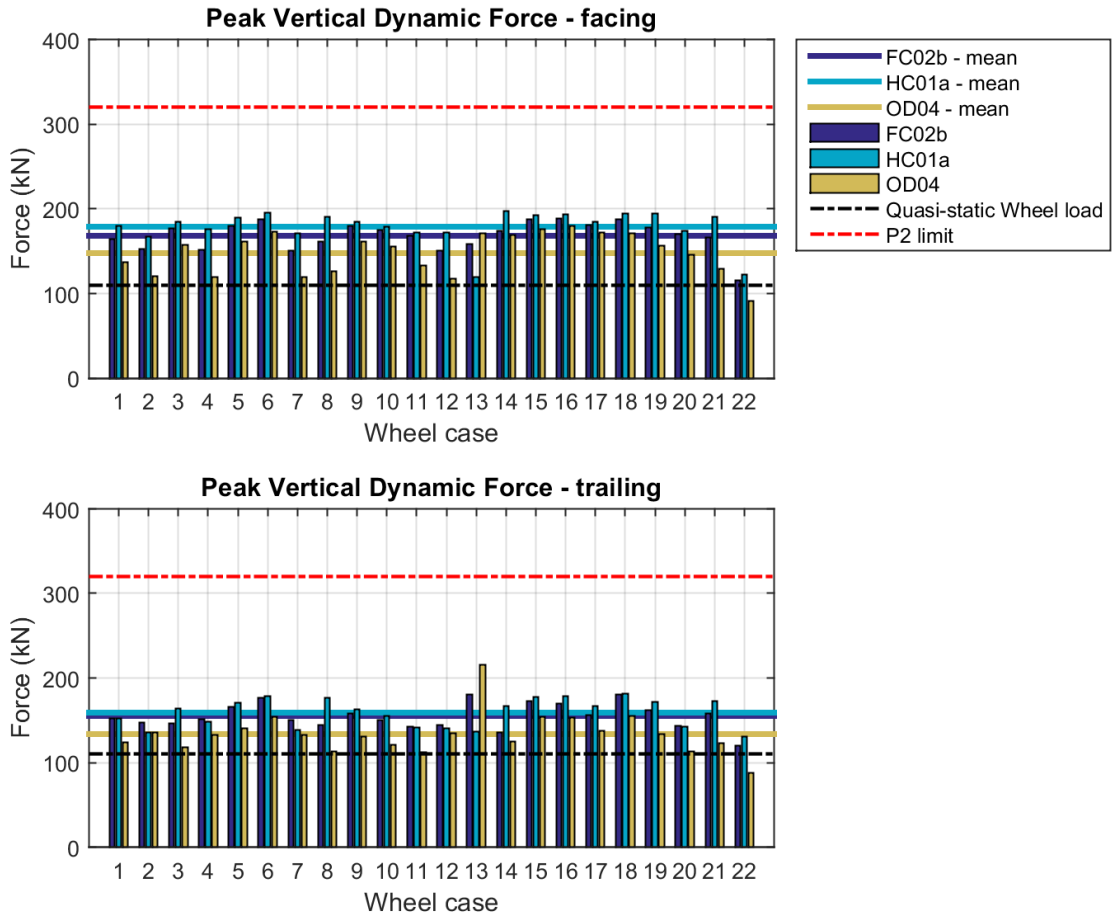

Figure 3.2.**37** shows the P2 filtered force. Table 3.2.3 summarises the average values and calculates the percentage difference with respect to FC crossing. The following are observed:

- On average the HC.design results in increased forces up to 30% (P1) and 16% (P2) with respect to FC. One specific wheel #14 leads to very high force, due to its high conical shape, resulting in an early contact with the nose at a lower vertical position. On the other hand this is the only design that shows benefits with respect to hollow wheels, because it provides a recessed position for the wheel to contact on the field side, without forcing the wheel up.
- On average the OD04 results in reduced forces up to 30% (P1) and 15% (P2) with respect to FC.
- P1 force increases with speed (80 to 120km/h) by up to 50%, 42% and 31% for FC, HC and OD04 respectively. OD04 therefore shows better adaptability to increased traffic speed.
- P2 forces are little affected by speed (80 to 120km/h) and often lead to few percents decrease as speed increases.

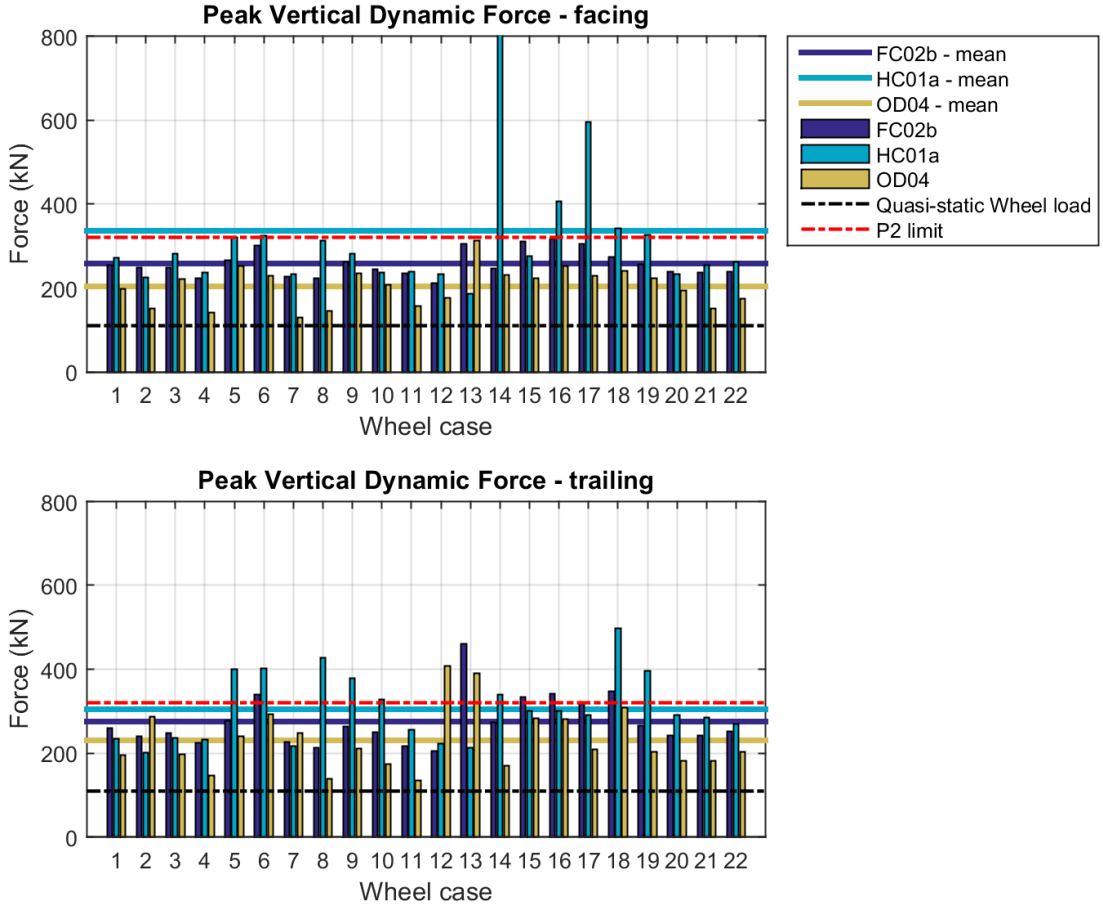

Figure 3.2.36 Peak P1 force for all cases of wheels and all three crossings at 80km/h in facing (top) and trailing (bottom) directions. Wheel #13 = hollow, wheel #21=P10 and wheel #22=P8.

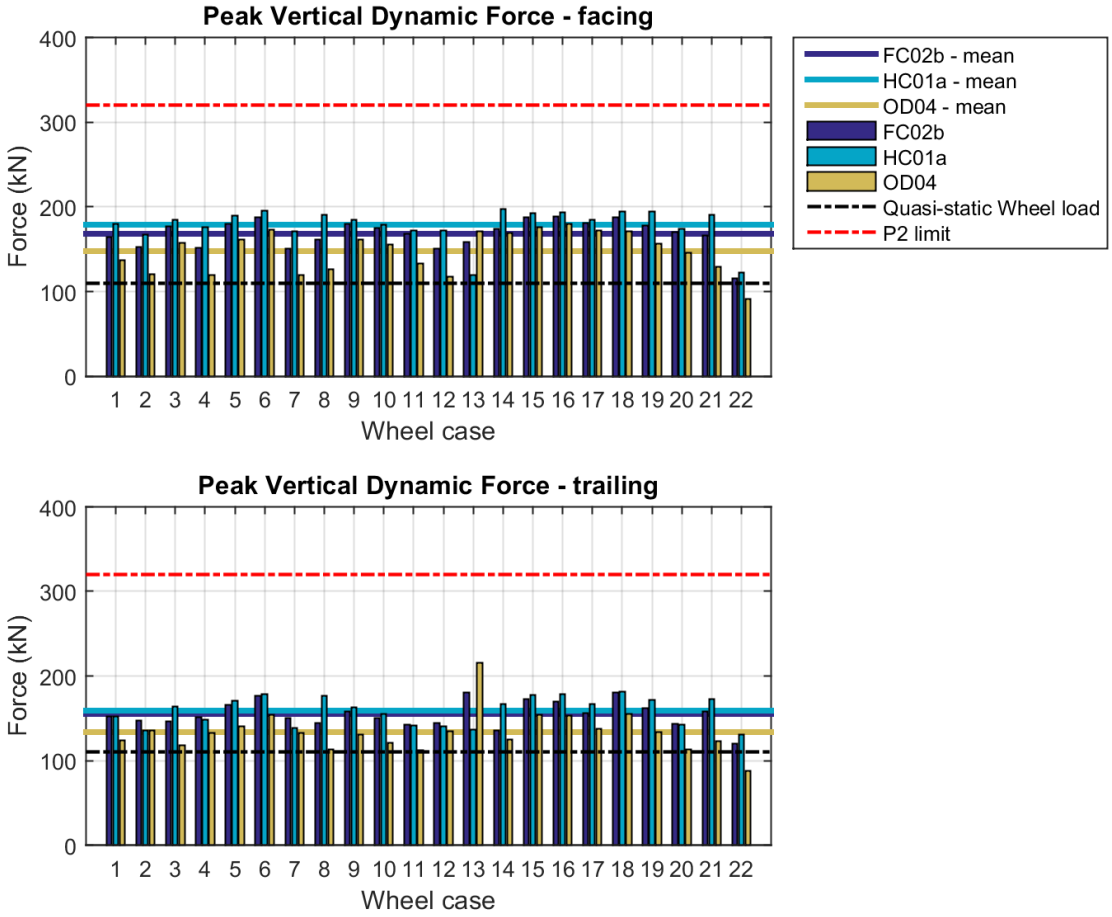

Figure 3.2.37 Peak P2 force for all cases of wheels and all three crossings at 80km/h in facing (top) and trailing (bottom) directions. Wheel #13 = hollow, wheel #21=P10 and wheel #22=P8.

Table 3.2.2 Peak P1 (top) and P2 (bottom) force comparison for all three crossing geometry

	P1 force average				% difference wrt FC		
		FC	HC	OD04	FC	HC	OD04
facing	80km/h	257.8	335.5	203.3	0%	30%	-21%
	120km/h	377.9	472.3	263.9	0%	25%	-30%
trailing	80km/h	274.5	305.5	231.1	0%	11%	-16%
	120km/h	413	433.9	301.6	0%	5%	-27%
	P2 force average				% difference wrt FC		
		FC	HC	OD04	FC	HC	OD04
facing	80km/h	168.3	178.4	147.3	0%	6%	-12%
	120km/h	162	187.7	144.2	0%	16%	-11%
trailing	80km/h	151.1	158.6	134.1	0%	5%	-11%
	120km/h	151.6	164.6	129.4	0%	9%	-15%

3.2.3.15 CONCLUSIONS ON SHAPE OPTIMISATION OF CROSSINGS

- Shape of the crossing geometry and how it interacts with the wheel shape has a big influence on the resulting unfiltered dynamic force (P1), that leading to rail material damage. There is less of an influence on the filtered (P2) force, that leading to support and ballast degradation.
- A representative range of wheel shapes needs to be considered to assess the performance of a crossing geometry, in particular high conicity wheels and hollow worn ones. Anterior knowledge of traffic types and states of wheel can enable a better comprehension of the performance of a crossing and specific instance (wheel-crossing shape combinations) to be improved.
- Some changes to the machining operation of the crossing rolling surface can lead to significant improvement in performance against high frequency impact load. The benefit is less observable on the supporting components and these needs to be mitigated through alternative methods, for example support resilience improvement (see following section 3.2.4 and 3.2.5). However both types of improvements have a mutual benefit.

3.2.4 OPTIMISATION OF RESILIENT SUPPORT IN BALLASTED TRACK CROSSING PANELS

The potential benefit of support optimisation has been demonstrated within INNOTRACK project, however this numerical optimisation was carried out with idealized constant moving track model [3.2.32]. Two S&Cs (UIC60-760-1:15) were eventually installed at Eslöv, Sweden and tested under dense traffic conditions, one of which had lower vertical stiffness and resilient baseplates. The modification of track support stiffness in the crossing panel indicates a high potential and advanced simulation techniques can be used to help identify such optimum designs. The Results showed in particular that reducing the track stiffness from 500 to 85 kN/mm leads to significant lower normal contact forces, and this reduction increases further with increasing speed. The worked carried out by the University of Huddersfield in this project aims to advance on the methodology used in Innotrack by introducing a discrete Finite Element description of the track support to show how this optimization process can be used more effectively to optimize the local pads properties in the crossing panel as to lower the risk of specific damages highlighted earlier in this project [3.2.1].

The work carried out in the project has been prepared in the form of a journal paper so that it could be submitted for publication. To not conflict with the requirement of originality of the journals only the summary and key results are presented here, as well as key information to be able to trace the eventual publications (under review at the time this is published).

3.2.4.1 PAPER SUMMARY

Turnouts are a key element of the railway system. They are also one part of the railway system with the highest number of degradation modes and associated failures. There are a number of reasons for this, including high dynamic loads resulting from non-linearities in the rail geometry and track support stiffness. The main aim of this study is to compare direct and indirect fixing in the context of the

crossing panel. A methodology to optimise the pad stiffness has been proposed in order to achieve a decrease in the indicators of the most common failure modes. A three-dimensional vehicle/track interaction model has been established, considering a detailed description of the crossing panel support structure. Genetic algorithm has been applied to find the optimum pad combination for various cases of travelling direction, travelling speed and support conditions.

3.2.4.2 ILLUSTRATION RESULTS

Figure 3.2.38 shows the type of results obtained from the optimisation methods for the direct fixing (top) and indirect fixing (bottom) turnout designs. Left hand side plots are showing the combination of rail pad stiffness as changed under the crossing panel in two difference locations. Black dots are the attempted combination by the optimisation routine, magenta the initial start point and the red dot the final optimised values. On the right hand side we have the initial (dashed line) overall stiffness along the crossing panel which increases mainly due to the crossing increased bending properties, while the adaptation of the rail pad stiffness enables a smoother overall stiffness profile along the panel.

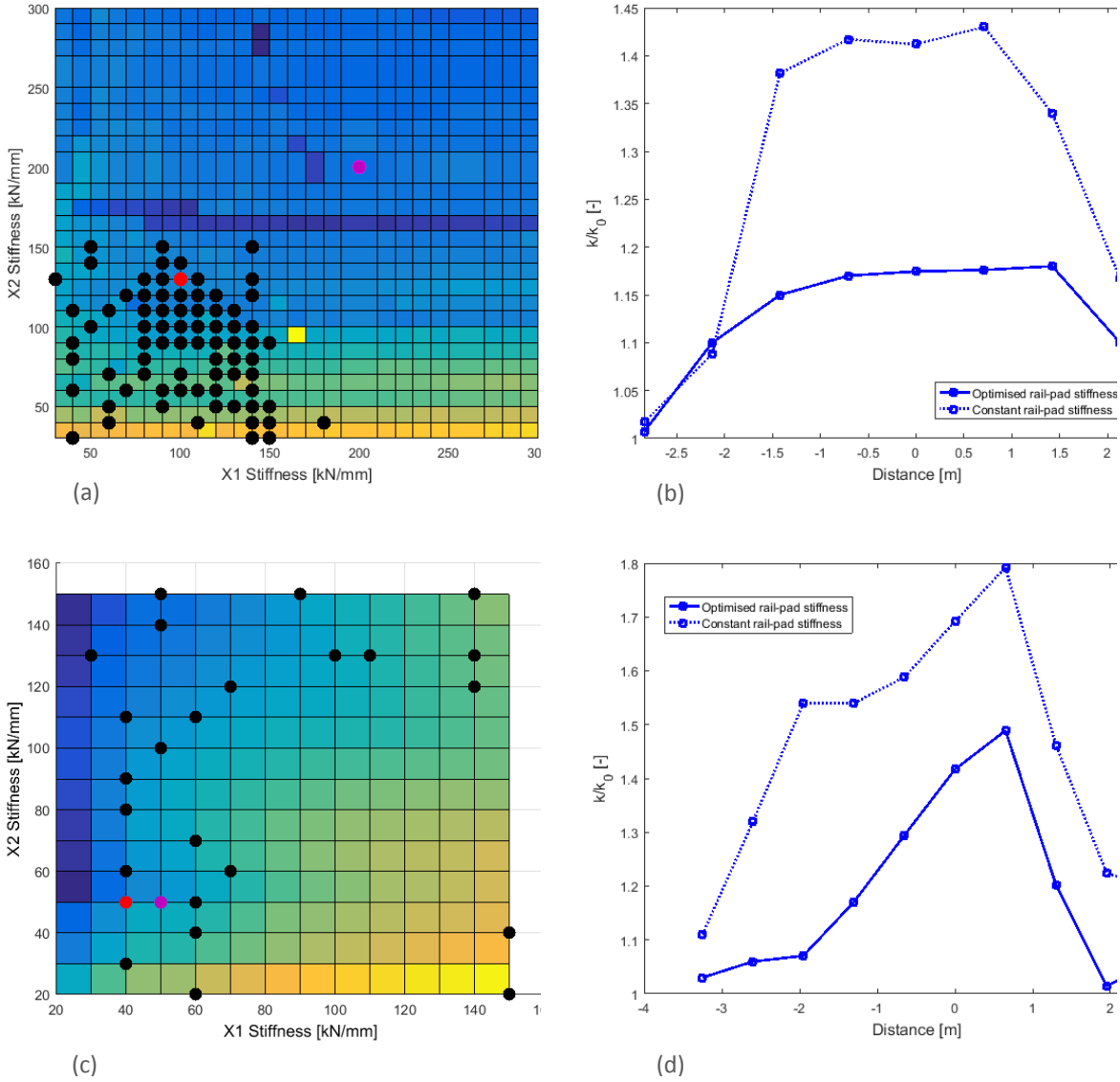

Figure 3.2.38 Example of results: function value and optimisation parameters for (a) direct fixing and (c) indirect fixing; track stiffness relative to the line track stiffness for (b) direct fixing and (d) indirect fixing [Speed = 80 km/h; Equivalent support stiffness=100 kN/mm]

3.2.5 Optimisation of support stiffness in ballasted track crossing panels using sleeper longitudinal linkages

It has been demonstrated how it is possible to improve significantly the performances of a given crossing panel changing the rail pad characteristics. In order to achieve even better results, it is necessary to go in the direction of a uniform support as in a ballastless track system. A medium-term solution has been proposed and consists in linking longitudinally the sleepers below the load transfer area in order to achieve a more continuously supported track system. Potential benefits may include reduction of sleeper vertical and lateral accelerations as well as forces transmitted to the ballast layer

with potential reductions in differential settlement. Another beneficial effect may be a reduction in sleeper roll limiting uneven loading between the left and right side on turnout with wide bearers. The practical details of how to implement such a solution are not discussed here and the work is intended to remain theoretical at this stage. It is however envisaged that this could be done rather simply by retro-engineering the desired properties at a low cost, so as to enhance ballasted S&C to behave more alike a slab track solution, without a complete renewal and associated costs.

This technology has been used in different contexts where an abrupt change in track stiffness may lead to non-uniform vertical displacements and, therefore, non-uniform dynamic loading. An example is transition zones, for example transition between slab track and ballasted track, transition between bridge abutment and ballasted track and transition between box culvert and ballasted track. In these cases, the main damage mechanisms are rail corrugation and wear, fatigue in the rail fastening system, cracked sleepers, in addition to non-uniform non-recoverable deformation of the ballast layer (i.e. called differential settlement).

For example, in case of high speed transition, Sañudo [3.2.42] shows a comparison of various track designs, including auxiliary rails, lighter sleeper and sleeper length variation, in terms of sleeper displacements and stresses on ballast. The best performance is obtained when extra-long sleepers in combination with additional rails are used.

Shahraki [3.2.43] also presents a comparison of different solutions at transition zones, such as auxiliary rails, longer sleepers and improved support conditions. Vertical deflection, acceleration and stresses at the rail and the ballast layer are considered and results show that auxiliary rails reduce the track dynamic characteristics due to the abrupt change in stiffness.

A gradual change in track stiffness by installing the auxiliary rails and placing the pads has been proven useful in Kang [3.2.44] in the context of transitions between precast slab track and ballasted track.

Similarly, Xin [3.2.45] analysed the transition between fixed and floating slab track, where the change in track modulus leads to a dynamic amplification factor of 1.76. A gradual increase in track modulus using additional rails in the low-stiffness side and gradual change in rail-pads in the high stiffness side has been demonstrated effective to reduce wheel/rail contact forces and rail deflection.

3.2.5.1 METHODOLOGY

The vehicle/track interaction model used in this pilot study is shown in Figure 3.2.39, and includes a number (2 or 4) of vertical connections (called ‘links’ hereafter) between adjacent sleepers under the load transfer area. Only vertical dynamic loads are considered in this initial study. The vertical irregularity input representing the vertical crossing geometry is calculated as explained in Grossoni [3.2.46].

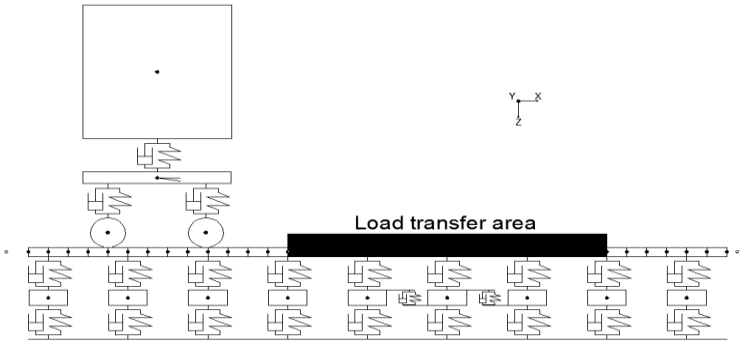

Figure 3.2.39 Two-dimensional vehicle/track interaction model with two longitudinal sleeper connections

The main input parameters adopted for the track system are as follows:

- Crossing type: CEN56 1 in 9.25 acute crossing;
- Rail type: 56E1 vertical profile;
- Sleeper type: concrete sleepers. The mass are variable between circa 410 kg and 470 kg as the length is not constant;

A freight vehicle is considered in this study and the main input data is as follows [3.2.47]:

- Unsprung axle mass: 1500 kg;
- Axle load: 22.5 t;
- Primary linear suspension stiffness: 10 MN/m;
- Secondary linear suspension stiffness: 6 MN/m.

Different conditions in terms of vehicle speed, number of links and vertical stiffness are considered, as following:

- Vehicle speed: 60/90/120/150 km/h;
- Number of links: 2/4;
- Support stiffness: 40/80/150/200 MN/m (to cover soft, typical and stiff track-bed [3.2.48]);
- Vertical link stiffness: 100/150/300/450 MN/m.

3.2.5.2 RESULTS

Figure 3.2.40 shows an example of the time history of ballast forces at the crossing nose for different vertical link stiffness, considering the speed equal to 90 km/m and the support stiffness equal to 80 MN/m.

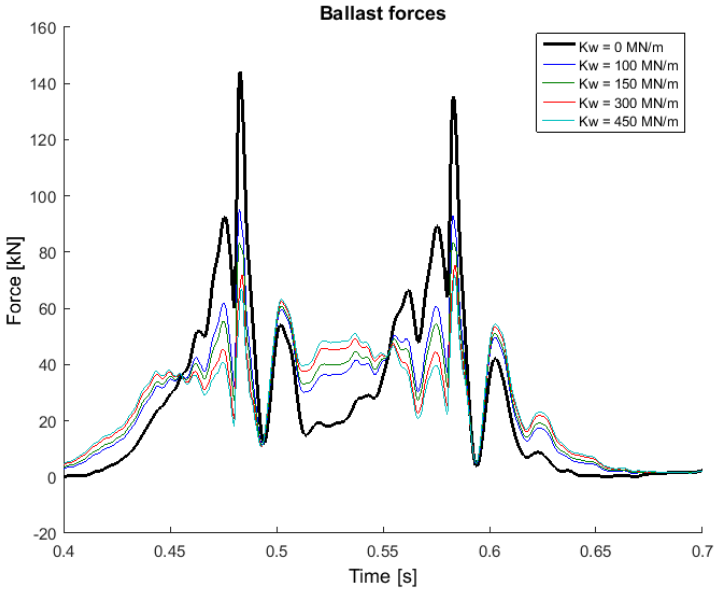

Figure 3.2.40 Time history of ballast forces varying the bar stiffness Kw (speed = 90 km/h; number of links = 2; Kb=80 MN/m)

From Figure 3.2.40, it is possible to conclude that the vertical connection between sleepers helps lower the ballast forces, as expected. This diminution depends on the stiffness value, with reduction from ca. 35% in case of low stiffness (100 MN/m) to ca. 50% in case of high stiffness (450 MN/m). Moreover, introducing a connection between sleepers is beneficial to homogenise the ballast force levels across the area considered, similarly to slab track systems [3.2.49].

Figure 3.2.41 shows the percentage difference of contact forces, rail-pad forces, support forces and sleeper acceleration with respect to the baseline scenario varying the number of links, the support stiffness and the speed. A negative difference means a decrease and a positive difference an increase in the quantity considered.

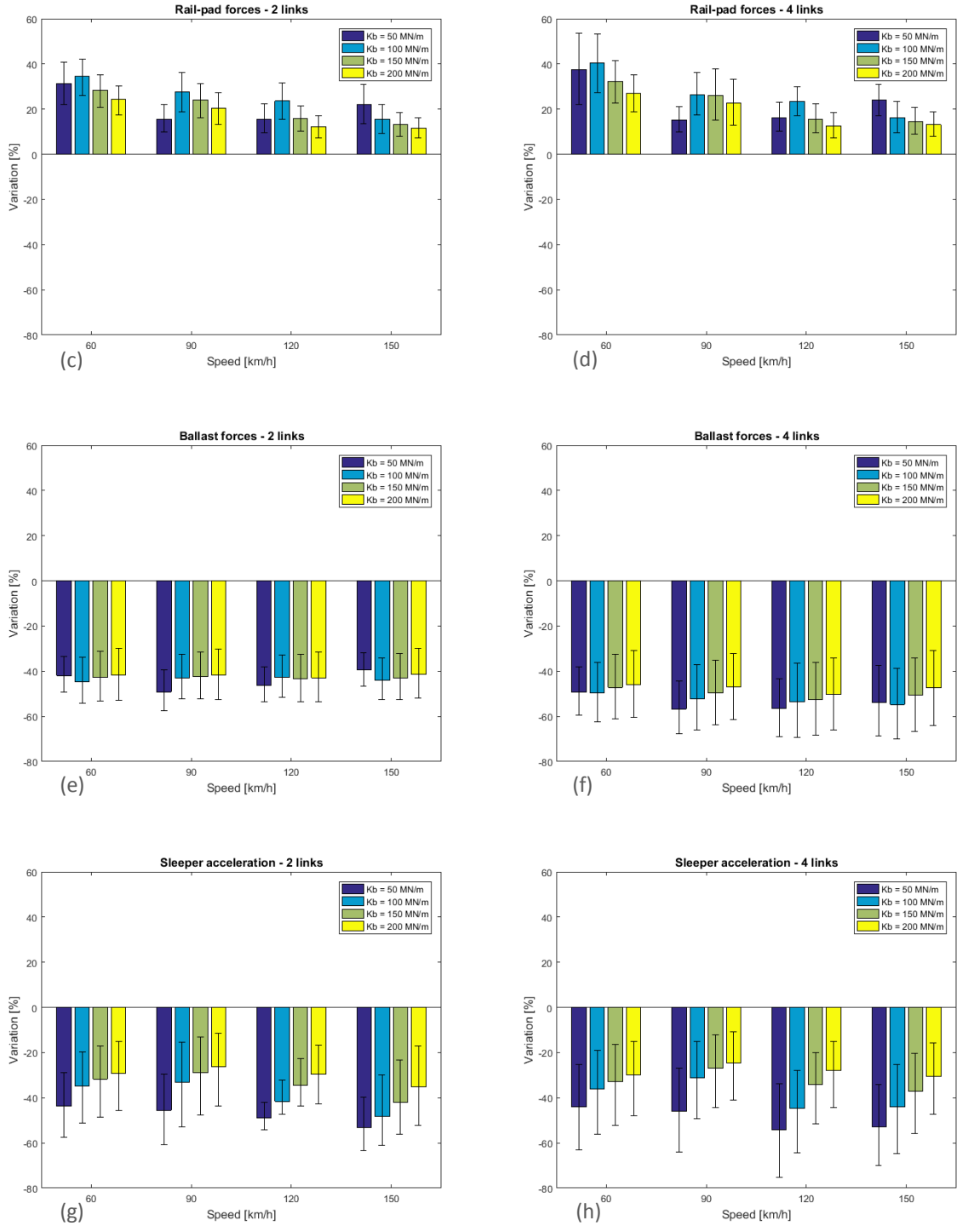

Figure 3.2.41 Percentage difference for (a,b) contact forces; (c,d) rail-pad forces; (e,f) ballast forces; (g,h) sleeper acceleration with respect to baseline scenario varying the travelling speed and the support stiffness (left column refers to 2 links and right column to 4 links)

The main conclusions that can be drawn from Figure 3.2.41 are:

- Contact forces: the change in the contact forces is reasonably negligible in case of two links for all the speed and support stiffness values considered. Nevertheless, the maximum reduction starts becoming noteworthy with four links at the highest speeds (i.e. 120-150 km/h) and at the lowest support stiffness values considered (i.e. 50-100 MN/m), reaching 15-20% decrease.
- Forces in rail-pads: generally speaking, there is an increase in the rail-pad forces in all the scenarios investigated. The increase is higher in case of low travelling speeds (60-90 km/h) and low/medium support stiffness (50-100 MN/m). This can be explained with the fact that a decrease in the support stiffness leads to high frequency vibrations that are absorbed by the pad layer. Therefore, as stated previously, this mid-term solution requires further investigations for an adequate fastening system in order to avoid sleeper fatigue.
- Force in the support: a remarkable decrease of forces in the support appears when sleepers are connected longitudinally. As pointed in the previous Section, there is also a beneficial effect of homogenising the force level along the interested area, similarly to the slab track concept. The effect of speed is almost negligible. On the other hand, the support stiffness becomes influential when 4 links are considered. The additional strength given by the vertical connection is beneficial especially in case of soft track bed.
- Sleeper acceleration: in addition to the decrease of forces in the support, further reduction in sleeper accelerations are found observed. The acceleration are further reduced for increasing speed and increasing number of links, while the apparent benefit is reducing with increasing support quality for a given speed value, as expected.

The last two quantities considered (force in the ballast and sleeper acceleration) are generally recognised as the main driver for the ballast settlement [3.2.50-3.2.51].

3.2.5.3 CONCLUSIONS

A pilot study has been carried out in order to assess the potential benefits of linking the sleepers longitudinally along the load transfer area at a crossing panel. This solution has been already applied and proven successful in situations where an abrupt change in track stiffness may lead to non-uniform vertical displacements and, therefore, non-uniform dynamic loading (e.g. transition zones).

A vertical vehicle/track interaction model was established considering half of the car-body, a bogie and two wheelsets. The influence of track parameters, including number of vertical links, vertical stiffness of the links and track support stiffness, and the vehicle parameters, including travelling speed, has been assessed considering contact forces, rail-pad forces, ballast forces and sleeper acceleration. The first quantity is generally recognised as the main drive rail-surface damage, such as squat, RCF and wear, while the last two as the main driver for the ballast settlement.

Results show that the highest reductions occur in ballast forces and sleeper accelerations, especially in case of soft track bed. Therefore, the proposed solution may be beneficial to help preventing differential settlement, geometry degradation, void generation and casting fatigue, and therefore a

mitigation measure could be envisaged on a case by cases basis to react against these specific problems. On the contrary, there is an important increase in the rail-pad forces. Therefore, as stated previously, this mid-term solution requires further investigations for an adequate fastening system in order to avoid sleeper fatigue.

3.2.6 MATERIAL CONSIDERATION

3.2.6.1 MATERIAL OPTIMISATION AT NETWORKRAIL

The optimisation of crossing profiles and/or of the materials they are made of requires consideration of the designs in current use which, based on the practice within the UK network, can be classified as:

- Fully fabricated crossings**:** As the name suggests, these are made by machining the appropriate rolled rail section to produce a point rail and a splice rail that are then secured together using high tensile steel bolts or multi-groove locking pins to form the crossing nose. The wing rails are also produced from rolled rails and are secured to the crossing using bolts or multi groove pins. (Figure 3.2.42)

Figure 3.2.42 Fully Fabricated Crossing [3.2.52]

- Part fabricated crossings**:** These crossings are also known as semi or part welded crossings and can be sub-categorised according to the process employed for the manufacture of the crossing nose; welded, cast, and forged. (Figure 3.2.43)

Figure 3.2.43 Part Fabricated Crossing [3.2.52]

- Cast monobloc crossings: These crossings are manufactured from cast steel as a single unit to which the pearlitic rails of the abutting track can be joined directly or through the use of a stainless insert that can be flash-butt welded to the cast austenitic manganese steel and to pearlitic rails. (Figure 3.2.44)

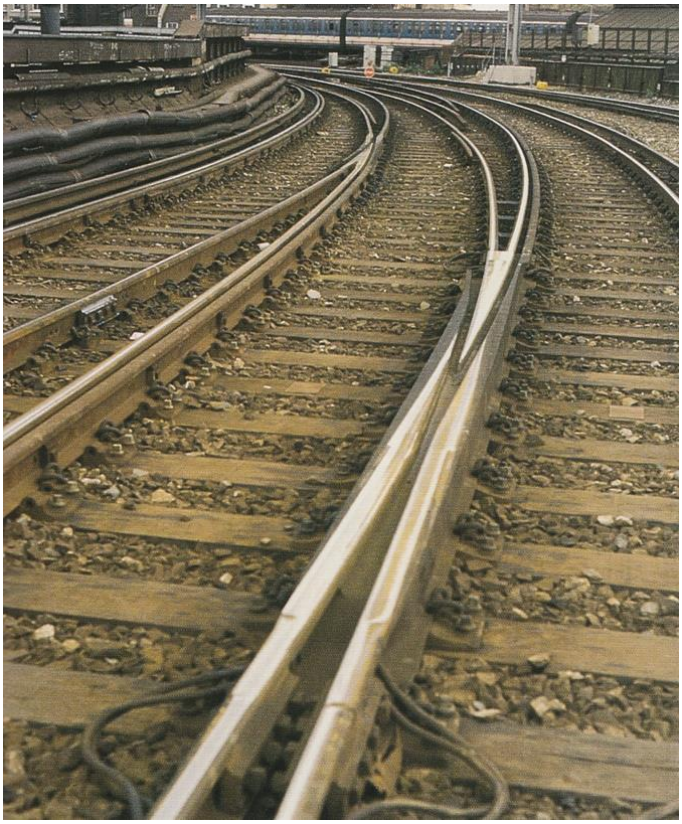

Figure 3.2.44 Cast Monobloc Crossing [3.2.52]

It is also worthwhile to establish the magnitude of potential usage of the various types of crossings and this is shown in Figure 3.2.45 below for the UK network [3.2.52].

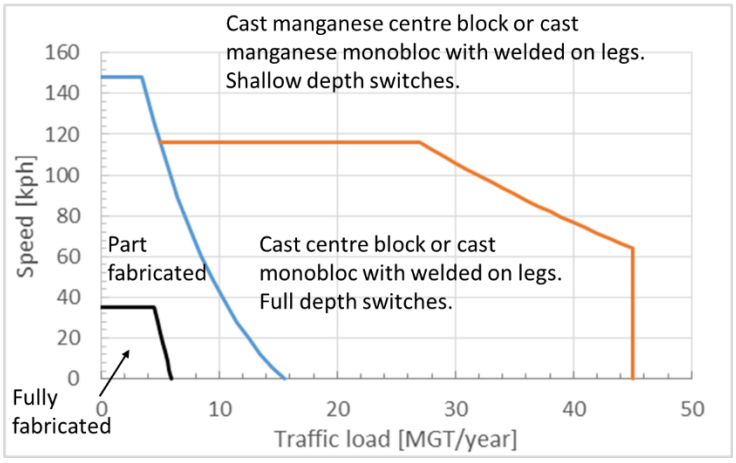

Figure 3.2.45 Usage Criteria for Various Crossing Types in UK

The optimised selection of material needs to be based on knowledge of expected degradation mechanisms. Based on both in-service observations and dynamic simulation of the wheel contact with various parts of the crossing layout, the commonly associated degradation mechanisms are wear, plastic deformation, and rolling contact fatigue. The available materials are assessed briefly with reference to their resistance to these degradation mechanisms.

Table 3.2.3 Comparative Metallurgical Properties of Available Rail Steels

Steel Grade	Fracture Toughness [MPa m1/2]		Max. Fatigue crack growth rate, [m/Gc]		Fatigue strength	Residual stress	Hardness	Tensile Strength	Elongation
	Min. single value	Min. mean value	Delta K= 10, [MPam1/2]	Delta K= 13, [Mpam1/2]		[MPa]	[HBW]	[MPa]	[%]
R200	30	35	Not specified		5X106 Cycles for total strain amplitude of 0.00135	<250	200-240	680	14
R220	30	35	17	55		<250	220-260	770	12
R260	26	29	17	55		<250	260-300	880	10
R260Mn	26	29	17	55		<250	260-300	880	10
R320Cr	24	26	Not specified			<250	320-360	1080	9
R350HT	30	32	17	55		<250	350-390	1175	9
R350LHT	26	29	17	55		<250	350-390	1175	9
R370CrHT	26	29	17	55		<250	370-410	1280	9
R400HT	26	29	17	55		<250	400-440	1280	9
HP335	27	31	<12	<34	Compliant	<250	335-380	1150	7
B320	Data not available but believed to be compliant with current specifications					<250	320-340	1100	14
B360						<250	360-390	1200	13
DOBAIN380						<250	380-420	1250	10
DOBAIN430						<250	>430	1400	9

3.2.6.2 RAIL MATERIAL

Vignole Rails used in the manufacture of the crossing layouts are governed by EN13674-1:2011 and the key properties are summarised in Table 3.2.3 Comparative Metallurgical Properties of Available Rail Steels below [3.2.49] and includes available data for some new rail steel grades developed by the major rail manufacturers but yet to be incorporated into EN 13674.

Hardness is often regarded as a key property of the rail steels and the relationship between this parameter and the three key degradation mechanisms of plastic deformation, wear, rolling contact fatigue. The data included in the relationships shown, include the grades specified in EN13674-1:2011 and a few additional grades developed by the major manufacturers and in use within selected railway networks.

Although tensile properties characterise most steels, and the older UIC rail steel grades were based on tensile strength, current rail steels are characterised by their hardness. At the same time determination of tensile strength and elongation are mandatory requirements of qualification and acceptance tests within EN13674-1 2011, which requires the derivation of predictive equations based on composition. However, the standard does not specify yield or 0.2% proof strength which could provide a better indication of the resistance of the grade to plastic deformation. The relationship between rail hardness and 0.2% proof strength is shown in Figure 3.2.46 for a wide range of rail steels [3.2.53].

Assessment of the resistance to wear and RCF (Rolling Contact Fatigue) of the full range of rail steel grades in commercial track is not a practical proposition because of the difficulty of ensuring controlled wheel-rail contact conditions on all rail grades. Hence controlled comparative tests have been undertaken using twin disk type test arrangements by many rail manufacturers and research organisations. The relationship shown in Figure 3.2.47 is based on a very large volume of data gathered over decades of testing on a twin disc test facility at a major rail manufacturer [3.2.53]. The similarity of the relationship between the steel grades specified in EN13674-1:2011 and a much wider range of pearlitic steels provides increased confidence in the dependence of wear resistance on hardness of pearlitic steels. Although the test programme spanning many years was undertaken on the same machine, subtle differences in procedure may have occurred and are reflected in the apparent scatter of results. Similar tests have also been undertaken on some novel hypereutectoid compositions in the as rolled and heat treated conditions and the results show the significantly greater resistance to wear of these grades even at the lower hardness values of the as rolled versions, Figure 3.2.48. Novel low carbon carbide-free bainitic steels, tested in a similar manner revealed a level of wear resistance similar to that of the standard grade (R260) but slightly lower when compared to EN pearlitic grades of similar hardness.

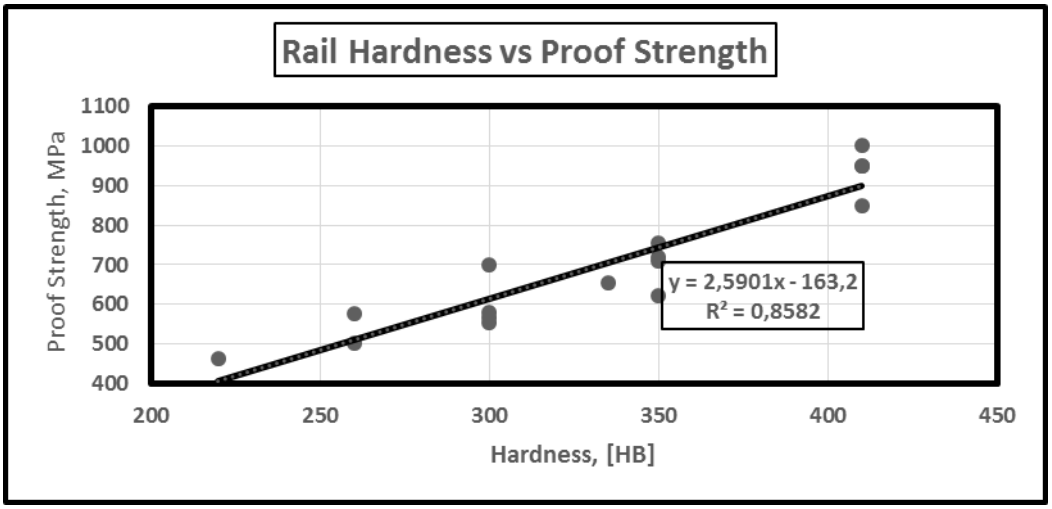

Figure 3.2.46 Relationship between Hardness and Proof Strength

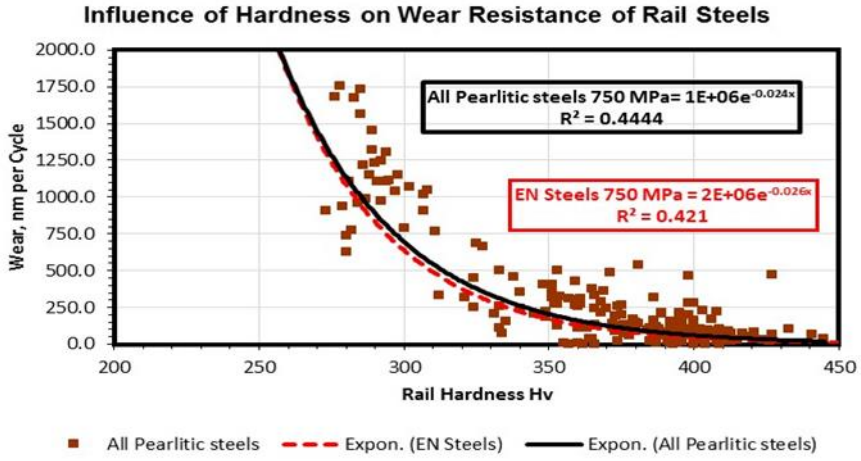

Figure 3.2.47 Relationship between Hardness and Wear Resistance

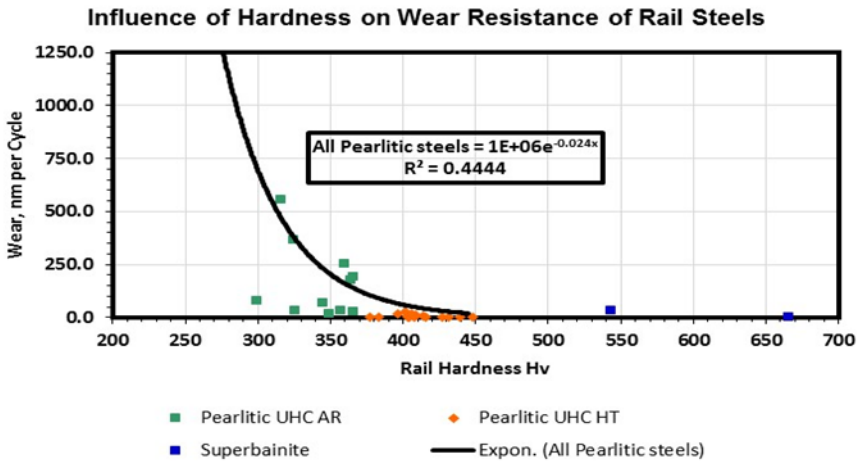

Figure 3.2.48 Relationship between Hardness and Wear Resistance - hypereutectoid

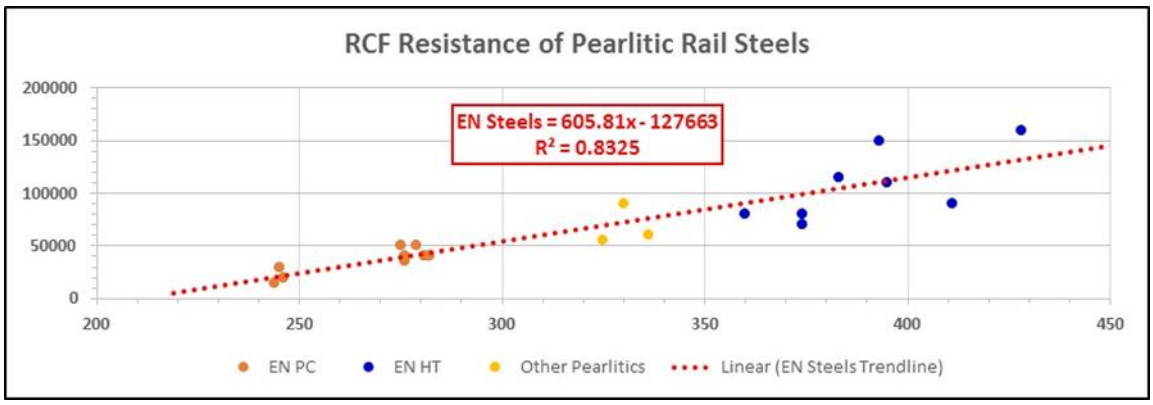

Figure 3.2.49 Relationship between Hardness and Resistance to RCF

The controlled tests to establish resistance to RCF were undertaken on the twin disc machine at a contact pressure of 900 MPa and the number of cycles to crack initiation was recorded. The results, shown in Figure 3.2.49, clearly indicate the strong positive influence of steel hardness on the resistance to RCF. A range of novel hypereutectoid steels in the as rolled and heat treated condition were also tested in a similar manner and the results revealed a near parallel relationship displaced to higher levels of resistance to RCF.

It is, therefore, apparent that a range of rail steels with greater resistance to the key degradation mechanisms of wear, RCF, and plastic deformation have been available for use in the manufacture of crossing layouts. However, the adoption of premium harder grades of rail steels has been thwarted by the key disadvantage of easy weld repair ability and restorability of such grades and points to the need for focused research. However, the advances in additive manufacturing offer the potential of a composite crossing nose or centre blocks welded to the appropriate premium grade rails to maximise the maintenance-free life of crossings.

3.2.7 Materials for Cast monobloc or Centre Block of Crossings

An alternative to fully fabricated or part fabricated crossing is the use of cast monobloc or cast centre block with welded on leg ends. The crossing nose and the immediate vicinity experiences high impact loading from the transfer of the wheel from the wing rail and although optimisation of the crossing nose and wing rail profiles provide very useful alleviation of the contact stresses, the maintenance of the desired profile is strongly dependent on the properties of the wing rail and crossing materials. Hence, the material choice for the monobloc or cast centre block has to be based on their resistance to those degradation mechanisms that are more closely related to material properties rather than their structural design. In particular, the chosen material must possess increased resistance to plastic deformation / lipping resulting from high impact loading. Furthermore, the wheel transfer area is also susceptible to spalling that may have its root cause in sub-surface initiation of cracking. Consequently, material choice has to be an intrinsic part of the design of any crossing. The two materials that require discussion are:

- Austenitic Manganese Steel (AMS) that continues to be widely used for crossings and

- Bainitic steels that have attracted significant research attention and one version (Titan) that was approved for use in UK network in 1980s.

In addition, use of a cast Cr-V steel in the Australian network [3.2.54] has been cited but there is little information available about their in-service performance.

3.2.7.1 AUSTENITIC MANGANESE STEEL (AMS)

The material choice for cast monobloc or centre block has been almost singularly restricted to unhardened austenitic manganese steel (AMS) for many decades and more recently to its use in the explosively hardened condition. However, AMS crossings are not used by some railway networks such as the national German network (DB). Composition and the key properties of the AMS material, determined from physical tests on crossings acquired from various networks [3.2.52], are summarised in Table 3.2.4 together with those of rail steel grades R260 and R350HT for comparison.

Table 3.2.4 Comparison of steel grades for crossings

	Composition			Proof Strength	Tensile strength	El	Hard-ness	Impact	K_{IC}
Steel	C	Si	Mn	MPa	MPa	%	HV	J at RT	MPa√m
Cast AMS Crossing	0.7-0.9	0.2-0.4	13-14	355-386	818-973	40-60	190-220	200-260	43-45
R260	0.73	0.31	1.1	502	926	12	280		33.7
R350HT	0.78	0.45	1.13	715	1134	11.5	370		37.2

The salient features of AMS steel are:

1. Low hardness and proof strength of the material in the as-received unhardened condition makes it susceptible to plastic deformation in the early stages after installation. However, AMS steel has been shown to possess a very high work hardening capacity and it is this property that has promoted its use for monobloc or centre block of crossings. Furthermore, explosive hardened AMS has much greater resistance to plastic deformation and wear.
2. Wear rates of AMS steel, measured using controlled twin disc tests in the laboratory, are very low despite its low levels of initial hardness [3.2.53] and this is attributed to rapid work hardening of the material raising the hardness to ~500HV. Figure 3.2.50 shows the results of the laboratory twin disc tests of AMS steels in comparison to the rail steel grades included in EN13674-1:2011. However, these results are based on weight loss after a fixed number of cycles and it does not reflect the true loss in the dimensions of the test piece some of which is lost to lipping through plastic deformation. Similarly, the effective rate of wear of this material in commercial track is a combination of the loss through wheel-rail contact and that through regular removal of lipping by grinding. Thus, the move to the use of explosively hardened AMS steel is justifiable as it minimises the loss through plastic deformation and the costs incurred

for remedial grinding. It would be of interest to undertake twin disc testing of explosively hardened material, although the loss of the hardened layer during machining needs to recognised.

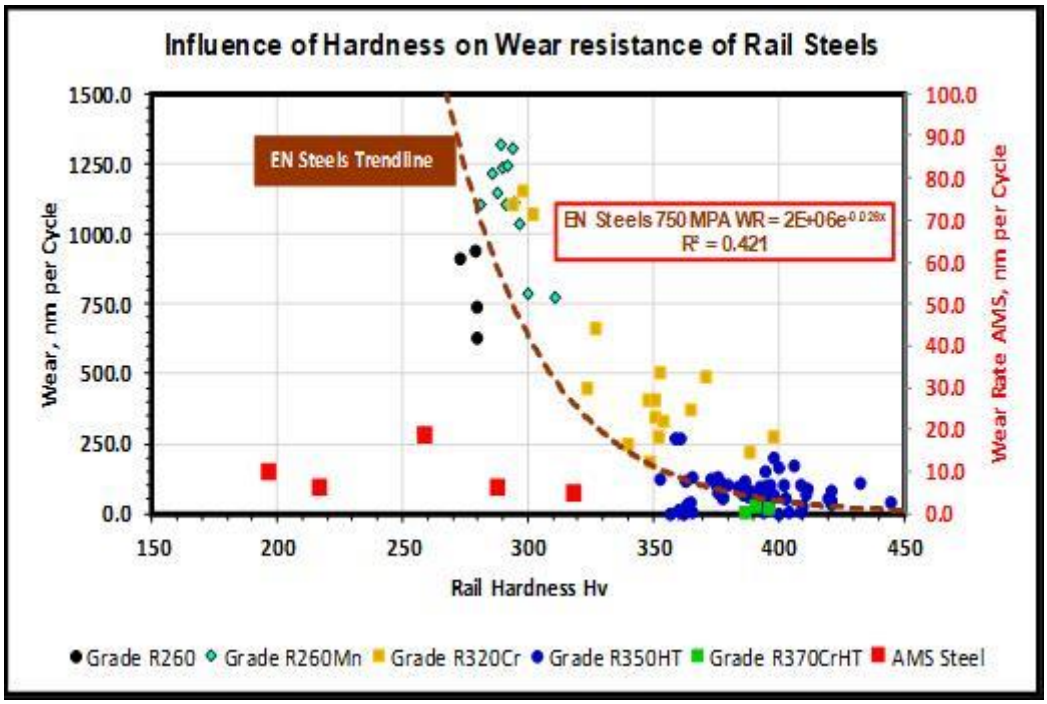

Figure 3.2.50 Wear Resistance of AMS Steel [3.2.55]

Another aspect of wear behaviour that appears not to have received as much research focus is side wear resulting from contact with the wheel flange where the contact conditions and the wear mechanisms operating are very different to the rolling contact between the rail and tread of the wheel. An interesting example of the use of AMS steel is shown in Figure 3.2.51, although the resulting longevity of the AMS insert is not known [3.2.56]. However, the approach opens the door for the use of composite components manufactured via the "additive manufacturing" route employing laser cladding or weld deposition techniques.

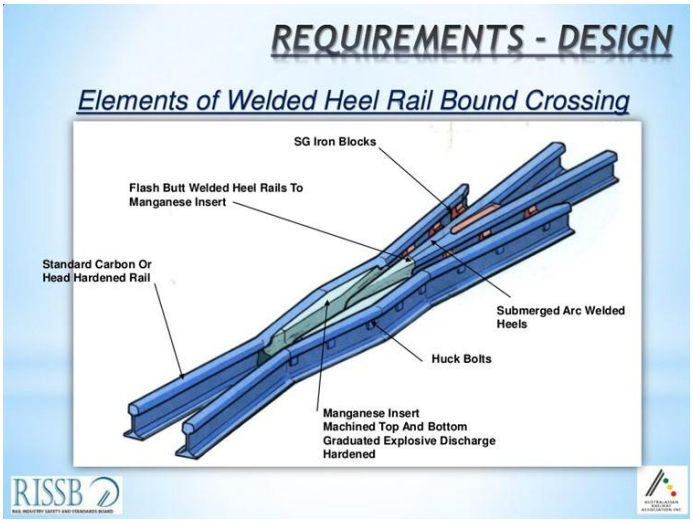

Figure 3.2.51 AMS Steel Inserts in Rail Bound Crossing [3.2.56]

3. Although field observations provide evidence of the increased resistance to RCF of AMS steels, there is very limited data on comparative testing under controlled laboratory conditions to quantify the magnitude of improvement compared to the available rail steels. The single data point depicting the resistance of this material to RCF initiation in Figure 3.2.52 illustrates the magnitude of improvement over standard rail grades. However, controlled tests on a rotary tribotester equipment investigating the effect of parameters of applied load, rolling speed and the number of cycles, confirmed the very high work hardening capacity of AMS steel but also revealed the presence of microcracks and micro-voids after around 150,000 cycles and suggested that these were the initiation of micro-spalling **[**3.2.57**]**.

Spalling is a key cause of maintenance intervention or even premature renewal of cast AMS crossings [3.2.57]. A school of thought associates such defects to rolling contact fatigue with merger of sub-surface initiated cracks initiated at casting defects or when the weld repairs are carried out without sufficient grinding to remove all the casting defects prior to welding. An example of a severely spalled AMS crossing is shown in Figure 3.2.53 which also reveals evidence of porosity in the original casting on the wing rails and on the rear portion of the nose [3.2.55].

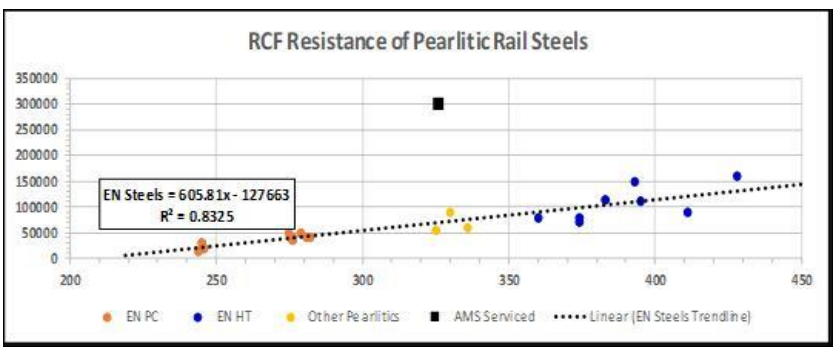

Figure 3.2.52 RCF Resistance of AMS Steel compared to pearlitic steels [3.2.53]

Figure 3.2.53 Spalling Damage in Cast AMS Crossing [3.2.58]

4. Coefficient of thermal expansion of AMS is ~ 50% higher compared to that of pearlitic rails, which when combined with a relatively narrow solidification range, makes them particularly prone to segregation and casting defects. Thus, as apparent from the example micrograph shown in Figure 3.2.54, almost all AMS crossings contain varying degrees of casting defects such as shrinkage voids, porosity and inclusions. Such defects can subsequently lead to the initiation of sub-surface fatigue cracks that merge together to result in the observed spalling. If detected in time, weld repairs can be undertaken to extend the life of the crossing.

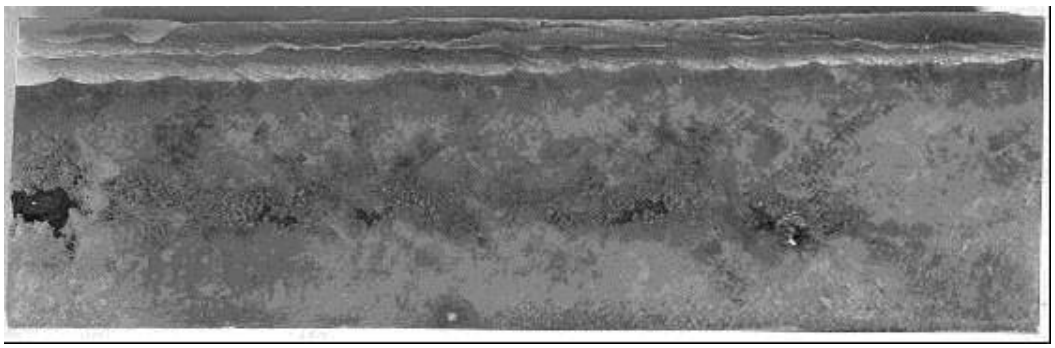

Figure 3.2.54 Extensive sub-surface shrinkage voids and porosity in a weld repaired cast AMS crossing [3.2.58]

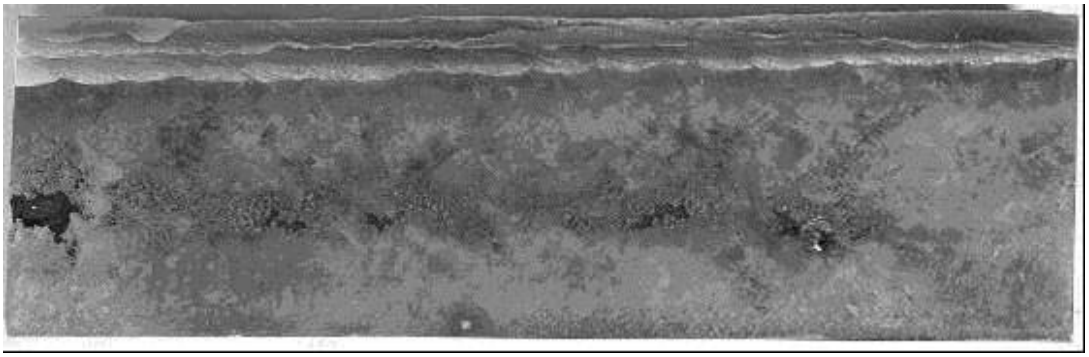

Figure 3.2.55 Extensive sub-surface shrinkage voids and porosity in a weld repaired cast AMS crossing [3.2.58]

5. AMS crossings are weld repairable but considerable precautions need to be taken during welding so as to prevent carbide precipitation and embrittlement that would otherwise be life curtailing **[**3.2.59**]**. Furthermore, as apparent from the example shown in Figure 3.2.56, the defects to be repaired cover relatively large areas which makes the control of temperature difficult and time consuming.

Figure 3.2.56 Example of the Extent of Weld Repairs Required [3.2.58]

6. AMS crossings cannot be directly welded to pearlitic rails and hence bolted fishplates have been used instead. A breakthrough in the Flash-butt (FB) of AMS crossings came through the use of two step FB welding operation in which a cast stainless steel rail is FB welded to the leg of the cast AMS crossing followed by sawing of the rail to leave a stainless steel slice approximately 25 to 30 mm thick at the end of the AMS crossing. The second FB weld is made

between the stainless steel slice and pearlitic rail leg with the welding operation reducing the thickness of the insert to ~10-15mm. The two stage FB welding process is time consuming and expensive as the operation needs to be repeated for each of the four leg ends. However, the metallurgical challenges of FB welding of significantly dissimilar compositions need to be emphasized. This is apparent in the failure [3.2.58] emanating from the interface area between the stainless insert and the pearlitic rail as shown in Figure 3.2.57.

Figure 3.2.57 Example of Fracture from Stainless Insert Interface [3.2.58]

The failure shown in Figure 3.2.57 highlights a small fatigued area at the base of the foot from the interface between the stainless insert and the pearlitic rail. The metallurgical investigation [3.2.58] attributed the failure to several contributing factors: microstructural phases present in the region, in-service dynamic stresses, and contribution from the deep manual grinding marks.

However, the chemistry of the interface region is sufficiently enriched with diffusion from the highly alloyed stainless steel insert to permit the formation of hard high carbon martensite even on natural air cooling. Contribution of other factors such as stress raising effects of grinding marks combine to initiate fatigue and subsequent fracture. Consequently, it is prudent to recognise challenges of FB welding of AMS crossings as a weakness of this material.

7. In-service inspection of cast AMS crossings is restricted to visual and dye-penetrant examination with no practical technique available for the assessment of sub-surface integrity of the cast material. Current ultrasonic inspection techniques are considered ineffective because of the coarse-grain microstructure resulting in interference from ultrasonic backscatter [3.2.60]. Magnetic particle inspection is also not applicable as the material is not magnetic. However, a recent project funded by the UK government called RailSAFT [3.2.61] has successfully developed an ultrasonic technique capable of reliable inspection of cast high-manganese steel railway crossings. The system utilises a combination of low-frequency ultrasonic transducers and a post-processing image reconstruction technique known as Synthetic Aperture Focussing Technique (SAFT) to minimise coherent noise contributions emanating from material back-scatter. It is claimed to be capable of full-volume inspection from the top surface of manganese steel crossings.

3.2.7.2 BAINITIC STEELS

A number of bainitic steel crossings have been proposed in the past and the compositions of a selected few are shown in Table 3.2.5.

Table 3.2.5 Composition of Bainitic Steel Crossings

	%C	%Si	%Mn	%Cr	%Mo	%Ni	%Cu	%P	%S	%B
Titan[3.2.62, 3.2.63] (UK)	0.1	0.3	1.0	2.0	0.5	3.0	2.0	<0.015	<0.015	0.003
USA[3.2.64]	0.26	1.85	1.75	-	0.5	3.0				0.004
China[3.2.65]	0.29	1.62	2.33	1.45	0.35	0.32				-

Several hundred Titan crossings were installed in the UK mainline and London Underground network. Although no in-service performance data is available, the innovation was deemed a success particular under the lower axle loads of the underground network. Typical mechanical properties is shown in table Table 3.2.6.

Table 3.2.6 Typical Mechanical Properties and Attributes of Titan Crossings

Property	Minimum value
0.2% PS, MPa	640
UTS, MPa	950
Elongation, %	6
R. of A, %	26
Hardness, HB	360
Charpy V notch at 15^0C, J	32
Key Attributes	
Easier to cast with reduced susceptibility to casting defects compared to AMS composition.	

Easier to Flash-butt weld without the need for stainless inserts and 2-stage operation. Also, weldable to pearlitic rails using aluminothermic process Can be weld repaired with no or minimal preheat Can be inspected using ultrasonics and magnetic particle Better resists plastic deformation under impact loading. However, lipping at the nose and wing area did occur and had to be removed by grinding.

Although data for the resistance to RCF for this steel is not available, the inspection and maintenance guideline issued by the manufacturer does confirm its susceptibility to gauge corner cracking and spalling and recommends grinding as the rectification measure.

However, in view of the lack of their widespread use, further discussion of the attributes of cast bainitic steels is not considered justified within the current project scope.

3.2.7.3 Specialist Wrought Materials for Crossings

The exposure of the crossings to high dynamic forces makes them more susceptible to the degradation mechanisms of plastic deformation, wear, and the many manifestations of rolling contact fatigue. Consequently, the introduction of specialist materials that are considered capable of better resisting the degradation mechanisms is understandable. Such crossings can either be of monobloc design constructed from wrought materials or fabricated built-up design comprising a crossing nose that is made from specialist wrought material. Composition and the key properties of the materials that have been used/proposed are shown in Table 3.2.7 followed by brief discussion of their key attributes in

Table 3.2.8 Key Properties of Specialist Wrought Materials for Crossings

Table 3.2.8.

Table 3.2.7 Chemical composition for Specialist Wrought Materials for Crossings

Crossing Steel	Composition, %											
	C	Si	Mn	Cr	Mo	Ni	Co	Al	Ti	B	Nb	V
VARIO 1800	0.03	0.1	0.1	-	4.6-5.2	18-19	8.5-9.5	0.05-0.15	0.5-0.8		-	-
Compact 1400	0.51	0.25	0.9	1.1	-	-	-	-	-		-	0.20
Q&T Fine Grained steels												
Dillidur400V [3.2.55]	≤0.20	≤0.50	≤1.80	≤1.50	≤0.50	≤0.80	-				≤0.05	≤0.08
Hardox[3.2.66] 500	≤0.27	≤0.50	≤1.60	≤1.20	≤0.25	≤0.25	-			≤0.005		
Aldur[3.2.67] Q	≤0.20	≤0.80	≤1.70	≤1.50	≤0.70	≤2.00	-	0.018 min			≤0.06	≤0.12
	Other additions include 0.5% Cu max, 0.15% Zr max											

Table 3.2.8 Key Properties of Specialist Wrought Materials for Crossings

Steel	HV	Proof Strength	Tensile Strength	Elon-gation	Impact	K_{IC}	Wear	RCF	Weldability	Other Disadvantages
		MPa	MPa	%	J at RT	MPa√m	mg/m Slip	Cycle		
VARIO 1800 crossing	520-620	1700	1800-2000	5-8	10-24	~80			Weld repairable. Flash butt welding with buffer layer	High cost of manufacture
Compact 1400		>900	1200-1400	>8	30				FB weldable, weld repair using preheat	Stress corrosion susceptibility
Dillidur 400V[3.2.55]	400-420	1000	1300	12	50		30		FB weldable, data on weld repair ability not available	Low wear resistance
Hardox[3.2.66] 500	470-530								Data not available	Limited thickness range
Aldur[3.2.67] Q		480-960	590-1150	10-17	30-40 (0^0C)					

3.2.7.4 VARIO 1800

Vario 1800 is an ultra-high strength maraging steel whose strength is not derived from high carbon content but instead from the precipitation of intermetallic compounds in a ductile matrix [3.2.68, 3.2.69]. The VAE crossing nose is made from a maraging W720 steel grade as per EN material grade 1.6358 to develop a tensile strength between 1700 to 1800 MPa and 0.2% proof strength of between 1600 to 1700MPa with elongation of >8%. Such maraging steels are suitable for the manufacture of moulds used in polymer processing, for die casting dies, drop-hammer dies, punches, and other non-cutting tools. However, there is a belief that maraging steels have poor resistance to abrasive wear [3.2.70] although specialist surface treatments such as plasma nitriding can be undertaken to improve this property.

The maraging crossing nose has good weldability to permit welding to the S355 base material and to the rails using electron beam welding. Furthermore, dies made of maraging steels can be weld restored and the same would be applicable to crossing nose inserts. The wing and closure rails can be of standard or heat-treated grades.

Although the high and costly alloying elements of the maraging steel makes it an expensive option, it is deployed in the very restricted area of the crossing nose and the volume of material used is minimised through the use of S355 base to which it is easily welded.

However, comparative data on the resistance of this grade to the degradation mechanisms of wear and RCF is not available nor is the in-service performance data. This gap in information needs to be bridged particularly since a range of maraging steels are available [3.2.71] including Fe-Ni-Mn compositions with much reduced costs of alloying elements. Furthermore, the availability of such grades in the wrought product dimensions that are suitable for the manufacture of crossing noses needs to be established since the current application of this material is in relatively thin gauges for rocket and missile skins and bars in a wide range of diameters for applications such as engine components (crankshafts and gears).

3.2.7.5 COMPACT 1400

Compact 1400 is a quenched and tempered Cr-V steel complying to the specification of EN material number 1.8159 with the composition shown in Table 5. The steel would need to be tempered at temperatures between 450^0C and 500^0C to develop tensile strength between 1200-1400 MPa and proof strength of between 1070-1250 MPa [3.2.72, 3.2.73].

The steel is used for general mechanical engineering, automotive components and gear parts. It is available in a range of bar diameters and thick plates. However, the company brochure does not elaborate on whether the crossing nose made of this material is full depth and how it is attached to the rails.

Data on comparative laboratory testing of resistance to wear and RCF from other sources [3.2.53] indicate that quenched and tempered microstructures do not have as high a resistance to wear and RCF as fine pearlitic steels. In-service performance of this grade of steel would be very useful to guide future research into the preferred microstructures for crossing noses.

The composition has a high Chromium content which may make weld repair and FB welding far more challenging.

3.2.7.6 QUENCHED & TEMPERED FINE GRAIN STEEL

Quenched and tempered fine grained steel plates are available from different manufacturers under different brand names such as Dillidur/Cogidur, Hardox, Aldur. There are many similarities in the steel compositions covered by these brands and the properties achieved reflect the product thickness and processing conditions. The grades are high strength steel plates for a wide range of applications but their ingress into the railway crossing nose world is at best very limited. The assessment described below is with reference to the Cogidur product from Vossloh primarily because of the availability of appropriate data.

Vossloh have an offering in the light rail sector of a crossing centre block layout accurately machined from a composite rolled plate. The active top part of the centre block is machined from ~80mm quenched and tempered plate of the composition shown in Table 3.2.9 while the bottom part of the layout is a “construction steel” plate. The concept of a composite plate for a crossing is attractive as it focusses the degradation resistant material to exactly where it is needed and minimises the overall

cost of manufacture. Therefore, there is a need to establish the resistance of the top material to the key degradation mechanisms. Figure 3.2.58 and Figure 3.2.59 show the influence of hardness on wear and RCF resistance as determined by testing on a twin disc rig [3.2.58].

It is apparent that resistance to wear of Quenched and Tempered (Q&T) microstructure is not as good as that of pearlitic steels. As the composition of Dillidur is similar to that of Abrazo plate, their resistance could also be expected to be similar. Vertical wear of the 400 HV Dillidur composition in a tramway network was significantly lower than that of the benchmark rail grade R260 but the reduction in side wear was not as high [3.2.58]. Consequently, it is not surprising that the Dillidur crossing material has not been offered for use in mainline networks. However, the caveat for the comparative results shown in Figure 3.2.58, is that the line contact conditions in a laboratory twin disc test does not emulate the contact conditions under the high dynamic loading experienced by the crossing nose. It is, therefore, necessary to develop specific tests to assess the resistance of various microstructures to wear, RCF, and plastic deformation.

Table 3.2.9 Compositions of Dillidur 400V and Abrazo 400 Steels

	Composition, wt %											
	C	Si	Mn	P	S	Cr	Mo	Ni	Nb	Ti	V	B
Dillidur 400V	≤0.20	≤ 0.50	≤1.80	≤0.025	≤0.010	≤1.50	≤0.50	≤0.80	≤0.05	-	≤0.08	≤0.005
Abrazo 400* Typical	0.16	0.35	1.25	0.015	0.002	0.25	0.50	0.20	0.03	-	0.03	0.002
* = for plate thicknesses between 40 and 80 mm												

The results (Figure 3.2.59) of controlled comparative testing indicates that the resistance to RCF of the Abrazo 400 quenched and tempered steel is closely aligned to the resistance of EN steels at similar levels of hardness suggesting that the performance of the Dillidur composition is likely to be similar. However, the caveat cited for the wear test results remains valid for the RCF resistance results because of the much simplified contact conditions.

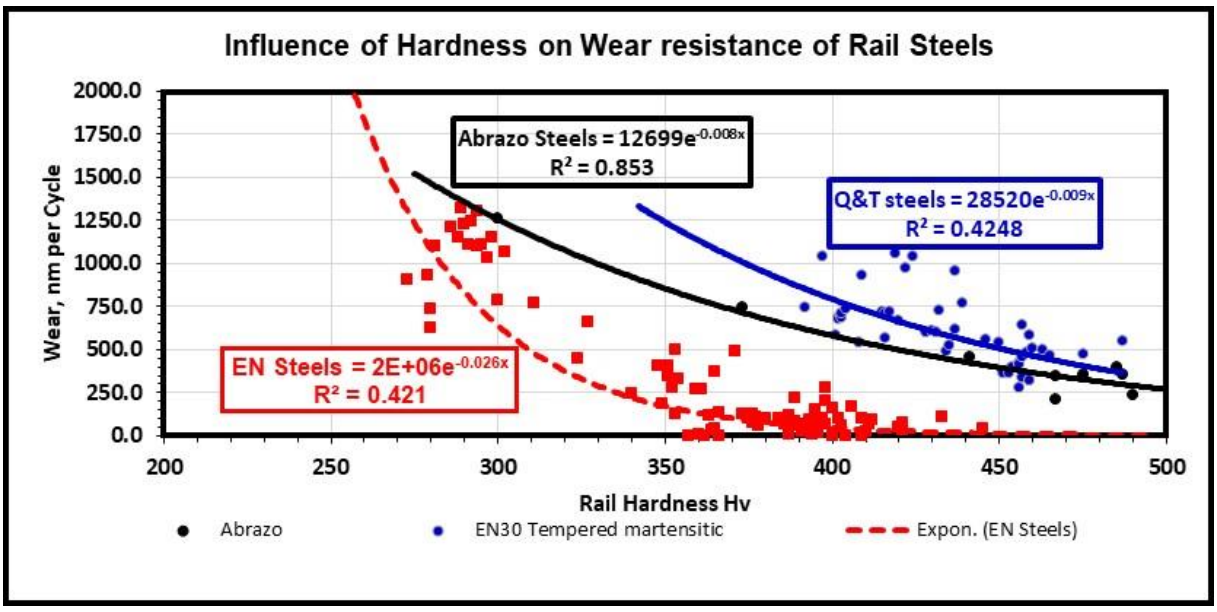

Figure 3.2.58 Influence of Hardness on Wear Resistance of Q&T Microstructures [3.2.58]

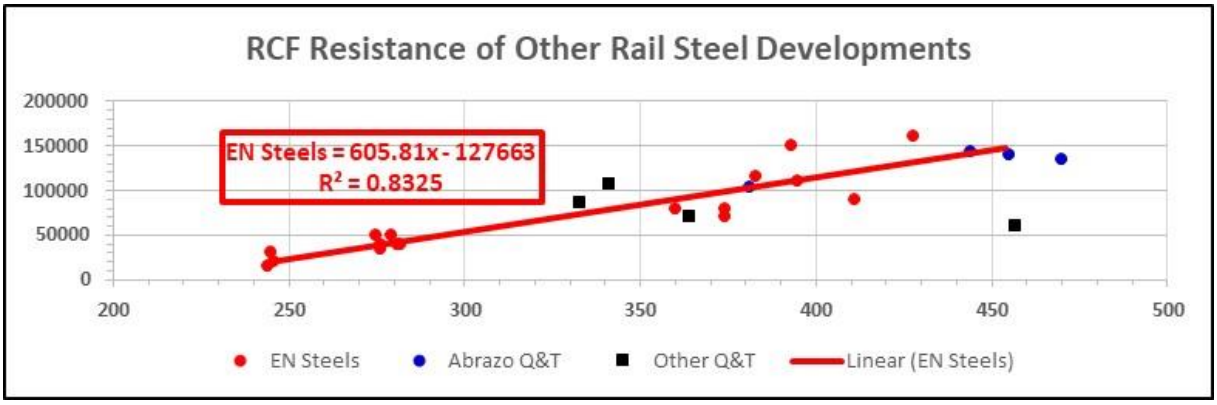

Figure 3.2.59 Influence of Hardness on RCF resistance of Q&T Microstructures [3.2.58]

3.2.7.7 MANGANESE – MOLYBDENUM STEEL

The desire to replace cast AMS with a precisely machined crossing manufactured from a degradation resistant wrought material prompted a research programme that resulted in the development of low carbon steel with the key alloying elements as per one of the example compositions included in the patent application [3.2.58, 3.2.71] is shown in

Table 3.2.**10**.

Table 3.2.10 Example Composition of Mn-Mo Steel

Chemical composition, wt%								
C	Si	Mn	P	S	Cr	Mo	Al	N
0.064	0.24	12.48	0.006	0.008	0.15	1.68	0.005	0.011

The composition has been designed to produce a fine, mixed microstructure comprising retained austenite, epsilon-martensite and 'normal' lath martensite giving the steel good levels of ductility and toughness. The steel addresses the vast majority of challenges that need to be met by any material that claims to overcome the disadvantages of cast AMS steel while matching the attributes of wear and RCF resistance. These are briefly discussed below:

1. As in the case of AMS, the appreciable proportion of retained austenite in Mn-Mo steel microstructure ensures rapid work hardening while the low carbon martensite provides additional hardness in the as-manufactured condition (~ 350 HB) and a higher yield stress than in cast AMS.
2. The low carbon content, typically ~0.06%, together with the higher integrity of a rolled product, makes weld repair much easier than in cast AMS. It also facilitates direct flash butt welding to pearlitic rails, thereby eliminating the need for costly stainless steel inserts that are currently needed when welding AMS crossings to pearlitic rail.
3. A significantly higher as-rolled hardness of the optimised Mn-Mo composition minimises plastic deformation of the crossing nose that necessitates profile grinding to remove the lipping commonly seen on non-hardened cast AMS crossings
4. A further attribute of the Mn-Mo composition is rapid work hardening rates relative to those of AMS steel.
5. The composition possesses a high resistance to the key degradation mechanisms of wear and RCF as is apparent from Figure 3.2.60 and Figure 3.2.61. The data shown is for a range of compositions that were evaluated.

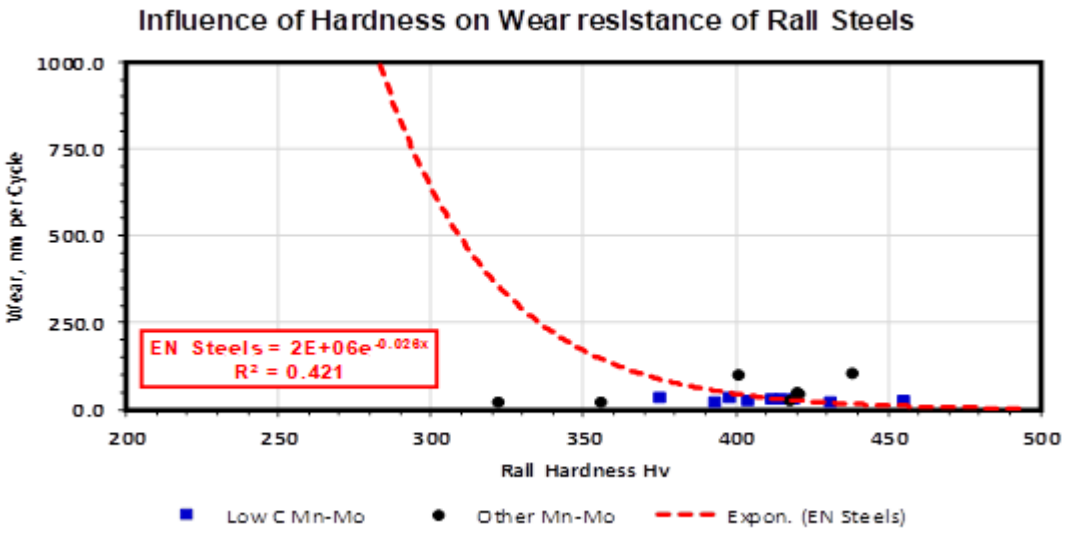

Figure 3.2.60 Influence of Hardness on RCF resistance of Mn-Mo Microstructure [3.2.58]

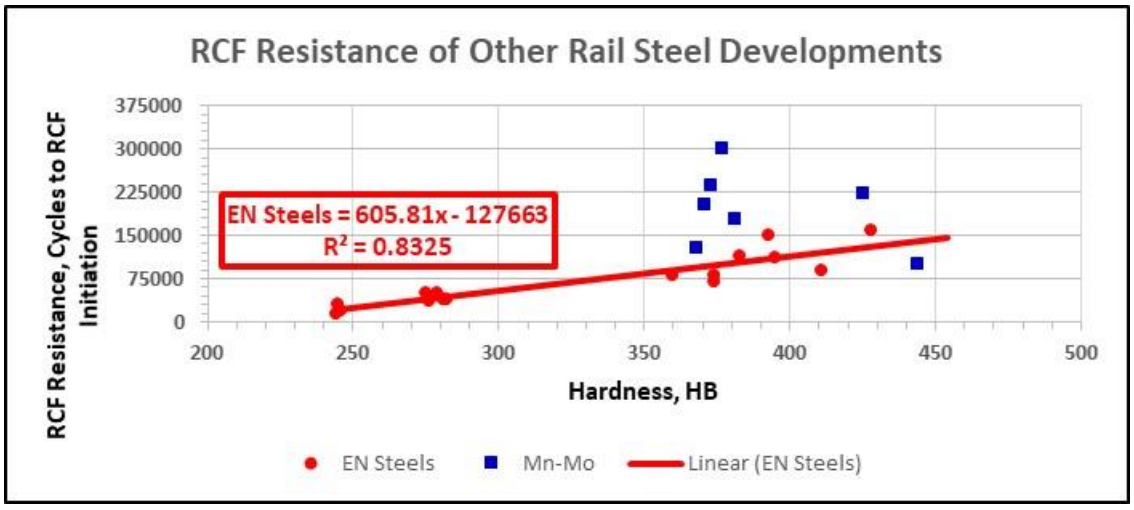

Figure 3.2.61 Influence of Hardness on RCF resistance of Mn-Mo Microstructures [3.2.58]

Although the refined mixed microstructure has provided attractive properties, optimisation of the composition to ease manufacturability while maintaining the attractiveness of properties is considered necessary.

3.2.8 New material

It is widely accepted that fixed point crossings are one of the most sensitive components of a switch and crossing (S&C) layout. The crossing is exposed not only to rolling contact, but also to dynamic high energy shocks during the transfer of the wheel from the crossing nose to wing rail or vice-versa.

A significant proportion of S&C for railway systems are currently manufactured from cast austenitic-manganese steel (AMS). AMS has traditionally been used owing to its good resistance to abrasion, high work hardening capacity on impact and excellent toughness following solution treatment and water quenching. The primary reason is the rapid work hardening rate that results in high hardness and the associated increase in resistance to wear. Without the rapid work hardening, resistance to abrasion, wear, and plastic deformation of AMS is poor. The nominal chemical analysis of AMS is 1.2% C, 13% Mn, 0.5% Si, which produces bulk hardness in the region of 200 to 250 HB. Following the passage of several MGT of traffic AMS S&C can reach hardness levels of 500 to 550 HB. However, there are a number of drawbacks with the use of AMS, which has prompted S&C suppliers to explore the use of alternative materials. Furthermore, AMS relies on work hardening to achieve optimum resistance to wear. Time taken to reach optimum hardness depends on axle load and for light rail applications the time to reach optimum hardness is inevitably considerably longer than that for heavy axle load applications. An alternative solution consists in pre-hardening the frog through explosion; this solution however means extra costs.

The low 0.2% yield stress (typically in the range 300-400 N/mm^2) can sometimes be a disadvantage in service as the deformation due to impact commonly experienced in railway switches and crossings increases the proof strength to levels more resistant to plastic flow but the associated dimensional changes are undesirable. Where work hardening is slow the AMS requires frequent weld repairs to restore deformation height loss as evidenced in Deliverable D13.1 "Operational Failure modes of S&C" *(**1.4.3** plastic deformation of the crossing nose for fixed crossings and **1.4.12** spalling of crossings)*

AMS is not an easy material to cast or machine into complex shapes needed for switches and crossings. The narrow freezing range of AMS results in many cavity type defects. Casting defects are common and are often the starting point of cracking seen in service. The presence of sub-surface casting cavities also increases the difficulty of weld restoration. Thus, the presence of such cavities restricts the permissible magnitude of vertical wear. This has been clearly demonstrated with the AMS points/crossings installed where the severe casting defects have resulted in cracking appearing on the running surface necessitating weld repair *(Deliverables D13.1 **section 1.4.4** casting defect leading to cracking and **1.4.5** transverse crack on the crossing nose)*. After approximately 10 years service the extent of the defects has become so severe that it has become uneconomical to continue remedial weld repair and the crossings have had to be replaced.

A further problem with AMS is the thermal instability of the austenitic structure, which renders it difficult to weld repair in track should material break-outs occur (as evidenced by *Deliverable D13.1 **section 1.4.10** material break-outs on manganese crossings)*. Another major disadvantage of AMS crossings is that they cannot be inspected by ultrasonic or eddy current techniques.

The direct weld connection between manganese crossings and carbon steel rails cannot be carried out with the usual welding processes (e.g., thermit welding, shielded manual arc welding, etc.) nor directly with processes such as flash-butt welding, This is due to the metallurgical incompatibility of the two steels. The crossing to rail connection is made possible by using a stainless steel insert that is flash-butt

welded, first to the frog and then to the carbon-steel rail, thus minimising the incompatible mechanical discontinuity between the parts to be connected. However this process of double welding while superior to bolted fishplated joints, can, if not carried out correctly lead to failures in track or can lead to a 'soft-spot' around the adaptor casting being created. (*Deliverable D13.1* ***section 1.1.3)***

The proposed answer to the defects identified in *Deliverable D13.1 "Operational Failure modes of S&C"* (described above) is to limit the initiation of such defects through the use of a special steel that provides a higher surface hardness.

The new material and its implementation developed by Vossloh Cogifer is different than existing steel grades (e.g. CrBainit [DB], B320, B360) and will offer significant benefits over traditional cast manganese crossings in terms of improved internal quality and the resulting extension to component life at the same time as reduced maintenance cost.

The target of the demonstrator is to confirm the effects that can indeed be avoided through the use of the proposed new material, and to quantify the resulting decrease in whole life costs.

In principle the Demonstrator would take the form of a crossing manufactured in the new steel that would replace an existing 60E1 crossing (Turnout TG 1/12 R500mm) manufactured from cast manganese.

The crossing would have the same geometry as the existing crossing and would match the existing crossing footprint with only 8 special replacement baseplates requiring to be provided.

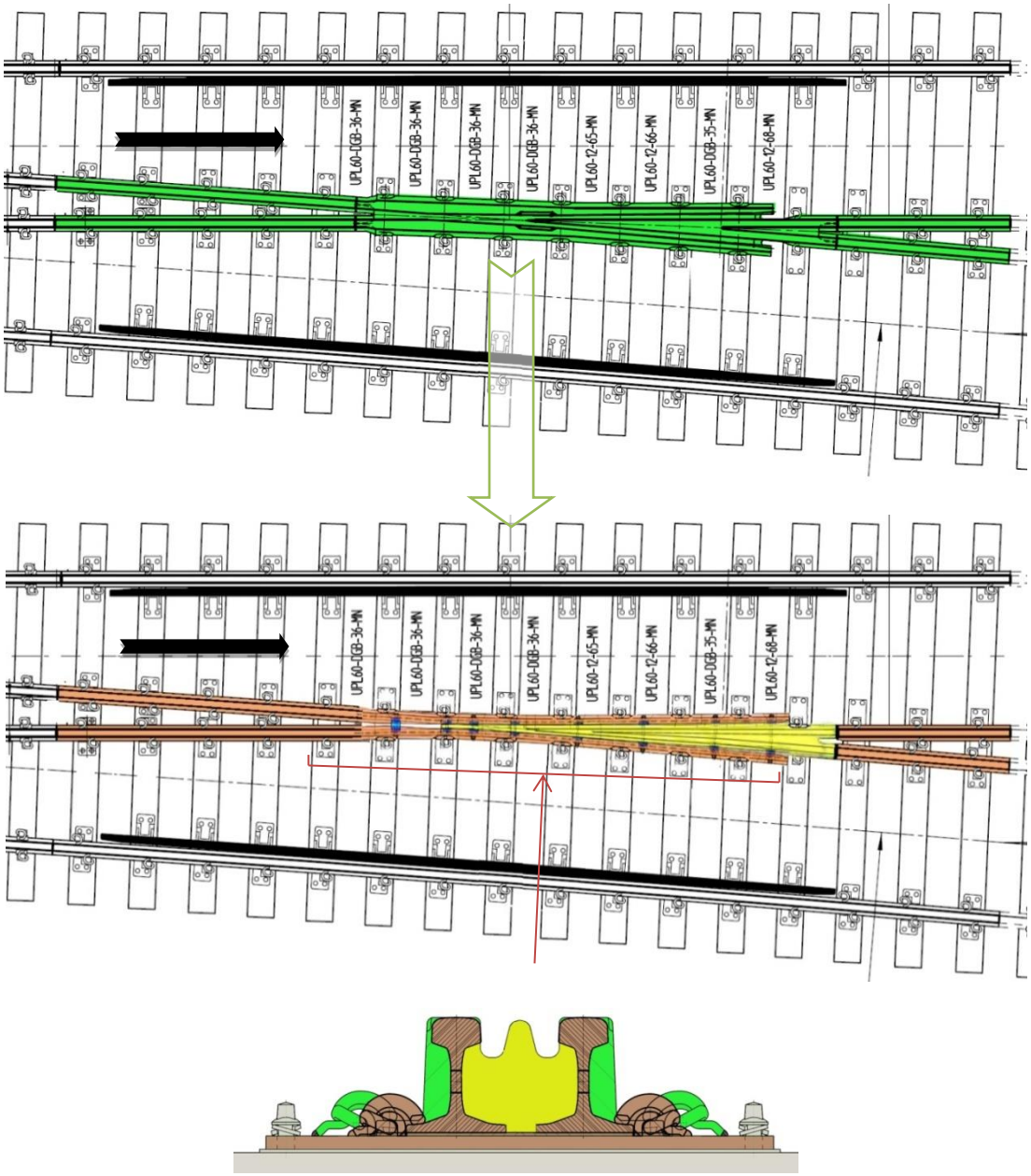

Figure 3.2.62 Demonstrator crossing

Same geometry and compatible baseplates (8 special provided with the test crossing). Tested material is implemented on the crossing point and represented in yellow on the drawing. The green section represents the monobloc Mn crossing shape replaced by the rails and point. The fasteners (Pandrol clip) are moved in order to be close to the rail. The baseplate has same holes as for Mn crossing, but adapted shoulders

3.2.9 CROSSING GEOMETRY AND WEAR MONITORING IN TRACK

Understanding the complex degradation mechanisms of wear, plastic deformation and fatigue damage in crossing and switches requires robust damage models supported by reliable material data as well as a mean of precisely measuring and quantifying the change in shape of the rails under traffic conditions.

Current industry practice relies on manual devices such as MiniProf and Calipri to do this. However surveying a full turnout at regular intervals implies costly operation with long track possession, often at night where quality of data can be compromised by a number of factors, most importantly the human factor.

Various semi-automated advanced solutions are available using a range of 2D or 3D laser scanner or 3D camera. The C4R consortium is interested in investigating those solutions able to improve the speed and reliability of track measurement to support the validation of models prediction as well as validating the demonstrator activities such as installation of a new material crossing in Sweden.

3.2.9.1 TROLLEY BASED MEASUREMENT

The University of Huddersfield in the H2020 project WRIST has been developing a laser based system to measure in details weld geometries. The prototype research instrument has been further modified and adapted in C4R for use on switches and crossings. The principle is to mount a laser head onto a fixed frame running parallel to rail of interest, through a length of about 1.1 m. The laser is moved along the rail at a constant speed and over a fixed reference frame so that a series of 2D cross sections are measured every 0.7 mm longitudinally, to enable a later 3D recomposition of the shape of the rails (weld, crossing, switches etc…). Figure 3.2.63 shows the system being trialled on a full S&C assembly in the UK and the details of the laser head used. Similar system are commercially available, such as GRAW scorpion (Figure 3.2.64), but they come at a high premium and this particular example is dedicated to measure the crossing nose area. One of the purpose of the instrument being developed here is that it can be deployed for entire S&C survey in a manner that the data can be used for the simulations shown earlier in this chapter of the report and that it can be faster and more accurate that using standard MiniProf or Calipri system.

This is achieved by having the laser installed on a trolley frame having three resting point, two in the measured rail (top of the rail) and one on the opposite rail. This way the horizontal plane of the track is known and the gauge face is used to align the trolley along the rail being measured. The laser head is fixed on a linear guide and moved along through a conveyor belt and electric motor. At the moment the laser travels over 1m in about 40~50 seconds, but this will be improved. Reference markers are placed onto the rail head at each ends and are part of the measurement, so that they can be used during the post processing to recompose the 3D geometry along a significant length (full crossing or full switch-stock assembly) – see Figure 3.2.45 and 3.2.46.

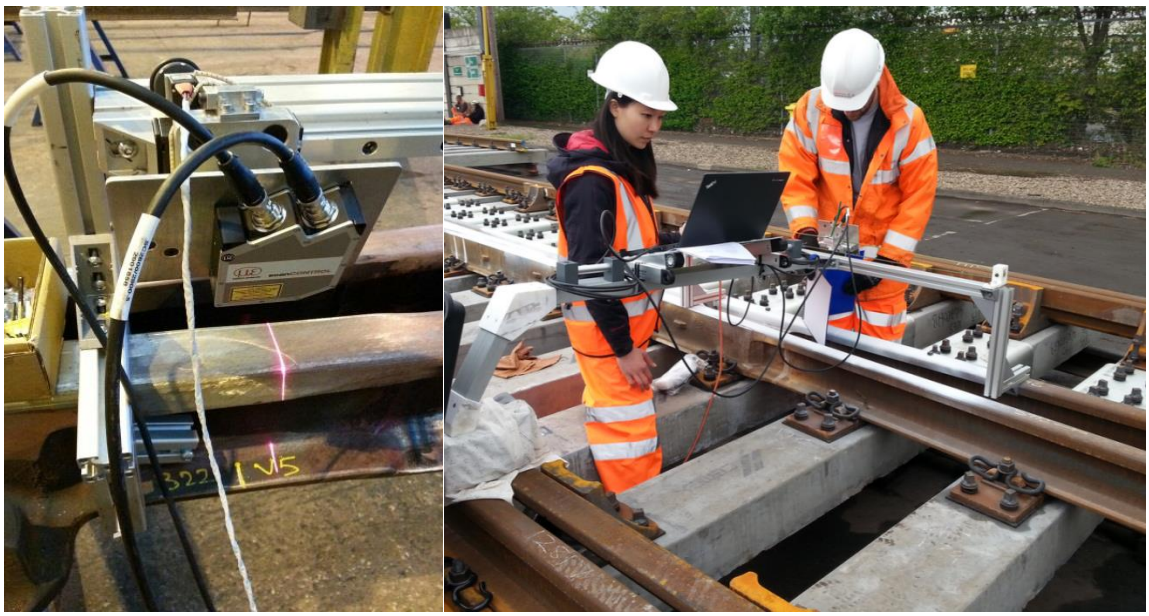

Figure 3.2.63 UoH Laser measurement trialed on crossing welded leg end (left) and on full S&C Assembly (right)

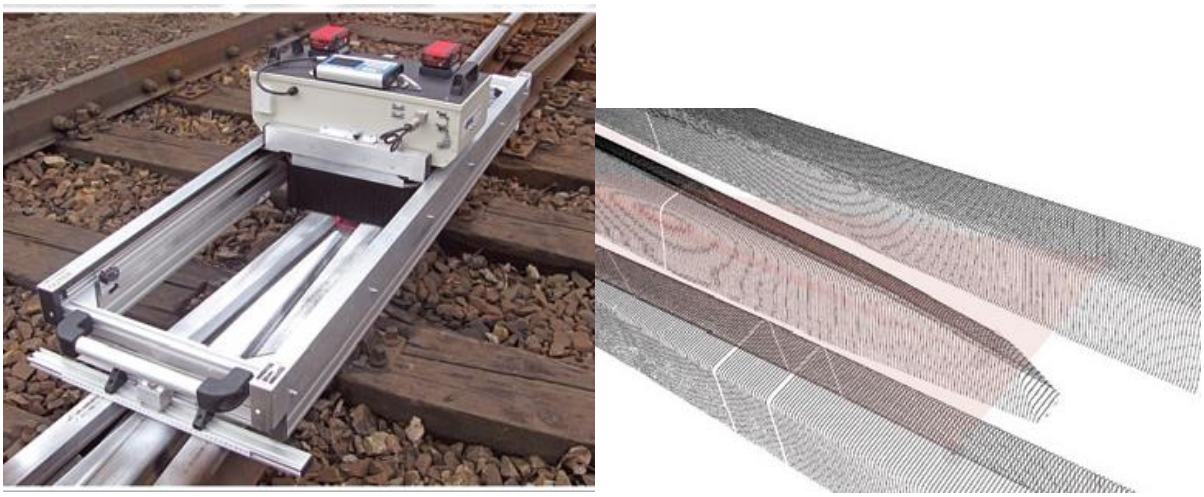

Figure 3.2.64 Graw Scorpion S&C measurement system (source http://graw.com)

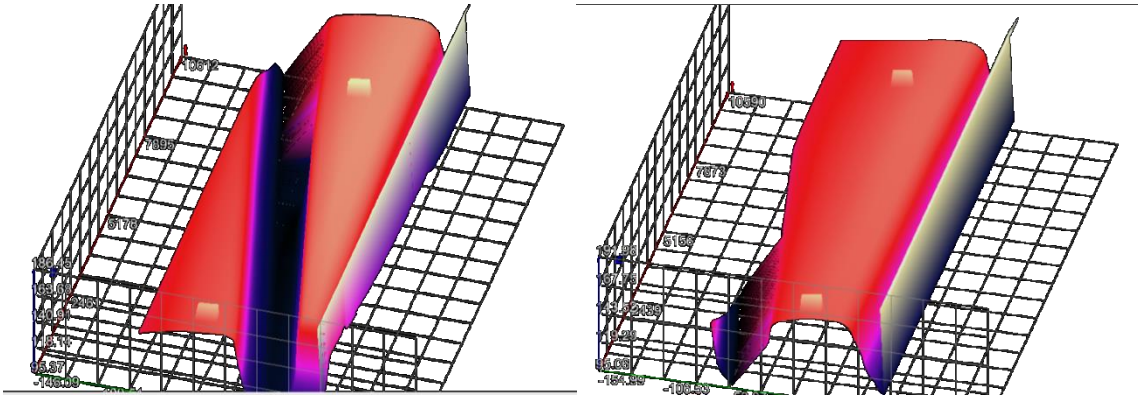

Figure 3.2.65 Resulting 3D image of two consecutive measures taken by UoH of a crossing (nose/wing). Markers used to locate consecutive measurements are visible.

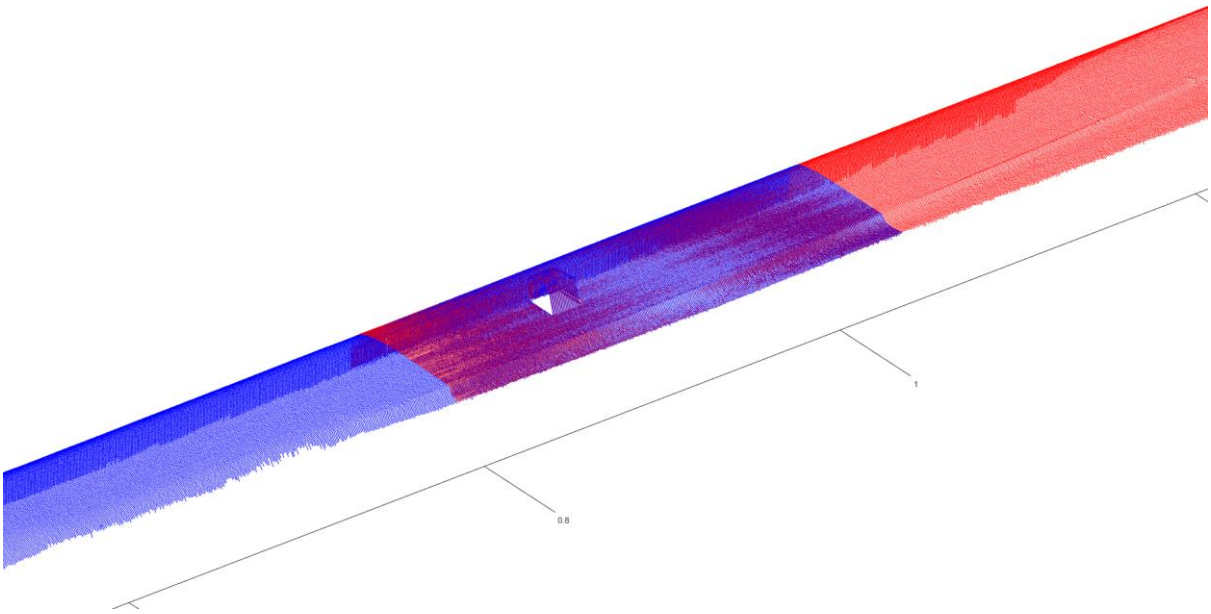

Figure 3.2.66 Example of the recomposition of the measured crossing section using Matlab and the measured markers for positioning.

3.2.9.2 HAND HELD MEASUREMENT

In addition Vossloh Cogifer plans follow up in track in order the evolution of the new crossing material installed in Sweden, to monitor the new material behaviour. The aim is to measure the running surface before traffic, after 1 month, 6 months, 12 months and, 24 months. Those measurements compared to the reference shape will show the wear at relevant sections and wear along the crossing point. The measurement will be done with a portable laser tool “creaform HANDY SCAN3D –700”, Figure 3.2.47. Resolution is 0.05 mm and accuracy 0.03 mm. VCSA has tested this tool and plan to buy this tool, see the CAD snapshot in Figure 3.2.68.

Figure 3.2.67 Portable 3D scanner by HandyScan 3D (source: http://www.creaform3d.com)

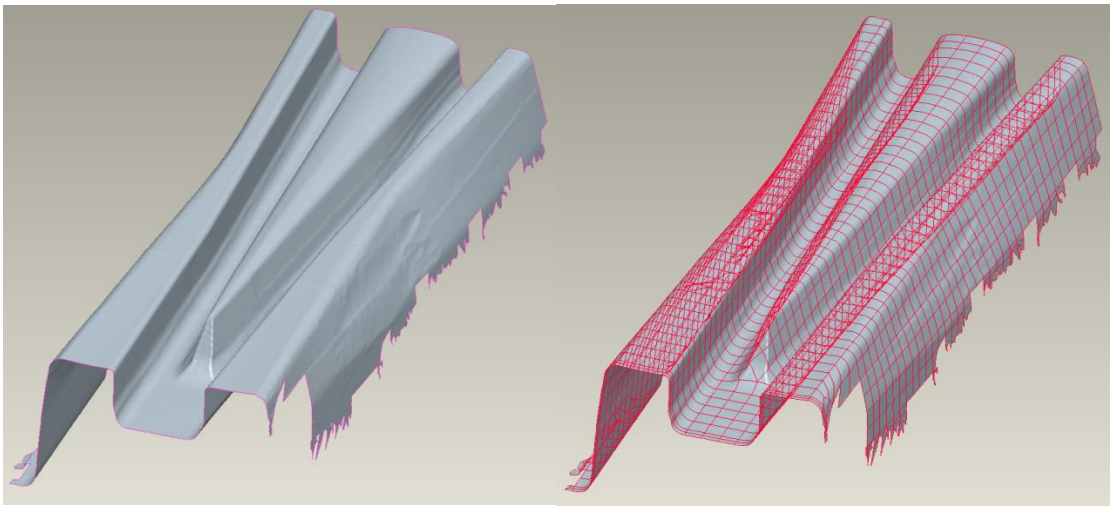

Figure 3.2.68 Meshed STEP model

3.2.10 REFERENCES

[3.2.1] C4R Deliverable 1.3.1

[3.2.2] SUSTRAIL Deliverable 4.4

[3.2.3] Jenkins, H., Stephenson, J., Clayton, G., Morland, G., & Lyon, D., The effect of track and vehicle parameters on wheel/rail vertical dynamic forces, *Railway Engineering Journal*, 1974, **3**(1), pp 2-16

[3.2.4] Innotrack Deliverable 3.1.4

[3.2.5] Pålsson, B. A., & Nielsen, J. C., Track gauge optimisation of railway switches using a genetic algorithm, *Vehicle System Dynamics*, 2012, **50**(Sup1), pp 365-387

[3.2.6] Wan, C., Markine, V., & Shevtsov, I., Improvement of vehicle–turnout interaction by optimising the shape of crossing nose, *Vehicle System Dynamics*, 2014, **52**(11), pp 1517-1540

[3.2.7] Andersson, C. and T. Dahlberg, Wheel/rail impacts at a railway turnout crossing, *Proceedings IMechE, Part F, Journal of Rail and Rapid Transit*, 1998, 212(2), pp 123-134

[3.2.8] Zhu, J.Y., On the effect of varying stiffness under the switch rail on the wheel—rail dynamic characteristics of a high-speed turnout, *Proceedings IMechE, Part F, Journal of Rail and Rapid Transit*, 2006, **220**(1), pp 69-75

[3.2.9] Kassa, E., C. Andersson, and J.C. Nielsen, Simulation of dynamic interaction between train and railway turnout, *Vehicle System Dynamics*, 2006, **44**(3), pp 247-258

[3.2.10] Alfi, S. and S. Bruni, Mathematical modelling of train–turnout interaction, Vehicle System Dynamics, 2009, **47**(5), pp 551-574

[3.2.11] Bruni, S., et al., Effects of train impacts on urban turnouts: modelling and validation through measurements, *Journal of Sound and Vibration*, 2009, **324**(3), pp 666-689

[3.2.12] Ren, Z., S. Sun, and G. Xie, A method to determine the two-point contact zone and transfer of wheel–rail forces in a turnout, *Vehicle System Dynamics*, 2010, **48**(10), pp 1115-1133

[3.2.13] Burgelman, N., Z. Li, and R. Dollevoet, A new rolling contact method applied to conformal contact and the train–turnout interaction, *Wear*, 2014, **321**, pp 94-105

[3.2.14] Sebes, M., et al., Application of a semi-Hertzian method to the simulation of vehicles in high-speed switches, *Vehicle System Dynamics*, 2006, **44**(sup1), pp 341-348

[3.2.15] Wiest, M., et al., Assessment of methods for calculating contact pressure in wheel-rail/switch contact, *Wear*, 2008, **265**(9), pp 1439-1445

[3.2.16] Pletz, M., W. Daves, and H. Ossberger, A wheel passing a crossing nose: Dynamic analysis under high axle loads using finite element modelling, *Proceedings IMechE, Part F, Journal of Rail and Rapid Transit*, 2012, **226**(6), pp 603-609

[3.2.17] Wiest, M., et al., Deformation and damage of a crossing nose due to wheel passages, *Wear*, 2008, **265**(9), pp 1431-1438

[3.2.18] Kassa, E. and G. Johansson, Simulation of train–turnout interaction and plastic deformation of rail profiles, *Vehicle System Dynamics*, 2006, **44**(Sup1), pp 349-359

[3.2.19] Pletz, M., W. Daves, and H. Ossberger, A wheel set/crossing model regarding impact, sliding and deformation—Explicit finite element approach, *Wear*, 2012, **294**, pp 446-456

[3.2.20] Sun, Y.Q., C. Cole, and P. Boyd, A numerical method using VAMPIRE modelling for prediction of turnout curve wheel–rail wear, *Wear*, 2011, **271**(1), pp 482-491

[3.2.21] Johansson, A., et al., Simulation of wheel–rail contact and damage in switches & crossings, *Wear*, 2011, **271**(1), pp 472-481

[3.2.22] Xiao, J., F. Zhang, and L. Qian, Contact stress and residual stress in the nose rail of a high manganese steel crossing due to wheel contact loading, *Fatigue Fract Engng Mater Struct*, 2014, **37**(2), pp 219-226

[3.2.23] Ekberg, A., E. Kabo, and H. Andersson, An engineering model for prediction of rolling contact fatigue of railway wheels, *Fatigue Fract Engng Mater Struct*, 2002, **25**(10), pp 899-909

[3.2.24] Vu, M., S. Kaewunruen, and M. Attard, Nonlinear 3D finite element modeling for structural failure analysis of concrete sleepers/bearers at an urban turnout diamond, 2016

[3.2.25] Eck, S., et al., Comparison of the fatigue and impact fracture behaviour of five different steel grades used in the frog of a turnout, *Proceedings IMechE, Part F, Journal of Rail and Rapid Transit*, 2014, **228**(6), pp 603-610

[3.2.26] Larsson-Kraik, P.-O., et al., Geometrical degradation of railway turnouts-a case study from Swedish heavy haul railroad, *Proceedings IMechE, Part F, Journal of Rail and Rapid Transit*, 2014, **228**(6), pp 611-619
[3.2.27] Li, X., J.C. Nielsen, and B.A. Pålsson, Simulation of track settlement in railway turnouts. *Vehicle System Dynamics*, 2014, **52**(Sup1), pp 421-439
[3.2.28] Kennedy, J., et al., Reducing railway track settlement using three-dimensional polyurethane polymer reinforcement of the ballast, *Construction and Building Materials*, 2013, **44**, pp 615-625
[3.2.29] SOLIDWORKS. Release 2015. Dassault Systèmes
[3.2.30] ANSYS Mechanical APDL. Release 15.0. ANSYS Inc.
[3.2.31] ANSYS Mechanical APDL. Release 15.0, Help system, ANSYS parametric design language guide. ANSYS Inc.
[3.2.32] Nicklisch, D., Kassa, E., Nielsen, J., Ekh, M., & Iwnicki, S., Geometry and stiffness optimization for switches and crossings, and simulation of material degradation. *Proceedings IMechE, Part F, Journal of Rail and Rapid Transit,*2010, **224**(4), pp 279-292.
[3.2.33] Lichtberger, B., Track compendium. Eurailpress Tetzlaff-Hestra GmbH & Co. KG, Hamburg, 2005
[3.2.34] Grossoni, I., Bezin, Y., & Neves, S. G. M., Optimization of support stiffness at a railway crossing panel. Paper presented at the Railways 2016, The Third International Conference on Railway Technology: Research, Development and Maintenance, Cagliari Italy
[3.2.35] Kaewunruen, S., & Remennikov, A. M., Sensitivity analysis of free vibration characteristics of an in situ railway concrete sleeper to variations of rail pad parameters, *Journal of Sound and Vibration*, 2006, **298**(1), pp 453-461
[3.2.36] Johansson, A., Nielsen, J. C.O., Bolmsvik, R., Karlström, A., & Lundén, R., Under sleeper pads—Influence on dynamic train–track interaction, *Wear*, 2008, **265**(9), pp 1479-1487
[3.2.37] du Grand Placitre, A., & Zuckerman, A., Benefits of Under Sleeper Pads (USPs) for ballasted track. Paper presented at the RAILWAY ENGINEERING 2015: 13th International Conference & Exhibition, Edinburgh, 2015
[3.2.38] Riessberger, A., Ballast track for high speeds. Proceedings "Tracks for High-Speed Railways", pp 23-44, Porto, Portugal, October 2006
[3.2.39] Grossoni, I., Bezin, Y., & Alonso, A., Modelling Uneven Support at Railway Crossings using a Vehicle-track Coupling System. in J. Pombo (Editor), Railways 2014, Ajaccio, Corsica, 2014
[3.2.40] Hunt, G.A., EUROBALT: vertical dynamic model for track damage studies. British Rail Research: Derby, 1998
[3.2.41] Bezin, Y., Farrington, D., Penny, C., Temple, B., & Iwnicki, S., The dynamic response of slab track constructions and their benefit with respect to conventional ballasted track, *Vehicle System Dynamics*, 2010, **48**(Sup1), pp 175-193
[3.2.42] Sañudo, R., Markine, V., Dell'Olio, L., Optimizing Track Transitions on High Speed Lines. IAVSD 2011 Dynamics of vehicles on Roads and Tracks, 2011.
[3.2.43] Shahraki, M., C. Warnakulasooriya, and K.J. Witt, Numerical study of transition zone between ballasted and ballastless railway track. Transportation Geotechnics, 2015. 3: p. 58-67.

[3.2.44] Kang, Y., et al., A study of track and train dynamic behavior of transition zone between concrete slab track and ballasted track. SPARK, 2008: p. 1-7.
[3.2.45] Xin, T., U. Kumar, and L. Gao, Dynamic design of track transition between two different slab tracks. 2014.
[3.2.46] Grossoni, I., Bezin, Y., & Alonso, A., Modelling Uneven Support at Railway Crossings using a Vehicle-track Coupling System. in J. Pombo (Editor), Railways 2014, Ajaccio, Corsica, 2014
[3.2.47] Zhai, W., Vehicle-track coupling dynamics. Beijing, China: Science Publishing House, 2007: p. 12-132.
[3.2.48] Hunt, G.A., EUROBALT: vertical dynamic model for track damage studies. British Rail Research: Derby, 1998
[3.2.49] Bezin, Y., Farrington, D., Penny, C., Temple, B., & Iwnicki, S.,, Vehicle System Dynamics, 2010, 48(Sup1), pp 175-193
[3.2.50] Sato, Y., Japanese studies on deterioration of ballasted track. Vehicle System Dynamics, 1995. 24 Suppl.(1): p. 197-208.
[3.2.51] Guerin, N., Approche experimentale et numerique du comportement du ballast des voies ferrees, in Structures et materiaux. 1996, Ecole nationale des ponts et chausses: Paris.
[3.2.52] Cope D L and Ellis J B: British Railway Track Volume 5, Switch & Crossing Maintenance, The Permanent Way Institution
[3.2.53] Private communications: Internal test data from rail manufacturer.
[3.2.54] Robin Stevens: Turnout Design & Components; National Turnout Workshop, Perth; Nov 2010
[3.2.55] Personal communications - Tata Steel Internal Research Reports.
[3.2.56] Craig Bishop, VAE Railway Systems - Turnout Manufacture in Australia; Published on Apr 10, 2014.
[3.2.57] R. Harzallah; A. Mouftiez; E. Felder; S. Hariri; J.-P. Maujean. - Rolling contact fatigue of Hadfield steel X120Mn12; Wear Volume 269, Issues 9-10, 17 September 2010, Pages 647-654
[3.2.58] Repair and rebuild of Manganese Crossing using Hardface Welding. Hardface Technologies, 2003.
[3.2.59] Welding austenitic manganese steel rail. Welding Technology Institute of Australia, TGN-R-01, Mar 1, 2006.
[3.2.60] P Ramuhalli et. al - Ultrasonic Characterization of Cast Austenitic Stainless Steel Microstructure: Discrimination between Equiaxed- and Columnar-Grain Material – An Interim Study: US Department of Energy – PNNL 18912; Oct 2009
[3.2.61] RailSAFT – Ultrasonic inspection of cast austenitic-manganese steel railway crossings – www.twi-global.com
[3.2.62] Edgar Allen Titan crossing Brochure
[3.2.63] D R. Pendleton, et al., "Welded and cast-centre crossings accepted after trial", Railway Gazette Int, 3, 1986, pp. 176-177
[3.2.64] K Sawley and J Sun, "Advanced rail steels: investigating the bainitic option", Railway Track Struct, 3, 1997, pp. 22-27
[3.2.65] F C Zhang, et al., "Effects of hydrogen on the properties of bainitic steel crossing", Engineering Failure Analysis, 2009, pp. 1461-1467
[3.2.66] SSAB Swedish Steel Ltd Brochure: www.ssab.co.uk/products/brands/hardox/hardox-500

[3.2.67] High-strength quenched and tempered fine-grained steels: www.voestalpine.com/heavyplates
[3.2.68] Bohler brochure – W720 DE - 11.05 – EM-WS
[3.2.69] VAE Crossings brochures
[3.2.70] Franjo Cajner, Darko Landek, and Vojteh Leskovek: SURFACE MODIFICATIONS OF MARAGING STEELS USED IN THE MANUFACTURE OF MOULDS AND DIES; ISSN 1580-2949; MTAEC9, 44(2)85(2010); Original scientific article: Izvirni znanstveni ~lanek
[3.2.71] Corus Engineering Steels Brochure
[3.2.72] Data Sheet Material No 1.8159 – Dorrenberg Edelstahl; www.doerrenberg.de
[3.2.73] Abrazo 400 Datasheets
[3.2.74] Steel for producing parts for railway, railway crossings and switches and method for producing said parts: EP 2807283 A1 /WO2013110798A1

3.3 LONG-TERM DESIGN SOLUTIONS

The overall design of the S&C has been fundamentally unchanged for the last 30 years. To tackle the significant increases in line speed, axle load and volume of traffic the S&C system has been incrementally further developed, but from a sub-system or component level. The future ambition of the S&C next generation is therefore to consider a whole-system approach to enhancing common S&C designs and to incorporate modern mechatronics for improved system kinematics and control.

Sections 3.3.1 – 3.3.4 have been written by VAE, while Section 3.3.5 has been written by VCSA.

3.3.1 S&C NEXT GENERATION – ENHANCED DESIGN, MATERIALS & COMPONENTS

Due to higher traffic loads, higher speeds and severe weather conditions and dirt, S&C components are affected by slip, wear and RCF. S&C rely on standard profiles that are machined to the specific shapes as required by the S&C configuration. Traditionally, the design application engineering is different across European and particularly worldwide railways. To progress beyond the current state of the art technology, transfer opportunities from other industries as well as developing materials science solutions shall be examined. The innovative approach is to adopt the growing trend of merging mechanical, electro-mechanics, electronic design and digital control system elements into one integrated S&C. The next generation of radical S&C designs will be based on new methodologies of switching trains between tracks in a manner that improves capacity, performance and reduce costs whilst maintaining safety as the most important consideration. The wheel-rail interface will be optimised to enable the development of radically new mechanisms for switching a train from one line to another.

3.3.2 S&C NEXT GENERATION – ENHANCED KINEMATIC & ELECTRIFICATION SYSTEMS

Existing S&C systems still use historical design feature originally intended for hand operation. Modern actuators and motors deliver increased switch actuation forces, which can reduce the asset operational life. The next generation of S&C design will incorporate a completely new switching function using novel kinematic elements and will be designed from a whole system perspective. The new design will also affect the failure modes of track circuits and provides an opportunity to integrate train detection with significantly reduced electrical failure modes.

3.3.3 S&C NEXT GENERATION – ENHANCED CONTROL, MONITORING & SENSOR SYSTEMS

Existing S&C systems do not utilise sophisticated sensor systems with feedback control loops. Through new technology development and transfer from other industries, the next generation S&C design will incorporate intelligent self-diagnostic systems with the capability to self-adjust, self-correct and self-heal within predefined system operating tolerances. The next generation of S&C will significantly reduce manual maintenance operations through self-management.

3.3.4 S&C NEXT GENERATION – MAINTENANCE AND DEGRADATION FREE S&C

It is vital that the S&C system has a stable position in vertical and lateral direction during its operational life time. To counter the dynamic forces over the total life time correct support conditions have to be guaranteed. It is common that the S&C is treated as an extension of the normal plain track system utilising the same design and construction techniques. The next generation of S&C will allow for a different approach to the S&C support elements and will be designed together as a whole system.

3.3.5 MCS Modular Continuous Support on turnout design

Modular Continuous Support (MCS) track developed by Vossloh Cogifer is a ballast-less beam track offering an efficient lower cost rail technology for all track configurations (including for turnouts) based on two main principles:

- Pre-fabricated modules for tracks and turnouts (a small gap appears between the modules, but with limited influence on the performance).
- Rail is continuously supported.

MCS track is a way to improve track design and S&C design in the following fields, see also Table 3.3.1:

- Reduced structure height and weight, facilitating the logistics.
- Maintenance costs amount to 20-30% of the maintenance costs for ballasted track.
- Increased service life, improved rail behavior in track and turnouts
- Higher track stability
- Abatement of noise and, in particular, vibration nuisance
- Track accessibility to road vehicles

Table 3.3.1 MCS track vs ballasted track

DESCRIPTION	Ballast track	MCS track
Maintenance	Need to check and upkeep geometry, high cost.	Stable geometry. Low cost, comparable to slab track.
Construction cost and LCC	Construction cost relatively lower but with high LCC	Construction cost comparable to ballast track, but with LCC comparable slab track.
Construction	Need for heavy, specialized machinery	No specific equipment for a modular layout.
Lifetime	Relatively lower.	Relatively higher: comparable to slab track.
Rail and turnout design	Wear, vibration and contact surface driven by sleepers layout	Better setting of the rail which implies less wear, vibration and a better stability. Les constraints on the rail.
Stability	Instability of the track on ballast	Comparable to slab track

MCS track technology includes the following features (cf. Figure 3.3.1):

- Longitudinal pre-cast reinforced concrete beams, continuously supporting the rail by a continuous pad. Beams can be designed for any capacity.
- Standard proprietary fastenings are used to fix rails on the beams with a spacing potentially longer than for ballasted track.
- The modular design system is delivered in convenient 5 to 8 m track modules consisting in the assembly of the two concrete beams connected together to ease and ensure alignment. Modules can be easily shipped by truck or rail.
- The absence of ballast implies a direct contact between the longitudinal beam and the platform through a certain thickness of grout.

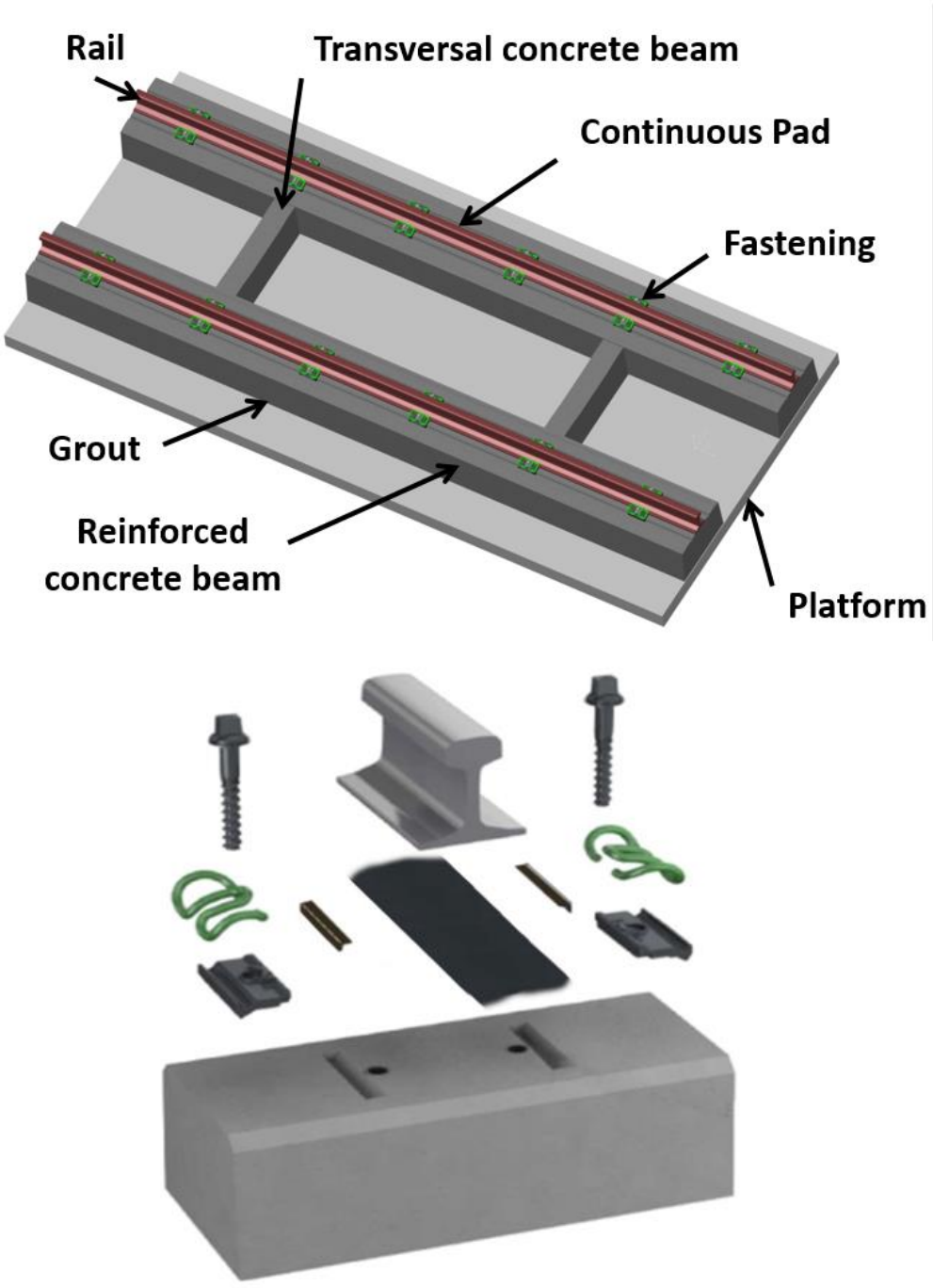

Figure 3.3.1 Modular Continuous Support description

Figure 3.3.1 shows a track module by Vossloh Cogifer with MCS principles developed at WP1.1 slab track workshops:

- A continuous elastic pad is supporting the rail.
- Six fastening systems are located on each beam.
- The distance between fasteners is around 1000 mm (R>3000 m), and 600-700 mm (R<3000 m).
- Vossloh W21T fastening system is used.
- Lateral adjustment is done by an adapted angle guide or insulator (+/-4mm).
- Curve is included in the concrete bloc (location of dowels and grove).
- Rail inclination is included in the concrete bloc section or rail head.
- TOP DOWN levelling is used: a mortar is applied between the module and the bituminous layer or sub layer.

Mechanically, it can be pointed out that MCS track is supposed to exhibit a better LWR resistance compared to conventional track (reduced rail warp risk when confronted to extreme temperatures).

3.3.5.1 MCS APPLICATION IN S&C

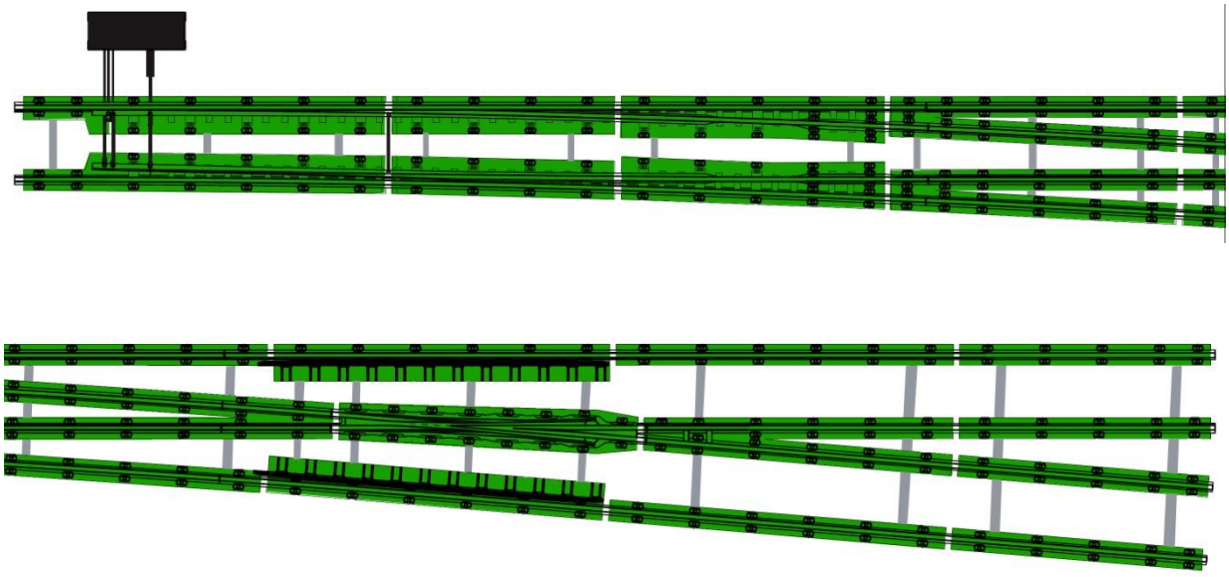

Figure 3.3.2 Modules (MCS)

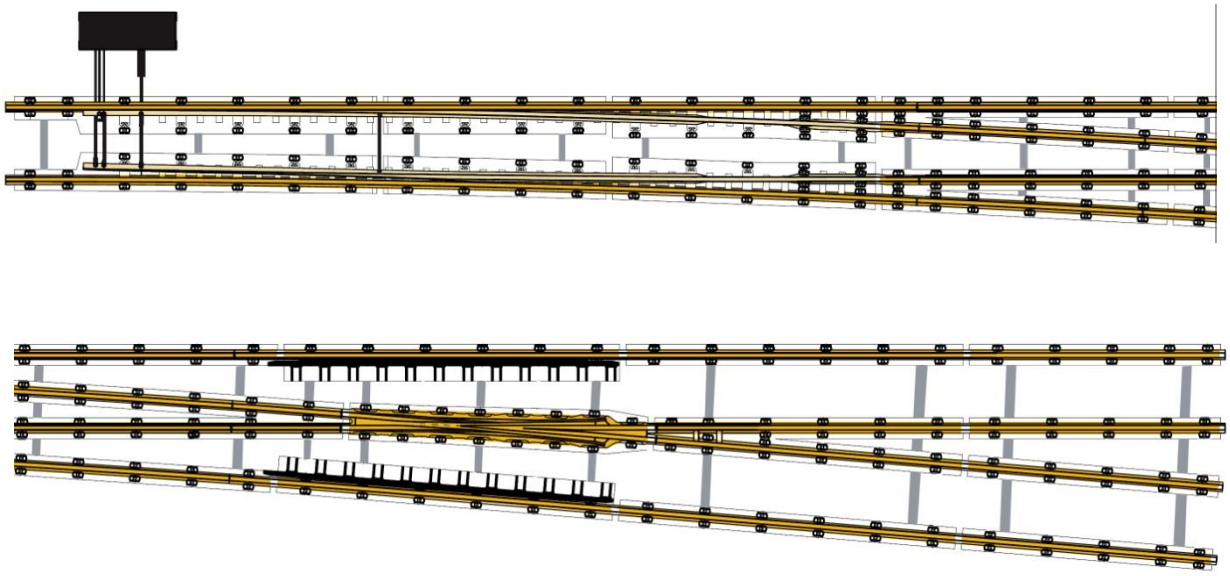

Figure 3.3.3 Continuous rail support (MCS)

4 S&C resilience to extreme weather conditions (C4R task 1.3.3)

4.1 DEFINITION OF EXTREME WEATHER

Extreme weather is a term used in the climate debate. It is normally used for heavy rains and storms as well as longer time with a dominating weather type, as long time with rain, high or low temperature.

Extreme weather is in another definition a weather state that effects the society. The meaning of extreme weather in this definition is “unexpectable weather that gives a severe impact on the society and infrastructure”.

In this report the following conditions are mentioned to be extreme in that sense that the infrastructure owner should be prepared to avoid the impact on S&Cs:

- Winter conditions
  - Drifting snow
  - Heavy snow falls
  - Hail
  - Freezing rain
  - Stress free temperature compared to rail temperature > 45 degrees
  - Long time with weather under 0 degrees
  - Temperature oscillating around 0 degrees
- Summer conditions
  - Rail temperature above 70 degrees
  - Rail temperature compared to stress free temperature > 45 degrees
  - Fast temperature changes within 24 hours (>25 degrees)
  - Sun radiation (Uvpart 200 W/m^2?) over longer time
- Rainy season/Windy season
  - Heavy rain fall (>90 mm/24 hour)
  - Flooding due to environment not capable to receive water
  - Heavy wind (>33 m/s – Hurricane class I)
- Other
  - Dry, arid zones which contains to areas with sand (critical wind speed 10 m/s)
  - Thunder

During winter it is snow, low temperature and temperature oscillating around 0 degrees that will give the most problems encounter in S&Cs.

During summer it is high temperature and sudden changes of temperature that will give most problems encounter in S&Cs.

Water in sub layer gives a more unstable foundation that will lead to faster deterioration of the track geometry. If the water comes during a short time due to heavy rain the deterioration can be very fast with “muddy sleepers”. Longer time with rain might give the same effect and even lead to undermining the ballast so that part of the sub layer is flushed away.

The definition of heavy rain is 50 mm within 24 hours according to [4.2.1]

Only heavy wind is assumed to not give any specific problem for S&Cs. In combination with drifting snow the problems for S&Cs are assumed to occur at 6 m/s and in combination with drifting sand at 10 m/s. The more heavy wind the more the transport of snow and sand will be.

Zones with sand will give problems with more wear and initiation of cracks, but also the sand will affect the quality of ballast so that the deterioration of track geometry goes faster.

Thunder may affect signalling equipment, but is not included in this report.

4.2 COLD CLIMATE

4.2.1 BACKGROUND

Snow and low temperature are meteorological phenomena that affect the reliability of the railway. As precipitation seems to increase in certain places in the scenario of warmer climate it might also become more frequent with extreme snowfalls in the future [4.2.2]. Track problems related to cold climate and potential solutions are discussed in Section 4.2, which has been written by Trafikverket.

4.2.2 TEMPERATURE AND SNOW IN EUROPE

Temperatures below zero are possible in all of Europe but are more common in the north and at high altitudes, such as in the Alps. The lowest temperatures are normally recorded in January and February, and large amounts of snow are obtained if the cold weather is combined with open water. In Figure 4.2.1, it is shown that this can affect nearly all of Europe. In many European countries, cold weather only leads to problems for the railways a few days in a year. Therefore the preparedness for snow and ice is less in these countries than it is for countries having temperature below zero up to 120 days per year (northern Europe). The amount of snow varies from a few centimetres up to 200 centimetres per year. According to SMHI (the Swedish Meteorological and Hydrological Institute), snowfall can result in up to 100 centimetres in just one day. It is the combination of strong winds and snow fall that gives the largest problems. Trafikverket has identified that even just 2 cm snow/hour is enough to create problems, especially if it is combined with winds above 6 m/s.

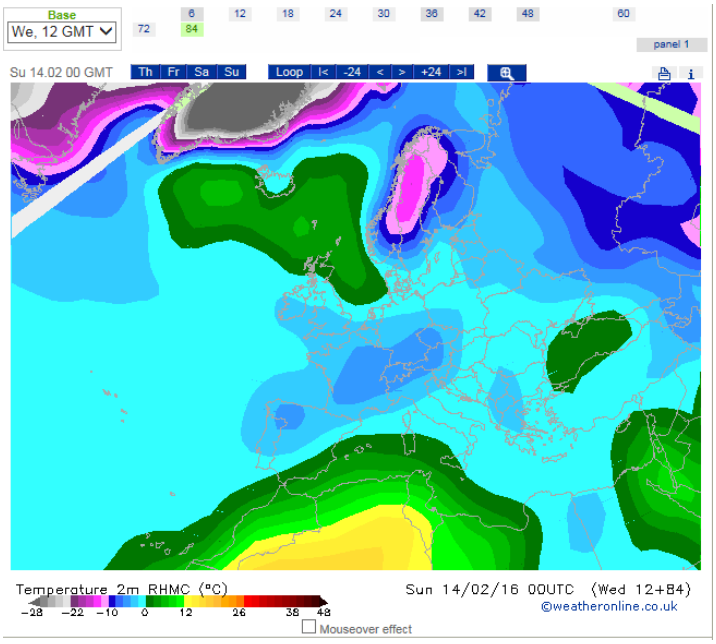

Figure 4.2.1 Night temperature 14th February 2016 [4.2.3]

4.2.3 TRACK RELATED PROBLEMS

There is a higher number of failures during winter than during any other season as shown in Figure 4.2.2. These failures are typically for rail, S&Cs and overhead wire (or 3rd rail). Those that affect traffic and how they can occur are for instance:

- Rails will have more rail breakage due to low temperature.
- On tracks where the wind can build snow piles due to drifting snow trains may get stuck.
- In switches, there can be a problem to move the switch blade due to snow.
- Overhead wires will have ice formation that can cause sparks and sometimes the overhead wire is torn down

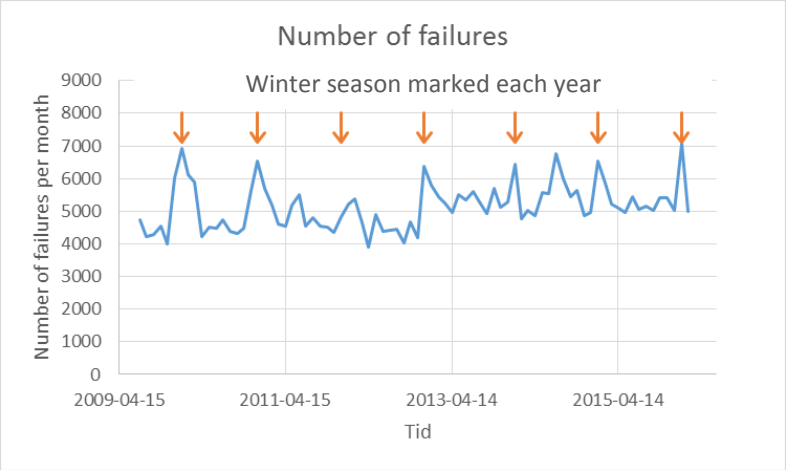

Figure 4.2.2 Number of failures for railway infrastructure in Sweden, orange arrows mark December/January each year

4.2.4 Implemented solutions

Heating by electrical or gas systems is generally the implemented solution. The energy flow is higher with gas solutions and therefore such systems can faster remove large amounts of snow. Heating with an electrical heater is more reliable and does not require as much maintenance. Electrical heating elements have a power of 200 – 400 W/m, which is enough to heat the rail to a temperature of at least 20 degrees higher than the ambient temperature. The heating elements are placed on the inside foot of the stock rail and on the foot or in the web of the switch rail. Most of the heat from a heating element is radiated out in the air. If the fastening of the heating element is not maintained properly there might be a distance between the heating element and the rail leading to reduced efficiency. Trafikverket's heating elements reaches 700 W/m at the tip of the switch rail and between 300 – 600 W/m in the rest of the heated area. The solution can guarantee removal of at least 20 cm snow per hour. The life time of a heating element is about 10 years.

4.2.5 Possible solutions under test

Trafikverket is investigating several new solutions that can make the heating system more efficient, more reliable and able to cope with more snow than previously. One solution is based on heating cables which are restricted in power output (to about 150 W/m per cable) but are more efficient as the energy to heat up the rail is not radiated to the air and most of the power is used to heat up the rail, see Figure 4.2.3.

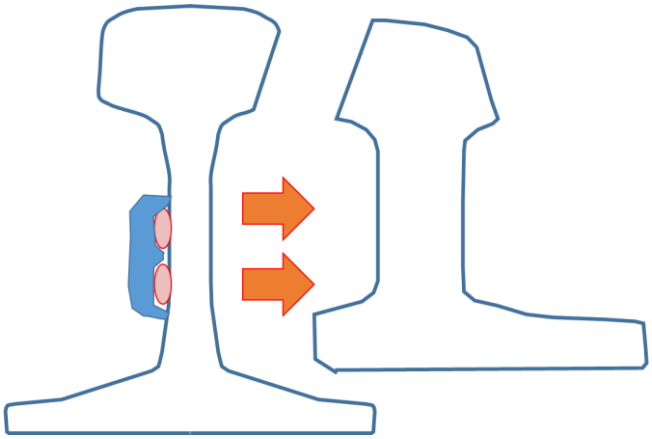

Figure 4.2.3 System with heating cables. The cables are protected by an insulating cover which reduces the heat loss to the air

Other tests are based on heating plates that can heat up the air between switch rail and stock rail by using from 100 W up to 900 W per sleeper gap. The maximum power is enough to heat more than 80 cm snow/hour which is the demand Trafikverket has asked for. The biggest challenge with these systems is how to control them. As the power output is so high it is even more important to limit the use to situations when there is heavy snow fall or drifting snow and hard winds than for the standard system.

4.2.6 Need for further development

Systems using cold or warm air as well as a system using warm water are in use in Japan. Some tests of this system have been performed in Europe. In Canada, anti-freeze liquid is used by manually spraying it on S&Cs and a Swedish company has offered a more automated system which is still under development.

4.2.7 References

[4.2.1] severe.worldweather.org.

[4.2.2] IPCC https://www.ipcc.ch/pdf/reports-nonUN-translations/swedish/ar5-wg2-spm.pdf

[4.2.3] www.weatheronline.co.uk

4.3 WARM CLIMATE

4.3.1 BACKGROUND

Railway operators operate within a variety of meteorological conditions, some of which are particularly problematic for rail transportation. Warm weather conditions influence railways in general. These conditions may affect operating efficiency, physical infrastructure, and the safe passage of freight and people. Precipitation and fog lead to decreased visibility of signals, flash floods can wash out tracks, and excessive heat can warp tracks. Crosswinds can reduce stability or lead to blow-over of railcars. Snow and ice may cause regional delays or shutdowns. Serious problems can also result from pre-existing accumulations of rain, ice and snow not associated with current weather conditions.

Despite the growing availability and sophistication of weather information and introduction of new technologies, adverse weather conditions continue to cause problems for operators. Weather phenomena present many real-time and forecast problems that challenge the abilities of railway operators and crews to confront, recover from, avoid and communicate specific weather hazards.

Sections 4.3.2 and 4.3.3 has been written by TCDD, while Sections 4.3.4 and 4.3.5 has been written by VCSA.

4.3.2 WARM WEATHER- RELATED PROBLEMS AT TCDD

As a result of examination of the records from TCDD accident and incident reports and speed restriction records for the period 2012-2014 it is found that 163 weather-related railway accidents and incidents have occurred, 46.6% of those were most closely associated with extreme heat causing track buckling and deterioration of track geometry.

Another problem is that due to adverse effect extreme heat on railway switches point machine protect itself and the signal turns into red. In addition, track buckling is also seen on steel railway bridges at TCDD lines.

So temperature extremes and temperature variability are the most frequently seen weather-related cause of derailments. Fast moving trains traversing tracks that are kinked, misaligned or broken have the potential to derail many railcars. Collisions are less common than derailments. Fast moving trains traversing tracks that are kinked, misaligned or broken have the potential to derail many railcars. Accidents during the summer months of June, July, and August are predominantly caused by high temperatures at TCDD networks.

Figure 4.3.1 Failure of track geometry due to warm weather

4.3.2.1 PRECAUTIONS FOR SUMMER AT TCDD

- Before summer, small fastening materials are loosened and those damaged are maintained and the screws are tightened to suitable torque values
- Making up deficiency of ballast, especially in curvy areas ballast shoulders are reinforced.
- Speed restriction to prevent any hazard during very high temperatures
- Track maintenance is performed by tamping machine except in July and August.

4.3.3 TEMPERATURE - EXTREMES AND VARIATIONS

The temperature at which railway track is laid or when repairs are made is referred to as the “rail stress free temperature.” Any significant deviation above or below this temperature may result in expansion or contraction in the steel rail. The TCDD network is divided into 7 regional directorates, see

Table 4.3**.1**.

Table 4.3.1 Temperatures in different directorates of the TCDD network

REGIONS	Max Air Temperature Measured (in 50 Years)	Minimum Air Temperature Measured (in 50 Years)	Average Rail Temperature (In 50 Years)	Corresponding Stress free temperature (In 50 Years)
REGION-1	44,1°C	-19,5°C	28,7°C	33,7°C
REGION-2	44,4°C	-31,4°C	25,6°C	30,6°C
REGION-3	44,6°C	-21,8°C	29,6°C	34,6°C
REGION-4	45,0°C	-37,0°C	24,7°C	29,7°C
REGION-5	46,0°C	-34,4°C	26,8°C	31,8°C
REGION-6	47,0°C	-28,0°C	30,1°C	35,1°C
REGION-7	43,8°C	-27,4°C	23,2°C	28,2°C

Thermal misalignments caused by sun induced kinks have often been identified as a cause of train derailments with the potential for injuries, fatalities and property damage. A kink that occurs at a rail joint can cause the joint to give way under the weight of the train. Thermal misalignment of railway tracks may be further compounded by poor ballast condition or a soft roadbed. A lead locomotive or railcars may derail when high heat causes a switch to open up, forcing the train up and over the switch. Extreme heat may also produce misalignment and slack, as well as damage to catenaries and pantographs. High stresses increases the risk of sun buckling close to the S&C, but also give longitudinal and lateral displacements within the switch panel. These displacements are causing failures due to "S&C not in control".

4.3.4 Temperature related problems– Experience from Network Rail

Switches and Crossings (S&C) work and the plain line immediately adjacent to S&C is at the highest risk of buckling and preparation work in these locations is the most critical. S&C with timber bearers are at greatest risk.

One method of monitoring or controlling temperatures around S&C, in the event of high temperatures is to deploy a permanent track watchman to remain on site, recording and watching the track every time a train passes over the location. Typically the watchman will have a temperature gauge and take regular readings of the rail temperature.

4.3.4.1 POINT WORK EXPANSION

Points and switches have moveable parts that have intricate mechanical interlocking systems. During periods of high temperature these are vulnerable to expansion and can foul other equipment and cause failures. If expansion occurs, switches may not be able to operate for the passage of a train or are able to detect the train and this will inevitably cause disruption to the network.

One of the first signs of a problem is when the signaller operates the points but does not get the required indication on the signalling panel. The points may have moved to the required position but will not lock into the position. Switch diamonds are more vulnerable than an ordinary switch.

Normal mitigations include, but are not limited to:

- Ensuring all equipment has been correctly adjusted
- Lubricating moveable parts where possible
- Painting the points with a reflective paint
- Arranging patrols to inspect vulnerable locations during periods of high temperatures
- Track Section Manager to monitor points lubrication and arrange enhanced lubrication to reduce risk.

Expansion and subsequent deformation can also occur on switches which incorporate stress transfer blocks, see Figure 4.3.2.

Figure 4.3.2 Misalignment at switch heel due to thermal forces

Maintaining a stable and high rail neutral temperature is critical for prevention of this type of buckling. Neutral or stress free temperature of CWR is usually different from initial installation or anchoring temperature. Rail longitudinal movement (creep) can be due to train braking and traction forces, or

due to differential thermal forces (sun and shade). Compressive and tensile forces can cause radial breathing of curves especially in weak ballast conditions. Vertical differential settlement of rails can occur on new or recently surfaced track, or in areas of weak subgrade conditions. Neutral temperature changes can be influenced by maintenance operations including: lifting, lining, and tamping, replacing broken rail, destressing, and installing CWR in cold weather.

4.3.4.2 PAINTING OF CRITICAL SWITCHES AND SWITCH DIAMOND CROSSINGS

The Track Managers in the UK arrange the painting of operationally critical switches and switch diamond crossings with heat-reflecting white paint, Figure 4.3.3. They would typically ask for this to be completed by 31st March each year. Painting rails at-risk white so they absorb less heat, reducing rail temperatures. Typically measurements have shown that a painted rail will be five to ten degrees cooler than an unpainted rail.

Figure 4.3.3 Switch diamond with heat-reflecting paint

4.3.5 TEMPERATURE – EXTREMES AND VARIATIONS CWR INCORPORATION PROCEDURE FOR S&C

The integration of the turnout section into a continuous rail is now a common practice. It can nevertheless be observed that the procedures to perform such integration are not yet normalized. The consequence is that those procedures are different from one network to another. Not known or not properly applied by the installation entity, the turnout section becomes a fixed point in the track where all forces are joining creating a particular stress condition and potentially unstable.

Integration procedures can be standardised and at least minimum requirements can be put into an EN standard.

The main topics to be addressed in such a standard should be:

- Phenomena**:** Fixed or moveable frogs are often considered as fixed points in the track, concentrating track forces close to the S&C.
- Problem**:** Toe of the switch: holding the safety equipment often allows creeping of the rail, thus disturbing the equipment. Increased risk for rail breakage when the temperature is low and sun kinks when the temperature is high.
- Caused by: Stress free temperature is not correct. Track maintenance work can introduce additional stresses and geometrical instability. Another cause is that traffic in one dominating direction moves the rail especially if there is change of speed in the area.
- Preventative measure: Regulary check the stress free temperature. Introduce minimal rules about how to design the turnout to avoid weak areas. Rules about ballast shoulders and stablizing after maintenance work that affects geometrical stability.

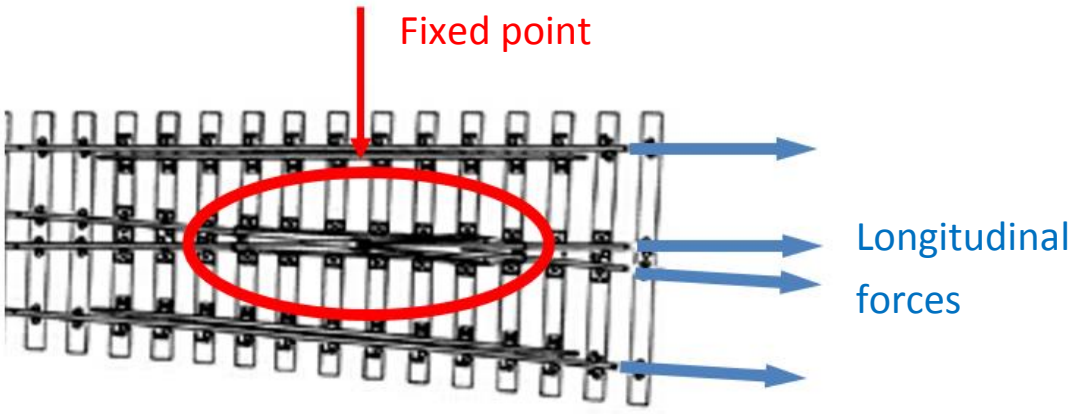

Figure 4.3.4. The crossing is forming a fixed point due to the two rails linked at the heel. This results in high forces on the welds

4.4 RAINY CONDITIONS

4.4.1 BACKGROUND

High waters from flash floods, river floods, persistent heavy rains, and hurricanes are one of the most known weather-related concerns facing the railway operators.

Washouts caused by runoffs from earlier heavy rains or rising waters have the potential to weaken bridge trestles, undermine ballast, and cause collapsed culverts. Derailments and spills can then occur when the roadbed or bridge gives out. Snowmelt causes similar saturation problems by removing ballast, making soft roadbeds. Deteriorated ties further increase these risks.

Slides can threaten the safety and efficiency of railway operations. Slide mitigation planning and implementation requires the development of warnings that allow trains to safely stop in advance of a hazard. Ground movements as a result of heavy rains, freeze-thaw cycles, tremors and other factors can disturb large boulders or large fields of rocks. These may derail a train in motion, or block tracks by debris from rock slides, mudslides, avalanches, fallen trees etc. and cause significant delays or damages.

Sections 4.4.2 has been written by TCDD, while Section 4.4.3 has been written by VCSA.

4.4.2 RAINY WEATHER –RELATED PROBLEMS AT TCDD NETWORK

As a result of examination of the records from TCDD accident and incident reports and speed restriction records for the period 2012-2014, it is found that 163 weather-related railway accidents and incidents, excluding winter conditions have occurred, 46.6% of those were most closely associated with extreme heat causing track buckling and deterioration of track geometry. The remaining 53.4% is closely associated with rainy conditions causing slides of mud and rocks, flood and saturated soil, precipitation etc. 10% of rainy condition cause precipitation, 59% is subsidence and track geometry deterioration, about 6% is rock sliding, about 19% is landslides, about 6% is flash flooding, river flooding.

We can schedule the failures due to precipitation at TCDD network as below:

- Unavailability of railway due to landslide
- Subsidence of track
- In case of choked culverts and arched bridges during heavy rain and flood, suspension of railway track is seen due to washed away ballast
- Geotextiles are used on the platform for the known subsidence locations to drain the water

Following heavy rain, flooding and earthquakes, civil structures like tunnels, bridges, culverts etc. and cuttings, embankments, ditches are checked at once.

If frost comes after rain, upon the melting of frost, railway track becomes more instable than usual. In such situations, the above-mentioned checks start at early hours of the day. If there is very hot weather prevailing, checks are carried out around noon and afternoon depending on the situation.

Figure 4.4.1 Landslide due to extreme rain

Figure 4.4.2 Drainage failure due to excessive rain

Figure 4.4.3 Fallen rocks due to rain

Figure 4.4.4 Landslide due to excessive rain (left) and unavailable track due to fallen rocks caused by excessive rain (right)

TCDD makes the following precautions to reduce failures due to winter, rain and flooding to a minimum:

- Cleaning of arched bridges and culverts
- Supporting of piers of steel bridges
- Due to signs of deviation in river bed and to protect the platform from water, spur diking is applied as a measure in advance
- Cleaning of cuttings
- In rocky areas, the rocks that have a risk to fall down are removed
- To prevent the flooding coming from a mountain side from moving to the railway line, head ditches are built as a mitigation measure and water is directed to culverts

The well-known problematic places are always under control by TCDD maintenance staff. In case of any sign for heavy rain or snow, a maintenance team is directed to those places for checking purposes. This team has close communication with a dispatcher to govern the traffic.

4.4.2.1 MOST COMMON FAILURES OBSERVED IN SUMMER AND WINTER AT TCDD NETWORK

In the TCDD network, climatic factors are considered as the external factors that have very large influence on railway infrastructure and catenary systems. Climatic factors affect large areas. To provide aggregated climatic data at country level is more realistic, see Table 4.4.1

Table 4.4.1 Climatic data in TCDD network

<table>
<tr><th>CLIMATIC DATA</th><th>AT COUNTRY LEVEL- TURKEY</th></tr>
<tr><td>Average Ambient Temperature</td><td>From 2009 to 2014;
Avg. of the min extremes: -33.6° C
Avg. of the max extremes: 46.1° C</td></tr>
<tr><td>Average Humidity</td><td>63.8%</td></tr>
<tr><td>Wind Speed</td><td>1.9 m/sec</td></tr>
<tr><td>Ice Loads</td><td>
<table>
<tr><th rowspan="2">*Region No</th><th rowspan="2">Ice load coefficient</th><th rowspan="2">Ice load kg/m</th><th rowspan="2">Ice load N/m</th><th colspan="2">Ambient Temperature</th></tr>
<tr><th>Highest</th><th>Lowest</th></tr>
<tr><td>1</td><td>0</td><td>0</td><td></td><td>50</td><td>-10</td></tr>
<tr><td>2</td><td>0.2</td><td>0,2√d [1)]</td><td>1.96√d [1)]</td><td>45</td><td>-15</td></tr>
<tr><td>3</td><td>0.3</td><td>0,3√d</td><td>2.94√d</td><td>40</td><td>-25</td></tr>
<tr><td>4</td><td>0.5</td><td>0,52√d</td><td>5.096√d</td><td>40</td><td>-30</td></tr>
<tr><td>5</td><td>1.2</td><td>1,2√d</td><td>11.76√d</td><td>40</td><td>-30</td></tr>
</table>
1) d=Radius of conductor; * Region numbers are indicated on the map
</td></tr>
</table>

	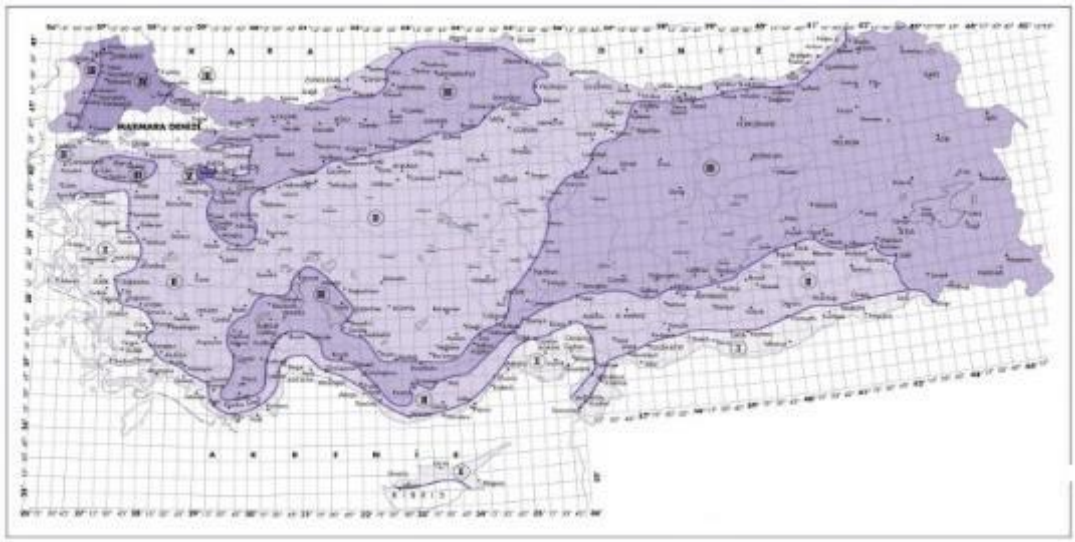 Ice Load map of Turkey
Air Quality	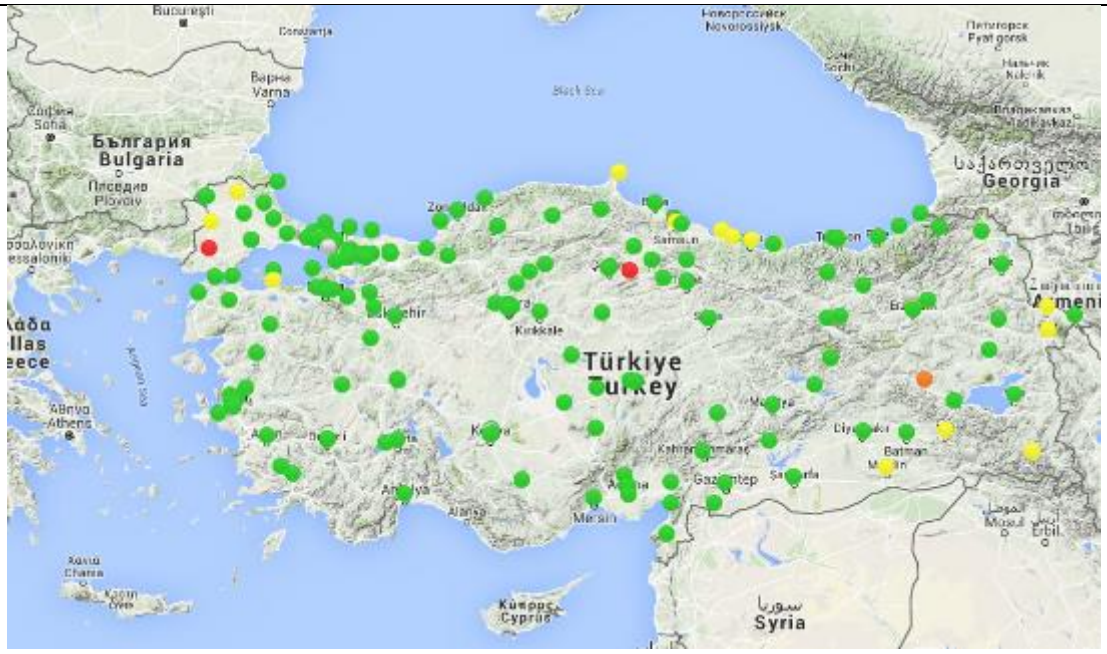

The most common climatic factors causing failures seen in the TCDD network are:

- Heavy rain
- Fallen tree on catenary system due to wind
- Precipitation

- Track geometry failure due to external factors
- Fire
- Stroke of lightning onto substation
- Flood
- Falling rocks on the track
- Track alignment problems

The TCDD network is divided into seven regions. For regions 2, 4, 5 and 6, statistics for the most commonly observed climatic factors leading to failures in 2014 to 2015 are presented in Tables 4.4.2 to 4.4.4.

Table 4.4.2 Number of failures in 2014 to 2015 for Region 2

REGION 2	2015											
EXTERNAL FACTORS	JAN.	FEB.	MAR.	APR.	MAY.	JUNE	JULY	1. Region	SEP.	OCT.	NOV.	DEC.
heavy rain	0	0	0	0	0	0	0	0	0			
fallen tree on OHL	1	0	0	0	0	1	0	0	0			
precipitation	0	0	0	0	0	1	0	0	0			
Track geometry failure due to external factors	0	0	0	0	0	0	0	0	0			
fire	0	0	0	1	0	0	1	1	0			
stroke of lightning onto substation	0	0	0	0	0	0	0	0	0			
flood	0	0	0	0	0	0	0	0	0			
falling rocks on the track	0	0	0	0	0	0	0	0	0			
storm	0	0	0	0	0	0	0	0	0			
track allighment problems	0	0	0	0	0	0	0	0	0			
REGION 2	2014											
EXTERNAL FACTORS	JAN.	FEB.	MAR.	APR.	MAY.	JUNE	JULY	AUG.	SEP.	OCT.	NOV.	DEC.
heavy rain	0	0	0	0	0	0	0	0	0	0	0	0
fallen tree on OHL	0	0	0	0	0	0	0	0	0	0	0	0
precipitation	0	0	0	0	0	0	0	0	0	0	0	0
Track geometry failure due to external factors	0	0	0	0	0	0	0	0	0	0	0	0
fire	0	0	0	0	0	0	1	0	0	0	0	0
stroke of lightning onto substation	0	0	0	0	0	1	0	0	0	0	0	0
flood	0	0	0	0	0	0	0	1	0	0	0	1
falling rocks on the track	0	0	0	0	0	0	0	0	0	0	0	0
storm	0	0	0	0	0	0	0	0	0	0	0	0
track allighment problems	0	0	0	0	0	0	0	0	0	0	0	0

Table 4.4.3 Number of failures in 2014 to 2015 for Regions 4 and 5

REGION4-REGION5	2015											
EXTERNAL FACTORS	JAN.	FEB.	MAR.	APR.	MAY.	JUNE	JULY	AUG.	SEP.	OCT.	NOV.	DEC.
heavy rain	0	0	0	0	0	0	0	0	0			
fallen tree on OHL	0	0	0	0	0	0	0	0	0			
precipitation	0	0	0	0	0	1	0	0	0			
Track geometry failure due to external factors	0	0	0	0	0	0	0	0	0			
fire	0	0	0	0	0	0	0	0	0			
stroke of lightning onto substation	0	0	0	0	0	0	0	0	0			
flood	0	0	0	0	0	0	0	0	0			
falling rocks on the track	0	0	0	0	0	0	0	0	0			
storm	1	0	0	0	0	0	0	0	0			
track allighment problems	0	0	0	0	0	0	0	0	0			
REGION4-REGION5	2014											
EXTERNAL FACTORS	JAN.	FEB.	MAR.	APR.	MAY.	JUNE	JULY	AUG.	SEP.	OCT.	NOV.	DEC.
heavy rain	0	0	0	0	0	0	0	0	0	0	0	0
fallen tree on OHL	0	0	0	0	0	0	0	0	0	0	0	0
precipitation	0	0	0	1	0	0	0	0	0	0	0	0
Track geometry failure due to external factors	0	0	0	0	0	0	0	0	0	0	0	0
fire	0	0	0	0	0	0	0	0	0	0	0	0
stroke of lightning onto substation	0	0	0	0	0	0	0	0	0	0	0	0
flood	0	0	0	0	0	0	0	0	0	0	0	0
falling rocks on the track	0	0	0	0	1		0	0	0	0	0	0
storm	0	0	0	0	0	0	0	0	0	0	0	0
track allighment problems	0	0	0	0	0	0	0	0	0	0	0	0

Table 4.4.4 Number of failures in 2014 to 2015 for Regions 5 and 6

REGION5-REGION6	2015											
EXTERNAL FACTORS	JAN.	FEB.	MAR.	APR.	MAY.	JUNE	JULY	AUG.	SEP.	OCT.	NOV.	DEC.
heavy rain	0	0	0	0	0	0	0	0				
fallen tree on OHL	0	0	0	0	0	0	0	0				
precipitation	0	0	0	0	0	0	0	0				
Track geometry failure due to external factors	0	0	0	0	0	0	0	0				
fire	0	0	0	0	0	0	0	0				
stroke of lightning onto substation	0	0	0	0	0	0	0	0				
flood	0	0	0	0	0	0	0	0				
falling rocks on the track	0	0	0	0	0	0	0	0				
storm	1	0	0	0	0	0	0	0				
track allighment problems	0	0	1	0	0	0	0	0				
REGION5-REGION6	2014											
EXTERNAL FACTORS	JAN.	FEB.	MAR.	APR.	MAY.	JUNE	JULY	AUG.	SEP.	OCT.	NOV.	DEC.
heavy rain	0	0	1	0	0	0	0	0	0	0	0	0
fallen tree on OHL	0	0	0	0	0	0	0	0	0	0	0	0
precipitation	0	0	0	0	0	0	0	1	0	0	0	0
Track geometry failure due to external factors	0	0	0	0	0	0	0	0	0	0	0	0
fire	0	0	0	0	0	0	0	0	0	0	0	0
stroke of lightning onto substation	0	0	0	0	0	0	0	0	0	0	0	0
flood	0	0	0	0	0	0	0	0	0	0	0	0
falling rocks on the track	0	0	0	0	0	0	0	0	0	0	0	0
storm	0	0	0	0	0	0	0	0	0	0	0	0
track allighment problems	0	0	0	0	0	0	0	0	0	0	0	0

4.4.3 Flooding – Problems related to Network Rail

During periods of heavy rain, routes may experience localised or in some cases extensive flooding. Floodwater has the ability to wash away large sections of track bed and cause signalling failures if equipment becomes waterlogged or track circuits become fully submerged.

Heavy rain bursts can cause two types of flooding in the summer months: ground water flooding and run-off flooding.

Ground water flooding is generally a result of heavy rain falling proceeded by a long wet spell. Low lying ground becomes saturated and can physically hold no more water, so the site becomes flooded.

Run-off flooding on the other hand, is caused by an intense burst of rain (normally associated with summer thunderstorms). The rain is so heavy that it cannot drain away quickly enough, or the drains cannot cope with the amount of rainfall so flooding occurs. Urban areas are more susceptible to run-off flooding due to the semi-impervious nature of the roads, pavements and drains. The flooding, however, is generally localised.

During the summer, if there has been a particular dry spell, the ground may be baked and hard, increasing demands on drainage.

Basic preparations include but are not limited to:

- Ensuring that track drainage is kept clear from obstructions (normally ballast, vegetation and litter)
- Ensuring that off track drainage is clear from obstructions (this type of drainage is important in controlling or diverting run off from adjacent land)
- Ensuring local authorities have adequate flood defences and that they are in a good state of repair
- The Rail Network's flood defences are in a good state of repair
- Reporting of any blocked drains or defective pumping locations to Route Control
- Deploy flood defence systems including modular ridged barriers with a membrane that seals to prevent water getting through, and inflatable barriers which are filled with flood water.
- Build pumping stations in locations which are prone to flooding so we can quickly pump flood water away

Many sections of railways were built in cuttings and tunnels which are lower than the surrounding area, and many other lines are on flat, low-lying land with limited drainage, making them prone to flooding.

Figure 4.4.5 Flooding in switches and crossings

Flood water can wash away ballast - the bed of stones which supports sleepers - making the line unsafe until it is re-laid.

The development of land near the railway can increase the risk of flooding. If the drainage system is inadequate, rain which previously soaked into the ground may run off tarmac and concrete and straight onto the tracks.

When the water level rises above the rails, trains have to reduce their speed to prevent damage to the train. If the track has a live conductor rail, flooding can cause a short circuit.

Points and signalling equipment can fail when water enters their housings and may need replacing before services can resume.

When lines that are at risk of flooding effort are renewed, care is taken to raise the tracks and signalling equipment to try to mitigate this.

5 Optimized S&C sensor strategies to minimize traffic disruptions (C4R task 1.3.4)

Today, the most common way to inspect S&Cs is by inspection performed by personnel walking in the track. Recorded measurements from such visits can be used for monitoring purpose, but most of the inspections are not quantified and are therefore not useful for predictions.

5.1 KEY OPERATIONAL PARAMETERS

S&Cs can be monitored in track, by stand off equipment, by the point machine, by the interlocking system or by vehicles.

5.1.1 MONITORING IN TRACK (EMBEDDED SENSORS)

Monitoring in track is investigated in the In2Rail project and therefore it is just briefly covered here. Sensors measuring acceleration, displacement or strain can be used on the rails and sleepers. In ballast pressure and acceleration can be measured. A commercial available technology is available for sleeper measurement. In Figure 5.1.1 is shown result from a measurement made in Sweden.

The measurement is valuable to understand the actual stiffness and how that changes over time. A second reason is to be aware if the sleeper is getting voided or the rail is so damage that the acceleration increases.

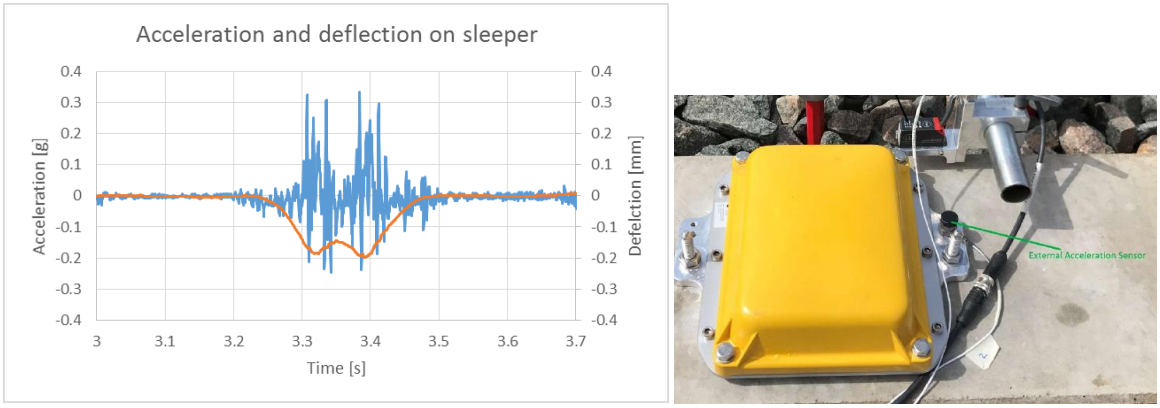

Figure 5.1.1 Acceleration and deflection on a bogie passage at Algutsgården (Sweden) May 11th 2017 (filtered to 40 Hz), to the left the setup with the wireless accelerometer in the yellow box as well as a laser deflection sensor to check the result.

Temperature is measured to control the heating elements.

Force is more difficult to measure than strain. In straight track, a wheel impact load detector can be used to indirectly measure the vertical wheel-rail contact force by measuring the force at the rail seat. These detectors are 7 metres long to cover twice the circumference of a wheel so it is not realistic to use them in an S&C. When using strain gauges applied on the rail web, the vertical force can only be determined if the contact points are known in advance, and in S&Cs double point contact occurs both

in the switch panel and in the crossing. Thus, to measure wheel-rail contact forces (vertical, lateral and longitudinal) in S&Cs, it is necessary to use an instrumented wheelset.

5.1.2 MONITORING BY POINT MACHINE AND INTERLOCKING SYSTEM

The point machine always controls in which position the S&C is. During the movement of the switch rail, time for movement, force, motor current, hydraulic pressure and/or the distance can be measured. Voestalpine offers the system Roadmaster [5.1] that is a system that includes both point machine measurements and track measurements in the S&C.

VCSA offers the systems SURVAIG [5.2] and SURTRACK, which are designed for predictive maintenance of track equipment and track circuits.

In digitalised interlocking systems, current, voltage and energy can be measured and time variant control signals can be registered. Even in relay based interlocking systems, it is possible to record the occurrence of and when in time different states occur.

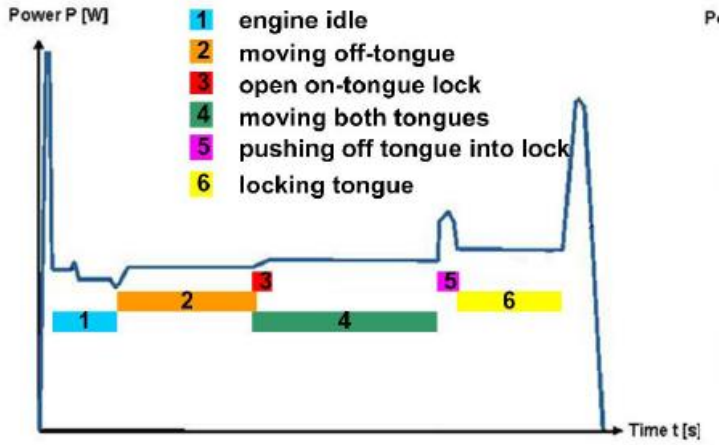

Figure 5.1.2 Illustration of different phases when moving switch-tongue measured by power (from [5.3])

5.1.3 MONITORING BY USING STAND OFF EQUIPMENT

Monitoring by using stand off equipment is investigated in the In2Rail project and is therefore just briefly covered here.

Stand off technology uses laser and/or camera technology to measure or observe. It normally also involves some kind of video analysis and pattern recognition. It is possible to measure distances and profiles, and also changes, over time. For instance if objects are stuck between switch rail and support rail this can be observed by a camera. Stand off technology can also used to observe settlement over time. A proposed technology here is to use satellite measurements that can be used to over time observe the height of the superstructure down to the order of millimetres.

A special possibility that is a mix between in track measurements and stand off technology is the use of sensors placed in track that communicate wirelessly with equipment outside the track. In WP1 and

WP4 strain sensors is embedded in concrete and activated by RFID technologies. For more simple applications, the energy of the sensor might be sent to the sensor with RFID technology. For more advanced applications, a battery or solar panel is needed for the sensors.

5.1.4 MONITORING BY VEHICLES

Measurement by vehicles is standard for track including the straight section (through route) of an S&C, and it is performed as often as it is for standard track. For diverging track, the measurements are performed more seldom. All infrastructure owners measure track geometry and, by ultrasonic equipment, internal rail defects. For surface initiated rail defects, eddy current, video inspection and even axle box accelerometers (squats) can be used.

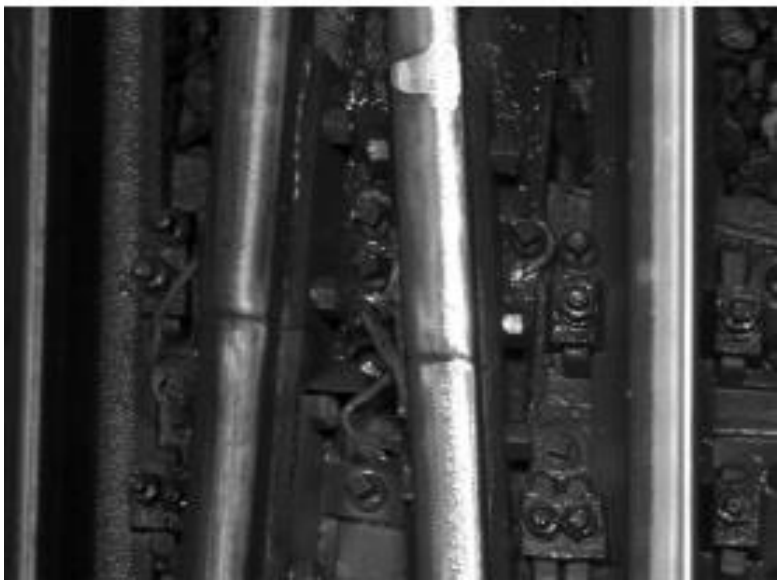

Figure 5.1.3 Video inspected rail in S&C [from 5.4]

5.2 EXPERIENCE FROM MEASUREMENT THAT IS IN UNDER DEVELOPMENT

5.2.1 DEFLECTION MEASUREMENT

Deflection measurement can be done if the track geometry car both can measure loaded and unloaded. At Trafikverket this is done when asked for and not a regular basis.

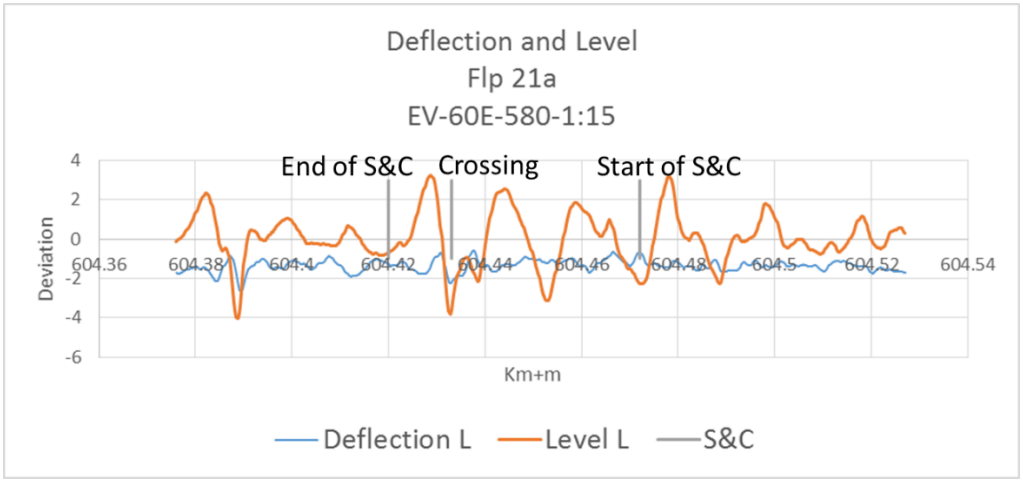

Figure 5.2.1 Deflection measurement and level for S&C Flp 21a

Larger deflection indicates either bad subsoil condition and/or voided sleepers. At positions where there is large deflection the deterioration of the level signal will go faster.

5.2.2 Measurement of rail profile

Rail profile measurement is done by ordinary track geometry cars, but the spacing is normally up to 1 meter so special measurement car has been developed for S&Cs where the spacing can be 20 mm or less. To get even better spatial resolution the equipment must be brought to track, see section 3.2.11. One of the demonstrators is discussing such a solution. With a spatial resolution of 10 mm or better it is possible to measure wear and longitudinal profile. Bothe of these values are of interest to take maintenance decisions. In Figure 5.2.2 is shown what is possible to do with today's measurement system.

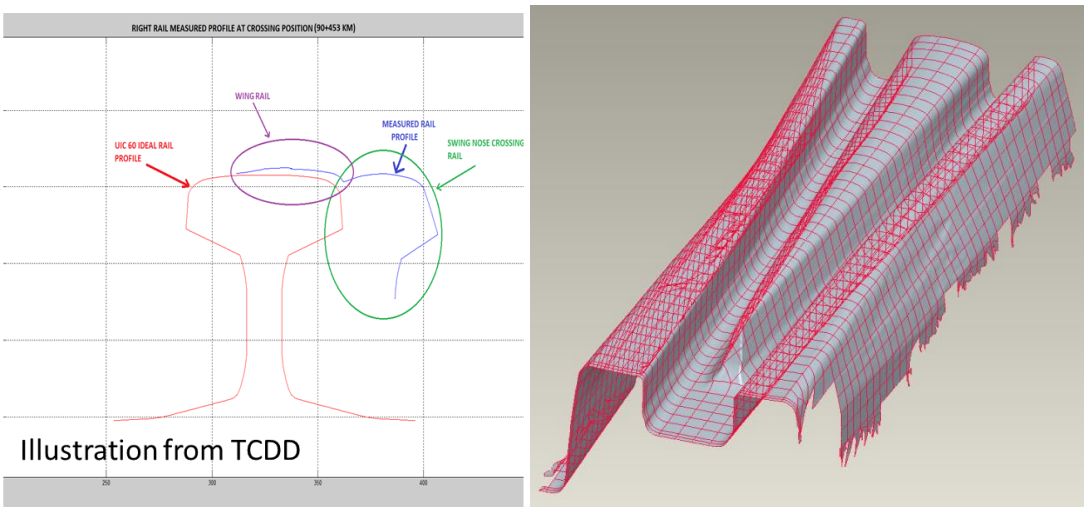

Figure 5.2.2 Rail profile measurement either from train (left) or by hand (right, Handyscan 700)

5.3 SENSOR STRATEGIES

The overall goal for all monitoring is to be able to take decisions of maintenance in time before failures are affecting the operation of traffic.

The condition data must therefore include a prediction of deterioration over time. When the signal passes the threshold value there must (in most cases) be a long enough failure development time to allow for safe traffic operation until adequate maintenance is performed.

5.3.1 RELATIONSHIP BETWEEN SENSOR DATA AND DETERIORATION LEVELS

Sensor data are first collected locally and can be either stored as raw data or summarized in mean values, standard deviation, minimum and maximum values. Measurements at different times can be used to follow trends and based on these trends it is possible to predict when in time to do maintenance.

This example is from a track geometry car measurement and in particular the development of the level signal. Level is the vertically position of the rail and is normally the signal from the track geometry car that changes fastest over time, see Figure 5.3.1. The S&C Åby 132a and Åby 133b was placed in track in 2013. The crossing had shortly after installation a dip of 6 mm, which is unusually much. Because of the bad initial situation and no performed maintenance, the dip has during the following two years developed to about 11 mm, which is close to the action limit for normal track.

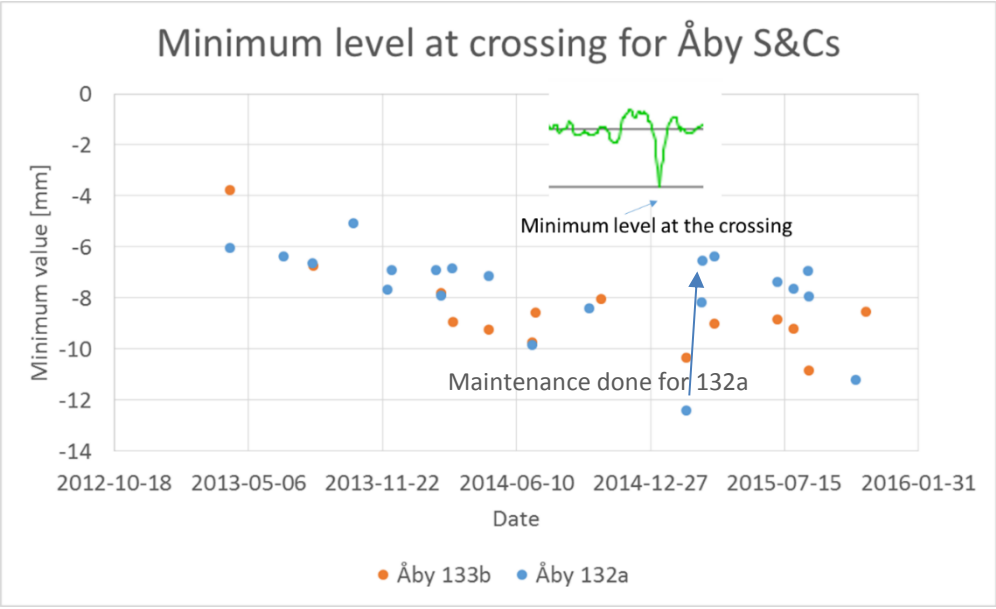

Figure 5.3.1 Time history of measured minimum level for the crossing at Åby 133b and 132a.

Measurement of track geometry in S&Cs is still an area where development is needed as each recording needs to be compared for nearly the same location (within 5 m) to be sure that the analysis is done in a correct way. For normal track, a larger deviation is acceptable. Today's system for

presenting track geometry gives possibilities to monitor track degradation over time, which has been proven by for instance the Technical University of Graz. To be able to perform a similar analysis for S&Cs it is necessary to identify the different panels of the S&C and use different parameters for each panel.

5.4 REFERENCES

[5.1] https://www.voestalpine.com/bwg/static/sites/c015/downloads/en/products/Roadmaster_en.pdf

[5.2] http://www.vossloh-cogifer.com/en/products_and_systems/track_monitoring_2/track_monitoring_3.html

[5.3] Böhm, Thomas und Schenkendorf, René und Lemmer, Karsten (2016) *Statistical Process Control for Modern Switch Failure Detection.* In: Proceedings of the 11th World Congress on Railway Research, e1-e6. 11th World Congress on Railway Research, 29. Mai - 02. Jun. 2016, Mailand, Italien

[5.4] http://www.eurailscout.com/services/switch/visual-switch-inspection-/

5.5 SENSOR STRATEGIES

The overall goal for all monitoring is to be able to take decisions of maintenance in time before failures are affecting the operation of traffic.

The condition data must therefore include a prediction of deterioration over time. When the signal passes the threshold value there must (in most cases) be a long enough failure development time to allow for safe traffic operation until adequate maintenance is performed.

5.6 RELATIONSHIP BETWEEN SENSOR DATA AND DETERIORATION LEVELS

Sensor data are first collected locally and can be either stored as raw data or summarized in mean values, standard deviation, minimum and maximum values. Measurements at different times can be used to follow trends and based on these trends it is possible to predict when in time to do maintenance.

Here the focus will be on data from track geometry cars and in particular the development of the level signal. Level is the vertically position of the rail and is normally the signal from the track geometry car that changes fastest over time.

An example for a crossing at Trafikverket is given in Figure 5.6.1. The S&C Åby 133 b was placed in track in 2013. The crossing had shortly after installation a dip of 6 mm, which is unusually much. Because of the bad initial situation and no performed maintenance, the dip has during the following two years developed to about 11 mm, which is close to the maintenance limit for normal track.

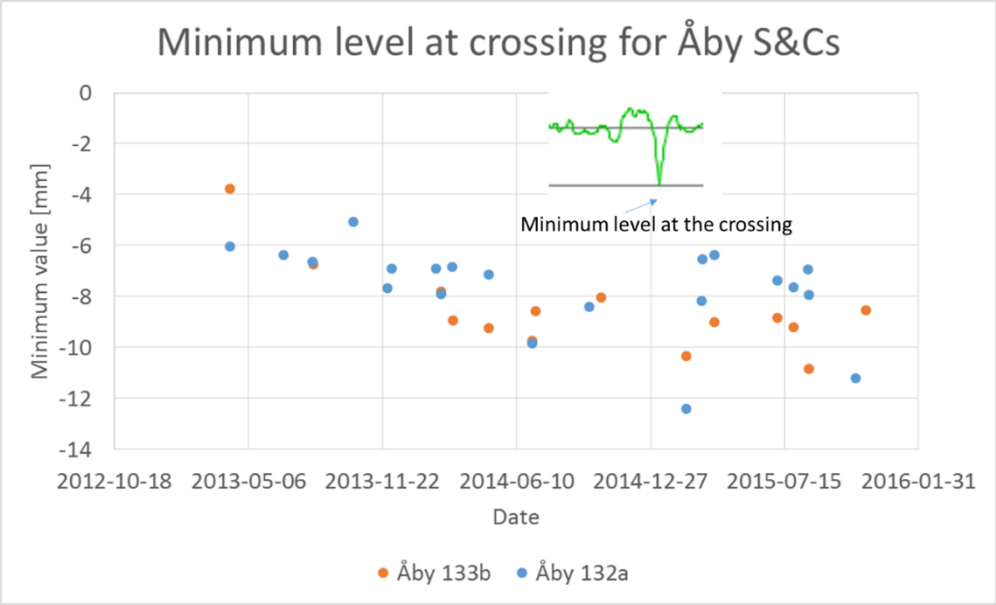

Figure 5.6.1 Time history of measured minimum level for the crossing at Åby 133b. Maintenance can be planned before the minimum level reaches a certain value

Measurement of track geometry in S&Cs is still an area where development is needed as each recording needs to be compared for nearly the same location (within 5 m) to be sure that the analysis

is done in a correct way. For normal track, a larger deviation is acceptable. Today's system for presenting track geometry gives possibilities to monitor track degradation over time, which has been proven by for instance the Technical University of Graz. To be able to perform a similar analysis for S&Cs it is necessary to identify the different panels of the S&C and use different parameters for each panel. The geometry at the crossing and the point machine are normally not within the tolerances of new laid track (+/- 2 mm) and should therefore be identified and monitored separately, while the rest of the S&C can be treated as normal track. For the diverging route, a special analysis of gauge, side wear and alignment also can be made. In the analysis, prediction models for each parameter is needed and these models need input of traffic volume in straight and diverging routes.

6. Conclusions

The present deliverable is the final report describing the work carried out in tasks 2, 3 and 4 of Capacity4Rail WP1.3.

Simulations has been made aiming towards improved railway turnouts (S&C) that reduces material deterioration (wear, plastic deformation, rolling contact fatigue) and failures (C4R task 1.3.2). Based on numerical simulations of dynamic vehicle-track interaction using validated models and software, it has been demonstrated how rail and track degradation can be reduced by optimisation of geometry and stiffness properties of the turnout, leading to reduced Life Cycle Cost (LCC).

The investigated *short-term solutions* for reducing loads and rail profile degradation in the switch panel have included selection of (1) rail profile and rail inclination, (2) rail grade, and application of (3) friction management. The calculations have shown that a design with inclined rails (1:30) is superior to the case with vertical rails. The selection of rail grade R350HT instead of R260 leads to an expected reduction in wear, but in order to more accurately quantify the improvement there is a need for validation of the implemented wear map model by further measurements of the influence of contact pressure and sliding velocity on wear coefficients for different rail grades. The predicted influences of rail grade and friction management on RCF are uncertain due to the wide range of factors influencing RCF initiation, such as the important interaction between crack growth and wear in situations with medium-high levels of energy dissipation (*Ty*) in the wheel-rail contact. Such situations have been shown to be common in the switch panel and in particular at rail sections where there are transitions between ‘one-point’ and ‘two-point’ wheel-rail contact. Thus, it is important that the implemented RCF damage model is validated by future field observations and measurements. It has been shown that both wear and RCF are reduced significantly by maintaining a low friction coefficient in the wheel-rail contact. In particular, situations with dry wheel-rail contact (high friction) should be avoided as these lead to very high RCF damage impact.

The investigated *medium-term solutions* have focussed on improving the performance of the crossing panel. These solutions have included (1) geometry optimisation of the crossing to minimise impact loads and reduce the steering force damage in the contact areas, (2) dynamic load mitigation (ballast protection) through rail pad stiffness optimisation and the use of under sleeper pads (USP) or connecting elements between sleepers, and (3) novel materials in crossing nose and wing rails to resist fatigue, wear and plastic deformation.

The investigation in crossing geometry has highlighted key differences in current design practice and machining tools used for half and full cant (UK terminology) geometries, leading to quantifiably different damage behaviour. The interaction between wheel shape and the crossing wing geometry is a determining factor in the level for vertical impact force, lateral dynamics and resulting rail damage. The crossing with a higher inclined wing rail showed better performance across all wheels simulated. The peculiar behaviour of hollow wheels has been quantified and shown to be more reactive to one of the crossing types. High conicity wheels are also potentially leading to higher dynamic impact. All this

needs to be considered in the design process. On that basis, the proposed methodology can enable a fast and effective optimisation process of the crossing wing rail geometry minimising vertical impact loads, wear and RCF on both wing rail and crossing vee. The topic of further work will focus on modifying the shape of the wing rail (inclined, length of inclined and slope of topping) to achieve an optimum solution in between the two investigated so far. Like for the short-term optimisation in switches, there is a crucial need for more material data to quantify their resistance to wear and RCF in high energy (*Tγ*) and high load regimes, with the particularity of cast manganese behaviour, having a very non-linear and unpredictable hardening process through the earlier cycles of utilisation. Such data is currently not available to make a full utilisation of the methodology developed here. Alongside, it is important to be able to measure precisely the evolution in shape of crossing both at the early stages and throughout their life by using advanced 3D scanning equipment.

A methodology has also been proposed for the optimisation of rail pad stiffness in crossing panel, showing that low stiffness rail pads (ca 80 kN/mm) provide a suitable mitigation for ballast pressure, sleeper acceleration and minimising contact forces, while maintaining acceptable bending stresses of rail components. This study can be extended to more crossing types, length and speed, as well as include baseplate systems. An investigation into the role of under sleeper pads (USP) in mitigating vertical dynamics loads has been presented, highlighting the importance of careful selection of USP properties, so that the system response is fully understood while designing or upgrading an S&C. Finally, an investigation in linking sleepers together in the areas of load transfer of a crossing panel has shown some benefits in protecting the ballast layer while making the panel behave more like a slab. It is proposed this is followed up by further investigation in lateral and combined vertical/lateral loading to highlight benefit and cross over between ballasted and non-ballasted tracks, possibly within the lighthouse project In2Rail under hybrid track scope.

Next generation S&C (*long-term solutions*) will be based on a whole-system approach including enhanced design, materials and components and incorporation of modern mechatronics for improved system kinematics and control. One example of a long-term solution that has been discussed in the report is the Modular Continuous Support (MCS) track, which is a ballast-less track design offering an efficient lower cost rail technology based on pre-fabricated modules and continuously supported rails. Next generation S&C will be an important topic for further work in Shift2Rail.

Operation of S&Cs in extreme weather conditions is a challenge to railway administrations (task 1.3.3). The report includes a survey of common problems occurring due to situations with high temperatures, strong winds, low temperatures and heavy snow fall, as well as heavy rain fall and flooding. In most cases the most economical solution is to send out personal to inspect the situation and remove obstacle and restrict the traffic until the condition has improved. Though a number of preventative actions should also be considered.

- Warm weather

  - Paint operational-critical switches with heat reflecting white-paint
  - Regulary check the stress free temperature. Introduce minimal rules about how to design the turnout to avoid weak areas. Rules about ballast shoulders and stablizing after maintenance work that affects geometrical stability
  - Ensuring all equipment has been correctly adjusted
  - Lubricating moveable parts that needs to be lubricated
  - Before summer, small fastening materials are loosened and those damaged are maintained and the screws are tightened to suitable torque values
  - Making up deficiency of ballast, especially in curvy areas ballast shoulders are reinforced
  - Track maintenance performed by tamping machine should not be done during hot season
- Heavy winds
  - Ensure that there are no high trees close to the track
- Heavy rain
  - Ensure that track drainage system are designed and maintained to lead water so the ballast not is affected
  - Ensure that track off drainage system are designed and maintained to lead water so the ballast not is affected
  - Install geotextiles at known subsidence locations to drain the water
  - Cleaning of arched bridges and culverts
  - Supporting of piers of steel bridges
  - Due to signs of deviation in river bed and to protect the platform from water, spur diking is applied as a measure in advance
  - Cleaning of cuttings
  - In rocky areas, the rocks that have a risk to fall down are removed
  - To prevent the flooding coming from a mountain side from moving to the railway line, head ditches are built as a mitigation measure and water is directed to culverts
  - At tunnels or other places which are situated so low that flooding can fill them a sealed and ridged barrier is built before the location so the ballast cannot lead the water down into the area. At the location pumps are installed to take care of water that comes

  - Places signaling and other sensitive equipment so high that flooding cannot damage them in areas where flooding might occur
- Heavy snow fall
  - Minimize the number turnout that needs to be moved so that maintenance personnel can concentrate on the active turnouts
  - Installation of equipment that can remove snow fast
  - Installation of high pressure equipment that can remove snow instantly

As part of task 1.3.4 monitoring of S&C has been covered. S&C can be monitored by using

- Embedded sensors in track or interlocking system
- Stand off equipment besides the track
- Vehicle based measurements

The most essential information that should be collected is the information of movement of switch blade, track geometry and rail profile. Other candidates are measurement of vehicle induced acceleration, stiffness and rail temperature in the switch heating system.

By using the measured values trending is possible, prediction can be made and preventative maintenance can be planned. The implementation of monitoring strategies and sensor technology is covered in more detail in Capacity4Rail SP4.

In task 1.3.5, the following innovative S&C concepts has been demonstrated.

- Installation of bainitic crossing
- Installation of wireless, battery based accelerometer sensor for dynamic measurements
- Material testing with a new twin disc equipment
- Laser profile measurement equipment for crossing
- Weather prognosis for switch heating

The present work and the writing of this deliverable were performed by Chalmers, University of Huddersfield, VAE, VCSA, INECO, TCDD and Trafikverket (lead contractor).